SPATIO-TEMPORAL ANALYSIS AND MODEL DEVELOPMENT FOR URBAN HEAT ISLAND EFFECT OVER INDIAN CITIES

Ph.D. Thesis

ANEESH MATHEW

(2014RCE9039)

DEPARTMENT OF CIVIL ENGINEERING
MALAVIYA NATIONAL INSTITUTE OF TECHNOLOGY, JAIPUR

August, 2018

Spatio-temporal Analysis and Model Development for Urban Heat Island Effect over Indian Cities

Submitted in

fulfilment of the requirements for the degree of

Doctor of Philosophy

In

Civil Engineering

By

Aneesh Mathew

2014RCE9039

Under the Supervision of

Dr. Sumit Khandelwal

Department of Civil Engineering, MNIT Jaipur

DEPARTMENT OF CIVIL ENGINEERING
MALAVIYA NATIONAL INSTITUTE OF TECHNOLOGY, JAIPUR

August, 2018

DECLARATION

I, **Aneesh Mathew**, declare that this thesis titled, "**Spatio-temporal Analysis and Model Development for Urban Heat Island Effect over Indian Cities**" and the work presented in it, are my own. I confirm that:

- This work was done wholly or mainly while in candidature for a research degree at this university.
- Where any part of this thesis has previously been submitted for a degree or any other qualification at this university or any other institution, this has been clearly stated.
- Where I have consulted the published work of others, this is always clearly attributed.
- Where I have quoted from the work of others, the source is always given. With the exception of such quotations, this thesis is entirely my own work.
- I have acknowledged all main sources of help.
- Where the thesis is based on work done by myself, jointly with others, I have made clear exactly what was done by others and what I have contributed myself.

Date: 14/08/2018

Aneesh Mathew
(2014RCE9039)

CERTIFICATE

This is to certify that the thesis entitled "**Spatio-temporal Analysis and Model Development for Urban Heat Island Effect over Indian Cities"** being submitted by **Aneesh Mathew (2014RCE9039)** is a bonafide research work carried out under my supervision and guidance in fulfillment of the requirement for the award of the degree of **Doctor of Philosophy** in the Department of Civil Engineering, Malaviya National Institute of Technology, Jaipur, India. The matter embodied in this thesis is original and has not been submitted to any other University or Institute for the award of any other degree.

Place: Jaipur
Date: 14/08/2018

(Sumit Khandelwal)
Associate Professor
Dept. of Civil Engineering
MNIT Jaipur

Acknowledgements

Any accomplishment requires blessings and efforts of numerous individuals and this work is no exception. I am extremely grateful to GOD Almighty and my beloved parents whose blessings have made this work possible.

It gives me great pleasure in conveying my heartiest thanks and profound gratitude to my thesis supervisor, Dr. Sumit Khandelwal, Associate Professor, Department of Civil Engineering, Malaviya National Institute of Technology Jaipur for providing me with the guidance, advice and support at each and every step in the completion of this work. His guidance helped me in all the time of research and writing of this thesis. I appreciate all his contributions of time, ideas, and funding to make my Ph.D. experience productive and stimulating.

The work of this magnitude could not have been accomplished without the valuable inputs of Prof. Jyotimay Mathur who shared his vast knowledge and expertise from time to time. I am indebted to him for his constant encouragement and keen interest; he has shown in the progress of the study. I whole heartedly acknowledge the support of Prof. Y.P. Mathur who readily cooperated throughout the discussions and whose crisp comments and suggestions have vastly enhanced the quality of the work.

Heartfelt thanks are put on record towards the Director, MNIT Jaipur for providing research facilities at MNIT Jaipur. Special thanks are due to Prof. Udaykumar R Yaragatti, Director, MNIT Jaipur for the encouragement and motivation for completing the work.

I gratefully acknowledge the co-operation, motivation and assistance extended by Prof. Gunwant Sharma, Prof. Rohit Goyal, Prof. Mahesh Kumar Jat, Prof. Rajesh Kumar and Dr. Nivedita Kaul. All my colleagues who have pushed and motivated me from time to time are thanked from the bottom of my heart. Mr. Kuldeep Tiwari and Mr. Gopala Rao, deserve a special mention.

I am also thanking our colleagues, research scholars and friends for their helpful suggestions and encouragement. Mr. Rishabh Chaudhary, Mr. Chander, Miss. Neha Gupta, Mr. Shivam Chauhan, Mr. Gitesh Bakolia, Mr. Subrata Nath, Mr. Sreenu Sreekumar and Miss Asha Bohra deserve a special mention. I wish to thank all the

M.Tech students in Water Resources Engineering (2015-2017 batch), MNIT Jaipur for their full support for conducting in-situ field survey for temperature measurements. My field study was made less obstacle ridden because of the immense support from these people.

Many thanks to the technical and office staff of Department of Civil Engineering, MNIT Jaipur especially Mr. Rajesh Saxena and Mr. Ramji Lal for their support.

I gratefully acknowledge the funding sources that made my Ph.D. work possible. This work was supported by the Department of Science and Technology (DST) Delhi, Government of India. I also wish to thank the Land Processes Distributed Active Archive Center (LP DAAC), located at the U.S. Geological Survey (USGS) Earth Resources Observation and Science (EROS) Center (lpdaac.usgs.gov) for making available the satellite data.

Last but not the least, I would like to thank my family: my parents and to my brother and sister for supporting me spiritually throughout writing this thesis and my life in general. I whole heartedly acknowledge the role and sound support of my brother Mr. Anooj Mathew and my sister Miss Anila Mathew whose support and prayers have made this work possible.

(Aneesh Mathew)

Date: August 15th, 2018 (Independence Day)
Jaipur

Spatio-temporal Analysis and Model Development for Urban Heat Island Effect over Indian Cities

Abstract

Congested and unsustainable planning, reduction in green covers and increased emissions from industries and vehicles have given birth to many climatic issues. One such issue is enhanced land surface temperature (LST) giving rise to urban heat island (UHI) phenomenon. The present study has been carried out to understand the UHI effect of areas surrounding Jaipur, Ahmedabad and Chandigarh cities in India. Remote sensing data from MODIS sensor (on board Aqua and Terra platforms), Landsat data and ASTER DEM data has been used. The study has been undertaken for summer, monsoon and winter seasons, prevailing over the study area, by utilizing data of thirteen years from 2003 to 2015. The study areas have geographical extent of approximately 1370, 887, and 511 square kms for Jaipur, Ahmedabad and Chandigarh, respectively.

LST is used as the key parameter for surface urban heat island (SUHI) studies in the present study. Inverse or negative surface UHI effect has been observed over Jaipur whereas very weak and moderate SUHI effect is observed over Ahmedabad and Chandigarh, respectively during the daytime. Clear SUHI effect is observed during night period over these cities. From the analysis of night-time images, overall average of maximum SUHI intensity of the Jaipur study area during summer, monsoon, and winter seasons is 8.39 K, 6.83 K, and 9.6 K, respectively. Similarly overall average of maximum SUHI intensity of the Ahmedabad study area during summer, monsoon, and winter seasons is 6.26 K, 5.79 K, and 7.69 K, respectively. Overall average of maximum SUHI intensity of the Chandigarh study area during summer, monsoon, and winter seasons is 5.67 K, 4.64 K, and 5.04 K, respectively. Annual average maximum SUHI intensity of the Jaipur, Ahmedabad and Chandigarh study areas for all seasons is 8.5 K, 6.75 K, and 5.17 K, respectively. The average night SUHI intensity for the entire 13 year duration for Jaipur, Ahmedabad and Chandigarh study areas is 2.87 K, 2.64 K, and 1.14 K, respectively. On the other hand corresponding average day SUHI intensity of the Jaipur, Ahmedabad and Chandigarh study areas is -0.99 K, 0.57 K, and 1.53 K, respectively. UHI_{index}, which is a normalized index with values between 0 and 1 corresponding to pixels of minimum and maximum temperature, respectively, has been used to compare the UHI intensity of different periods and different seasons. The average value of UHI_{index}

for the entire study period will indicate the combined UHI effect over different parts of the study area. Maximum of average UHI_{index} of Jaipur city is 0.95 which is very close to 1 and hence indicating that this pixel encounters consistent maximum LSTs. Similarly, the maximum of average UHI_{index} of Ahmedabad and Chandigarh are 0.92 and 0.89, respectively. Pixels with average value of UHI_{index} more than 0.90 can be considered to indicate that high LST normally occurs on these pixels and they can be considered as hot spots (HS).

A new criterion for classifying the growth of SUHI effect based on UHI_{index} and transect analysis has been proposed in this study. Methods such as UHI_{index} growth analysis and transect analysis through HS have been applied to study spatio-temporal changes in SUHI growth over Jaipur, Ahmedabad and Chandigarh cities in India. Analysis of 8-day night-time LST data shows that significant SUHI growth exists over the study area. Increase in area enclosed by different isothermal lines, vary from 20% to above 400% during different seasons between 2003 and 2015 which indicates that there is a continuous increase in LSTs of all the three cities. The temperature gradient between HS and area adjacent to it is falling i.e. more and more area is noticing temperatures close to the temperature of HS and there is consequent growth in the UHI effect.

In-situ temperature monitoring has been conducted at 7 points spread within the study area (3 inside the urban boundary and 4 outside the urban boundary but inside study area boundary) of Jaipur city, in order to study the thermal pattern of various surfaces at these locations as well as to compare the SUHI and AUHI effects. AUHI and SUHI intensity has been calculated at the time of satellite pass (10.30 AM and 10.30 PM). Positive AUHI intensity has been observed at most of the locations irrespective of time periods. Negative SUHI intensity has been observed at most of the locations during day period, whereas positive SUHI intensity has been observed during night. Direct relationship has been observed between AUHI and SUHI during night, whereas inverse relationship has been observed between AUHI and SUHI during day. i.e. AUHI has been observed during both day and night period.

Contrast diurnal LST variations have been observed during different time intervals by analyzing Aqua and Terra LST data. Regression analysis of all the images (two day-time and two night-time) has been carried out for Jaipur and Ahmedabad cities. Good correlation, with R^2 value as high as 0.90, is observed between night images (Aqua night

and Terra night). The corresponding R^2 values for day images of the two satellites are comparatively lower (ranges from 0 to 0.82), whereas the coefficient of correlation is very low for day and night images (ranges from 0 to 0.59). In order to understand these varying relationships, images corresponding to Ludhiana city have been used. This city shows nearly similar SUHI effects during both the day and night times. The vegetation density in and around Ludhiana city is higher compared to Ahmedabad and Jaipur areas. The analysis indicates that night time images can be used for the analysis of SUHI effect over any area. The use of day time images for this analysis depends on the surface cover and may show a false temporary effect which may not be similar to AUHI. Time of observation is very important for analyzing the efficacy of remote sensing data for surface temperature variations for different land covers and SUHI studies. UHI varies during the day, and it is more significant during the evening/night. Diurnal LST relationship with various land surface parameters like vegetation, built-up, soil, water, etc. has also been investigated in the present research. Various land surfaces play a significant role in the diurnal variations of LSTs. Diurnal relationship of LST with various parameters representing vegetation, urbanization, soil, water and elevation has been investigated.

In the present study, LST has been predicted by LTS model, using 10 years LST values along with NDVI, %ISA, RD and elevation as input parameters to the model for Ahmedabad, Chandigarh and Jaipur study areas. From the graphs and scatterplots, it can be concluded that good correlation exists between the model predicted and observed LST values, where R^2 values range from 0.84 to 0.97. MAE and MAPE of the model range from 0.23 K to 0.36 K and 0.08 % to 0.12 %, respectively. The LTS model has been compared with ANN model to estimate the skill score factor of the LTS model (Forecasted) with reference to the ANN (Referred) model. The validation statistics have been calculated based on skill scores, taking into consideration a reference prediction using ANN, since there will be inherent autocorrelation in the data. Skill scores calculated for most of the periods show positive values which clearly depicts the efficacy of LTS model compared to ANN model for better LST prediction.

Table of Contents

List of Figures

List of Tables

Abbreviations

%ISA	:	Percent Impervious Surface Area
AHI	:	Atmospheric Heat Island
ANFIS	:	Adaptive Neuro Fuzzy Inference Systems
ANN	:	Artificial Neural Network
ASTER	:	Advanced Spaceborne Thermal Emission and Reflection Radiometer
AUHI	:	Atmospheric Urban Heat Island
AVHRR	:	Advanced Very High Resolution Radiometer
BLUHI	:	Boundary Layer Urban Heat Island
BRDF	:	Bidirectional Reflectance Distribution Function
CBD	:	Central Business District
CHS	:	Centroid of Hot Spots
CLUHI	:	Canopy Layer Urban Heat Island
CS	:	Cold Spots
DEM	:	Digital Elevation Model
DHS	:	Distance from Hot Spots
DL	:	Developed Land
DOWV	:	Day Of the Week Variation
DVI	:	Difference Vegetation Index
EROS	:	Earth Resources Observation and Science
ETM+	:	Enhanced Thematic Mapper Plus
EVI	:	Enhanced Vegetation Index
FTP	:	File Transfer Protocol
F_v	:	Fractional Vegetation
GDEM	:	Global Digital Elevation Model
GDP	:	Gross Domestic Product
GP	:	Genetic Programming
GIS	:	Geographical Information System
HS	:	Hot Spots
IGBP	:	International Geosphere Biosphere Programme
IMD	:	Indian Meteorological Department
IPCC	:	Intergovernmental Panel on Climate Change
LC	:	Land Cover

LPDAAC	:	Land Processes Distributed Active Archive Center
LSMA	:	Linear Spectral Mixture Analysis
LST	:	Land Surface Temperature
LTS	:	Linear Time Series
LU	:	Land Use
LU-LC	:	Land Use/ Land Cover
MAE	:	Mean Absolute Error
MAPE	:	Mean Absolute Percentage Error
MIR	:	Mid Infrared
MLR	:	Multivariate Linear Regression
MNDWI	:	Modified Normalized Difference Water Index
MNF	:	Maximum Noise Fraction
MNIT	:	Malaviya National Institute of Technology
MODIS	:	Moderate Resolution Imaging Spectroradiometer
MRT	:	MODIS Re-projection Tools
MSE	:	Mean Squared Error
MVI	:	Microwave Vegetation Indices
NASA	:	National Aeronautics and Space Administration
NDBI	:	Normalized Difference Built-up Index
NDVI	:	Normalized Difference Vegetation Index
NDISI	:	Normalized Difference Impervious Surface Index
NDBaI	:	Normalized Difference Bareness Index
NDWI	:	Normalized Difference Water Index
NIR	:	Near Infrared
OLI	:	Operational Land Imager
PLS	:	Partial Least Squares
PCA	:	Principle Component Analysis
PCR	:	Principal Component Regression
PHS	:	Prospective Hot Spots
QA	:	Quality Assurance
RD	:	Road Density
RMSE	:	Root Mean Square Error
RZ	:	Rural Zone
SDL	:	Semi Developed Land

SDS	:	Science Data Sets
SE	:	Surface Emissivity
SEB	:	Surface Energy Balance
SNR	:	Signal-to-Noise Ratios
SST	:	Sea Surface Temperature
SUCI	:	Surface Urban Cool Island
SUHI	:	Surface Urban Heat Island
SUHS	:	Surface Urban Heat Sink
SVM	:	Support Vector Machines
SWIR	:	Short Wave Infrared
TIR	:	Thermal Infrared
TM	:	Thematic Mapper
TOA	:	Top of the Atmosphere
UCI	:	Urban Cool Island
UCII	:	Urban Cool Island Intensity
UL	:	Undeveloped Land
UTM	:	Universal Transverse Mercator
UHI	:	Urban Heat Island
UHII	:	Urban Heat Island Intensity
UR_{UHI}	:	Urban-Rural UHI intensity
UZ	:	Urban Zone
VI	:	Vegetation Index
VNIR	:	Visible Near Infrared
WGS	:	World Geodetic System
WIST	:	Warehouse Inventory Search Tool

Chapter 1

Introduction

Many cities of the world are experiencing drastic variations in the thermal environment which is affecting the thermal comfort levels. Urbanization has been considered as one of the primary reasons for the increase in temperatures at local scale. This increase in temperature has resulted in a variety of environmental issues not only at local levels but also at regional and global scales. Urbanization has led to the conversion of natural land covers into impervious built-up surfaces. The replacement of natural land covers into urban land causes variations in the energy balance of the urban climate. Heat storage capacity of urban regions increases due to the effect of built-up and anthropogenic materials resulting in the development of urban heat island (UHI) phenomenon where city areas are hotter than neighbouring rural and semi-urban areas, particularly at night (Voogt and Oke, 2003). This local difference in temperature between city and its surroundings creates an adverse impact on inhabitants and environment and hampers air quality by elevated emissions of air pollutants and greenhouse gases, increases energy consumption, loses biological control, impairs water quantity and affects human health and comfort (Konopacki and Akbari, 2002; Pantavou et al., 2011; Santamouris and Kolokotsa, 2015; Sakka et al., 2012; Stathopoulou et al., 2008).

Materials used in urban areas for pavement and roofs, such as concrete, bitumen, and asphalt have different thermal bulk properties and surface radiative properties than the materials present in rural regions which cause a change in the energy balance of the urban area, often leading to higher temperatures than neighbouring rural areas (Oke, 1982). The primary reason for the night-time warming is that unlike suburban and rural areas, urban surfaces absorb energy in the form of short wave radiation during the day which is then slowly released during the night as long wave radiation. Urban street canyon effect results in lower rates of long wave radiation loss during the night and consequent higher temperature of urban surfaces than the rural surfaces. Severe impacts of UHI on humans, animals, climate, and environment have been reported (Kolokotroni et al., 2012; Konopacki and Akbari, 2002; Zhao et al., 2015; Patz et al., 2005). Thus, there is a need to look into the matter as mitigation is the sole thing which can help us out to fight from this deteriorating condition. The United Nations (2013) has reported that an additional two

billion population will live in cities by 2050, so building sustainable cities plays a vital role in accomplishing global sustainability targets. Thus, UHI mitigation strategies should be incorporated into future city design and planning to lessen the inverse effects caused by the UHI effect.

1.1 Types of Urban Heat Island and Their Measurement

UHI refers to the excess warmth of the urban land or atmosphere compared to non-urbanized surroundings. When land surface temperature (LST) is used for analyzing the UHI effect, it is called surface UHI (SUHI). The difference in air temperatures between urban and their surrounding rural areas is expressed as atmospheric urban heat island (AUHI), which may be divided into two categories: canopy layer urban heat island (CLUHI) for urban canopy layer (layer of urban atmosphere extending from surface to mean building height), and boundary layer urban heat island (BLUHI) for urban boundary layer (layer above canopy layer that is influenced by the underlying urban surface) (Voogt and Oke, 2003). Traditionally, CLUHI is measured by recording air temperatures, at standard meteorological height of 1.5 to 2.0 meter, at stationary weather station networks (Landsberg, 1981; Kukla et al., 1986; Karl et al., 1988; Changnon, 1992; Gallo et al., 1993; Gallo et al., 1996). Temperature measurements at isolated weather stations and by vehicle mounted sensors are designated as in-situ measurements which are widely used for the AUHI studies, and have the advantage of a high temporal resolution and a long data record. However, in situ data also have a poor spatial resolution.

The advent of high resolution Earth monitoring satellites has made it possible to study the effects of urbanization on meteorology and climate on continental and global scale. Satellite imageries have become an effective tool for UHI studies as satellite data, in comparison to ground sensors, is more uniform, larger and regular (Hung et al., 2006). The study of SUHI has been largely dependent on remote sensing data and LST has extensively been used for SUHI studies (Zhangyan et al., 2006; Tran et al., 2006; Jusuf et al., 2007; Yuan and Bauer, 2007; Liang and Qihao, 2008; Cheval and Dumitrescu, 2009). LST is the skin temperature of the ground surface (Qin and Karnielli, 1993). LST is determined by the effective radiating temperature of the Earth‘s surface, which controls surface heat and water exchange with the atmosphere (Yuan and Bauer, 2007). Climate studies, climate activities, environmental conditions and management practices of Earth

surfaces and its surrounding atmosphere require LST information on a useful scale (Becker and Li, 1993). High spatial resolution remote sensing thermal data acquired in the daytime have been extensively used to study SUHIs on meso or large scales when UHI intensities are highest (Roth et al., 1989). Many previous studies have validated the fruitful application of satellite thermal infrared (TIR) data with varying spatial and temporal resolutions, including Advanced Very High Resolution Radiometer (AVHRR) (8 km), Moderate Resolution Imaging Spectroradiometer (MODIS) (1 km), HJ-1 B (300 m), Landsat TM (Thematic Mapper) (120 m), Advanced Spaceborne Thermal Emission and Reflection Radiometer (ASTER) (90 m), and Landsat Enhanced Thematic Mapper Plus (ETM+) (60 m), due to their low cost, beneficial spatial coverage, and temporal repetition (Aniello et al., 1995; Chen et al., 2006; Dousset and Gourmelon, 2003; Jusuf et al., 2007; Lo and Quattrochi, 2003; Pongrácz et al., 2010; Yang et al., 2010; Yue et al., 2012; Zhang et al., 2013). Landsat TM/ ETM+ data have been extensively used, among the available remotely sensed satellite data, for numerous UHI studies worldwide (Srivastava et al., 2009; Stathopoulou and Cartalis, 2007; Weng, 2001; Xian and Crane, 2006), due to free open-access for data procurement, long life span, and better spatial coverage for most of the UHI hotspot areas.

1.2 Issues Related with UHI Effect

Studies have shown that the UHI effect results in higher energy and water consumption (Santamouris, 2014; Santamouris et al., 2015; Konopacki and Akbari, 2002; Kolokotroni et al., 2012). A substantial increase in energy requirement for cooling has been identified (Asimakopoulos et al., 2012; Hassid et al., 2000) by the rise in urban surface and air temperatures due to urban climate change like UHI effect (Synnefa and Santamouris, 2012). Greater demand for air conditioning, consequently increases the production of ground-level ozone, which has direct consequences on human health (Akbari et al., 1996; Akbari et al., 2001). The average rise of the cooling demand and average reduction of the heating have been observed to be 23% and 19%, respectively. Overall, average energy consumption for heating and cooling of the buildings has been found to have increased by 11% (Santamouris, 2014). Built-up areas are mainly responsible for the increase in energy consumption and account for about 40% of the annual energy consumption worldwide. New design tools for better energy efficiency are therefore essential (Pisello et al., 2015).

This temperature increase not only impacts the comfort and health of urban dwellers, but also contributes to heat wave disasters. Heat waves have been considered as one of the major risk factors of UHI as they can affect human health resulting in exhaustion, dehydration, circulatory disorders, and potential deaths (Buchin et al., 2016). Heat wave disasters have been reported as the predominant cause of human mortality resulting from natural hazards in post-industrial societies worldwide (Poumadere et al., 2005). Borden and Cutter (2008) have reported that in the US heat/drought ranks the highest for natural hazards mortality (19.6%) among flooding, lightning, severe weather, tornado, wildfire, mass movement, coastal and geophysical hazards. The summer of 2003, the hottest one in Europe since 1500, shocked the world with almost 15,000 deaths in France (Poumadere et al., 2005).

1.3 Motivation of the Study

The world is facing a continuous increase in global temperature, which is mainly due to the rapid urbanization. Urbanization has been contemplated as one of the major global problems with changes in emergent properties of different land surface materials. One such emergent property is the temperature difference between urban and rural surfaces that affects health; energy budget; local and regional planning; and climate (Clinton and Gong, 2013). Urbanization is resulting in a lot of environmental problems like global warming, air pollution, and environmental degradation which adversely affect the quality and comfort of urban living and the urban population (Ash et al., 2008). Urbanization is one of the most obvious aspects of human impacts on the Earth, resulting in greenhouse gas emissions and land use/ land cover (LU-LC) changes, both of which, in turn, affect daily mean surface and air temperatures (Gallo and Owen, 1999; Owen, 1998; Kikon et al., 2016). Major anthropogenic alterations on Earth's environment result in UHI effect where urban areas show higher air and surface temperatures compared to the countryside, and geospatial pattern of UHI remains poorly understood over large areas (Zhou et al., 2014). Significant variations have been reported in the day to day temperature variations between urban and rural areas (Tam et al., 2015).

Studies regarding UHI have become authoritative due to its consequence on energy demand, thermal comfort, human health and environmental or climatic conditions related to pollution dispersion (Crutzen, 2004; Harlan et al., 2006). Hence, many researchers

around the world have intensively studied the UHI effect of various cities in the last 30 years. Study of UHI is of high significance as many environmental, economic and social considerations are associated with it which directly affect the comfort and health of the residents of a city. **Hence future research should be more concentrated on better understanding of the heat island effect and design and planning of various parameters capable for mitigating the effects of UHI and ultimately enabling condition for living in a better environment.**

When the entire world is facing the impacts of climate change, UHI studies are important in creating substantial knowledge about the UHI phenomenon and its spatial growth which might be further used in developing strategies for mitigating its effects on the global climate. Therefore, the magnitude and pattern of UHI effect have been one of the major concerns of many urban climatological studies (Cheval and Dumitrescu, 2009; Streutker, 2002; Tiangco et al., 2008; Hung et al., 2006). Yamashita et al. (1986) have reported that city size affects UHI intensity and the UHI intensity increases with increase in the size of the city. Besides the size of a city, main factors affecting UHI are, urban canyon; built-up density; building and road geometry; road density; thermal and optical characteristics of urban materials; canyon geometry; urban structures; anthropogenic heat produced due to human activities; coverage of vegetation and water features in the city; evapotranspiration in the cities (Kovats and Hajat, 2008; Imhoff et al., 2010; Kolokotroni and Giridharan, 2008; Santamouris et al., 2001; Rizwan et al., 2008). UHI effect is also affected by differences in land cover (LC) mainly due to the variation in the composition of different land features at urban and rural locations. Understanding spatial SUHI growth impacts on human comfort and health are crucial for making rational and scientifically sound decisions in urban planning applications. So it may be possible to overcome obstacles and better manage the UHI effects. There is a dearth of research that have used remote sensing images to conduct long-term, multi-temporal studies on the impacts of SUHI growth on spatial variations of thermal behaviors during different seasons. **Hence, a better understanding of the heat island effect and its spatiotemporal growth is required for more efficient city planning.**

Limited reference of UHI effect of cities of hot-semi arid climate is available and limited research on UHI of cities of developing nations like India has been reported in the literature. **Thus, it is critical to understand and improve the knowledge about the**

UHI phenomenon in developing cities so as to upgrade energy efficiency in the urban building standards and accomplish higher quality of life standards. A better understanding of diurnal variations of the heat island effect and its relationship with the urban landscape parameters is required, for more effective city planning. Cool islands have been observed in many cities and are attributed to the strong influence of specific and diverse climatic parameters occurring for each city. The primary reason for surface urban cool island (SUCI) effect over semi-arid Indian cities has to be investigated to analyze the contrast diurnal SUHI variations. Existence of diurnal UHI effect has been reported in literature with significant variations in UHI intensity during the diurnal cycle. **Contrast diurnal SUHI pattern has been observed in semi-arid cities of India which contradicts the findings of previous studies. Hence it is felt important to study the diurnal UHI effect of semi-arid cities of India as well as to further investigate the reasons of contrast diurnal thermal behaviour.**

Variations in the LST (LST dynamics) and its relationship with various land surface parameters like vegetation, urbanization, etc. have also been discussed in many studies. Understanding of relationships coupled with spatial SUHI growth impacts on human comfort and health are crucial for making rational and scientifically sound decisions in urban planning applications. India has witnessed unprecedented development in recent past and due to that many of Indian cities have developed at a rapid pace. The projected growth rate of Indian cities is much higher than the corresponding rate of other big metropolitan cities of the World. The high growth rate will cause a lot of burden on the city infrastructure and large scale development will be required for the increased population. A better understanding of the heat island effect and its relationship with the urban landscape parameters is required, for more effective city planning. The UHI effect is a common worldwide phenomenon irrespective of size and location. Numerous studies have been done to understand this effect and the factors responsible. A large percentage of the studies have been mostly carried out for cities of developed nations, mainly falling in cold climate. Also, previous studies have fundamentally been based on studying either the night time or daytime effect with no emphasis on its diurnal existence. The present study documents this gap in previous studies by comparing the diurnal SUHI effect. The influence of various land surfaces on contrast diurnal and spatial variations of LSTs has also been investigated in the research.

In most of the studies on UHI, effect of single parameter on LST is studied for single time frame and then the comparison of various parameters is done. However, no study is available which considers the simultaneous effect of various parameters on diurnal LST variations. Similarly, limited models are available for predicting the temperature at a particular location corresponding to the values of other parameters. It is very necessary to develop a model incorporating all the parameters affecting UHI. This will serve as a tool for the city planners to help them in preparing the master plan of a city on scientific lines. If the master plan of a city is prepared after considering the effect of various parameters in such a fashion that it can help to contain the UHI effect to a predetermined extent, both the UHI effect and its consequent effect on environment can be reduced.

It may be important to investigate the significance of time of observation for SUHI studies while using satellite data as time of the satellite observation may play an important role. The proposed research is a step towards increasing the understanding of diurnal LST variations over Indian cities for SUHI assessment and also investigating the role of time of observation of remote sensing data as well as thermal profile of various land surfaces for SUHI analysis.

1.4 Objectives of the Present Study

It seems that there is an urgent need to conduct comprehensive research to study the characteristics of UHI effect of Indian cities. Looking into these aspects, the objectives of the proposed research work have been framed as under

1. To study the spatial and temporal variations in the UHI effect over three Indian cities of Ahmedabad, Chandigarh and Jaipur cities in India.
2. To carry out spatio-temporal SUHI growth analysis of the three cities using UHI_{index} and Transect methods.
3. To study the diurnal thermal behavior of various land surface materials viz-a-viz air temperature, by in-situ temperature monitoring, for comparing diurnal SUHI and AUHI effects.
4. To analyze the efficacy of remote sensing data of different times during the day/night for SUHI studies, in order to understand the importance of time of observation.

5. To explore the diurnal relationship of LST with various parameters representing vegetation, urbanization, soil, water and elevation.
6. To use the relationship of LST with different parameters to develop a model to predict the LST at any location for the assessment of SUHI effect.

1.5 Organization of the Thesis

The chapter wise organization of the thesis is as follows;

Chapter 1 contains the Introduction. It describes various types of UHI and their monitoring methods. It also discusses about LST and issues associated with UHI effect which is followed by motivation of the candidate for this research and the objectives of the study.

Chapter II presents a comprehensive review of relevant literature. It brings out the gaps in the existing knowledge and outlines the requirement of the present research.

Chapter III describes the details and features of the data used in the research. It also gives insight to the methodology adopted for procuring data, its pre-processing and methodology adopted for studying the relationship of various parameters along with the methodology for data analysis and interpretation.

Chapter IV presents results and discussion and is broadly divided into *six* sections. The *first* section describes the diurnal patterns of LST, hot spots (HS) dynamics and SUHI Intensity variations over the study areas. Spatio-temporal SUHI growth analysis using UHI_{index} and transect methods have been explained in the *second* section. *Third* section explains the efficacy of satellite data for SUHI studies by analysing aqua-terra MODIS LST relationship. *Fourth* section describes the diurnal thermal behaviour of various land surfaces from in-situ temperature measurements. The diurnal relationship of LST with different parameters has been given in the *fifth* section, while the *sixth* section contains the descriptions and details of LTS based model.

Chapter V outlines the conclusions of the research findings, including the contribution of the candidate in the present research. It also discusses the scope for future research in the area.

Chapter 2

Literature Review

Urbanization has modified various aspects of human living conditions (Rizwan et al., 2008) and created drastic environmental issues like global warming, air pollution, environmental deterioration, etc. which negatively influence the quality and comfort of urban living (Qiao et al., 2013). Urbanization is a process of altering natural land surface materials with manmade features. The anthropogenic changes of natural surfaces significantly alter the energy balance in cities and affect the urban thermal environment (Hart and Sailor, 2009). Under foreseen climate change scenarios global mean temperatures are projected to increase by about 1.4–5.8 ◦C by the end of 21st century (Intergovernmental panel on climate change (IPCC), 2007). Heat stress in urban areas is projected to worsen in the future due to the adverse effect of growing urbanization and global warming on human health (Johnson et al., 2012; Kovats and Hajat, 2008). Urban surfaces generally have higher solar radiation absorption and a better thermal capacity and conductivity as they are comprised of built-up areas like buildings, pavements and other impervious surfaces. Heat is stored by urban covers during the day and released during night. This thermal behaviour, in conjunction with waste heat released from urban houses, transportation and industry, contributes to the development of UHI effect - an excess warmth of the urban land surfaces and atmosphere than the neighbouring rural areas. Long-term temperature records have shown that the impact of urbanization on thermal environment is not only limited to big cities, but also have been noticed in many cities with human population less than 10,000 (Karl et al., 1988). UHI is a global phenomenon, which causes many environmental and social consequences (Li et al., 2013).

Contrast in surface energy balance (SEB) in urban and rural areas as a consequence of the thermal imbalance in the amount of heat energy stored during the day is the major cause of the formation of UHI (Oke, 1982). Urbanization leads to the replacement of Earth's natural vegetation cover of reasonably uniform surface roughness and evapotranspiration properties with urban fabrics (such as asphalts, concretes, bricks and metals) characterized with high thermal properties (Rosenfeld et al., 1998; Taha, 1997; Yang, 2013; Landsberg, 1981). The surface modifications caused by canyon like geometry and

altered thermal properties of natural vegetation enable built-up areas to store more radiated heat during the day than rural areas. After sunset, urban and rural temperatures begin to diverge thereby generating the heat island in the canopy-layer of the built-up areas. As a result of the open exposure and unobstructed clear sky view factor of rural areas, cooling starts quickly after sunset, unlike built-up areas with slow cooling rate due to reduced sky view factor and re-radiation of the stored heat energy during the day (Offerle et al., 2005; Taha, 1997). The heat island stays in the canopy-layer overnight, until sunrise when daily solar radiation cycle begins and rural areas start warming up (Giannaros et al., 2013).

2.1 Remotely Sensed Surface Temperature

The conversion of rural land uses to urban land uses consequences substantial climate changes in urban areas, and LST change has been a key parameter of urban climate research (Voogt and Oke, 2003). LST is described as the skin temperature of the surface which refers to soil surface temperature for bare soil, canopy surface temperature of vegetation for densely vegetated ground. For sparsely vegetated ground, LST is determined by the temperature of the vegetation canopy, vegetation body and soil surface (Qin and Karnieli, 1999). Since Rao (1972) demonstrated the application of satellite images in retrieving the thermal footprints of urban areas, satellite data have been used to study LST and the UHI, with many studies using data from AVHRR (Gallo and Owen, 1998; Streutker, 2002), TM, ETM+ (Weng, 2001; Nichol and Wong, 2005), and MODIS sensors (Anniballe et al., 2014; Khandelwal et al., 2017; Qiao et al., 2013). The satellite thermal data can provide better spatial coverage and more information about the urban canopy layer or surface heat island effect (Hung et al., 2006).

LST is generally defined as the skin temperature of the surface which refers to soil surface temperature for bare soil and canopy surface temperature of vegetation for densely vegetated ground. For sparsely vegetated ground, LST is determined on the basis of temperature of the vegetation canopy, vegetation body and soil surface (Qin and Karnieli, 1999). LST is a key parameter for examining SUHI effect (Oke, 1982; Streutker, 2003; Weng et al., 2004), and assessing heat-related risks and vulnerability in cities (Harlan et al., 2006; Lafortezza et al., 2009; Buscail et al., 2012). LST is determined by the effective radiating temperature of the Earth‘s surface, which controls

surface heat and water exchange with the atmosphere (Yuan and Bauer, 2007). Solar radiation, open space, vegetation cover, building rooftops, and water bodies strongly influence LST (Chun and Guldmann, 2014). Satellite TIR sensors measure top of the atmosphere (TOA) radiances, from which brightness temperatures can be determined using Planck's law. The brightness temperature is converted into LST using ground surface emissivity. Brightness temperatures differ from actual LST ranging from 1 K to 5 K, due to several atmospheric effects like partial water vapor absorption, variable ground surface emissivity, subpixel variation of LST, urban geometry and non-vertical satellite viewing angle (Dousset and Gourmelon, 2003). Therefore, atmospheric effects and then, spectral emissivity values should be considered in estimating actual LST.

Three methods have been employed to compute LST from space. The single infrared channel method uses surface emissivity (SE) and an accurate radiative transfer model and atmospheric profiles, which are given by either satellite soundings or conventional radiosonde data (Schmugge et al., 1998). The split window method makes atmospheric correction and correction for the SE effects with SE as an input based on the differential absorption in a split window (Wan and Dozier, 1996). New day–night MODIS LST method requires day–night pairs of TIR data in seven MODIS bands for simultaneously retrieving LST and band-averaged surface emissivities without knowing atmospheric temperature and water vapour profiles to high accuracy (Wan and Li, 1997). Further, the 3D roughness of urban surfaces, which is scale-dependent on satellite images, is to be taken into consideration for creating more regionally representative urban temperature estimates (Voogt and Oke, 2003).

2.2 UHI Phenomenon: Causes and Effects

UHI primarily depends on the alteration of energy balance in urban areas which is due to numerous factors like urban canyons and geometry (Landsberg, 1981), thermal properties of the different building materials (Montavez et al., 2000), replacement of vegetation cover with impervious surfaces that restrict evapotranspiration (Imhoff et al., 2010; Takebayashi and Masakazu, 2007), and reduction in urban albedo (Akbari and Konopacki, 2005).

Anthropogenic heat strongly contributes to the formation of the UHI effect (Hirano and Fujita, 2012). Major sources of anthropogenic heat include buildings, industrial

processes, air conditioners and vehicles (Rizwan et al., 2008). Building fabric materials absorb solar and infrared radiation during day time as shortwave radiation. The stored heat is released by convection to the atmosphere and by longwave radiation to other surfaces or to the sky with subsequent rise in ambient temperature (Santamouris et al., 2011).

In general, the primary mechanisms contributing to the UHI phenomenon are building, canyon and road geometry, thermal and optical characteristics of different materials used in urban spar, anthropogenic heat and lack of evaporation in the cities, air pollution and aerosols (Kolokotroni and Giridharan, 2008; Santamouris et al., 2001; Rizwan et al., 2008; Vardoulakis et al., 2013). Development associated with urbanization and temperature rise causes increase in energy demand. The rising energy demand can be met with increase in energy production which will also result in increase in the emission of greenhouse gases.

The present population growth projections indicate that by 2050, out of estimated world population of about 9.1 billion, nearly 70% of population, i.e. about 6.3 billion people will reside in urban areas (United Nations, 2014). Therefore, substantial population growth and urban sprawl will continue in the foreseeable future, and thus, the spatial extent and the magnitude of UHI effects will also continue growing (Zhang et al., 2013). Mirzaei and Haghighat (2010) have reported that diseases caused as an effect of UHI, result in a large number of deaths annually. Human health is harmfully affected by heat stress in urban areas, and the health of urban atmosphere may worsen in the future due to rapid urbanization resulting from urban sprawl and fast development of cities and global warming (Rotem-Mindali et al., 2015: Johnson et al., 2012; Kovats and Hajat, 2008).

The major adverse effects of UHI includes the deterioration of living environment, increase in energy consumption (Konopacki and Akbari, 2002), elevation in ground-level ozone (Rosenfeld et al., 1998), alterations in local and regional atmospheric circulations (Feng et al., 2012; Marrapu, 2012; Miao et al., 2009) and even an increase in mortality rates and heat related discomforts (Changnon et al., 1996; Enete et al, 2012; Ihara et al., 2011; Md Din et al., 2014; Uejio et al., 2011; Frumkin, 2002; Gong et al., 2012) destroy habitat (Kareiva and Wennergren, 1995). UHI can generate profound impacts on socioeconomics, human life, and the environment such as increased energy consumption

for cooling (Kolokotroni et al., 2012), compromised human health and comfort (Patz et al., 2005), and degraded water and air quality (EPA, 2003; Sarrat et al., 2006; Rosenfeld et al., 1998). The worsening of physical well-being of a city's population (Fujibe, 2011), damage of thermoregulatory system caused by heat stress in the form of heat syncope, cardiovascular stress, thermal exhaustion, heat stroke and cardiorespiratory diseases (Kleerekoper et al., 2012; Rydin et al., 2012) are the adversarial effects on residents of a city. Elevated air temperature has an inverse effect on the micro-climates within cities compared to rural areas (Erell et al., 2011; Hathway and Sharples, 2012; Wilby, 2003), by formation of ground level ozone (Kleerekoper et al., 2012), modification of local micro and macro climates i.e. wind patterns, humidity changes, storms, floods, and change in local ecosystems (Lee, 1991; Sailor and Fan, 2002) and exacerbation of global warming by increased energy consumption for air conditioning and increased heat emissions released into the local environment (Kolokotroni et al., 2012). Each of these effects concerning to climate bears a secondary implication and in most cases a resonating drift on other effects directly involving the city's inhabitants.

2.3 SUHI Studies: Present State of the Art and Gaps in Existing Literature

Urbanization is one of the most important human activities, creating enormous impacts on the ecosystem at the local, regional and global scales (Turner et al., 1990). It involves transformation of natural land surfaces into anthropogenic impervious surfaces due to the introduction of low and high albedo materials which may lead to dramatic climate changes. Surface and atmospheric modifications due to urbanization generally lead to a modified thermal climate that is warmer than the surrounding rural areas, particularly at night. This phenomenon is known as UHI (Voogt and Oke, 2003) and when LST is used for analysing the UHI effect, it is called SUHI. The main cause of SUHI is modification of the land surfaces through urban development with the use of materials that effectively retain heat. On the other hand, urbanization negatively affects the environment due to pollution thus modifying the physical and chemical properties of the atmosphere, and the soil surface (Kaya et al., 2012). Building materials such as bitumen, asphalt, brick, rock, concrete etc. absorb and store solar radiations during the daytime and release it gradually at nighttime. Hence, SUHI intensity is observed to be stronger at night as compared to day time (Abutaleb et al., 2015). Urban geometry is also one of the main factors causing

UHI effect. Urban canyons are normally represented by narrow streets and wind speed is reduced by tall buildings which cause heat storage by increase in reflective surfaces (Abutaleb et al., 2015). It has been suggested that simple methods have to be implemented to calculate the UHI intensity within urban areas, as a function of time, climatic conditions and structural attributes (Arnfield, 2003).

Rapid urbanization and industrialization are the most effective reasons of the rise of regional temperature than global warming in the recent half century (Chung et al., 2004). The magnitude and extent of the UHI mainly depend on the size, geometry, and population of a city (Oke, 1981). As East Asian cities continue to grow rapidly in both population and physical infrastructure, the UHI phenomenon is much more evident in those cities (Hulme et al., 1994; Hung et al., 2006). Ichinose et al. (1999) have observed that urbanization over the past 135 years has produced a warm bias of 2.8 ◦C as the lowest air temperature in the climate record of Tokyo. Chung et al. (2004) have reported the minimum temperature warming up to 0.7 ◦C for 1971 to 2000 compared with 1951 to 1980 in Seoul. Boonjawat et al. (2000) have noticed a rise of 1.23 ◦C as the lowest air temperature in the urban heating of Bangkok over the last 50 years. Zhou et al. (2004) have reported that, accompanied with rapid urbanization in southeast China, the surface temperature has been increasing by 0.05 ◦C/decade since 1978. Lokoshchenko (2014) has studied the UHI intensity of Moscow from long term temperature records and has observed a mean UHI intensity of 1.0–1.2 K at the end of the 19th century, 1.2–1.4 K during first two decades of the 20th century and 1.6–1.8 K during both the middle and at the end of the 20th century.

The magnitude of UHI can be expressed in terms of UHI intensity (UHII) which is the difference between urban and rural temperatures (Clinton and Gong, 2013). When the difference is positive (urban hotter than rural), there is a SUHI; when the difference is negative, an urban heat sink (SUHS) has been observed. SUHI and SUHS are temporally variable both diurnally and seasonally (Clinton and Gong, 2013). Numerous UHI studies have been carried out over the past few years to understand the change in temperatures using both remotely sensed thermal data (Chen et al., 2012; Friedl, 2002; Seguin and Itier, 1983) and ground measurements data (Dash et al., 2002; Golden and Kaloush, 2006; Snyder et al., 1998). UHII is the most important parameter of climatic alteration of a city in environmental science (Stewart and Oke, 2012). In most cases, air-temperature based

UHII is calculated from weather station data referred as atmospheric UHII (AUHII), whereas LST based UHII is estimated from satellite imagery refereed as surface UHII (SUHII) (Memon et al., 2009). It is usually noticed that the maximum UHI intensity is best developed during the warm period of the year (Oke, 1973; Mihalakakou et al., 2004) especially during calm and clear nights (Arnfield, 2003; Ripley et al., 1996). This is attributed to the greater cooling rates in the rural areas compared to the urban zones that quicken the temperature reduction in the rural zones, and upsurge the temperature difference between the city and its environment (Oke, 1982). Theoretical and experimental research conducted mainly in North American cities has reported that the maximum UHI intensity happens 3–5 hours after sunset (Oke, 1987). Though, many recent field studies have found that the extreme UHI intensity may occur at different times of the day, before and after sunset or midnight or even during the daytime, and this is primarily explained by the thermal balance in the specific urban and rural regions (Skoulika et al., 2014; Livada et al., 2002).

Giannaros et al. (2013) have investigated that the city of Athens exhibits higher air temperatures than its surroundings during the night (>4 ^{o}C), whereas the temperature contrast is less evident in the early morning and mid-day hours. The simulations, in agreement with concurrent observations, showed that the intensity of the canopy-layer heat island had a typical diurnal cycle, characterized by high night time values, an abrupt decrease following sunrise, and an increase following sunset. Tan and Li (2015) have observed that daytime UHI intensity is higher than the night time UHI intensity, especially for big cities. For cities with an area >100 km^2, the mean daytime UHI intensity (2.90 K) has been observed to be higher than the night time UHI intensity (2.30 K). On the basis of analysis of a large number of clusters, it has been concluded that daytime UHI intensity is more significant than night time UHI intensity for clusters with an area >2 km^2. Satellite-derived LST data for pixels corresponding to ground stations measuring T_{air}, showed that LST can be up to 5 K lower than the respective T_{air} during night time, while it can be up to 15 K higher during the rest of the day (Kourtidis et al., 2015).

Hung et al. (2006) have investigated the UHI effects in eight Asian mega cities and have found out seasonal variations in the maximum intensity of UHI of Tokyo which is minimum at 3 ^{o}C around January-February and maximum at 13 ^{o}C around July-August.

Similar observations have also been made at other cities of temperate and tropical climates However, Karl et al. (1988) have suggested that urbanization within the United States exerts its greatest impact on minimum (compared to maximum or mean) temperature (which is mainly a nocturnal phenomenon) and have found that the UHI effect is most significant during the night. All these observations indicate that not only the UHI intensity is highly variable, but any generalization about its behavior may not be universally applicable.

UHI indicates a major local climatic phenomenon, increasing the temperature of urban areas significantly. The increase in temperatures in urban areas is causing increase in air conditioning demands, raised pollution levels and is modifying precipitation patterns. Therefore, the magnitude and pattern of UHI effect have been one of the major concerns of many urban climatological studies. This has important energy, environmental, economic and social consequences while it deteriorates the comfort and health of the residents of a city and subsequently the quality of life of the inhabitants. Existing knowledge on UHI is quite rich but is overshadowed by various discrepancies as related to the performed experimental and theoretical analysis. Thus there is a need for an objective experimental and communication etiquette to be followed in forthcoming UHI studies. Comprehensive and precise knowledge of the magnitude and the characteristics of UHI is a prerequisite for a proper and complete scientific planning of urban mitigation and adaptation technologies.

2.3.1 UHI Growth Studies

The spatial extent of UHI has been related to total urban population, and the magnitude of the UHI has been shown to be more closely related to urban population density than the overall population (Streutker, 2003). The temperature of a surface is affected by vegetation due to both the cooling effect as well as the shadow effect. However, in urban areas, both the vegetation cover and density are low and built-up density is maximum at the central business district (CBD) of the city. The large built-up areas and low levels of vegetation are the main reason of higher temperature at and around the CBD. Built-up areas are usually well defined in the temperature images and form hot spots (HS). Similarly, cold spots (CS) are characterized by open and vegetated areas and can be

regarded as cool islands (Tiangco et al., 2008).

Karl et al. (1988) have reported a warm bias of 0.06 K in the annual average temperature from weather record of the USA and rapid urbanization occurred throughout the last century has been attributed as the main reason. They have also reported that human population has a significant effect on rise in temperature and regions with human population of about 10,000 are 0.1 K warmer than neighbouring regions having a population less than 2000. In a study on UHIs throughout China an average temperature rise of 0.1 K per decade has been observed (Weng et al., 1990). It has also been observed that UHIs have significant seasonal dependence and it shows considerable variations across the country. Cui et al. (2007) have found that the UHI intensity has increased at a rate of 0.21 K per decade during the period from 1959 to 2005. Zhang et al. (2009) have observed a rate 0.75 K per decade in rise of UHI intensity over Shanghai during the past three decades. IPCC (2007) has reported that there is a substantial increase in the temperature worldwide and the mean global LST has increased by around 0.74 K in the past century. Hung et al. (2006) have observed severe UHI effect in Tokyo with UHI magnitude as high as 12 K. They have also found strong SUHI in the range of 5-8 K in other selected tropical cities in their study. Streutker (2003) has observed that the magnitude of average nighttime SUHI in Houston, Texas has increased by 0.82 ± 0.10 K during 12 years from 1987 to 1999. Inverse correlation has also been observed between UHI magnitude and rural temperatures. It has also been identified that the spatial extent of the UHI is independent of both the magnitude of UHI and rural temperature.

Effat and Hassan (2014) have detected changes in LC and heat islands over Cairo and have found that Cairo city has experienced large growth in the urban areas that reached from 14.9 to 39.3% from 1984 to 2013. The magnitude of the UHI over Cairo ranged from 3.11 ^{o} C to 5.7 ^{o} C. It has been noticed that the UHI intensity and spatial distribution were higher and more dominant in the dense built-up areas of the city. Cheval and Dumitrescu (2009) have investigated the UHI of the city of Bucharest (Romania) and have reported higher thermal variability during daytime (12.5 ^{o}C) than during night time (4.6 ^{o}C). They have also found that the heat island extends between 5 to11 km radius from CBD. It has been observed that the thermal difference between the UHI and the surrounding area is higher and more variable during the daytime, and is strongly related to the LC.

Yamashita et al. (1986) have reported that city size affects UHI intensity and the UHI intensity increases with increase in size of the city. Besides the size of a city, main factors affecting UHI are, urban canyon; built-up density; building and road geometry; road density; thermal and optical characteristics of urban materials; canyon geometry; urban structures; anthropogenic heat produced due to human activities; coverage of vegetation and water features in the city; evapotranspiration in the cities (Kovats and Hajat, 2008; Imhoff et al., 2010; Kolokotroni and Giridharan, 2008; Santamouris et al., 2001; Rizwan et al., 2008). UHI effect is also affected by differences in LC mainly due to the variation in the composition of different land features at urban and rural locations. Thus, the extent of UHI over an area is affected by numerous parameters and UHI extent varies in respect to those parameters as well as the effect usually increases over a period of time. **It is necessary to estimate the extent of spatio-temporal SUHI growth over a city. New criterions based on UHI_{index} and transects analysis have been introduced in the present study to analyze the spatio-temporal areal SUHI growth over three cities for better understanding of the heat island effect and its spatio-temporal growth.** One of the objectives of the current research is to analyze the spatial and seasonal patterns of UHI effect over three Indian cities. Further, the study aims at examining the location of HS within the study area as well as the increase in area under UHI has also been investigated. Main focus of the research is to find the increase in area, over a period of time, for fixed temperature gradient from the LST of HS. This increase in area can be used as a measure to indicate UHI growth of the city. **The study of UHI growth is of high significance as many environmental, economic and social considerations are associated with it which directly affects the comfort and health of the residents of a city. Hence, a better understanding of the heat island effect and its spatiotemporal growth is required for more efficient city planning.**

2.3.2 Diurnal Variations of the UHI

Zhou et al. (2014) have reported the diurnal and seasonal SUHI intensity over 32 major cities in China and showed that the annual average SUHI intensity varied from 0.01 to 1.87 °C during the Moreover, the SUHII differed significantly by season, characterized by a higher SUHI intensity in summer season than in winter season during the day, and the opposite during the night for most of the cities. Variations in daytime and night time SUHI intensity for a city strongly depend on the geographic location and research period.

Hu et al. (2013) used remotely sensed LST in studying the SUHI of Texas and Houston from 2001 to 2010. It has been observed that the SUHI values are more notably enhanced in the daytime than night time with an increasing trend with larger composite periods. The temporal aggregation impacts the spatial pattern of the SUHI implying that the higher SUHI regions are more likely to have a larger gap between two composite scales and this is related to the amount and distribution of clouds.

Anniballe et al. (2014) have done the analysis of the surface and air heat island in Milan, Italy and used SUHI and CLUHI maps to monitor the spatial and temporal evolution of surface and air heating. They have pointed out that summer months points out that the SUHI effect is a noticeable phenomenon throughout the whole diurnal cycle and has a stronger intensity in the daytime with peaks around 9–10 K while in the night time, in the absence of solar forcing, it decreases by a factor of 2. In contrast, the canopy layer heat island during the daytime is absent: the CLUHI emerges after sunset with an average intensity around 3–4 K, showing features similar to the night time SUHI.

UHI intensity in the area has significant seasonal variability, and the maximum is always shown during the warm period except in cities of the humid climate. Night time UHI has been observed to be greater than the average daytime UHI especially during the summer months in the coastal and arid cities (Ramamurthy and Sangobanwo, 2016). Klok et al. (2012) have shown that the daytime SUHI intensity of Rotterdam can be as high as 10 ◦C. Differences in the SUHI between the neighbourhoods can be better described by urban surface characteristics. A statistical analysis indicates that the SUHI is largest for neighbourhoods with scarce vegetation that have a high fraction of impervious surface area, and a low albedo. Average surface temperature differences between the warmest and coolest districts are maximum 12 ◦C during day, and 9 ◦C during night. Districts with a large night-time SUHI differ from districts with a large daytime SUHI.

Tan et al. (2010) have reported that the highest UHI intensity observed during the night especially during autumn and winter months in Shanghai, China, while observations during the summer season illustrate that the maximum UHII is more noticeable during the noon and afternoon period. Saito et al. (1990) have observed the daily UHI maximum during the daytime in Kumamoto, Japan due to the very high LST of the materials used in the city, though a second peak UHI is detected during the night period. Similarly, the

UHII is equally presented during the night and day periods in Guwahati, India (Borbora and Das, 2014). Sofer and Potchter, (2006) have observed that the maximum UHI befalls during the afternoon period during the summer season in Eilat Israel from urban temperature measurements. Similarly, measurements carried out during the summer period, have depicted that the highest UHII is noticed during the daytime in Hong Kong, China (Giridharan et al., 2005), while in the tropical city of Muer, Malaysia, the maximum UHI occurs equally during the day, while a second UHI peak is detected during the night (Rajagopalan et al., 2014). In Muscat, Oman the maximum magnitude of UHI has been reported 6–7 hours after sunset (Charabi and Bakhit, 2011), while in Beijing, China the maximum UHII has been detected at the late night period or evening (Miao et al., 2009; Liu et al., 2007), and the weakest during the day period. The maximum UHI intensity has been noted during the late afternoon and the night period in Delhi, India (Mohan et al., 2012), while in Ulan Bator, Mongolia the UHII during the night-time is five times greater than during the day period (Ganbat et al., 2013). **Existence of diurnal UHI effect has been reported in many literatures with significant variations in UHII during the diurnal cycle. It is necessary to estimate the diurnal UHII of semi-arid cities of India as well as to find out the actual reasons behind contrast diurnal thermal behaviour.**

2.3.3 Daytime Urban Cool Islands

The existence of daytime urban cool islands (UCI) has been reported in several urban climatological studies (Runnalls and Oke, 2000; Figuerola and Mazzeo, 1998; Chang et al., 2007; Rasul et al., 2015). Vardoulakis et al. (2013) have observed that UCI has been observed early in the morning in many urban temperature stations and also the relationship between the UHI intensity and local airflow has been investigated using wind speed measurements. High UHI intensities are related with low wind velocity conditions, whereas for wind velocities greater than 7.5 km/h, UHI intensity is minimum (<2 ^{o}C) and even tend to be eliminated. Vegetation, mainly through evapotranspiration and direct shading, can lessen temperatures and form a local cool island within an urban area (Tyrväinen et al., 2005). Rasul et al. (2015) have observed that UCI intensity (UCII) of the Erbil city in Iraqi Kurdistan ranged from 3.5 to 4.6 ^{o}C. Reduced anthropogenic heat flux and shading in dense urban canyons where the incoming solar radiation can't penetrate are also the major reasons of UCI (Erell et al., 2011). Lazzarini et al. (2013)

have observed inversion of UHI in Abu Dhabi city due to the higher amount of vegetation density inside the city compared to suburban/rural areas where bare land and sand is more predominant. Jauregui (1997) has reported that 75% of the total observations for UHII have been recorded during the night period while only 25% have been obvious during day period. Heat is absorbed by urban surfaces during day period and emitted during night time (Carnahan and Larson, 1990; Leroyer et al., 2011; Oleson et al., 2008; Oleson et al., 2010). As a consequence of this behaviour, urban areas with low thermal inertia surroundings can experience both night-time SUHI and daytime SUHS (Clinton and Gong, 2013). In Beijing, UCIs have been noticed during the morning period continuing until noon time (Miao et al., 2009).

Pandey et al. (2012) have reported the formation of daytime UCI over central parts of Delhi, India during low wind conditions in November and December. The daytime LSTs over Delhi are observed to be cooler by about 5–6 °C than the nearby rural areas during these months. During the night time, the central parts of Delhi are noticed to be warmer by 5–6 °C than the neighbouring rural areas. The air-temperature based UHIIs have been higher and positive during the night-period, but lower and negative during the daytime (Hafner and Kidder, 1999; Montavez et al., 2000). On the other hand, most of the LST based UHIIs, observed through satellite data have been positive during both the day and night periods (Hung et al., 2006; Pongracz et al., 2006; Memon et al., 2009). Montavez et al. (2000) have reported that the highest UHIIs occur during the night and the least during the day while Kim and Baik (2002) have noticed that the UHII during the night has been around 3.3 times greater than during the day. **Most of the comprehensive spatio-temporal patterns of higher UHIIs have been noticed during solar off-peak time (i.e., night-time, evening and early morning when solar radiation is not the leading source of heating).** Ramamurthy and Sangobanwo (2016) have investigated hourly and seasonal variations in atmospheric UHI of ten cities in the U.S. and reported that in most of the inland cities have experienced the positive day UHI, in contrast most coastal cities with the exception of Seattle experienced negative UHI during the late afternoon period. Cool islands in Singapore are detected in forested and less developed areas of the city (Chow and Roth, 2006), while the development of UCIs is also reported for the CBD area mainly because of the important shading caused by the tall buildings during the daytime and the proximity to a local river and the sea (Chow and Roth, 2006). **When, the diurnal thermal flows are quite reduced because of the protracted shading in urban canyons,**

reduced anthropogenic heat and the possible cooling effect of sea breeze in coastal zones, the urban temperature may be lower than the rural one and cool islands may appear. Cool islands are observed in many Indian cities and are attributed to the strong influence of specific and diverse climatic parameters occurring for each city. The primary reason for SUCI effect over semi-arid Indian cities has to be investigated to analyze the contrast diurnal SUHI variations.

Frey et al. (2007) have investigated the presence of daytime a distinct surface cool island for Dubai city and cool surface areas at Abu Dhabi city and its neighbouring mangrove regions. The albedo mainly regulates net radiation. The albedo in downtown areas is lower than in their neighbouring desert environments. Consequently, the net radiation is greater in the urban areas. LST behaves opposite to the net radiation and is higher in land use (LU) classes, where water is available. Estoque and Murayama (2017) have investigated the influence of landscape composition on the variability of LST that results in altered thermal patterns in the megacities of Southeast Asia. Average LST of the impervious surface area has been observed to be around 3 K higher than that of green vegetation cover which clearly depicts the effect of impervious surface and the green cover on the formation of UHI and cool island effects, respectively. The spatial pattern of UCIs has been strongly correlated with greenspace patterns; land with greenspace spatial configuration provided an efficient means of enhancing the cooling effects, and the intensity of the cooling effect has been reflected in cool island characteristics (Kong et al., 2014). Urbanization brings substantial changes in the properties of various land surfaces. The replacement of the Earth's natural vegetation and evapotranspiration properties with near-uniform surface roughness and urban fabrics like asphalts, concretes, bricks and metals characterized by high thermal properties cause modification of the SEB of urban areas (Rosenfeld et al., 1998; Taha, 1997; Yang, 2013). The contrast in SEB of urban and rural areas and consequent imbalance of heat energy stored during the day is the primary reason for UHI development (Oke, 1982). Urban parks can mitigate UHI effects and decrease cooling energy consumption during summer season (Cao et al., 2010).

Some of the studies have reported the existence of SUCI effect during day time. Attenuation of net radiation due to the smoke and pollutants has been considered as the major reasons of SUCI effect (Memon et al., 2009; Pandey et al., 2012). Shading of the

area due to tall buildings, i.e. building height, has a significant role in daytime cooling (Oke, 1982; Memon et al., 2009; Nasser et al., 2016). Soil moisture within the urban area has an influence on the thermal environment because evaporation decreases LST via latent cooling (Rasul et al., 2015; Lazzarini et al., 2013). Usage of new reflective surfaces produces greater Landsat cooling than the increase of normalized difference vegetation index (NDVI) (Mackey et al., 2012). Vegetation and Water bodies play a significant role in urban cooling (Sun et al., 2012; Chang et al., 2007; Rizwan et al., 2008; O'Malley et al., 2015; Hathway and Sharples, 2012). Different temperature profiles have been observed in some areas where cool island effect is encountered during daytime and the nighttime behavior is UHI effect. Most of the studies have reported the existence of diurnal SUHI effect, whereas some of the limited studies have reported the existence day SUCI effect over some cities. The reasons behind this contrast diurnal SUHI effect have also been discussed in various literatures discussed above. For semi-arid cities in India, those reasons do not validate the contrast diurnal SUHI variations. **The present study documents this gap in previous studies by comparing the diurnal UHI effect and its relationship with thermal behaviour of various land surfaces like concrete, road, soil, vegetation, etc. and the influence of time of observation on diurnal SUHI variations. Contrast diurnal LST variations during day and night times have been investigated for select cities of India. The thermal dynamics of different types of land surfaces has been investigated.** The time of satellite pass over any area is fixed but this pass is at different time of the day for different cities of a country as well as different cities of different countries. Energy interactions of the Earth's surface with incident solar radiations are different during different time of the day. **It may be important to investigate the significance of time of observation for SUHI studies while using satellite data as time of the satellite observation may play an important role.**

2.3.4 LST Relationship with Various Parameters

Changes in LU-LC, urban sprawling, and population shifts have resulted in large variation in the spatio-temporal patterns of the UHIs due to the elimination of different water features and vegetated surfaces (Zhang et al., 2013). Oke (1981) has identified that areas with high built-up density have the highest temperature which is associated with the thermal properties of the existing structures and the street geometry. Li et al. (2012) have observed that surrounding rural areas show lower LSTs and relative lower variation in

LSTs than urban areas. Also, significant relationships between LST and fractional vegetation (Fv), population density, and road density have been observed. Urban land surfaces strongly influence LST and its spatial heterogeneity within UHI. Remote sensing based urban surface biophysical composition such as vegetation abundance, impervious surface, water bodies and soil fractions have been found to be the best indicators of surface temperature variations across space (Deng and Wu, 2013; Zhang et al., 2009; Guo et al., 2015). Intensive and rapid urbanization is an illustration of human-induced LU-LC change, which has worsened the ongoing impacts on the climate system by changing the thermal pattern (Jin et al., 2005). Variations in LU-LC conditions significantly influence the climatological diurnal temperature range (Gallo et al., 1996).

Urbanization is one of the primary driving factors of LC changes and subsequently increase of LST (Pal and Ziaul, 2016). As an important environmental factor, LST plays a significant role in describing energy exchanges of the Earth's land surface and atmosphere (Quattrochi and Luvall, 1999; Weng et al., 2004). Correlation of LST with various parameters representing surface properties of the ground has been the core of many studies on UHI effect. Linear positive correlation has been observed between LST and percent impervious surface area (%ISA) (Dousset and Gourmelon, 2003; Lazzarini et al., 2012; Yuan and Baur, 2007; Deng and Wu, 2013; Chen et al., 2006; Civco et al., 2002; Zhang et al., 2009). Imhoff et al. (2010) have shown, after analysing 38 of the most populous cities in the continental United States that ISA is the primary driver for increase in temperature explaining 70% of the total variance in LST. Xu et al. (2012) have used normalized difference impervious surface index (NDISI) to investigate the impact on the regional thermal environment and have shown that impervious surface is positively exponentially correlated with LST, while vegetation and water are inversely related to LST. They have also found that contribution of impervious surface to regional LST change can be up to six times higher than the sum of vegetation and water contributions and each decrement of 10% impervious surface cover with additional 10% green or water space could lower LST by up to 2.9 or 2.5 °C, respectively.

The extent of urbanization increases with increase in population density and consequent development takes place which results in increase in %ISA and road density (RD, length of road per unit area). Clear patterns of high temperature area along highways have been found in previous studies on SUHI effects (Tiangoco et al., 2008; Weng et al., 2004;

Yuan and Bauer, 2007). %ISA combined with LST and Normalized Difference Built-up Index (NDBI) can quantitatively explain the spatial distribution and seasonal variation of urban thermal patterns and associated LU-LC conditions (Zhang et al., 2009). Zhang et al. (2009) have indicated that %ISA is an accurate indicator of UHI effects with strong linear relationships between LST and percent ISA, whereas, the relationship between LST and NDVI suffers due to seasonal effect. They also show that variations in surface temperature could be better accounted for by differences in imperviousness than by the commonly used NDVI. NDVI and NDBI are well correlated with the changes of LST whereas normalized difference bareness index (NDBaI) has a weaker correlation with LST (Guo et al., 2015). Zhao and Chen (2005) have used NDBaI to classify the barren lands, according to different values of NDBaI. The NDBaI that represents soil distribution in urban areas, showing a negative relationship with LST (Chen et al., 2006). Positive correlation has been observed between LST and NDBI in many studies (Deng and Wu, 2013; Chen et al., 2006; Pal and Ziaul, 2016; Zhang et al., 2009; Guo et al., 2015; Sun et al., 2012).

Weng et al. (2004) have shown that LST is not only negatively related to NDVI but also to F_v across the entire range of values, which indicates that F_v is an appropriate predictor of LST more than NDVI in forest areas. Furthermore, the landscape composition and the spatial configuration both influence UHIs. Rotem-Mindali et al. (2015) have compared the cooling effect of residential areas with high vegetation cover to that of small to medium size (2-40 ha) public parks. They have suggested that 'greening' areas within the private urban space should be encouraged at the expense of building new small-medium parks in metropolitan areas that lack the sufficient free space for larger parks. Vegetation cover is one of the most readily controllable variables in urban landscapes and is the primary target for intervention strategies to mitigate SUHI effect (Clinton and Gong, 2013; Jonsson, 2004). Previous research shows that vegetated areas show lower surface temperatures than impervious ones (Owen et al., 1998). LST has significant negative correlations with the NDVI (Liang and Weng, 2011; Hung et al., 2006; Mackey et al., 2012; Deng and Wu, 2013; Guo et al., 2015; Gillies et al., 1997; Weng et al., 2004; Gallo et al., 1993; Alshaikh, 2015) as well as Fv (Wu et al, 2014; Li et al., 2012; Weng et al., 2004). Various vegetation indices and fractional vegetation cover have been used to indicate UHI effects (Epperson et al., 1995; Gallo and wu, 1998; Guo et al., 2015; Lo et al., 1997). Skelhorn et al., (2014) have reported that increase in vegetation by 5% could

reduce average LST by 1 ^{o}C and also the replacement of vegetation with asphalt could rise air temperature up to 3.2 ^{o}C. Gallo and Owen (1999) have evaluated seasonal trends in NDVI and temperature and have found that about 40% of the variations in urban-rural temperature difference, i.e. UHI intensity, can be accounted for by the difference in NDVI and LST. The relationship between biophysical composition and LST also varies with seasons and is thought to be nonlinear (Chen et al., 2006; Owen et al., 1998). Based on landscape metrics derived from different LST zones, Liu and Weng (2008) found that the seasonal variations in landscape pattern have been correlated with LST. Previous studies that focused on the correlation between urban thermal behaviour and landscape patterns indicated that LST is strongly subject to both the composition and configuration of land cover/use (Buyantuyev and Wu, 2010; Li et al., 2011; Weng et al., 2007; Zhou et al., 2011; Guo et al., 2015).

Pu et al. (2006) have analyzed the relationship between NDVI and LST for five LU-LC types and have found a strong negative correlation between LST and NDVI for all LU-LC types. They have suggested that moisture availability from vegetation cover allows a large fraction of net radiance flux to be balanced by evapotranspiration and by the latent heat flux, thus reducing the sensible heat flux and hence LST. LC types or indices show positive correlation with LST except for vegetation (Ali et al., 2016). Changes in LC (the biophysical attribute of the Earth‘s surface) and LU (the utilization of land surface for a given human purpose) have been reported to be the main driver of environmental change, while climate change and the climate variability may influence land-use preferences differently in various parts of the world (Brunsell, 2006). Lo et al. (1997) have studied changes in the thermal responses of urban LC types and have found a strong negative correlation between NDVI and irradiance of residential, agricultural, and vacant/transitional LC types, indicating that the irradiance of a LC type is significantly influenced by the amount of vegetation present.

Xu et al., (2013) have investigated the methods of observation statistics and remote sensing retrieval, using remote sensing information including the UHI intensity index, the NDVI, the normalized difference water index (NDWI), and the difference vegetation index (DVI) to analyze the relationship between the UHI effect and the spatial and temporal concentration distributions of atmospheric particulates in Beijing. It has been observed that if UHI intensity is in the weak heat island or green island range (below 0.1),

the DVI value increases and the atmospheric particulate concentration decreases as the UHI intensity index increases. If the UHI intensity is largely in the range of a medium heat island, strong heat island, or extremely strong heat island (greater than 0.1), then increases in the UHI intensity index lead the DVI value to decrease and the atmospheric particulate concentration to increase.

Sun et al. (2012) have observed that the correlations of NDBI, NDBaI with LST have been positive, and the correlations of NDVI, modified normalized difference water index (MNDWI), digital elevation model (DEM) with LST is negative. Sun et al. (2012) have reported the inverse relationship between MNDWI and LST which implied that pure water would reduce the LST and the polluted water would rise the surface temperature. Ogashawara and Bastos (2012) have used a quantitative approach to explore the relationships among temperature, different LC areas and several indices, and have observed that urban areas represented by NDBI are positively correlated with high LSTs. Conversely, areas covered in vegetation represented by NDVI and water represented by NDWI correlated positively with low temperatures. Ibrahim (2017) has used linear regression analysis to produce relationships of LST with NDVI, NDBI, NDBaI and NDWI and reported that NDVI and NDWI correlated negatively with low LSTs while NDBI and NDBaI correlated positively with high LSTs. Chen et al. (2006) have observed that correlations between NDVI, NDWI, NDBaI and LST have been negative when NDVI is limited in range, but positive correlation has been found between NDBI and LST. **It is possible that the utilization of different indices like NDVI, MNDWI, NDBaI and NDBI could represent LC types quantitatively so that the relationships between different indices and LST can be established in UHI studies.**

Variation in LST due to change in elevation of different areas has been observed to be different from environmental lapse rate, and a negative correlation has been observed between LST and elevation. The effect of variations in LSTs due to change in elevation shall also be considered when LST studies are performed over large areas where the land terrain is not flat (Khandelwal et al., 2017; Sun et al., 2012).

A lot of research has been carried out for analyzing the association of LST with various surface and other physical characteristics of urban areas. Most of this research has been carried out for developed countries as well as for cities in cold climates and limited

research is available for cities of hot and arid regions. The reference literature available for Indian conditions is also limited.

In the present times, when the entire globe is reeling under the impacts of climate change, studies of such nature might prove to be helpful in generating substantial knowledge about the UHI phenomenon which might be further used in developing strategies for mitigating its effects on the global climate. Hence, it is very important to explore the diurnal relationship of LST with various parameters representing vegetation, urbanization, soil, water and elevation. The proposed research is a step towards increasing the understanding of the UHI and the factors responsible for it. The study will also help in the quantification of the effect of these factors on UHI effect.

2.3.5 Predictive Models

There are several modeling approaches that have been applied in various studies to estimate different ecological and meteorological parameters, both linear and nonlinear. Among the linear techniques are multivariate linear regression (MLR), partial least squares (PLS) regression, and principal component regression (PCR) and among the nonlinear are artificial neural networks (ANN), genetic programming (GP), support vector machines (SVMs), and adaptive neuro fuzzy inference systems (ANFIS) (Borhani et al., 2016a, 2016b). Application of modeling such as ANN or regression models is one approach to determine the relationship between various environmental variables especially for land surface features. MLR is one of the most widely used statistical methods, which attempts to model the relationship between two or more interpretive variables (independent) and a response variable (dependent) by fitting a linear equation into the observed data. Regression models have been used to simulate future rainfall projections using either linear or nonlinear correlation between local scale surface variables and atmospheric variables (Wilby and Wigley, 1997; Wilby et al., 1999; Dettinger et al., 2004; Feng et al., 2014). Regression analysis comprises many techniques for modeling and analyzing several variables. In previous literatures, the linear regression analysis has frequently been preferred to fit experimental data. In recent years, several studies have been performed for the comparison of both linear and nonlinear regression analysis (Gunay, 2007; Aşıkgil and Erar, 2013).

El-Fouly et al. (2008) have used linear time series (LTS) model for the prediction of wind speed and direction from historic wind data. One year and two year LTS models have been developed using data of one and two years, respectively. The accuracy of the model has been investigated using two sets of data recorded during winter and summer season. Many previous studies have used the application of time series models for the prediction of various factors like rainfall, thermal load, etc. (Bagirov et al., 2017; Saengsawang et al., 2017; Aghdaei et al., 2017).

Gobakis et al. (2011) have studied the applicability of ANN and learning paradigms for UHI intensity prediction in Athens, Greece. Shwetha and Kumar (2015) have used ANN model for the prediction of LST under clear and cloudy conditions using microwave vegetation indices (MVIs), LU-LC, elevation, latitude, longitude and Julian day as input parameters. Lee et al. (2016) have also used neural network model for UHI prediction in Seoul, Korea. Prediction results from the neural network model have been compared with the measured data. It has been observed that the coefficients of correlation of the developed models range from 0.95 to 0.99. Kumar et al. (2013) have developed ANN model for prediction of LST image from LU-LC image.

Mushore et al. (2017) have estimated the impact of urban growth on future micro-climate of Harare, Zimbabwe located in Southern Africa by predicting future distribution of LU-LC, as well as LST using Cellular Automata Markov Chain analysis. Using UI as predictor of LST, it has been predicted that the 18 to 28 ^{o}C class will reduce in coverage between 2015 and 2040, while the 36 to 45 ^{o}C category will increase in proportion covered from 42.5 to 58% of the city. Continued urban sprawl will rise warming and result in high forthcoming temperatures unless mitigation strategies are strengthened.

Chen et al. (2014) have simulated the UHI effect over Hangzhou, East China by a weather research and forecasting model coupled with an urban canopy model. An average temperature rise of 0.74 K in the city center has been observed under high urbanization conditions in the simulation. The UHI peak has been observed to reach the maximum value of 1.6 K around sunset, and the analysis of the surface energy balance has shown that the primary cause of UHI is a large amount of heat storage in the urban fabric during the day period and the release of this heat after the sunset. UHI intensity in the area has significant seasonal variability, and the maximum is always shown during the warm

period except in cities of the humid climate.

Limited models are available for predicting the temperature/UHI intensity at a particular location corresponding to the values of other parameters. Additionally, a number of UHI prediction studies are based on the ANN techniques (Gobakis et al., 2011; Lee et al., 2016; Şahin, 2012). A neural network architecture has been developed to predict the UHI intensity in Athens, Greece, during both day and night (Mihalakakou et al., 2004) using data for a two-year time period. Another study uses input data from meteorological stations as well as historic measured air temperatures within the city to predict the UHI intensity in London based on neural network architecture (Kolokotroni et al., 2010). High rate of development is causing a lot of burden on the city's infrastructure, and large-scale development is required for the increased population. For planned development of a city master plan is prepared in which area for different type of activities are earmarked, but they are decided without taking into account the role of various parameters on UHI. If in addition to various principles of planning, the information available on UHI is also utilized during the process of development, it may enable the city planners to design the physical urban layout in such a manner that it helps to contain UHI associated with the development. Preparing master plan of a city, after considering the effect of various parameters in such a fashion that it can help to contain the UHI effect to a predetermined extent, can result that both the UHI effect and its consequent effects on the environment can be reduced.

Chapter 3

Data & Methodology

The primary objective of the present work is to analyze the intensity and characteristics of spatio-temporal UHI variations over study areas around Jaipur, Ahmedabad and Chandigarh cities in India. Spatio-temporal SUHI growth analysis of the three cities has also been conducted. Large amount of remote sensing data has been used for the study. The data has been downloaded from the United States National Aeronautics and Space Administration (NASA) website through internet. Details of the data, its properties and pre-processing have been documented below.

3.1 Remote Sensing Data Used for the Present Study

Table 3.1 shows the remote sensing data used for the present study.

Table 3.1: Remote Sensing Data used for the Present Work

Remote Sensing Product	Short Name	Sensor	Platform	Temporal Resolution	Spatial Resolution (m)
Land Cover Type	MCD12Q1	MODIS	Combined Aqua & Terra	Yearly	463.3
Various Bands	-	TM/ETM+/OLI	Landsat	16 Day	30 to 120
Land Surface Temperature and Emissivity	MYD11A1/MOD11A1/ MYD11A2	MODIS	Aqua/Terra	1 Day/ 8 Day	926.6
Vegetation Indices	MYD13Q1	MODIS	Aqua	16 Day	231.7
Global Digital Elevation Model (GDEM)	ASTGTM	ASTER	Terra	-	24.8

3.1.1 Landsat Data Products

TM and operational land imager (OLI) sensor data have been used for the present study. TM sensor features seven bands of image data (three in visible wavelengths, four in infrared) all of which have 30 meter spatial resolution. TM is a whisk broom scanner which takes multi-spectral images across its ground track. TM has become a useful tool in the study of albedo and its relationship to global warming and climate change. Landsat 8 carries two instruments: The OLI sensor contains six refined heritage bands, along with three new bands (a shortwave infrared band for cirrus detection, a deep blue band for coastal/aerosol studies and a Quality Assessment band) and TIRS sensor has two thermal

bands. These sensors provide improved signal-to-noise (SNR) radiometric performance quantized over a 12-bit dynamic range. Improved signal to noise performance enables better characterization of land cover state and condition. Products are delivered as 16-bit images (scaled to 55,000 grey levels). For the calculation of various parameters like NDVI, NDBI, NDBaI, MNDWI and %ISA, TM and OLI sensor data have been used in the present study.

3.1.2 MODIS Products

MODIS is a sensor on board Terra and Aqua platforms that provides information about the Earth‘s surface in 36 wavebands covering the visible, NIR, shortwave infrared (SWIR) and thermal ranges. It has a viewing swath width of 2330 km and views the entire surface of the Earth every one to two days. It acquires data at three spatial resolutions of 250 m (first two bands), 500 m (bands 3 to 7), and 1000 m (remaining bands). The MODIS products are available with different level of processing and processed at temporal resolution of one-day, 8-day, 16-day, one-month, quarterly and yearly (LP DAAC, USGS).

3.1.2.1 Land Cover Type

MODIS LC type product (MCD12Q1) is useful in describing the LC properties which is done by utilizing year-long observations of Aqua and Terra data. MODIS land cover product incorporates five different LC classification schemes which are derived through a supervised decision-tree classification method. The primary land cover scheme includes 17 classes defined by the International Geosphere Biosphere Programme (IGBP), which includes 11 natural vegetation classes, three human-altered classes (developed and mosaicked land classes), and three non-vegetated classes.

3.1.2.2 Land Surface Temperature

One-day MYD11A1 and MOD11A1 LST product are available at two time frame for both night and day time. Eight-day MYD11A2 LST product is available for both night and day time. It is calculated by averaging the view-time LST of two to eight days for clear-sky conditions (Wan, 2007). It has 12 Science Data Sets (SDS) layers which give day and night images of LST and information such as view angle, view time and clear sky conditions during the recording of LST observation, both for day time and night time LST. The

emissivities of bands 31 and 32, which have been used to derive LST, are also available as separate SDS layers.

The TIR signature received by satellite sensor is determined by thermal radiation from the Earth's surface. A database has been developed for MODIS thermal band radiance values from accurate atmospheric transfer simulations for an extensive range of atmospheric and surface conditions. Based on this simulated database, a look-up table and interpolation scheme have been developed to study the effects of LST and emissivity, atmospheric water vapour, and temperature profiles on MODIS TIR band radiance. A view-angle dependent split-window LST algorithm has been developed for correcting atmospheric and emissivity effects. A day/night LST algorithm is used for calculating LSTs without knowing the atmospheric temperature and water vapour profiles to high accuracy. This algorithm uses day/night pairs of TIR data in seven MODIS bands for simultaneously retrieving LST and band-averaged emissivities for all LC types. The emissivities in MODIS bands 31 and 32 are inferred from the land-cover types based on thermal infra-red BRDF (bidirectional reflectance distribution function) models (Snyder and Wan, 1998; Snyder et al., 1998). MODIS is particularly useful for the LST product because of its global coverage, radiometric resolution and dynamic range for a variety of LC types. It has high calibration accuracy in multiple TIR bands designed for retrievals of SST (Sea Surface Temperature), LST and atmospheric properties (Wan, 1999).

The MYD11A1/ MOD11A1/MYD11A2 product has a quality flag also, for LST, in the form of SDS layers. This quality flag provides information on algorithm results that can be viewed in a spatial context for each pixel (LP DAAC, USGS). The quality flag, can be used to analyze the algorithm results to know if the algorithm result for a particular LST is nominal, abnormal or if some other defined condition has been encountered for a pixel. The QC information can be obtained by reading the flags stored in an 8-bit unsigned integer. The quality flag enables the user to establish the quality of the LST results and use only that data which meets the predetermined quality requirements. The QC information has been used to determine the usefulness of the LST data in the present study and pixels of best quality only (having zero value for bit numbers 0, 2 and 6 indicating an error of ≤ 2 K in the calculation of LST) have been used for the study.

3.1.2.3 Vegetation Indices

MODIS vegetation indices, provide consistent spatial and temporal comparisons of vegetation canopy greenness, chlorophyll and canopy structure and a composite property of leaf area. Two vegetation indices derived from atmospherically-corrected reflectance in the red, near-infrared, and blue bands are; the NDVI and the enhanced vegetation index (EVI). The two products more effectively characterize the global range of vegetation states and processes. MYD13Q1, gridded vegetation indices product, provides global land coverage at temporal interval of 16 days and has 12 SDS layers and it gives reflectance values for red, blue, NIR and MIR bands in addition to NDVI and EVI values (spatial resolution of 231.7 m for the study here). It also includes quality assurance (QA) flags with statistical data that indicate the quality of the VI product. This enables the user to include only those pixels for which the VI flag indicates good quality. Thus, it is also possible to remove pixels on the basis of adjacent clouds detected or for which atmosphere bidirectional reflectance distribution function (BRDF) correction has not been performed. 250m_16 days_NDVI layers giving NDVI image has been used in the present study. 250m_16_days_VI_Quality layer has been used to remove the influence of clouds and hence only good quality pixels have been used for the study.

3.1.3 ASTER Product – Global Digital Elevation Model

ASTER is an imaging instrument built by a consortium of the Japanese government, industry, and research groups and operates on the NASA‘s Terra platform (LP DAAC, USGS). ASTER is one of the five state-of-the-art instrument sensor systems on-board Terra with a unique combination of broad spectral coverage and high spatial resolution in the visible near-infrared (VNIR) through short wave infrared (SWIR) to the TIR regions. ASTER is an advanced optical sensor and images are acquired in 14 spectral bands using three separate telescopes and sensor systems. These include three VNIR bands with a spatial resolution of 15 meters, six SWIR bands with a spatial resolution of 30 m, and five TIR bands that have a spatial resolution of 90 m.

Global Digital Elevation Model (GDEM) is produced from optical stereo data acquired by ASTER. ASTER is capable of collecting in-track stereo using nadir- and aft-looking near infrared cameras. Since 2001, these stereo pairs have been used to produce single-scene (60x 60 kilometre (km)) DEM having vertical (RMSE) accuracies generally between 10

and 25 meters. Automated processing including stereo-correlation of the ASTER DEM scenes is done to produce scene-based DEMs. Residual bad values and outliers are then removed and selected data is averaged to create final pixel value. The residual anomalies are then corrected and the data is partitioned into 1 x 1 degree tiles. For each 1 x 1 degree tile, two files are delivered: a) DEM data file; and b) a quality assessment (QA) file, which is a file that gives the number of scene-based DEMs contributing to the final DEM value at each pixel or the positon of data anomalies that have been corrected and the data source utilized for the correction. The ASTER GDEM covers surfaces between 83°N and 83°S and is comprised of 22,702 tiles. Tiles that cover at least 0.01% land area are encompassed. The ASTER GDEM is distributed as Geographic Tagged Image File Format (GeoTIFF) files with geographic coordinates (latitude and longitude). The data are posted on a 1 arc-second (about 30–m at the equator) grid and referenced to the 1984 World Geodetic System (WGS84)/ 1996 Earth Gravitational Model (EGM96) geoid.

3.2 Methodology

Various data products have been ordered/requested from the LP DAAC website using NASA Warehouse Inventory Search Tool (WIST). WIST enables the user to search for the data on the basis of its discipline (atmosphere, land, ocean, etc.), sensor (MODIS, ASTER, AVHRR etc.), location (through latitude/longitude, orthographic, equatorial search, etc.) and date/time range (start date/time and (or) end date/time). The search result is in the form of list of data granule(s) and request for desired data granule(s) is then submitted. All the files associated with the ordered product(s) are included in a unique directory on the Earth Resources Observation and Science (EROS) EOSDIS Core System (ECS) server, the link of which is communicated through the mail and the data can be downloaded through anonymous file transfer protocol (FTP) pull. Landsat data has been directly downloaded from the Earth Explorer website.

Data of 13 years from 2003 to 2015 (referred as study period) has been utilized for the present study. 46 LST images of 8-day period and 23 VI images of 16-day period are available for a year. GDEM and LC type images of 2011 have been used. In addition, Landsat TM, ETM+ and OLI sensor data have also been used for calculation of %ISA, NDBI, NDBaI, MNDWI, and NDVI.

3.2.1 Pre-Processing of Remote Sensing Data

3.2.1.1 Pre-Processing of MODIS and ASTER Data

The MODIS data is in HDF-EOS format and in Sinusoidal Projection System. The Earth gridded tile area of each MODIS image covers approximately 1100 km x 1100 km. Pre-processing of downloaded MODIS images has been done using MODIS Re-projection Tools (MRT). MRT is used for sub setting of the data to a smaller area. The data has also simultaneously been re-projected from Sinusoidal projection to UTM Zone 43N projection system with WGS84 datum and has been reformatted from HDF-EOS to GeoTIFF format. The ASTER GDEM is in GeoTIFF format with geographic lat/long coordinates and a 1 arc-second (30 m) grid. Since, single image of ASTER data covers approx. 60 km x 60 km area only, multiple images covering the entire study area have been downloaded and have been mosaic together. This image has also been re-projected to the UTM Zone 43N projection system with WGS84 datum. Various data layers in GeoTIFF format have been analyzed using ArcGIS and spread sheets software.

3.2.1.2 Pre-Processing of Landsat Data

The Landsat images have been geometrically rectified to the UTM projection system (datum WGS 84, Zone 43). The ground control points have been carefully selected in order to make sure that the RMS errors lie below 0.5 pixels. A second-order polynomial and the nearest neighbour resampling method have been employed for implementing the georectification. The digital numbers of the Landsat images have been converted to the ex-atmospheric reflectance using the methods provided by (Chander and Markham, 2003) and the Landsat Science Data Users Hand book.The pre-processing of Landsat data has been done by using ENVI software.

3.2.2 Study Areas and Its Features

SUHI effect over three cities (Jaipur, Ahmedabad and Chandigarh), located in four states of India (Rajasthan, Gujrat, Panjab and Haryana, respectively) has been analyzed. MODIS Yearly LC type image (LP DAAC, USGS) of 2011 has been utilized to extract the urban area and the urban area polygon has been automatically created from the LC type image. Fig. 3.1 shows the geographical location of study areas. The study areas broadly encounter three seasons in a year: winter season from November to February, summer season from

March to June and monsoon season from July to October (with wide fluctuations in daily average air temperature due to atmospheric conditions). About 70% of total rainfall over these cities falls during the monsoon season. Remaining 30% rainfall is distributed during the remaining part of the year (Indian Meteorological Department (IMD), Pune).

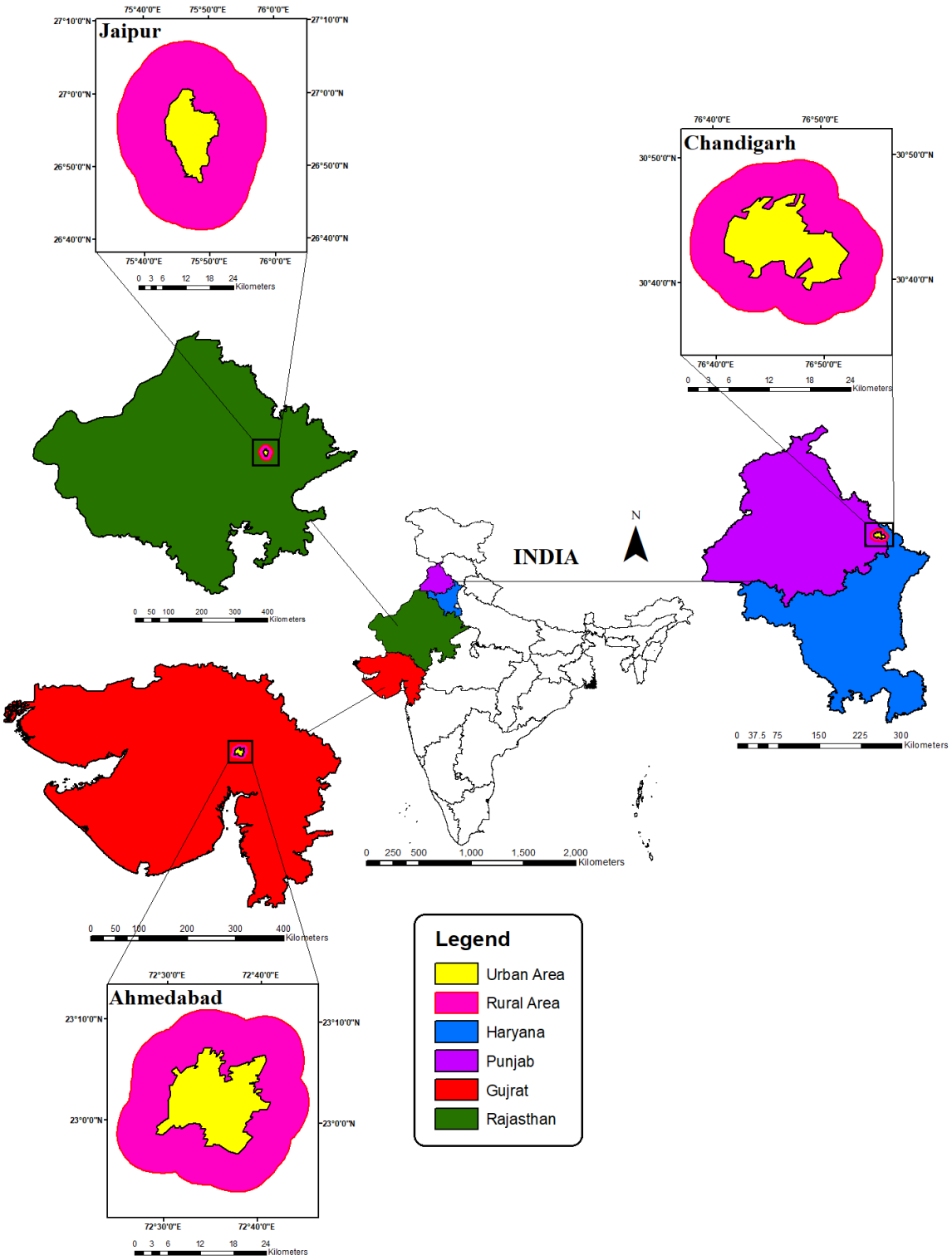

Fig. 3.1. Geographical Location of Jaipur, Ahmedabad and Chandigarh Study Areas

a) Jaipur

Jaipur is the capital of Rajasthan state of India (biggest state by area) and is the 10th largest city of India. Population of Jaipur city is about 3.15 million (census, 2011). The city is situated on a predominantly flat plain and is surrounded by Aravalli hill ranges on the North, North-East and East sides. The remaining part of the city has a mixture of barren land, low to medium height vegetation and built-up areas in the form of roads, buildings, industries, etc. The climate of the study area is mostly semi-arid under the Köppen Geiger climate classification "BSh" and is described by low precipitation, low humidity, and extremes of diurnal and annual temperatures. The area surrounding Jaipur city broadly encounters cold nights with average air temperature dropping up to 3 ^{o}C during the winter season. It extremely hot during daytime with maximum air temperature rising up to 48 ^{o}C during the summer season and extensive variations in daily average air temperature due to atmospheric conditions during monsoon season. The region is mostly water scarce with annual average precipitation of about 55 cm concentrated mostly during monsoon season (Tyagi et al., 2011; IMD, Pune). Cultivation in the various parts of the region is mainly dependent on precipitation during monsoon season. In other seasons crops having low water requirements are practiced, and the water requirement for those crops is met out using groundwater. Vegetation cover and agriculture in the city and its surroundings are dependent on precipitation during monsoon season, and it decreases considerably during the summer season.

The urban boundary of Jaipur city has been derived by extracting urban area polygon from the LC type image of MODIS sensor (MCD12Q1, available at a spatial resolution of 463.3 m). The extent of urban area polygon of Jaipur city is 16 km in the East-West direction and 24 km in the North-South direction. The study area shall encompass sufficient non-urbanized/rural area also. A buffer of 12 km i.e. half of the maximum extent of the urban area, outside urban area polygon has been created to mark the boundary of study areas for the cities, and the study has been carried out for area falling within this boundary. The study area is located between 26◦42'57.44" and 27◦04'39.13" North latitudes and 75◦40'12.26" and 75◦51'37.02" East longitudes. The study area covers an area of about 1370 km^2 (1595 pixels) and it covers adequate rural/suburban areas and satellite towns of the city for comparison with urban area (Fig. 3.2).

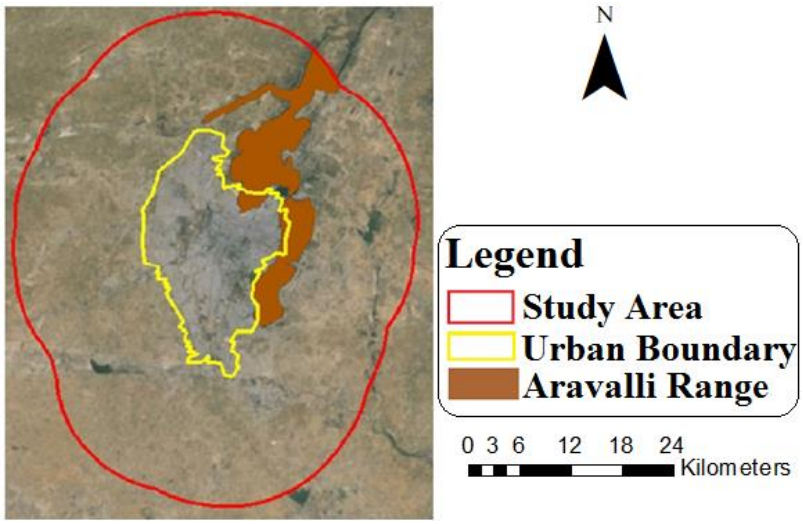

Fig. 3.2. Google Earth© Image of the Jaipur Study Area

b) Ahmedabad

Ahmedabad, former capital of the state of Gujrat, is the biggest city in the state and is located on the banks of Sabarmati river. It is the fifth largest city and seventh largest metropolitan area of India. According to the 2011 census, the urban population of Ahmedabad city was 6,352,254. Ahmedabad has a hot semi-arid climate with scanty rainfall throughout the year. The weather is warm from during the summer season (mean maximum and minimum temperature of 42 ^{o}C and 27 ^{o}C, respectively). Winter season experiences cold weather (mean maximum and minimum temperature of 30 ^{o}C and 15 ^{o}C, respectively) and wide fluctuations in daily average air temperature during monsoon season due to atmospheric conditions. The study area is mostly water scarce with average annual rainfall of approximately 800 mm concentrated mostly during the monsoon season. According to Köppen and Geiger, the climate of Ahmedabad city is classified as BSh, hot steppe climate (semi-arid) with marginally less rain than required for a tropical savanna climate.

The urban area polygon extracted from MCD12Q1 image has been automatically generated by using raster to polygon conversion tool in ArcGIS. The size of urban area is about 12 km and 17 km, in the North-South and East-West directions, respectively. The urban boundary has been enclosed by a buffer of 7 km to mark the boundary of the study area. The size of buffer has been chosen such that it covers sufficient rural/suburban area for the analysis as well as to avoid the influence of Gandhinagar city. The study area is located between 23^{o} 09' 54.68"N 72^{o} 33' 40.02"E and 22^{o} 54' 19.90"N and 72^{o} 39' 51.62"E

according to the geographic coordinate system. The study area covers approximately 887 km^2 (1053 pixels). Fig. 3.3 shows the Google Earth© image of the study area and urban area of Ahmedabad city.

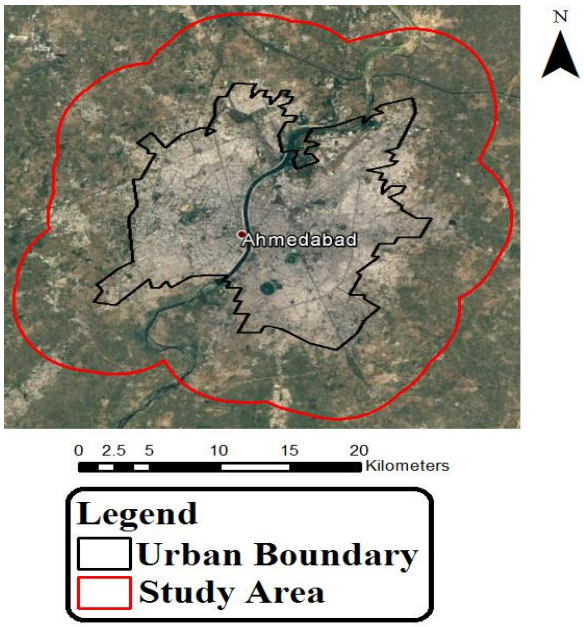

Fig. 3.3. Google Earth© Image of the Ahmedabad Study Area

c) Chandigarh

Chandigarh, one of the largest cities in Northern India, serves as the capital of the states of Punjab and Haryana. The population of the city was 1,055,450 with a population density of about 9258 persons per square kilometer (Census of India, 2011). Chandigarh is situated near the foothills of Shivalik hill range of the Himalayas in North. The average annual rainfall is approximately 1111 mm. Climate of the study area is mostly humid subtropical climate under the Köppen Geiger climate classification "Cwa" and is characterized by temperate or subtropical dry winter, hot-summer and sub-tropical monsoon climates. Climate of Chandigarh is characterized by a seasonal rhythm: unreliable rainfall and great variation in annul minimum and maximum temperatures (−1 °C to 45 °C) with mild winters and very hot summers (City Development Plan Chandigarh).

The length and width of urban area polygon (hereafter referred as urban boundary), from MCD12Q1 image is approximately 12 km in North-South direction and 18 km in East-West direction. A buffer of 5 km has been added to the urban boundary to mark the boundary of study area including North Eastern hill areas and the study has been carried

out for area falling within this boundary. The study area covers approximately 511 km^2 (595 pixels). Fig. 3.4 shows the Google Earth© image of the study area and urban area of Chandigarh city.

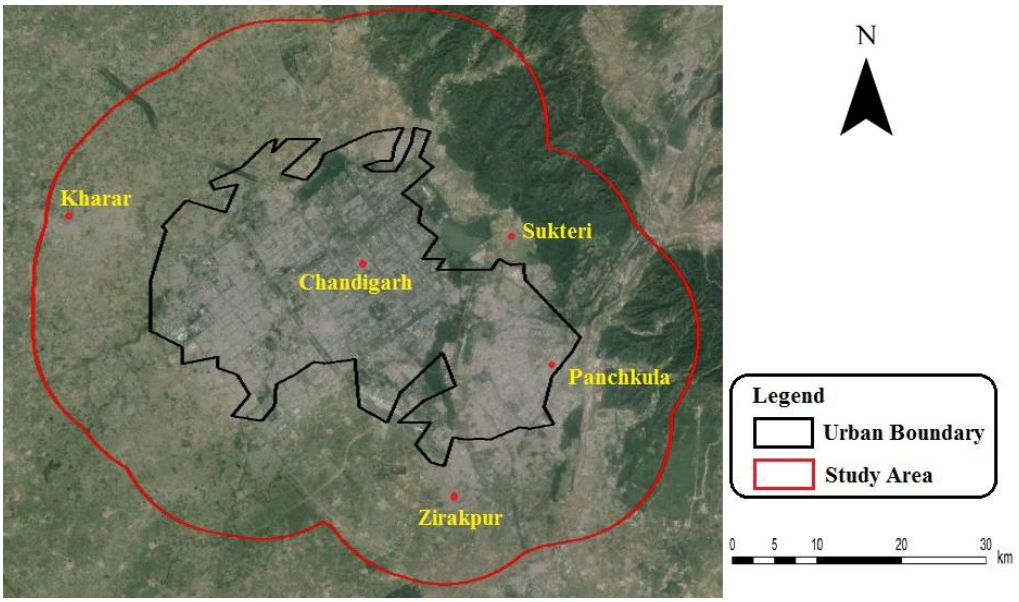

Fig. 3.4. Google Earth© Image of the Chandigarh Study Area

3.2.3 SUHI Growth using Hotspot and Transect Analysis

It is a commonly known fact that, within a city and its surrounding area, the maximum temperatures, at any time, are usually observed at one or other part of the CBD. On the other hand, the minimum temperatures at the same time are usually observed at the suburban or rural locations, and this location can be anywhere on or near the outer boundary of the area of interest, depending on a variety of physical, meteorological or other parameters (Khandelwal et al., 2017). UHI intensity over a city usually indicates the difference in temperature between two points/locations, one being at the CBD (corresponding to the location where the maximum temperature is recorded/observed) and other being at a rural/suburban location. Maximum UHI intensity (referred hereinafter as UHI intensity only) over a city corresponds to the condition when rural/suburban location is that where minimum temperature within the area of interest (can also be mentioned as study area) has been recorded. It has been shown in many studies that the primary important consideration, in any study on UHI effects, is the absolute value of UHI intensity. Location of the points, within the study area, where maximum and minimum temperatures are observed, is usually not same at all the times. These locations can be at different points in the study area and their placement in the study area is not very important. In any area, the

range of temperature during different periods of different years is highly variable. Due to seasonal and diurnal variations in the temperature range, the UHI intensity over the study area during any period may also be different i.e. UHI intensity over a study area, during different times, is not constant.

SUHI intensity over a city can be calculated, as the difference between the maximum and minimum LST values observed within the study area, using a thermal infrared image of the city. However, due to the varying UHI intensity as well as due to the shift/change in the locations corresponding to maximum and minimum LST observations, comparison of UHI intensity over a city, during different time periods is difficult. Similarly, it is not possible to compare the UHI effect of different cities during same or different time periods. Further, it is also not possible to consolidate and analyze the UHI effect over the study area from multiple images of LST data. In order to facilitate the UHI effect analysis using multiple images, UHI_{index} has been used. The UHI_{index} is calculated, from the LST values observed in any image, as per equation 3.1

$$\mathrm{UHI_{index}} = (\mathrm{LST_i} - \mathrm{LST_{min}})/(\mathrm{LST_{max}} - \mathrm{LST_{min}}) \tag{3.1}$$

where, LST_i is the LST of the location/pixel of the study area, where UHI_{index} is to be calculated. LST_{max} and LST_{min} correspond to those locations/pixels of the study area where maximum and minimum LSTs are observed while considering the same image from which LST_i has been extracted. In this fashion, UHI_{index} for each pixel of the study area, corresponding to an image can be calculated. The UHI_{index} is a normalized index with values between 0 and 1 only and due to this it can be used to compare the UHI intensity of different periods and different seasons. The UHI_{index} has been used to bring the variable LST range (and thus the UHI intensity), through normalization, into a normal range (between zero and one). This range is indicative of comparative UHI effect over different parts of a city (study area) and does not in any way indicate the actual UHI intensity. This way effect of the extreme events, observed due to any specific reason, can be eliminated, so that the analysis for seasonal effects as well as the analysis for a long term effect, as attempted in the present study, can be conveniently carried out. The UHI_{index} has been used to find the location of hot spots.

Due to the UHI effect, a temperature gradient, from the HS to the outer boundary of the study area, can be observed. This gradient may, however, be different in different

directions. Transects have been run, from HS to outer boundary of the study area, for transect analysis to find the temperature gradient along different transects. Transect analysis has been carried out by taking centroid of HS as the center point of the UHI. The transects pass through this center point. Two transects have been marked in the N-S and E-W directions, and two transects have been drawn at 45^{o} from these transects. This makes a total of four transects and eight directions from the HS. Absolute temperature difference (i.e. the relative difference between the maximum temperature observed at the HS and temperature of the place under consideration) has been calculated. This relative difference is then plotted along the transects. UHI_{index} and transect methods have been applied to find the growth in SUHI effect, over the study area.

3.2.4 In-Situ Temperature Measurement

In-situ surface and air temperatures have been collected for 27 hours duration (2 PM to next day 5 PM) at seven locations of the Jaipur study area, simultaneously where 3 are inside the urban boundary and 4 are in rural area. Table 3.2 gives the details of date and time of the field observations. The purpose of this exercise is to study the comparative thermal pattern of various surfaces at these locations as well as to compare the SUHI and atmospheric UHI (AUHI) effects. Fig. 3.5 shows the geographical positions of seven in-situ field survey locations. Table 3.3 gives the details of geographical location of in-situ field survey locations. The temperature has been recorded at fixed intervals between 1-2 hours. The time interval has been fixed on the basis of variations observed in the surface temperature and the interval has been kept as one hour during day time, 1 hour 30 minutes during evening and morning time and 2 hours during night. 10-12 measurements have been taken at each land surface material and average value of these measurements has been considered as the LST of that material at the particular time.

Infrared thermometers have been used for the surface temperatures measurement for different land surface materials. Mini infrared thermometer (make Fluke, model 59) has been used for in-situ measurements which is capable of measuring temperature in the range from 255 K to 548 K. The instrument operates on 9 V battery. The optical resolution (distance to spot size ratio) is 8:1. The accuracy of the system is about ±2% of the observation and is based on operating the system within the ambient temperature range of 273 K to 323 K and relative humidity of 10-90% @ 303 K. In addition to the surface temperature measurement, air temperature has also been measured at 1.5 m above the

ground level using data logger and sensor devices and heat stress meter instrument make precision that calibrated devices have been used for the field temperature measurement. AUHI and SUHI intensity have been calculated at the time of pass of AQUA/TERRA satellite over the study area (10:30 AM and 10:30 PM). UHI intensity has been calculated with respect to the location where minimum air temperature has been recorded at 10:30 PM.

Table 3.2: Date and Time of the Field Observations

SL. No.	Season	Observation Time
1	Monsoon	2 PM on 21/08/2015 to 5 PM on 22/08/2015
2	Winter	2 PM on 20/01/2016 to 5 PM on 21/01/2016
3	Summer	2 PM on 19/05/2016to 5 PM on 20/05/2016

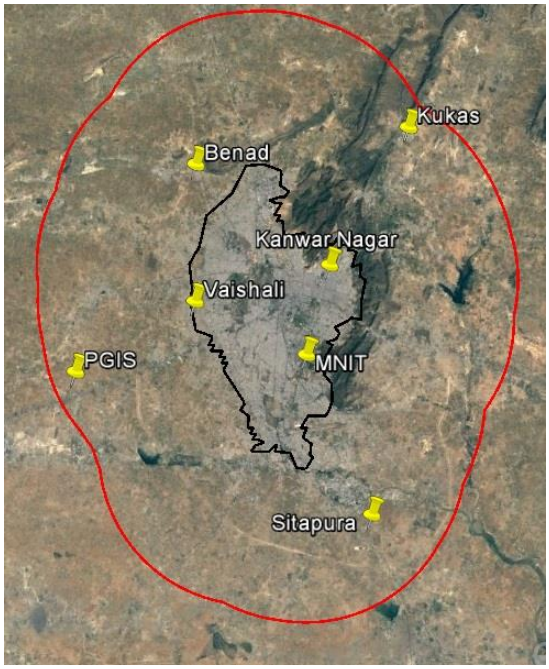

Fig. 3.5. In-Situ Field Survey Locations

Table 3.3: Geographical Location of In-Situ Field Survey Locations

ID	Name	Class	Latitude (ºN)	Longitude (ºE)	(m.s.l.)
1	Kanwar Nagar	Urban	26°55'46.69"N	75°49'37.99"E	431
2	Vaishali Nagar	Urban	26°54'14.62"N	75°43'14.37"E	424
3	MNIT	Urban	26°51'58.75"N	75°48'32.02"E	427
4	Sitapura	Semi urban	26°45'12.45"N	75°51'37.40"E	348
5	PGIS	Rural	26°51'15.77"N	75°37'33.67"E	392
6	Kukas	Rural	27° 1'36.31"N	75°53'23.27"E	401
7	Benad	Rural	27° 0'2.59"N	75°43'17.00"E	461

The in-site measurement has been carried out for four different surfaces and temperature of these surfaces has been recorded simultaneously. The surfaces considered are concrete pavement over a course of well compacted stones (concrete surface), a road surface with bitumen wearing course over well compacted water bound macadam layers (road surface), soil surface having zero vegetation cover (soil) and grass surface having no visible soil under it and having dense grass or shrub (vegetation). No external moisture was added to any of the surfaces during the observations.

3.2.5 Calculation of NDVI, MNDWI, NDBaI and NDBI

Various land surfaces of different spectral characteristics have been represented by different indices like NDVI or EVI for vegetation, MNDWI for water, NDBaI for soil, and NDBI for built-up areas. Estimation of these indices mainly depends on the spectral reflectance pattern of various surfaces for different spectral bands.

NDVI is an indicator of the amount of vegetation cover at the Earth surface (Kumar et al., 2012; Purevdorj et al., 1998). NDVI and EVI have been used to distinguish green belts over the study area. The value of NDVI ranges between -1 and +1. NDVI can be estimated by the following equation (Rouse et al. 1974; Holme et al., 1987).

$$\mathrm{NDVI} = (\mathrm{NIR} - \mathrm{RED})/(\mathrm{NIR} + \mathrm{RED}) \tag{3.2}$$

where, RED = Red Reflectance; NIR = Near Infrared Reflectance.

Zha et al. (2003) have developed the NDBI to identify and extract urban and built-up areas. NDBI has been used to highlight built-up areas, and it can be calculated by the following equation (Liu and Zhang, 2011).

$$\mathrm{NDBI} = (\mathrm{SWIR} - \mathrm{NIR})/(\mathrm{SWIR} + \mathrm{NIR}) \tag{3.3}$$

where, NIR = Near Infrared Reflectance; SWIR = Shortwave Infrared Reflectance.

MNDWI is calculated by equation 3.4,

$$\mathrm{MNDWI} = (\mathrm{R_{GREEN}} - \mathrm{R_{MIR}})/(\mathrm{R_{GREEN}} + \mathrm{R_{MIR}}) \tag{3.4}$$

Where, $\mathrm{R_{GREEN}}$ = reflectance in green band, $\mathrm{R_{MIR}}$= reflectance in mid infrared band

To retrieve bare land from the Landsat imagery, NDBaI has been used (Zhao and Chen, 2005): NDBaI is calculated by equation 3.5,

$$\mathrm{NDBaI} = (\mathrm{R_{TIR}} - \mathrm{R_{MIR}})/(\mathrm{R_{TIR}} + \mathrm{R_{MIR}}) \quad (3.5)$$

Where, $\mathrm{R_{TIR}}$ = reflectance in thermal infrared band, $\mathrm{R_{MIR}}$= reflectance in mid infrared band

3.2.6 Estimation of Impervious Surfaces of the Study Areas

Extraction of impervious surfaces at the subpixel level can be done by using the linear spectral mixture analysis (LSMA) (Wu and Murray, 2003). In pixel unmixing model, water bodies are to be masked from the spectral data since they cannot be considered as an end member due to its low albedo. The analytical procedure for LSMA is discussed below.

3.2.6.1 Water Body Masking

MNDWI has been used to extract water bodies from remote sensing data (Xu, 2006). In the present study, MNDWI has been used for removing water features from the TM/ETM+/OLI spectral data before conducting LSMA.

3.2.6.2 MNF Transform

The maximum noise fraction (MNF) transformation fixes most of the variances of the spectral bands into the first two or three resultant components. It is a modified variant of Principle Component Analysis (PCA) by ordering components according to Signal-to-Noise Ratios (SNR) (Green et al., 1988).

3.2.6.3 Linear Spectral Unmixing

In order to perform linear unmixing model, four types of end members are selected in the present study: vegetation, low albedo, high albedo, and soil by making a scatter plot using the first two MNF components. Finally, constrained mixture spectral analysis are used to process the pixel values of the masked image with the end members' spectra.

In the linear spectral unmixing model, the spectral value of an image pixel can be treated as a linear combination of different types of end members.

$$\mathrm{R_b} = \sum_{i=1}^{N} \mathrm{f_i R_{i,b}} + \mathrm{e_b} \quad (3.6)$$

$$\text{RMSE} = \sqrt{\frac{\sum_{b=1}^{M} e_b^2}{M}} \quad (3.7)$$

$$\sum_{i=1}^{N} f_i = 1 \text{ and } f_i > 0$$

where, R_b= reflectance in band b

$\text{RMSE} = \text{Root Mean Squared Error}$

f_i= fraction of end member in band b

$R_{i,b}$= reflectance of end member in band b

e_b= error in band

N = total number of endmembers

M = total number of bands

3.2.6.4 Endmember Fractions

By resolving the LSMA (equation 3.6) using the least error method, the pixel values of the masked TM/ ETM+/ OLI sensor images can be separated into fractions for the four endmembers. As urban areas with a wide range of spectral properties, impervious surfaces possess both high and low albedo values. Therefore, a linear mixture of low albedo and high albedo can be considered as a good representation of imperviousness (equation 3.8), and the fraction of impervious surface for each pixel can be estimated as the sum of fractions of high albedo and low albedo (Wu and Murray, 2003).

$$R_{imp,b} = f_{low}R_{low,b} + f_{High}R_{High,b} + e_b \quad (3.8)$$

where, $R_{imp,b}$, $R_{low,b,}$ $R_{High,b}$ = reflectance of impervious surfaces, low albedo and high albedo for band b; $f_{low,}f_{High}$= fraction of low albedo and high albedo; e_b = error for band b.

3.2.7 Calculation of Road Density (RD)

Road network map of Jaipur (Khandelwal, 2012), Ahmedabad and Chandigarh study areas have been created by on screen digitization of the roads from Google Earth. All the roads, major or minor have been digitized within the study area. This road map has been used for calculating road density by line density tool in the spatial analyst tool box using ArcGIS

software. Line density is calculated as magnitude per unit area of the feature that falls within a defined radius using centroid of the pixel as the centre of the circle. As the pixel size of LST is 926.626m, the radius for calculating RD has been taken as 655m. The area of the circle considered for calculating RD of a pixel is 57% more than the area of corresponding pixel.

3.2.8 Linear Time Series Model

El-Fouly et al. (2008) have used LTS model for the prediction of wind speed and direction from historic wind data. One year and two year LTS models have been developed using data of one and two years, respectively. The accuracy of the model has been investigated using two sets of data recorded during winter and summer season at Madison weather station (El-Fouly et al., 2008). The presented results reveal the effectiveness and the accuracy of the proposed new technique for wind speed and direction prediction. The proposed models have been used to predict wind speeds for one day ahead with an improvement over the persistent model up to 54.4% for the mean absolute error (MAE) and up to 55.3% for the RMSE. The corresponding improvements over the persistent model are up to 45.3% and up to 26% for the MAE and RMSE, respectively. The proposed models have been able to produce reduced scatter, higher coefficients of correlation, and higher scaling factors than those produced by the persistent model (El-Fouly et al., 2008).

3.2.8.1 One Year Linear Time Series Model

One year model is based on using data (Y) of n points from the year K and predicts the data (Y) for the year K+1, for the same time interval/points. The one year model can be represented by the formula, which is a single step version (El-Fouly et al., 2008).

$$Y_{K+1}(n) = a + b * Y_k(n) \tag{3.9}$$

where, Y_K represents data from year K, Y_{K+1} represents prediction for the year K+1; n represents number of points/values; a and b are model parameters which are estimated using least-square method expressed as equations 3.10 and 3.11. The parameters a and b have been estimated using MATLAB software.

$$A = \begin{bmatrix} a \\ b \end{bmatrix} = [B^T \quad B]^{-1} B^T Y_k \tag{3.10}$$

$$B = \begin{bmatrix} 1 & Y_k(1) \\ 1 & Y_k(2) \\ 1 & Y_k(3) \\ \vdots & \vdots \\ 1 & Y_k(n) \end{bmatrix} \quad Y_k = \begin{bmatrix} Y_k(1) \\ Y_k(2) \\ Y_k(3) \\ \vdots \\ Y_k(n) \end{bmatrix} \tag{3.11}$$

3.2.8.2 Two Year Linear Time Series Model

Two years model, uses data of n points from previous two years K and K-1. The model then predicts data for the year K+1, for the same time interval/points. The two year model can be represented by the formula, which is also a single step version (El-Fouly et al., 2008).

$$Y_{K+1}(n) = a + b * Y_k(n) + c * Y_{k-1}(n) \tag{3.12}$$

where, Y_K, Y_{K-1} represents data from year K and K-1, respectively, Y_{K+1} represents prediction for the year K + 1; n represents number of points; a, b and c are model parameters which are estimated using least-square method expressed as equations 3.13 and 3.14. The parameters a, b and c have been estimated using MATLAB software.

$$A = \begin{bmatrix} a \\ b \\ c \end{bmatrix} = [B^T \quad B]^{-1} B^T Y_k \, [B^T \quad B]^{-1} \tag{3.13}$$

$$B = \begin{bmatrix} 1 & Y_k(1) & Y_{k-1}(1) \\ 1 & Y_k(2) & Y_{k-1}(2) \\ & \vdots \quad \vdots & \vdots \\ 1 & Y_k(n) & Y_{k-1}(n) \end{bmatrix} \quad Y_k = \begin{bmatrix} Y_k(1) \\ Y_k(2) \\ Y_k(3) \\ \vdots \\ Y_k(n) \end{bmatrix} \tag{3.14}$$

In a similar fashion m year LTS model uses data of past m years for the prediction of the desired parameter for the year subsequent to the 10 years.

In the present study, remote sensing LST data of ten years has been used as input parameter for ten year LTS model to predict the LST for one year subsequent to the 10 years. In addition to the LST data, various input parameters (NDVI, RD, ISA and elevation) have also been used for the prediction of LST for SUHI analysis. The input parameters of NDVI, RD, ISA and elevation have been entered into Minitab corresponding to each LST data for each pixel of the study area for the entire 10 year period. Linear equations of NDVI, RD, ISA and elevation with LST have been developed using Minitab. One unique equation has

been developed for each pixel of the study area on the basis of 10 year values of NDVI, RD, ISA and elevation in addition to the LST i.e. the input parameters have been incorporated into the model using linear equation of LST as a function of these parameters.

3.2.9 Data Analysis

The various data layers used for the present study have been analyzed using ArcGIS and ENVI software. First of all various data layers have been extracted for the study areas. This has been done by 'Extract by Mask' spatial analyst tool, in which the data layer to be extracted has been taken as the input raster and study area boundary has been taken as the feature mask. Spatial and seasonal variations in extracted LST and VIs have then been studied. For the retrieval of various parameters like NDVI, NDBaI, MNDWI, NDBI and %ISA from Landsat data, ENVI software has been used.

The LST product has a resolution of 926.6 m, whereas the VI and ASTER GDEM products are available at 231.6 m and 24.8 m ground resolution, respectively. In order to study relationship of LST with various parameters, it is necessary to have all of them at same resolution and hence GDEM and VI layers have to be aggregated to the resolution of 926.6 m. Resample data processing tool has been used to produce GDEM image at a resolution exactly same as that of the LST image. Nearest neighbour algorithm has been used as the resampling technique. After, changing the resolution of all the images of different data products, the diurnal relationship of various parameters with LST has been studied individually.

Aggregation of VI, NDBI, NDBaI, MNDWI, and %ISA image has been done by Aggregate-Generalization spatial analyst tool. The output value of each aggregated pixel is calculated as mean of the value of input pixels that the coarser output pixel encompasses. Aggregation of VI values can be done by two methods. Firstly, by aggregating the finer resolution VI values themselves or secondly by aggregating the reflectance values of various bands and then to calculate VI values from the aggregated reflectance values. All parameters for study area have been extracted and overlay analysis has been done using ArcGIS software. Raster images have been exported to ASCII format and transferred to MS Excel to study the relationship of LST with various parameters.

Fig. 3.6 shows the flowchart of the entire methodology.

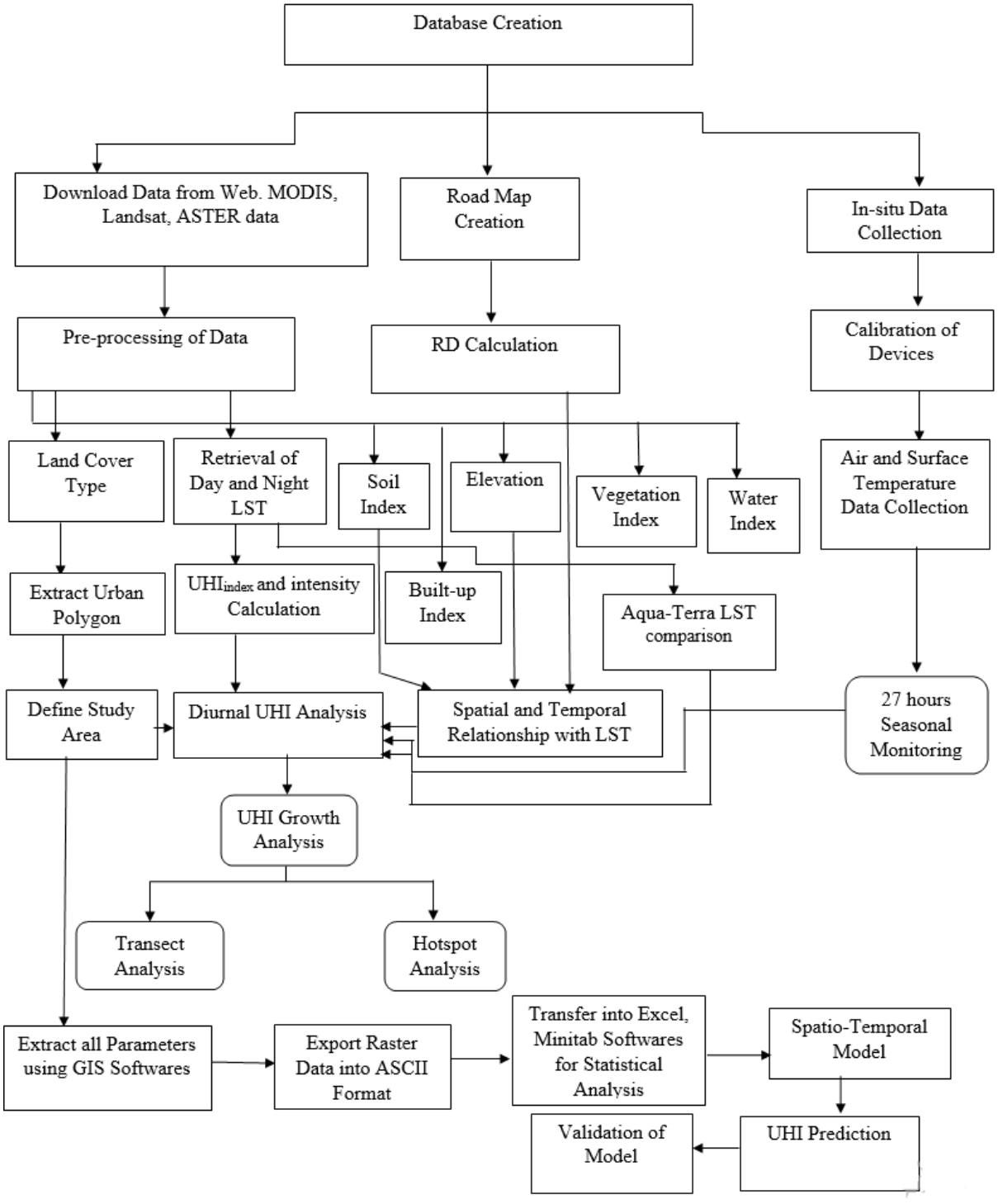

Fig. 3.6. Flowchart of Methodology

Chapter 4

Results and Discussion

This chapter documents the comprehensive results of diurnal UHI variations, spatio-temporal SUHI growth and the relationship of various parameters with LST and presents the details of the LTS model developed. Spatio-temporal SUHI pattern and variations have been discussed in section 4.1. Spatio-temporal SUHI growth analysis has been discussed in section 4.2. Diurnal LST relationships, variations, and field survey validation have been discussed in sections 4.3 and 4.4. Diurnal relationships between individual parameters with LST have been analyzed in section 4.5. Section 4.6 summarizes the details of the LTS model developed for predicting the LST at a particular location for known values of other parameters and discusses the results of the model validation.

4.1 Spatio-Temporal SUHI Pattern

This section documents the comprehensive results and discussion of the spatial and temporal variations in the UHI effect over the three Indian cities. Seasonal, diurnal and spatial patterns of LST, spatial and temporal variations in the UHI intensity and spatio-temporal SUHI pattern and its variations, have been discussed in subsequent paragraphs. The details of UHI_{index} for SUHI studies has also been discussed.

Diurnal LST variation during different seasons has been studied by creating a buffer of 12 km outside urban area boundary and LST profile has been plotted and studied for the urban and rural zones thus created.

4.1.1 Diurnal LST Variations over Jaipur City

Seasonal analysis of LST of Jaipur city has been done for thirteen years (2003-2015) by dividing the year is into winter, monsoon and summer seasons. Day time and night time images have been considered separately.

a) Day Time LST Images

General Day LST profile over the study area is similar throughout the research period, in spite of the fact that the study area encounters high seasonal variations in the LST. However, significant spatial and seasonal variations in LSTs can also be observed during

day period. In addition, large variations are observed, especially over the rural area, during different seasons. The spatial pattern of day LST images clearly indicate the inverse SUHI or negative SUHI over the study area during all seasons.

A large part of the area outside the urban boundary appears red in colour indicating high temperatures in this area during daytime. The rural area shows higher LSTs than the urban area for all seasons (Fig. 4.1a, c, and e). High LST pixels are almost non-existent during day time inside the urban boundary. Southern and Eastern parts of rural area show higher temperatures than the urban area. Most of the area falling in this zone is barren land. Energy interactions of barren land and vegetated ground are known to be different as no moisture is available at barren land and the rate of cooling of two types of land is also different, and these cause different temperature profiles over various parts of the study area. This difference is less prominent during the winter season as the temperature is lower during the winter season and the effect of differential cooling rate is not high. North Eastern parts of rural area show low LSTs due to the presence of agricultural fields areas around this location.

The daytime LST images show similar patterns during different season. However some variations can also be observed. Eastern part of the urban boundary exhibits low LST pixels during summer season whereas the Eastern part of the urban area shows higher LST compared to Western part of the urban area. The Southern part of the study area shows high LST pixels and maximum LST is also observed in this part only during the winter season.

b) Night Time LST Images

The LST pattern over the study area, during night time, is opposite to that observed during day time LST pattern and now the urban area shows higher LST compared to the rural area. LST pattern over the study area, as a whole, does not change significantly throughout the year.

The urban area near the Eastern side of urban boundary encounters maximum LST. This part of the urban area has predominantly built-up and paved areas, and consequently, the nighttime LST of this area is the highest in the night images during all the seasons. Some part of the rural area, near this part and outside the urban boundary, corresponds to Aravalli hill range and this part also has some high-temperature pixels. Mining has been done in this region to meet the demand for stones for construction purposes that has resulted in rock

surfaces being exposed to direct solar radiation. The energy interaction of rocks is similar to that of built-up area thereby resulting in high temperature in this region. Most part of the rural area exhibit low LSTs corresponding to LST for vegetated/agricultural ground or barren land. It is evident from the images that a thermal gradient exists as we progress from the high-temperature pixels towards the rural area or other parts of the urban area.

Minimum LSTs are observed over the area at the boundary of the study area, especially on the North-Western side. LST of Eastern and Southern parts of the rural areas is higher than other parts of the rural area (Figs. 4.1 (i) b, d, and f). Some parts of the rural areas show large variations in LST during monsoon season. However, winter season exhibits a large difference in urban and rural LSTs compared to other seasons.

LST of different parts of a city shows both diurnal and temporal variations. UHI intensity has been described as the difference in temperature between two points, within the area of interest (study area in this case), during simultaneous observations. UHI intensity corresponding to pixels/points observing the maximum and minimum temperatures has been referred as maximum UHI intensity.

UHI intensity exhibits diurnal and seasonal cycles and is modulated by meteorological conditions, such as cloud, wind conditions as well as anthropogenic heat release. Table 4.1 gives the seasonal and annual average of maximum UHI intensity for Jaipur study area. For the study duration between 2003 and 2015, the nighttime maximum UHI intensity varies from 9.80 K to 13.90 K during summer season and 7.58 K to 12.42 K during monsoon season and 10.04 K to 15.10 K during winter season. Similarly, nighttime minimum UHI intensity varies from 3.96 K to 6.22 K, 2.12 K to 5.26 K, and 6.28 K to 8.78 K for summer, monsoon and winter season, respectively. Overall average maximum SUHI intensity of the study area during summer, monsoon and winter seasons is 8.39 K, 6.83 K, and 9.60 K, respectively. Overall average maximum SUHI intensity of the study area for the entire study period is 8.50 K.

Table 4.1: Seasonal and Annual Average of Maximum Night SUHI Intensity for Different Seasons of Jaipur City

Season	2003	2004	2005	2006	2007	2008	2009	2010	2011	2012	2013	2014	2015	overall average
Summer	8.50	8.66	9.35	7.54	8.71	8.65	8.84	8.28	8.68	8.32	8.49	7.62	7.43	8.39
Monsoon	8.35	5.47	6.08	7.91	6.39	6.46	6.72	6.60	7.98	7.16	6.64	6.31	6.69	6.83
Winter	8.81	9.98	9.81	11.40	10.20	10.20	9.71	8.64	9.36	9.55	8.91	9.23	9.05	9.60
Annual	8.58	8.25	8.71	9.14	8.75	8.95	8.47	8.10	8.87	8.67	8.40	7.86	7.79	8.50

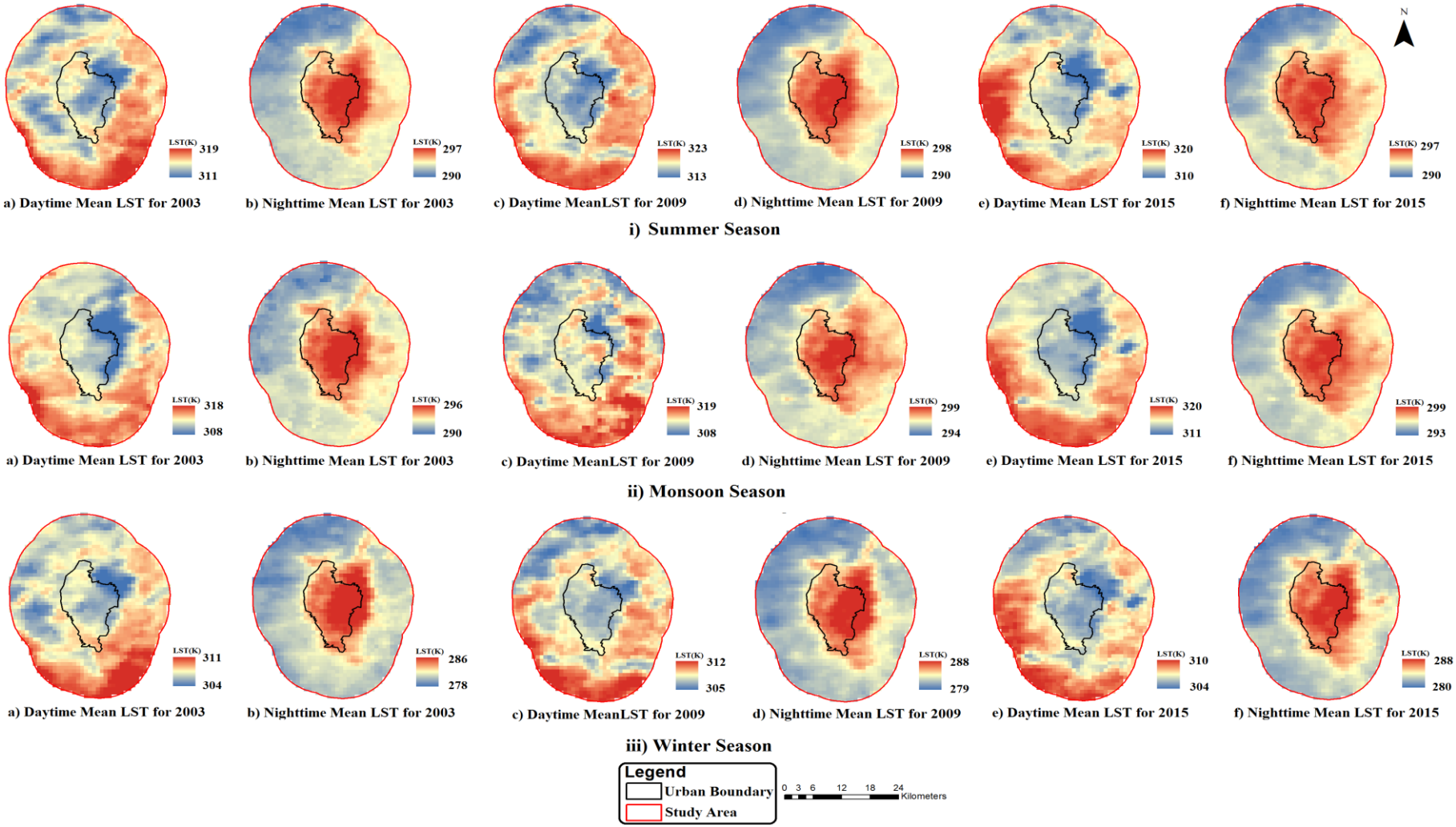

Fig. 4.1. Spatial and Diurnal Variation of Mean LST over Jaipur

Average LST of urban and rural areas has been calculated separately. Difference between the average LST of urban and rural areas give the urban-rural UHI intensity (UR_{UHI}). UR_{UHI} corresponding to each image of the study area has been calculated. Mean UR_{UHI} for each season of a particular year is then calculated by considering LST images for that season only. Mean UR_{UHI} from day time and nighttime images has been calculated for all the three seasons of the entire study period and it has been shown in Fig. 4.2.

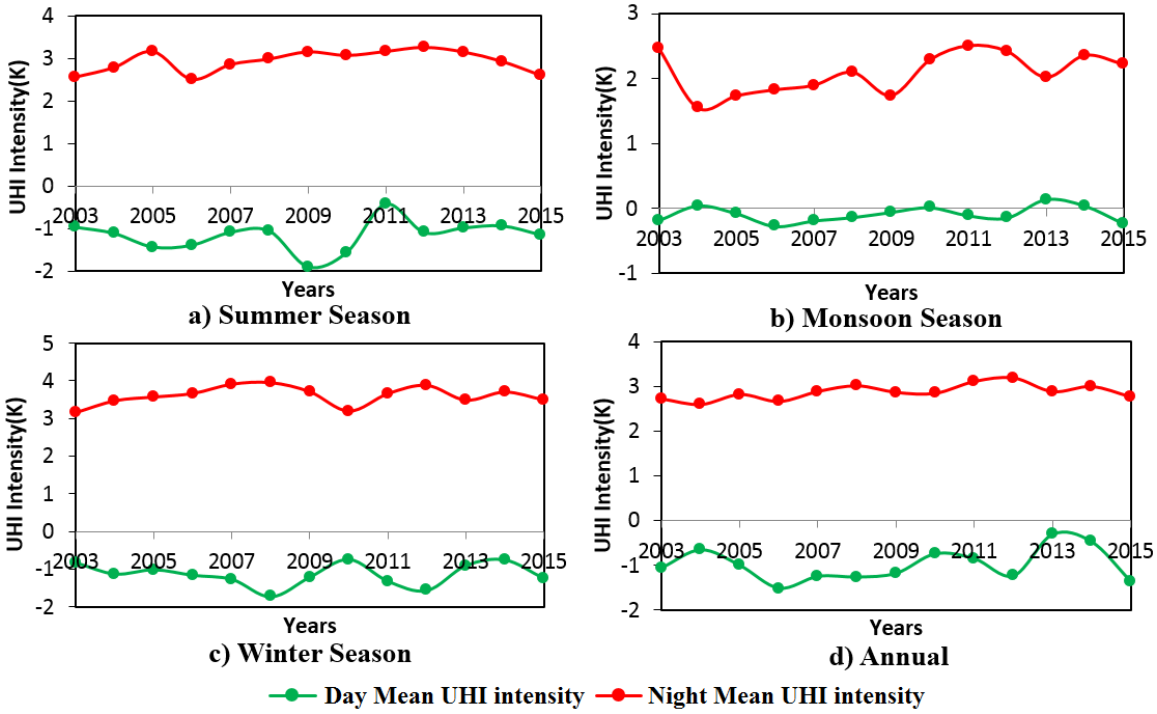

Fig. 4.2. Temporal and Diurnal Variation of Mean UHI Intensity (Jaipur)

Mean UR_{UHI} during daytime of summer season varies from -1.90 K to -0.43 K (Fig. 4.2a). The negative values indicate that the rural area is warmer than the urban area during daytime, which corresponds to negative SUHI or cool island effect. Most part of the rural/suburban area of Jaipur city comprises of barren land and the temperature of soil surface, during peak solar radiation, is higher than the temperature of built-up surfaces, thereby resulting in apparent cool island effect. For the 13 year study period, the overall average of mean UR_{UHI} is -1.16 K. The corresponding mean UR_{UHI} during nighttime of summer season varies from 2.51 K to 3.26 K (Fig. 4.2a). This means that the average LST of the entire urban area, for nighttime observations, is higher than the average LST of the entire rural area. The overall average mean UR_{UHI} for summer season is 2.93 K.

During monsoon season, daytime mean UR_{UHI} varies from -0.27 K to 0.14 K with an overall average of mean UR_{UHI} of -0.09 K and the nighttime mean UR_{UHI} varies from 1.54 K to

2.51 K with an overall average of mean UR_{UHI} of 2.09 K (Fig. 4.2b). Arnfiled (2003) has suggested that rural thermal admittance has a very important role in generating a heat island and moist soil possess thermal admittance values that are not dissimilar from those for typical dense urban building materials. Due to this reason the LST ranges inside the urban area are similar to those outside it, during monsoon season, thereby giving very low values of mean UR_{UHI}. However, during nighttime the LST of rural areas is little lower than the urban area thereby showing a positive SUHI effect. The mean day time UR_{UHI}, during winter season, varies from -0.75 K to -1.72 K with an overall average of mean UR_{UHI} of -1.15 K (Fig. 4.2c). It can be seen that the daytime observations indicate negative SUHI effect during all seasons. The mean UR_{UHI}, during nighttime of winter season, varies from 3.15 K to 3.91 K with an overall average of mean UR_{UHI} of 3.60 K (Fig. 4.2c). Therefore, the winter season UR_{UHI} is strongest with a high intensity of 3.60 K.

Significant diurnal surface temperature variations during different seasons have been observed in the Jaipur study area. The diurnal thermal pattern shows a clear contrast in temperature between urban and rural areas with clear existence of strong SUHI during night time (all seasons), while negative SUHI (during summer and winter seasons) or nonexistence of SUHI (during monsoon season) during day time is also noticeable over the study area.

The mean LST of the urban area shows increasing trend from 2003 to 2015 for nighttime observations of all seasons. The trend of mean LST for daytime observations from 2003 to 2015 is negative, during winter and summer seasons and no significant trend can be observed for monsoon season.

4.1.2 Diurnal LST Variations over Ahmedabad City

The analysis of Ahmedabad has been carried out similar to that of Jaipur city by considering the day and night images, separately.

a) Day Time LST Images

The LST pattern over the study area is not consistent and undergoes seasonal changes (Fig. 4.3). It can be seen that in almost all the images, corresponding to daytime LST, there is no clear pattern and the urban and rural areas have both high and low temperature pixels. However, the part of rural area where higher LST is observed is not constant and it spreads

in different parts of the rural area depending on the season. But on the other hand, the part of the urban area, where higher LST is observed is fixed and is consistently in the Eastern part of the urban area.

Very few high temperature pixels are observed inside the urban boundary and most of the high temperature pixels are located outside this boundary (Figs. 4.3 (i) a, c and e). Western part of the study area has concentration of higher temperature pixels and maximum LST is also observed in this part only. Conversely, the area near the Eastern boundary of the urban boundary has higher temperature pixels compared to other parts of the urban area. Southern and Eastern parts of the rural area show lower LSTs compared to other parts of the rural area. Some part of the urban area, around the centre and corresponding to Sabarmati river, consistently shows low LSTs. A large part of the rural/suburban area also contains low temperature pixels. Few high temperature pixels can also be observed on the Northern part of study area (monsoon and winter seasons). Similarly few low temperature pixels can be observed in the South-Western part of the study area (winter season) due to higher vegetation density. Monsoon LST images exhibit moderate or very weak day SUHI effect over the study area.

b) Night Time LST Images

Nighttime LST images for all seasons show similar spatial pattern. Most part of the urban area appears red in colour and the remaining part has orange colour [Figs. 4.3 (b, d, and f)]. The area outside urban boundary is predominantly blue, indicating that the LST of this area is in the lower range compared to the urban area. Red colour corresponding to high temperature pixels is almost absent in the rural area and some pixels appear orange coloured. Very few pixels inside the urban boundary are of light colour i.e. the LST of very small area falling inside the urban boundary is in the moderate range. Winter LST images, compared to other two seasons, shows striking SUHI effects with clear contrast in temperature of the urban area and the rural area.

The comparison of nighttime and daytime LST images depict existence of SUHI effect during nights, whereas weak or no such effect during daytime can be observed. The main reason for this variation is the difference in the properties of the surfaces present in the urban and rural area. The urban area surfaces comprise mainly of built up and anthropogenic material, whereas the surroundings of the city comprise of agricultural

fields, barren soil, and forest. Night time images exhibit a clear pattern of SUHI in the study area, where urban areas show higher surface temperatures than rural areas. The pattern of LST for the entire study area, as a whole, does not change significantly throughout the year during night time.

It can be observed from figures that during day-time, some parts of the rural area exhibit higher surface temperatures than the urban area which indicate nonexistence of SUHI effect during daytime in Ahmedabad especially during winter and summer seasons, i.e. negative UHI has been observed in the Ahmedabad during day time. On the other hand, during day time of the monsoon season, high LST pixels can be observed in both the urban as well as the rural area.

During night time, there is clear existence of SUHI and the LST of most parts of the urban area is higher than that of the rural area. As we move from center of the urban area to the boundary of study area, in any direction, shows that central area is hotter than outer area during the night. During day time the average temperature difference between urban and rural area is 0.57 K, whereas this difference is 2.64 K during night time.

Table 4.2: Seasonal and Annual Average of Maximum Night SUHI Intensity for Different Seasons of Ahmedabad City

Season	2003	2004	2005	2006	2007	2008	2009	2010	2011	2012	2013	2014	2015	overall average
Summer	5.85	6.71	6.90	6.11	6.08	6.67	6.15	6.36	6.14	6.06	6.34	5.86	6.15	6.26
Monsoon	7.76	5.20	5.72	4.63	5.45	6.05	5.24	5.60	7.46	6.56	5.56	4.36	5.72	5.79
Winter	8.25	8.07	7.80	7.81	7.60	8.11	7.69	7.22	7.35	7.34	7.32	7.58	7.85	7.69
Annual	7.20	6.91	7.00	6.55	6.62	7.18	6.53	6.64	6.86	6.68	6.59	6.25	6.79	6.75

Table 4.2 gives the average UHI intensity during different seasons of the study period. The maximum UHI intensity varies from 8.32 to 11.86 K during summer season; 6.42 to 11.22 K during monsoon season and 8.96 to 13.82 K during winter season. Similarly minimum UHI intensity varies from 2.38 to 4.60 K, 2.26 to 5.78 K, and 4.60 to 7.04 K for summer, monsoon and winter season, respectively. Average maximum UHI intensity of different seasons vary from 4.36 K to 8.25 K. Overall average maximum UHI intensity of the study area during summer, monsoon, and winter seasons is 6.26 K, 5.79 K, and 7.69 K, respectively and average maximum SUHI intensity of the study area for the entire study period is 6.75 K.

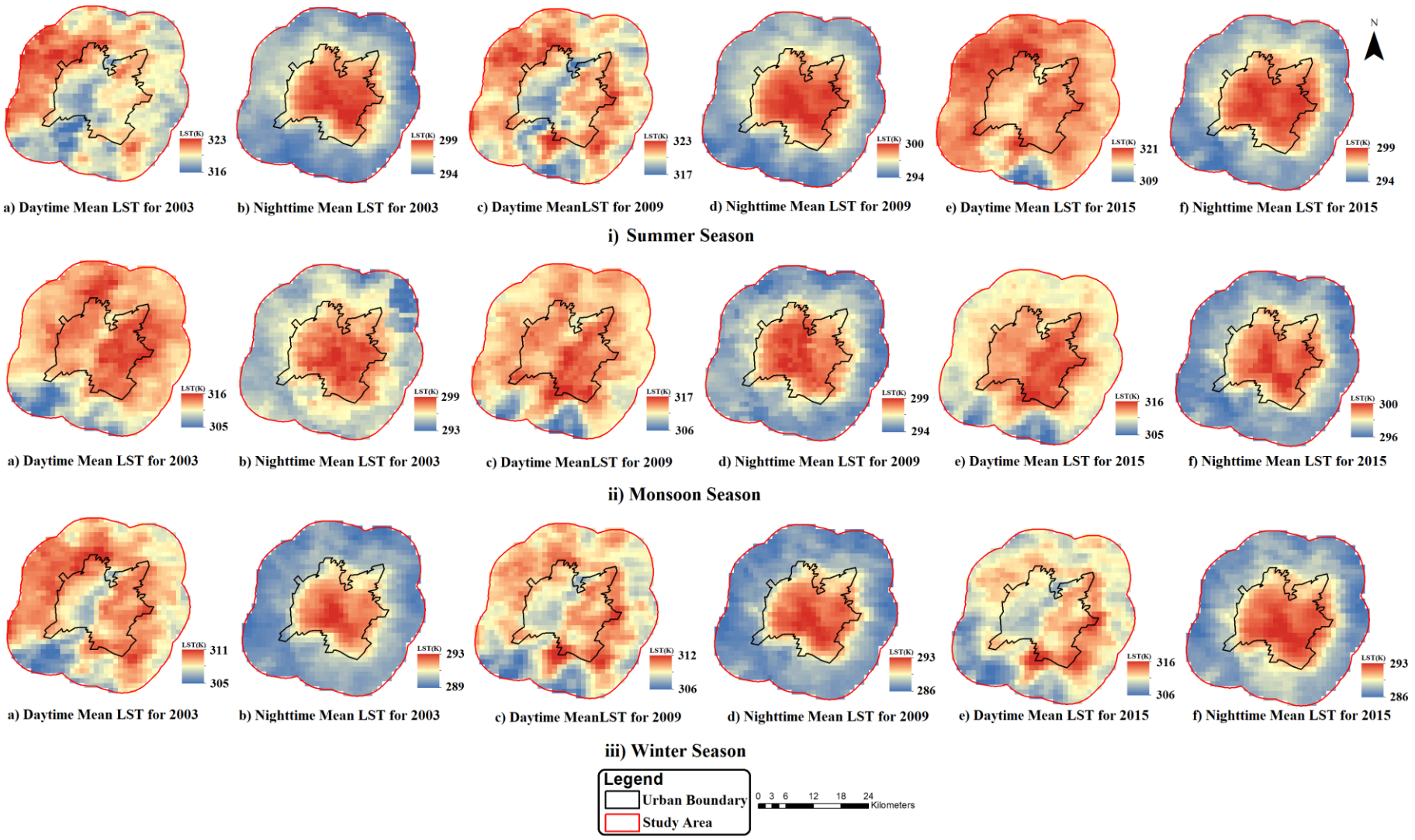

Fig. 4.3. Spatial and Diurnal Variation of LST over Ahmedabad

Fig. 4.4 shows the temporal and diurnal variation of annual mean UR_{UHI} of Ahmedabad study area. It can be seen from the figure that the urban area is consistently warmer than the rural area. Mean day UR_{UHI}, during summer season, varies from -0.31 K to 0.73 K with overall summer mean day UR_{UHI} of 0.07 K (Fig. 4.4a). Mean day UR_{UHI} varies from 1.44 K to 3.59 K, during monsoon season, with overall mean UR_{UHI} of 2.56 K (Fig. 4.4b). Similarly, during winter season, mean day UR_{UHI} varies from 0.30 K to 0.79 K with overall mean UR_{UHI} of 0.48 K (Fig. 4.4c). This indicates that day time SUHI of low intensity exists over Ahmedabad study area during summer and winter seasons. However, the overall mean UR_{UHI} intensity is relatively higher during monsoon season. On the other hand, the overall mean nighttime UR_{UHI} is 2.51 K (varies from 2.27 K to 2.71 K), 1.71 K (varies from 1.30 K to 2.11 K) and 3.20 K (varies from 2.89 K to 3.37 K) for summer, monsoon and winter seasons, respectively. There is significant mean UR_{UHI} during nighttime and it is much higher than the corresponding daytime mean intensities during summer and winters seasons. However, the daytime UR_{UHI}, during monsoon season, is higher than the nighttime UR_{UHI}. This can be due to the effect of vegetation and soil moisture. The flow in Sabarmati river, during monsoon season, is more than the flow during other seasons and the increased flow has increased cooling effect during the day compared to night, which results in lower UHI intensity during nighttime than during day time.

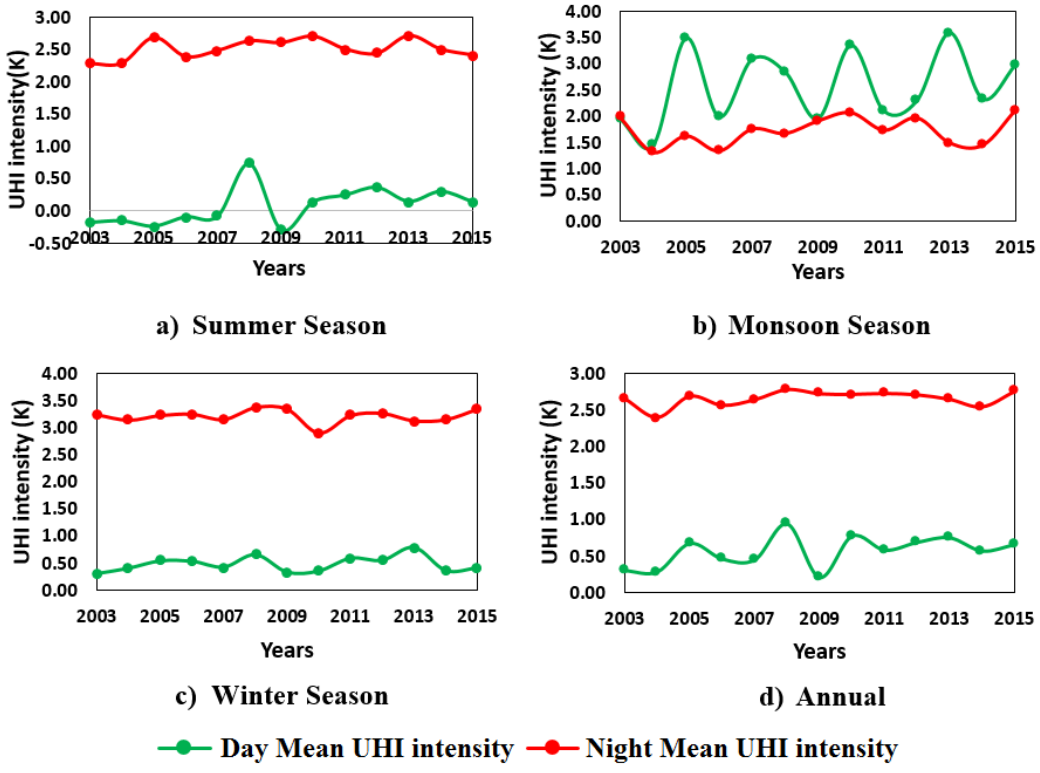

Fig. 4.4. Temporal and Diurnal Variation of Mean UHI Intensity (Ahmedabad)

There is higher difference between day and night UHI intensity during summer and winter season which shows the extremes of diurnal UHI (Figs. 4.4a and 4.4c).

The mean LST of the urban area shows increasing trend from 2003 to 2015 for nighttime observations of all seasons. The trend of mean LST for daytime observations from 2003 to 2015 shows a negative trend, during winter and summer season and no significant trend can be observed for monsoon season.

Hence significant diurnal surface temperature variations with respect to different seasons have been observed in the Ahmedabad study area, and contrast diurnal behaviour in the thermal pattern for heat island effect has also been observed. The clear contrast in temperature between urban and rural areas is evident, showing the clear existence of SUHI during night time, while the existence of low-intensity SUHI is also noticeable over the study area during day time. From the graphs and discussions above, it is evident that SUHI is a season dependent phenomenon and it also depends on the time of observation.

4.1.3 Spatio-Temporal SUHI Pattern and Comparison (Chandigarh)

The Chandigarh city is largely different from Jaipur and Ahmedabad due to its geography and climate. Chandigarh lies at the foothills of Shivalik mountain ranges and has the sub-tropical humid climate whereas Jaipur and Ahmedabad have semi-arid climate and mostly flat terrain.

a) Day Time LST Images

Urban areas and some parts of rural areas exhibit higher surface temperatures and large variations in LSTs in rural areas has also been observed (Fig. 4.5a, c, and e). Western and South-West part of rural areas show higher LSTs during most of the seasons. Eastern and North Eastern Shivalik hill regions show very low LSTs during day time compared to other areas due to the effect of vegetation. However, some variations are observed, especially over the rural area. North Eastern part of the urban areas near to urban boundary shows low LSTs due to the presence of Sukhna lake. During daytime, in addition to urban areas, some parts of rural areas exhibit higher LSTs and vary with seasons. Hence during the day time, the study area shows moderate SUHI effect.

During day time, urban areas show higher LSTs than rural areas especially during summer and winter season. During monsoon season, strong SUHI has been observed over the study area during the day time. During daytime, Eastern parts of the rural areas especially Shivalik hill ranges experience low LSTs due to the effect of vegetation cover in those areas.

Decreasing trend of LSTs has also been observed in both rural and urban areas during these seasons. Conversely, during monsoon season, increasing trend of LSTs has been seen in both rural and urban areas, and urban areas show higher LSTs than rural areas.

b) Night Time LST Images

During night time, urban areas show higher LSTs than rural areas and exhibit a clear SUHI effect over the area (Fig. 4.5b, d, and f). Similar LST pattern can be observed throughout the year. Some high-temperature pixels are also visible outside the urban boundary especially on Eastern and North Eastern regions which is the Shivalik hills area. The energy interaction of rocks is similar to that of built-up area thereby resulting in high temperature in this zone. It is evident from the images that a thermal gradient exists as we progress from the high-temperature pixels towards the rural area or other parts of the urban area. During monsoon season, large variations in rural LSTs have been observed especially in South Western parts and Shivalik hill areas. The value of maximum temperature during any period of monsoon season is similar to the corresponding range during the summer months. Rainfall during monsoon period causes an increase in the soil moisture of all soil types. This results in higher LSTs of the rural area during monsoon season than during other seasons. This explains comparatively smaller UHI intensities during monsoon season than during other seasons. The effect of dense vegetation during monsoon season dominating exposed rock surfaces resulting low LSTs in that areas.

The urban area shows higher surface temperatures than rural area. Increasing trend of LSTs has also been observed in both rural and urban areas during all seasons. Winter LST shows noticeable SUHI effects with a clear contrast in temperature of the urban area and the rural area.

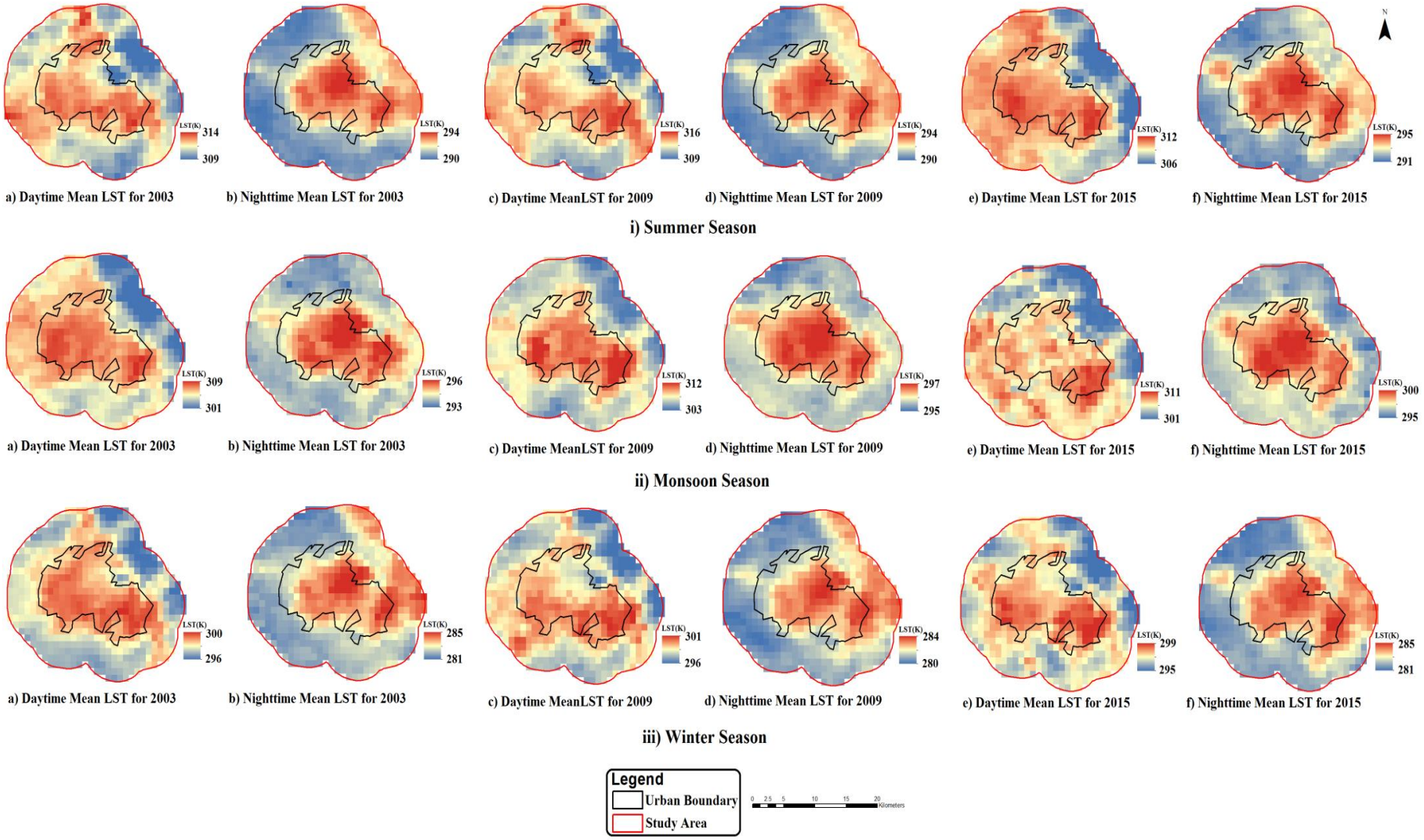

Fig. 4.5. Spatial and Diurnal Variation of LST over Chandigarh

Day and night LST images show the existence of SUHI effect over the Chandigarh study area. General LST profile during day and night period is almost same during all seasons where some significant variations have been observed over rural areas. Urban areas show higher LSTs than rural areas for all seasons. Eastern and North-East part of rural areas comprising of Shivangi hill ranges show significant diurnal LST variations due to effect of vegetation and exposed rock surfaces. The LST of this region is lower than the LST of most of the other parts of study area due to the effect of vegetation during daytime. However, during night time the rocks under the vegetation release some energy and consequently the LSTs of this part of rural area is higher than other parts of the rural area but similar to the urban area. Also, Western, South-Western and North-Western part of the rural areas shows significant diurnal LST variations due to effect of mixed barren and agricultural land.

Table 4.3: Seasonal and Annual Average of Maximum Night SUHI Intensity for Different Seasons of Chandigarh City

Season	2003	2004	2005	2006	2007	2008	2009	2010	2011	2012	2013	2014	2015	overall average
Summer	5.29	5.27	6.39	4.99	5.58	5.72	6.08	5.91	5.66	5.83	5.59	6.06	5.36	5.67
Monsoon	4.66	4.70	5.25	4.63	5.52	4.10	3.76	4.85	4.26	4.58	5.04	4.30	4.70	4.64
Winter	4.55	5.50	5.05	4.95	5.36	5.00	5.11	4.94	5.38	5.11	4.94	4.82	4.76	5.04
Annual	4.87	5.21	5.59	4.89	5.48	5.00	5.04	5.30	5.24	5.26	5.20	5.17	4.95	5.17

Table 4.3 gives the average maximum night UHI intensity during different seasons of the study period. The maximum UHI intensity varies from 6.94 to 9.50 K during summer season and 6.24 to 13.36 K during monsoon season and 5.80 to 10.20 K during winter season. Similarly minimum UHI intensity varies from 2.58 to 4.30 K, 2.34 to 3.54 K, and 3.00 to 4.30 K for summer, monsoon and winter seasons, respectively. Overall average of maximum UHI intensity of the study area during summer, monsoon, and winter seasons is 5.67 K, 4.64 K, and 5.04 K, respectively. Overall average of maximum SUHI intensity of the study area for the entire study period is 5.17 K. Low maximum average UHI intensity has been observed over Chandigarh study area compared to Jaipur and Ahmedabad cities. Chandigarh is a well-planned city with sub-tropical climate, and the city comprises of parks, water bodies (Sukhna lake), forest (Daria reserved forest in between Chandigarh and Panchkula) which probably affect the UHI growth.

Fig. 4.6 shows the temporal and diurnal variation of mean UR_{UHI}. The observation shows a clear picture of the existence of SUHI during the night for all the seasons, with hotter urban area than the surrounding non-urbanized areas. During the summer season, average

day UR_{UHI} varies from 1.02 K to 1.73 K with a mean day UR_{UHI} of 1.47 K, during a span of 13 years. The average seasonal intensity during night time in summer season ranges from 1.21 K to 1.51 K with a mean night UR_{UHI} of 1.36 K. Day UR_{UHI} is slightly higher than night UR_{UHI} during summer season. During monsoon season, average day UR_{UHI} varies from 1.92 K to 2.97 K with a mean day UR_{UHI} of 2.53 K. Corresponding intensity during night time in monsoon season ranges 0.89 K to 1.25 K with a mean night UR_{UHI} of 1.06 K. During the winter season, average day UR_{UHI} varies from 0.92 K to 1.48 K with a mean day UR_{UHI} of 1.17 K. The average intensity during night time in winter season ranges from 0.83 K to 1.16 K with an average mean night UR_{UHI} of 0.98 K. Annual night and day mean UHI intensities have been observed to be 1.14 K and 1.53 K, respectively. SUHI has been found to be the strongest and the weakest during summer and winter season, respectively during night time. Conversely, during the day time, SUHI has been observed to be weak for summer and winter season and strong for monsoon season with higher mean UR_{UHI} values than night time. Hence significant diurnal surface temperature variations on different seasons have been observed over the study area.

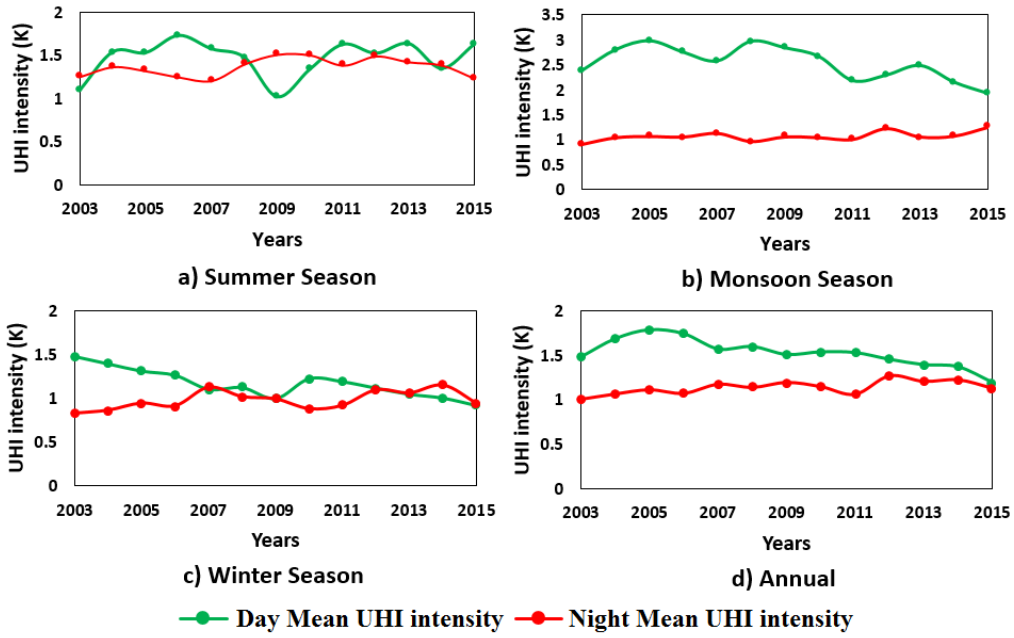

Fig. 4.6. Temporal and Diurnal Variation of Mean UHI Intensity (Chandigarh)

4.1.4 Spatio-Temporal UHI_{index} Pattern

The maximum and minimum temperatures for different periods of different years are highly variable, depending on the season of the year. Similarly, the UHI intensity at a particular location also varies considerably. Due to these reasons, it is very difficult to compare UHI

intensity at a particular location during different periods. Further, it is not possible to calculate the consolidated UHI effect over the study area from the LST data for a long period. In order to facilitate such calculations, UHI_{index} has been used which is a normalized index with values between 0 and 1. For any LST image, pixels of minimum and maximum temperature have UHI_{index} value between 0 and 1, respectively, while rest of the pixels have a value between 0 and 1. The average value of UHI_{index} for the entire study period will indicate the combined UHI effect over different parts of the study area.

4.1.4.1 Diurnal Average UHI_{index} Pattern of Jaipur City

Diurnal variation of UHI_{index} has been analyzed in the study. Fig. 4.7 shows the average UHI_{index} images of the study area derived separately from daytime and nighttime images. Contrast diurnal UHI_{index} pattern has been observed over the study area. Discrete UHI_{index} pattern can be observed during day period. As the distance from CBD increases, increasing trend of the values of UHI_{index} has been noticed over the study area, while inverse trend has been observed during night period.

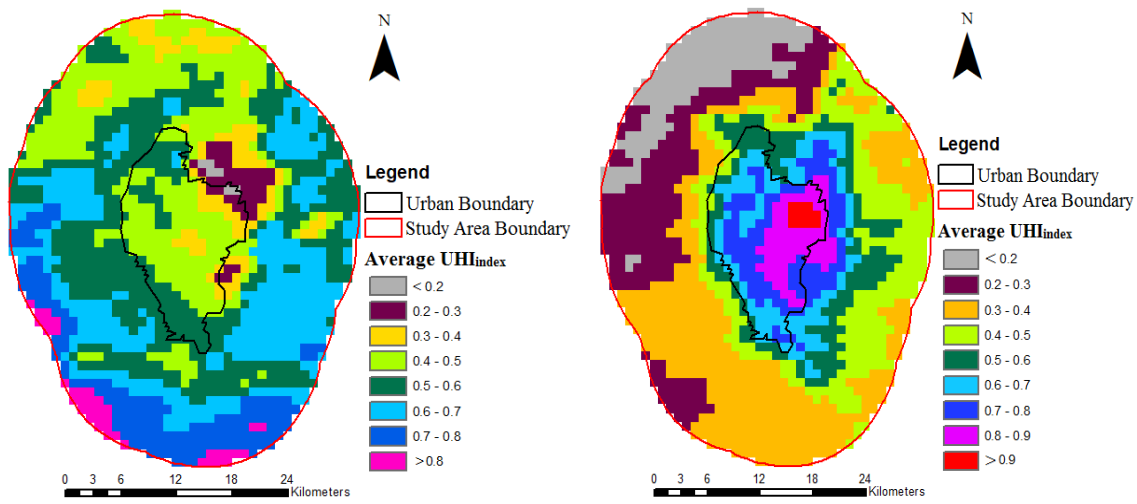

a) Day Period **b) Night Period**

Fig. 4.7. Average UHI_{index} Image of the Jaipur Study Area

a) Day Time Average UHI_{index} Pattern

UHI_{index} of all the pixels of the study area has been calculated for each image separately thus normalizing the LST of each pixel of the LST image between 0 and 1 and the process is repeated for the entire study period (258 day time images of 13 years from 2003 to 2015). Average of the UHI_{index} of all the images has been calculated. Fig. 4.7a shows the average

UHI_{index} image of the study area during day period. Rural areas show higher average UHI_{index} values that range from 0.60 to 0.88. Most of the urban areas has average UHI_{index} range of 0.30 to 0.60. From the image, it is clear that there is no existence of SUHI effect during day period.

The maximum value of average UHI_{index} is 0.88, and all the pixels in pink colour in Fig. 4.7a correspond to the average UHI_{index} value of more than 0.80. These higher temperature pixels are located at the Sothern and South-West part of the rural area near the study area boundary. The urban area has low-temperature pixels and the maximum and minimum values of average UHI_{index} in the urban area are 0.60 and 0.14, respectively and mean of average UHI_{index} of the urban area is 0.46. The maximum and minimum values of average UHI_{index} corresponding of rural area are 0.88 and 0.14, respectively. Mean of Average UHI_{index} corresponding to the rural area is 0.57, i.e. mean of average UHI_{index} of rural area is higher than the urban area which clearly depicts the existence of inverse or negative SUHI over the study area during day period. Very low UHI_{index} values ranging from 0.14 to 0.30 have been observed on the Eastern part of the urban boundary comprising of Aravalli hill ranges. North-Western part of the rural area comprising of agricultural field show average UHI_{index} range from 0.30 to 0.50. South and South-West part of the rural area near to the study area boundary shows higher UHI_{index} (greater than 0.80) pixels.

b) Night Time Average UHI_{index} Pattern

Average UHI_{index} of all the pixels of the study area has been calculated (451 night time images of 13 years from 2003 to 2015) similar to the daytime average UHI_{index}, and Fig. 4.7b shows the average UHI_{index} over the study area. The maximum value of average UHI_{index} is 0.95, and all the pixels in red colour in Fig. 4.7b correspond to the average UHI_{index} value of more than 0.90. These pixels which are the part of the CBD of Jaipur city, are the centre of the heat island. Other high-temperature pixels are located around these pixels. Average UHI_{index} of 11 pixels falling in CBD is more than 0.90 which indicates that high LST normally occurs on these pixels and they can be considered as hot spots (HS). The HS act as the centre of UHI of Jaipur city and other high-temperature pixels are located around these pixels.

The urban area has only high-temperature pixels and the minimum value of average UHI_{index} in the urban area is 0.41 and mean of average UHI_{index} of the urban area is 0.73.

The maximum and minimum values of average UHI_{index} corresponding of rural area are 0.87 and 0.09, respectively. Though the average UHI_{index} values in some parts of the rural area are also high, but most of these pixels fall in the Aravalli hill range, and the high temperature over these pixels is due to the exposed surface of rocks. The minimum average UHI_{index} value of 0.09 indicates that minimum temperature pixels of the entire study area are not same during different periods. Mean of Average UHI_{index} corresponding to the rural area is 0.38. Clear picture of SUHI has been observed during night period, i.e. as the distance from HS increases, LST decreases. The overall temperature pattern is similar to that discussed earlier, and the UHI_{index} can be conveniently used for comparison of UHI intensity at a particular location during different periods or UHI intensity of different locations during different periods.

Significant diurnal LST variations during different seasons have been observed in the study area, and contrast diurnal behavior in the thermal pattern for heat island effect has also been observed. The clear contrast in temperature between urban and rural area is evident, showing the clear existence of SUHI during night time, while inverse or negative SUHI is noticeable during day period.

4.1.4.2 Diurnal Average UHI_{index} Pattern of Ahmedabad City

Fig. 4.8 shows the diurnal average UHI_{index} images of Ahmedabad study area. Discrete UHI_{index} pattern has been observed during daytime, whereas clear SUHI has been observed during nighttime.

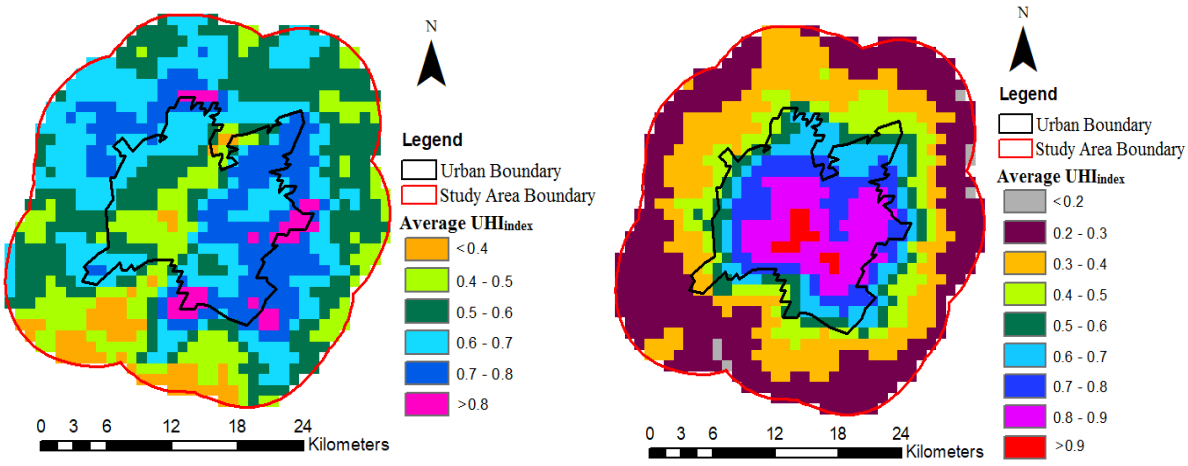

a) Day Period **b) Night Period**

Fig. 4.8. Average UHI_{index} image of the Ahmedabad study area

a) Day Time Average UHI_{index} Pattern

Fig. 4.8a shows the average UHI_{index} image of the study area during day time, calculated from 339 daytime images of 13 years from 2003 to 2015. From the image, it can be interpreted that there is no clear effect during daytime. High UHI_{index} pixels are located at both urban and rural areas in a discrete manner. Eastern part of the urban area (old city) shows higher UHI_{index} values than Western part of the urban area (new city). Centre of the city shows very low UHI_{index} values (0.33 to 0.50) due to the influence of Sabarmati River. Most of the UHI_{index} values greater than 0.80 are located at the Eastern and Southern location of the urban boundary. UHI_{index} pixels having minimum values (less than 0.40) can be observed at the Southern part of the rural area where vegetation density is very high. Maximum and minimum average UHI_{index} values for urban area are 0.87 and 0.33, respectively and corresponding maximum and minimum average UHI_{index} values for rural area are 0.86 and 0.32, respectively. i.e. higher and lower range UHI_{index} values are more or less equally distributed at both urban and rural areas. Mean of average UHI_{index} values for urban and rural area is 0.63 and 0.58, respectively.

b) Night Time Average UHI_{index} Pattern

491 good quality night time images have been used to calculate average UHI_{index} map of Ahmedabad study area (Fig. 4.8b). The maximum value of average UHI_{index} is 0.92, and all the pixels in red colour in Fig. 4.8b correspond to the average UHI_{index} value of more than 0.90. Average UHI_{index} of 13 pixels is more than 0.90 which indicates that high LST normally occurs on these pixels. These pixels can be considered as the center of the heat island and they can be considered as HS with other high-temperature pixels are located around these pixels.

The urban area has only high-temperature pixels and the minimum value of average UHI_{index} in the urban area is 0.31 and mean of average UHI_{index} of the urban area is 0.74. The maximum and minimum values of average UHI_{index} corresponding of rural area are 0.85 and 0.18, respectively. Mean of Average UHI_{index} corresponding to the rural area is 0.35. Clear picture of SUHI has been observed during night period, i.e. distance from HS increases, UHI_{index} decreases.

4.1.4.3. Diurnal Average UHI_{index} Pattern of Chandigarh City

Fig. 4.9 shows the diurnal average UHI_{index} images of Chandigarh study area. SUHI existence can be observed for both day and night periods with different thermal patterns.

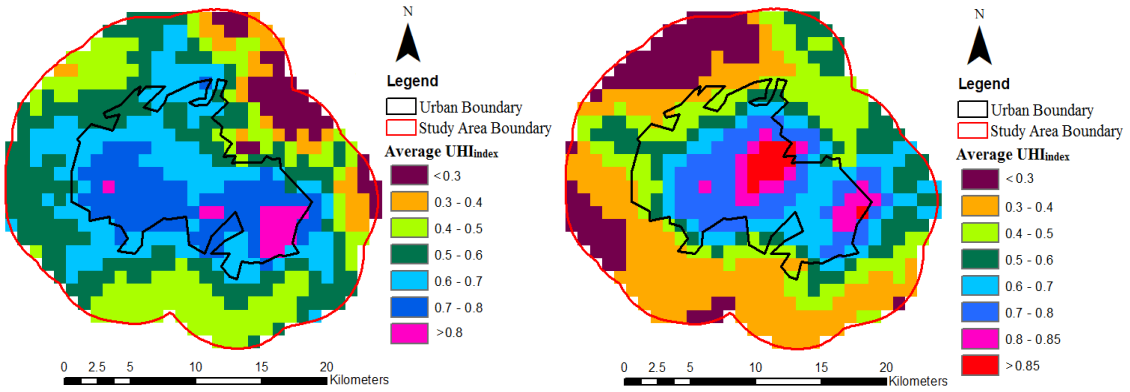

a) Day Period **b) Night Period**

Fig. 4.9. Average UHI_{index} Image of the Chandigarh Study Area

a) Day Time Average UHI_{index} Pattern

UHI_{index} has been calculated for 453 day time images of 13 years from 2003 to 2015, and average of the UHI_{index} of all the images has been calculated. Fig. 4.9a shows the daytime average UHI_{index} image of the study area. Existence of moderate SUHI effect can be observed during day period. High UHI_{index} pixels are located within the urban area in a discrete manner. However, these are less random compared to corresponding daytime average UHI_{index} images of Jaipur and Ahmedabad. Maximum and minimum average UHI_{index} values for urban area are 0.85 and 0.54, respectively and corresponding maximum and minimum average UHI_{index} values for rural area are 0.77 and 0.20, respectively. Mean of average UHI_{index} values for urban and rural area are 0.70 and 0.50, respectively. Most of the UHI_{index} values greater than 0.80 have been located at the Eastern part of the urban area. Most of the urban area covers UHI_{index} values in the range of 0.60 to 0.85. UHI_{index} pixels having minimum values (less than 0.30) are observed at the North-Eastern part of the rural area comprising of Shivangi hill ranges where vegetation density is very high. Most of the rural area covers UHI_{index} values in the range of 0.20 to 0.60. Urban area shows higher UHI_{index} values compared to rural areas which clearly shows that moderate SUHI effect observed over the study area.

b) Night Time Average UHI_{index} Pattern

UHI_{index} has been calculated from 555 night time images, and an average UHI_{index} of all the images has been calculated (Fig. 4.9b). The maximum value of average UHI_{index} is 0.89, and all the pixels in red colour in Fig. 4.9b correspond to the average UHI_{index} value of more than 0.85. Average UHI_{index} of 11 pixels falling in CBD is more than 0.85 which indicates that high LST normally occurs on these pixels and they can be considered as hot spots (HS).

The minimum value of average UHI_{index} in the urban area is 0.36 and mean of average UHI_{index} of the urban area is 0.66. Most of the urban area covers UHI_{index} values in the range of 0.60 to 0.89. The maximum and minimum values of average UHI_{index} corresponding to rural area are 0.85 and 0.23, respectively. Mean of Average UHI_{index} corresponding to the rural area is 0.42. UHI_{index} pixels having minimum values (less than 0.30) are observed at the North-Western and Western part of the rural area comprise of agricultural fields. Clear picture of SUHI has been observed during night period, i.e. as distance from HS increases, pixels of lower UHI_{index} value are observed. The overall temperature pattern is similar to that discussed earlier, and the UHI_{index} can be conveniently used for comparison of UHI intensity at a particular location during different periods or UHI intensity of different locations during different periods.

Day and night images show the existence of SUHI effect over the study area. But the daytime and nighttime SUHI patterns are entirely different and show significant variations. Diurnal and temporal variations in UHI effect over three Indian cities has been studied. There is no existence of surface heat island during day period especially for Jaipur and Ahmedabad cities, whereas clear SUHI has been observed during night for all cities. i.e. SUHI is predominantly a nocturnal phenomenon. Day SUHI effect has also been observed over Chandigarh city, where day SUHI intensity has been observed to be higher than night SUHI intensity. However, the daytime SUHI pattern is random whereas the nighttime SUHI pattern is similar to an island with high UHI_{index} pixels as the center and low value pixels around the high value pixels. For Ahmedabad and Jaipur, night SUHI intensity has been observed to be higher than day SUHI intensity. Diurnal and seasonal LST variations have been observed in these cities which may depend on a number of factors and parameters. Some of these have been discussed in subsequent sections.

4.2 Spatio-Temporal SUHI Growth Pattern and Variations over Indian Cities

This section documents the results and discussion on SUHI growth of the three cities using UHI_{index} and transect methods. The analysis has been carried out using LST data at a gap of six years (2003, 2009 and 2015) from 2003 to 2015. UHI_{index} has been used to determine the HS locations. As the analysis has been carried out with respect to the location of HS, it is very important to determine the HS location very carefully. Though, LST data at a gap of six years has been used for analyzing the SUHI growth, data of 13 years i.e. from 2003 to 2015 has been used to fix HS location. Only night time LST images have been used for carrying out the analysis.

UHI effect causes a temperature gradient from the HS to the outer boundary of the study area. This gradient may, however, be different in different directions. Transects have been run, from HS to outer boundary of the study area for transect analysis. Two transects have been marked in the N-S and E-W directions, and two transects have been drawn at 45^o from these transects (For Jaipur and Chandigarh). This makes a total of four transects and eight directions from the HS. Absolute temperature difference (i.e. the relative difference between the maximum temperature observed at the HS and temperature of the place under consideration) has been calculated. This relative difference is then plotted along the transects.

UHI_{index} and transect methods have been used to find the growth in SUHI effect, over the study area.

4.2.1 Spatio-Temporal SUHI Growth Pattern and Variations over Jaipur

4.2.1.1 SUHI Growth Analysis Using UHI_{index} Method

UHI intensity over a city is not constant and it varies in response to the constant changes happening within and around a city. As Jaipur is a growing city, SUHI effect over Jaipur city is expected to grow over a period of time. The mean UHI_{index} image shows that there are 11 pixels having mean UHI_{index} value above 0.90. It may be expected that over a period of time the UHI_{index} value of different pixels may change. If different categories are formed on the basis of mean UHI_{index} values and the number of pixels falling within a particular category does not change appreciably, over a period of time, it can be considered as the

case of stable SUHI pattern. However, if there is an increase in the number of pixels towards the higher range of UHI_{index}, it can be considered as the incidence of higher LST on some pixels which otherwise had relatively lower temperature compared to the pixels having maximum LST i.e. HS. This shall mean that, in comparison to the previous time period, LST of more number of pixels gets close to the LST of HS. This indicates that more area is encountering higher LSTs and thus increase in UHI effect over the city can be established.

In order to analyze the change in SUHI effect over Jaipur city, all the pixels of the study area have been classified into different categories on the basis of their mean UHI_{index}. Pixels with mean UHI_{index} value above 0.90 have been classified as falling in category HS. The average of mean UHI_{index} values of all the pixels inside the urban boundary is 0.78. All the pixels having mean UHI_{index} value between 0.75 and 0.90 have been classified prospective HS (category PHS). LST of these pixels is close to the LST of HS and these pixels can soon be converted into HS due to continuing growth of the city. Minimum value of UHI_{index} of urban area is 0.41. Pixels having UHI_{index} values above 0.50 but less than 0.75 have been considered as developed land (DL) and all pixels with mean UHI_{index} value above 0.50 are mostly within the urban boundary and have been jointly classified as urban zone (category UZ). All the pixels with mean UHI_{index} value below 0.25 have been considered to be falling in undeveloped land and categorized as UL. Pixels not falling in the undeveloped land have undergone some extent of development i.e. pixels with mean UHI_{index} value above 0.25 but less than 0.50 have been categorized semi developed land (SDL) and both UL and SDL have been jointly classified as rural zone (category RZ) also.

The change in SUHI has been analyzed using LST images of three years at six years' time interval (2003, 2009 and 2015). The analysis has been carried out on seasonal basis and images corresponding to summer, monsoon and winter season of the three study seasons have been considered separately. Annual mean UHI_{index} for each pixel has been calculated by averaging the UHI_{index} from images of a particular season for each year separately. A comparative plot of the area of pixels falling in different categories during different years has been given in Figs. 4.10, 4.11 and 4.12 for summer, monsoon and winter seasons, respectively. The number of LST pixels corresponding to area is shown on the top of each bar (Figs. 4.10, 4.11 and 4.12). The number of pixels having annual mean UHI_{index} value more than 0.90, for the year 2003, is 6, 7 and 13 for summer, monsoon and winter season,

respectively. The thermal coefficient of different surfaces is different and the range of LST during different seasons is also different. The behavior of different surfaces for different range of LST is highly varying, which results in different number of pixels representing HS, during different seasons. HS area, in 2003, is about 5.2 km^2, 6.0 km^2, and 11.2 km^2 in summer, monsoon and winter seasons, respectively. The corresponding area increases to 12.9 km^2, 14.6 km^2, and 13.7 km^2, respectively in 2009 and further increases to 15.5 km^2, 19.7 km^2, and 28.3 km^2, respectively in 2015. Consistent increase in area under HS has been observed during the two 6 year intervals. The increase is different during different seasons which can be due to varied reasons. Overall, an increase of 150% to 225% can be observed, in the HS area, during different seasons between 2003 and 2015. The total number of pixels under HS in 2015 (18, 23 and 33 pixels for summer, monsoon and winter seasons, respectively) is more than the number of pixels under HS as observed from mean UHI_{index} in Fig. 4.7 (11 pixels). This is because 13 year data from 2003 to 2015 has been considered for calculating mean UHI_{index} shown in Fig. 4.7 and the overall effect of averaging the data for a long period results in toning down the effect that can be observed during later years. On the other hand data of different seasons of 2015 has been utilized in finding HS during 2015. **This indicates that the SUHI growth over Jaipur city is still continuing and more area is becoming warmer with the passage of time.**

Similar trend can also be observed for the other category representing PHS. Between 2003 and 2015, the increase in area under category PHS, during different seasons, has been observed to be between 35 to 45 km^2. Area of pixels under the category PHS has increased by 10% to 35% during different seasons between 2003 and 2009 whereas this increase is from 40% to 65% during different seasons between 2003 and 2015. Area under category DL shows mixed trends with both increase and decrease in area under DL can be observed during different time intervals depending on the season. However, when the analysis is extended using UZ, it can be seen that total area under UZ increases by up to 12% for the period from 2003 to 2009 and the increase is up to 31% for the period from 2003 to 2015. This indicates that area of urban zone is increasing consistently with time. Some reduction in area under DL is due to shifting of more area from DL to higher LST categories of HS/PHS as compared to shifting to DL category from lower LST category of SDL/UL. Increase in UZ area means that the rural area of Jaipur city or the area near the urban boundary of Jaipur city that used to be relatively cooler earlier is becoming warmer and more and more part of the city is shifting from lower category to next category thereby

indicating an overall increase in the UHI effect. **Overall growth in SUHI, represented by increase in area under different categories, has been observed over Jaipur city during the period from 2003 to 2015 which indicates the clear picture of heat island growth in the study area and consequent decrease in human thermal comfort level.**

Categories SDL and UL that represent rural area also show different pattern than that by the HS/PHS categories. It can be seen from Figs. 4.10, 4.11 and 4.12 that the area under categories RZ and UL either increases or reduces during different seasons and also during different 6 years periods. Between 2003 and 2009, area under SDL increases during summer season but reduces during monsoon and winter seasons, whereas the area under UL decreases during summer season but increases during monsoon and winter seasons. Similarly, the trend between 2009 and 2015 is also mixed. The change in area under category SDL is absolutely opposite to that of the category UL during different seasons of all the periods. However, when the total area under categories SDL and UL is considered, a consistent decrease in the total area can be observed. The total area represented by rural categories is 947.1 km^2, 920.5 km^2, and 1063.8 km^2 during summer, monsoon and winter seasons, respectively, for 2003. The corresponding area reduces to 930.8 km^2, 916.2 km^2, and 1026.1 km^2, respectively, during 2009 and further reduces to 904.1 km^2, 882.7 km^2, and 968.5 km^2, respectively, during 2015. LST of any place is dependent on a variety of factors and the quantum of vegetation as well as the magnitude of impervious/built-up surface in the area of interest (or pixel) are very important parameters which are linked to each other and are related to the process of urbanization. In the rural area the change in magnitude of impervious/built-up surfaces is gradual and once this change has taken place, this is not reversed usually. In such a case the change in the area under the rural category shall have been similar and in one direction i.e. either increasing or decreasing order. However, LST has been observed to change with vegetation type also and agriculture practiced in the desert area shows the highest LST, followed by rainfed agriculture, irrigated agriculture, and forest. The variation in surface temperature is also determined by various vegetation covers on the Earth‘s surface in addition to rapid changes in climate attributable to climate sources in the study area (Parida et al., 2008). In general, for image pixels those are not entirely occupied by single homogenous vegetation or barrens soil, LST measurements indicate a mixture of soil and vegetation canopy temperatures, resulting from composite signatures. During monsoon season, the amount of vegetation determines LST by the latent heat flux from the surface to atmosphere via evapotranspiration and lower

LSTs are usually observed in areas with high vegetation density. The amount and quantum of vegetation depend on rainfall as well as on the quantity of water available. In the event of good rainfall, the vegetation density may be more resulting in comparatively lower temperature at those places and the area may fall under UL category. On the other hand, in the times of deficient rainfall, the area may move from UL category to the higher LST category of SDL. Due to the effect of this movement though the area under categories SDL and UL, independently does not show any pattern, but it follows a falling pattern if these are considered together as RZ.

The UHI effect is in terms of increase in the temperature of urban area compared to its rural surroundings. Area under category UZ has increased with the passage of time. The increase in area of UZ has been due to increase in LST of some part of the study area and hence movement of some area from lower UHI_{index} category to higher UHI_{index} category. The categories representing rural area have reduced area under them as development has been undertaken in this area resulting in the migration of that land from lower temperature to higher temperature categories and movement of some area of these categories to category SDL. This clearly indicates that there is an increase in the urban area and reduction in rural/UL. Increase in LST of some parts of the city is causing continuous growth in SUHI over Jaipur city.

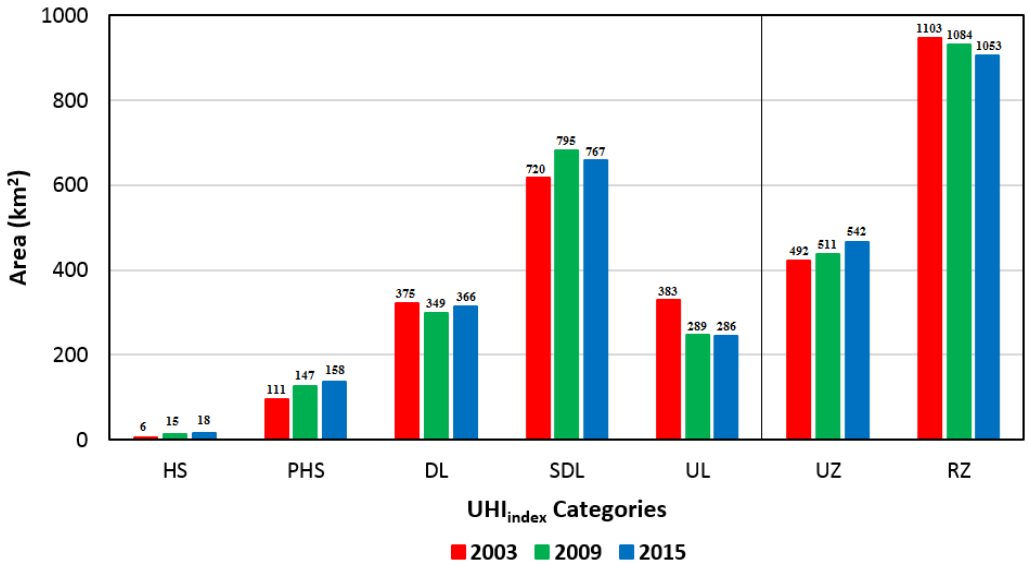

Fig. 4.10. SUHI Growth during Summer Season (Jaipur)

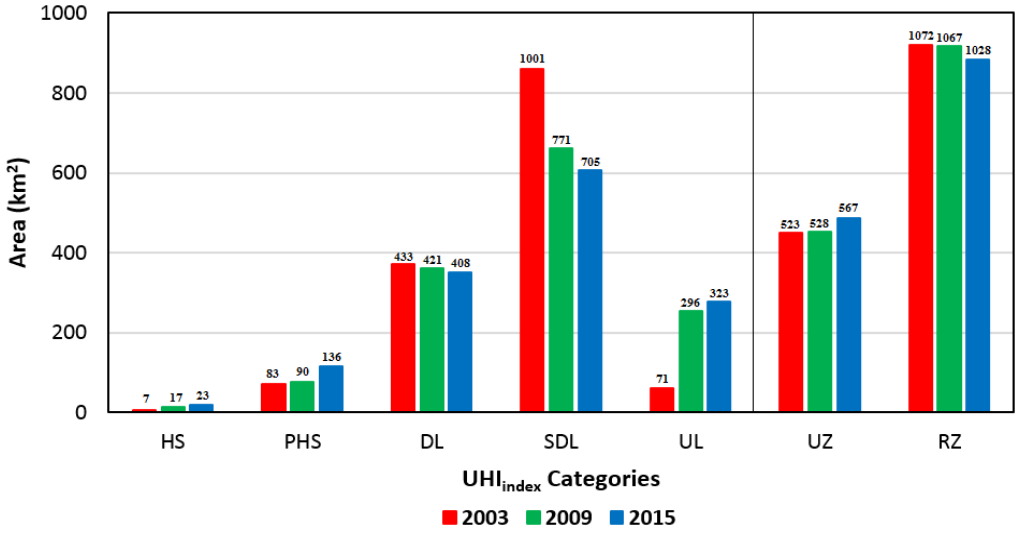

Fig. 4.11. SUHI Growth during Monsoon Season (Jaipur)

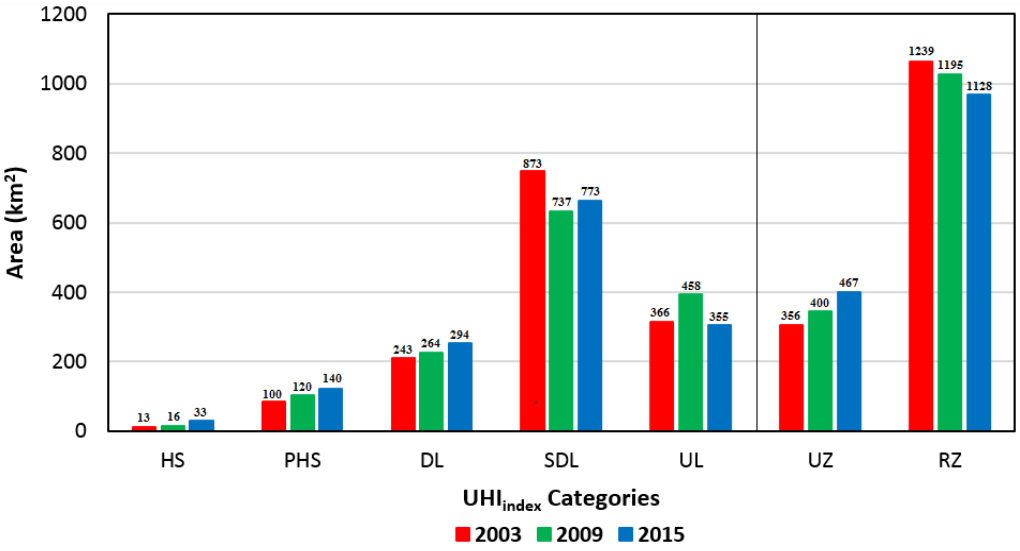

Fig. 4.12. SUHI Growth during Winter Season (Jaipur)

4.2.1.2 SUHI Growth Analysis using Transect Method

It has been observed from UHI_{index} analysis that number of pixels under HS of Jaipur city has consistently increased. Growth of SUHI has also been analyzed using transects. Transect analysis has been done by analyzing the LST of various pixels with respect to the LST of pixels of maximum temperature i.e. HS. Seasonal analysis has been carried out and for the purpose of this analysis, all the image of a particular season of a particular year have been taken, and the mean LST of each pixel of the study area corresponding to all the images of a particular season for each study year (2003, 2009 and 2015) has been calculated. Mean LST images for summer, monsoon and winter seasons have been shown in Figs. 4.13, 4.14 and 4.15, respectively. Centroid of the HS (CHS) has been marked on

the mean LST image and transects have been run, as explained earlier, in different directions through the CHS. Average of mean LST of all pixels falling under HS has been considered to be the temperature at the CHS. Pixels corresponding to every 1° C fall in temperature with respect to the CHS are marked along each transect. Lines passing through these pixels corresponding to each 1° C fall in LST with respect to the LST of CHS i.e. isothermal lines of fall in LST have been marked as -1° C, -2° C, -3° C, -4° C, and -5° C in Figs. 4.13, 4.14 and 4.15. Negative sign indicates that the isothermal line under consideration has LST lower than that of the average LST of the CHS.

The CHS is near the East and North-East of the urban boundary. The isothermal line of -1° C is nearly a circle in most of the images. An increase in the area enclosed by this isothermal line, can be seen from images of the same season, corresponding to each six year time period. This represents an increase in area where the LST is within 1° C of the LST of CHS. Images corresponding to each season show similar patterns but the pattern shown by images of different seasons is quite different.

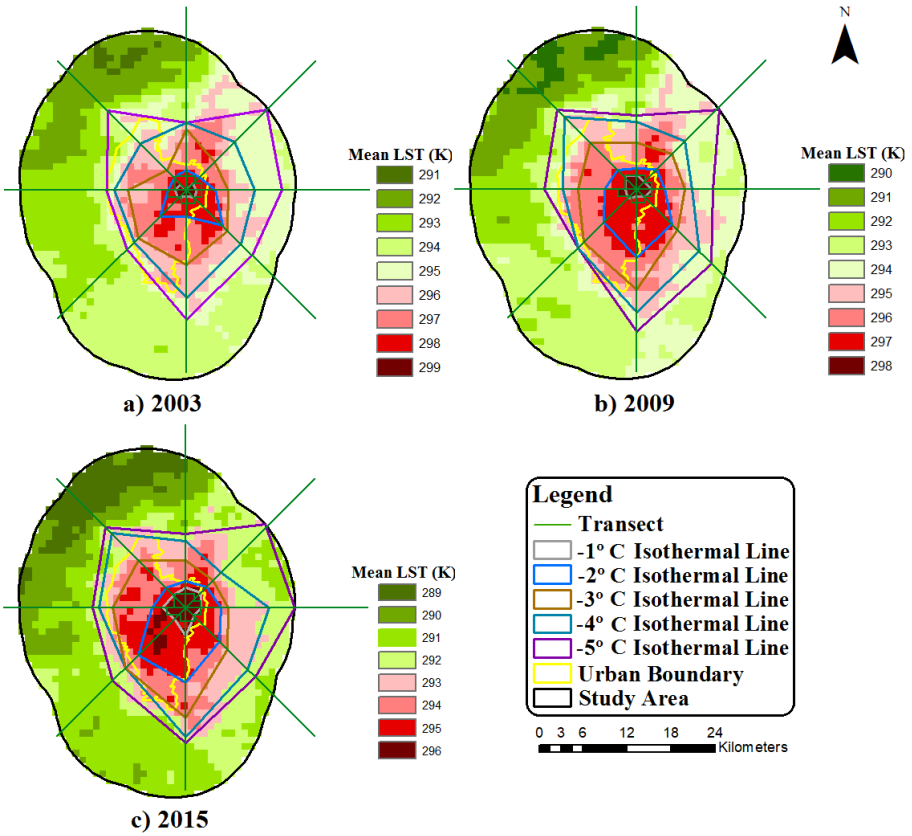

Fig. 4.13. Mean LST Images and Isothermal Lines for Summer Season (Jaipur)

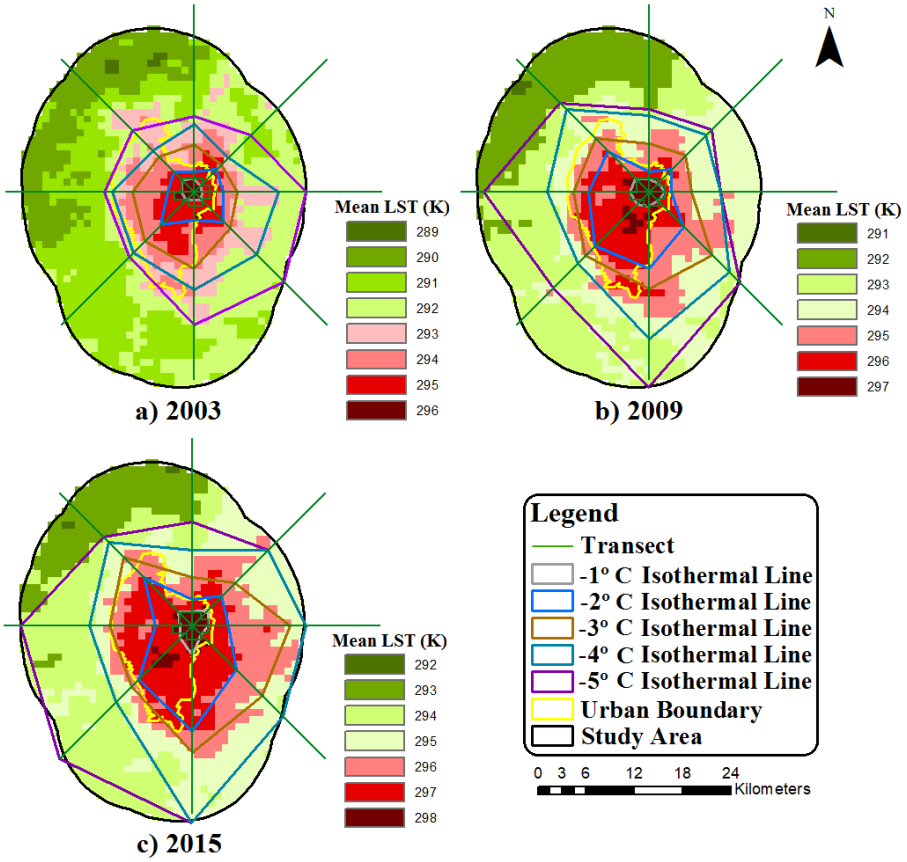

Fig. 4.14. Mean LST Images and Isothermal Lines for Monsoon Season (Jaipur)

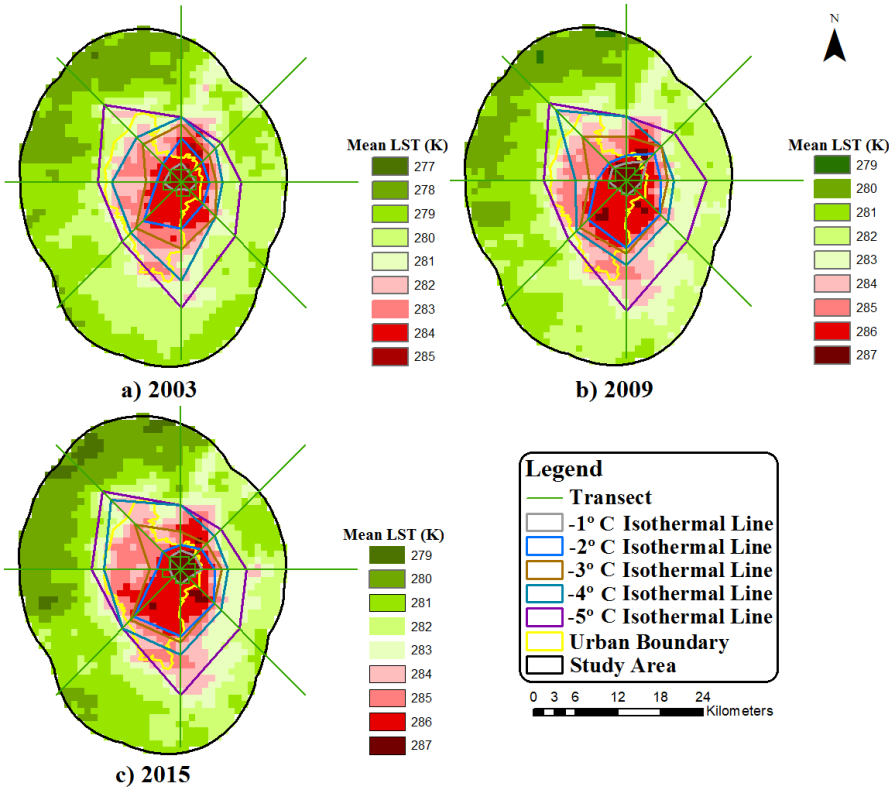

Fig. 4.15. Mean LST Images and Isothermal Lines for Winter Season (Jaipur)

Spacing between different isothermal lines of an image is not uniform and it is different in different directions. The spread of summer images is more towards the East as compared to the west direction which means that the temperature gradient is steeper in West direction. Monsoon images show a spread in both directions whereas winter images are very compact. The difference in the images is due to the development of different parts of the city during different times and also due to different extent of development of these areas. Oke (1973) indicated that the UHI magnitude mainly depends on the size and geometry of the city.

The concentration of lowest temperature pixels can be seen in the North Western part of the study area. The predominance of the agricultural area in North Western parts of the study area contains the temperature in this area. The harvesting of crop reduces the cooling effect of vegetation, and the soil behaves similarly to that of a barren land (mainly during winter season). During winter season also Eastern parts of the study area shows significant variations in temperature growth for each one degree fall in temperatures from the HS similar to summer season.

Mean UHI intensity corresponding to summer seasons is 8^{o} C for 2003 and 2009 while it is 7^{o} C for 2015. For monsoon seasons the mean UHI intensity is 7^{o} C for 2003 and 6^{o} C for 2009 and 2015. The mean UHI intensity for winter seasons is uniformly 8^{o} C. As the mean UHI intensity, for a season, does not vary by large extent, any increase in area enclosed by isothermal line shall be a clear signature of increase in LST over some area and hence growth in SUHI effect. Total area enclosed within each isothermal line has been calculated and has been given in Table 4.4. It can be seen from the table that the area within each isothermal line of fall in LST steadily increases from 2003 to 2015. The increase in area enclosed by different isothermal lines, during monsoon season, is 17% to 30% between 2003 and 2009. Total increase between 2003 and 2015 varies from 19% to 27%. This increase is minimum across all seasons. The corresponding increase for summer season varies from 7% to 120% between 2003 and 2009 and 20% to above 400% between 2003 and 2015. It can be interpreted from the Table 4.4 that there is a continuous increase in LST of the Jaipur city and the temperature gradient between HS and area surrounding it is falling i.e. more and more area is noticing temperatures which are moving close to the temperature of HS.

Table 4.4: Total Area Enclosed within Various Isothermal Lines (Jaipur)

Legend/ Category	Summer			Monsoon			Winter		
	2003	2009	2015	2003	2009	2015	2003	2009	2015
Area of pixels within 1°C isothermal line	3.7	8.1	18.8	6.4	12.1	15.2	10.6	13.1	14.2
Area of pixels within 2°C isothermal line	40.3	81.2	106.3	49.3	133.9	166.9	76.4	93.2	97.3
Area of pixels within 3°C isothermal line	153.5	213.1	240.2	154.1	263.5	385.5	120.6	141.2	143.8
Area of pixels within 4°C isothermal line	299.2	363.7	402.1	298.4	517.8	712.5	214.9	267.8	285.0
Area of pixels within 5°C isothermal line	486.8	519.7	582.9	506.4	801.8	1047.0	302.4	393.2	415.3
Total area of all the pixels of study area	1369.5	1369.5	1369.5	1369.5	1369.5	1369.5	1369.5	1369.5	1369.5

In order to know the comparative increase in area between different isothermal lines, area falling within two consecutive isothermal lines has been calculated by subtracting area under inner isothermal line from the area under next isothermal line of fall, and is given in Table 4.5. It can be seen from the table that there is a continuous increase in area between different isothermal lines which indicates that there is an increase in the area of different parts of the city that are encountering higher LSTs with the passage of each six year time interval. Increase in percentage of area between higher order isothermal lines (representing lower difference in LST between HS and area under consideration) is multiple times that of corresponding increase between lower order isothermal lines (representing higher difference in LST between HS and area under consideration). The change in area is higher during summer and monsoon season as compared to during winter season.

Table 4.5: Total Area Enclosed Between Consecutive Isothermal Lines (Jaipur)

Difference in temperature with respect to LST of HS	Summer			Monsoon			Winter		
	2003	2009	2015	2003	2009	2015	2003	2009	2015
Up to 1° C	3.7	8.1	18.8	6.4	12.1	15.2	10.6	13.1	14.2
Between 1° C and 2° C	36.7	73.1	87.5	42.9	121.8	151.6	65.9	80.0	83.1
Between 2° C and 3° C	113.2	131.9	133.9	104.8	129.6	218.6	44.2	48.0	46.5
Between 3° C and 4° C	145.6	150.6	161.9	144.3	254.3	327.1	94.3	126.6	141.3
Between 4° C and 5°	187.6	156.0	180.9	208.0	284.0	334.5	87.5	125.4	130.3
More than 5° C	882.7	849.8	786.6	863.1	567.7	322.6	1067.2	976.3	954.2

There is a consistent change in the position of different parts of the city with respect to the isothermal lines. There is a gradual shift of area from low order isothermal lines towards higher order isothermal lines. This indicates an increase in the LST of this area signified by lower difference from LST of HS. The area falling outside 5^{o} C isothermal line is reducing in each consecutive time interval indicating that some part of the area that was relatively cooler earlier, compared to the HS, has undergone some modifications that have resulted into increase in its LST indicated by the lower difference between the LST of this part and that of HS. Rise in SUHI growth from 2003 to 2015 for six years' time interval in the study area indicates huge expansion of urban areas which directly affects the comfort and health of the residents of a city.

4.2.2 Spatio-Temporal SUHI Growth Pattern and Variations over Ahmedabad

4.2.2.1 SUHI Growth Analysis Using UHI_{index} Method

HS of the Ahmedabad study area have been extracted in the same fashion as that of Jaipur study area, discussed earlier. The cutoff limits for different categories have been kept same as those of Jaipur study area. A comparative plot of the area of pixels falling in different categories during different years has been given in Figs. 4.16, 4.17 and 4.18 for summer, monsoon and winter seasons, respectively. The number of LST pixels corresponding to area is shown on the top of each bar (Figs. 4.16, 4.17 and 4.18). The number of pixels having annual mean UHI_{index} value more than 0.90, for the year 2003, is 11, 5 and 20 for summer, monsoon and winter season, respectively. This variation is due to the difference in thermal coefficient of different surfaces for different temperature range. HS area, in 2003, is about 9.44 km^2, 4.29 km^2, and 17.17 km^2 in summer, monsoon and winter seasons, respectively. The corresponding area increase to 18.89 km^2, 16.31 km^2, and 25.76 km^2, respectively in 2009 and further increases to 33.49 km^2, 30.05 km^2, and 29.19 km^2, respectively in 2015. Consistent increase in area under HS has been observed during the two 6 year intervals. The increase is different during different seasons which can be due to varied reasons. Overall, an increase of 70% to 600% can be observed, in the HS area, during different seasons between 2003 and 2015. The total number of pixels under HS in 2015 (39, 35 and 34 pixels for summer, monsoon and winter seasons, respectively) is more than the number of pixels under HS as observed from mean UHI_{index} in Fig. 4.8 (13 pixels), which has been developed by averaging 13 year data from 2003 to 2015. More number of HS pixels in 2015 indicate that the SUHI growth over Ahmedabad city is still continuing

and more area is becoming warmer with the passage of time.

Similar increasing trend can also be observed for the other category representing PHS. Between 2003 and 2015, the increase in area under category PHS, during different seasons, has been observed to be about 29 to 46 km^2. Area of pixels under the category PHS has increased by 10% to 30% during different seasons between 2003 and 2009 whereas this increase is from 25% to 156% during different seasons between 2003 and 2015. Area under category DL and SDL shows mixed trends with both increase and decrease in area under these categories during different time intervals depending on the season. Changes in various land covers depending on different seasons may result in shift of area into different categories especially in rural zone resulting in different trends in rural categories. Total area under category UZ increases by up to 19% for the period from 2003 to 2009 and the increase is up to 29% for the period from 2003 to 2015. This indicates that area of urban zone is increasing consistently with time. Increase in UZ area means that the rural area of Ahmedabad city or the area near the urban boundary of Ahmedabad city that used to be relatively cooler earlier is becoming warmer and more and more part of the city is shifting from lower category to next category thereby indicating an overall increase in the UHI effect.

Categories SDL and UL that represent rural area also show different pattern than that by the HS/PHS categories. It can be seen from Figs. 4.16, 4.17 and 4.18 that the area under categories RZ and UL shows decreasing trend during different seasons and also during different 6 years period and mixed trend in UL category during winter season. Total area under categories SDL and UL, i.e. under RZ consistently decreases between 2003 and 2015. The total area represented by rural categories is 1236.44 km^2, 1248.46 km^2, and 1289.67 km^2 during summer, monsoon and winter seasons, respectively, in 2003. The corresponding area reduces to 1194.36 km^2, 1191.79 km^2, and 1279.37 km^2, respectively, during 2009 and further reduces to 1142.84 km^2, 1163.45 km^2, and 1229.57 km^2, respectively, during 2015. The UHI effect mainly depends on size and location of the place. i.e. UHI intensity tends to increase with increasing city size. Morris and Simmonds (2000) have reported that the location and features of differing synoptic conditions influence the magnitude of UHI. SUHI growth has been shown to be influenced by intrinsic nature of the city and other external parameters of the city such as size of the city, building density, land-use distribution, etc.

The UHI effect is in terms of increase in the LST of urban area compared to its rural surroundings. With respect to UHI effect, area of urban zone has increased with the passage of time. The increase in area of urban zone has been due to increase in LST and hence movement of some area from lower UHI_{index} category to higher UHI_{index} category. However, the categories representing rural area have reduced area under them as development has been undertaken in this area resulting in the migration of that land from lower temperature to higher temperature categories. This clearly indicates that there is an increase in the urban area and reduction in rural/undeveloped land and this is causing increase in LST of some parts of the city and continuous growth in SUHI over Ahmedabad city.

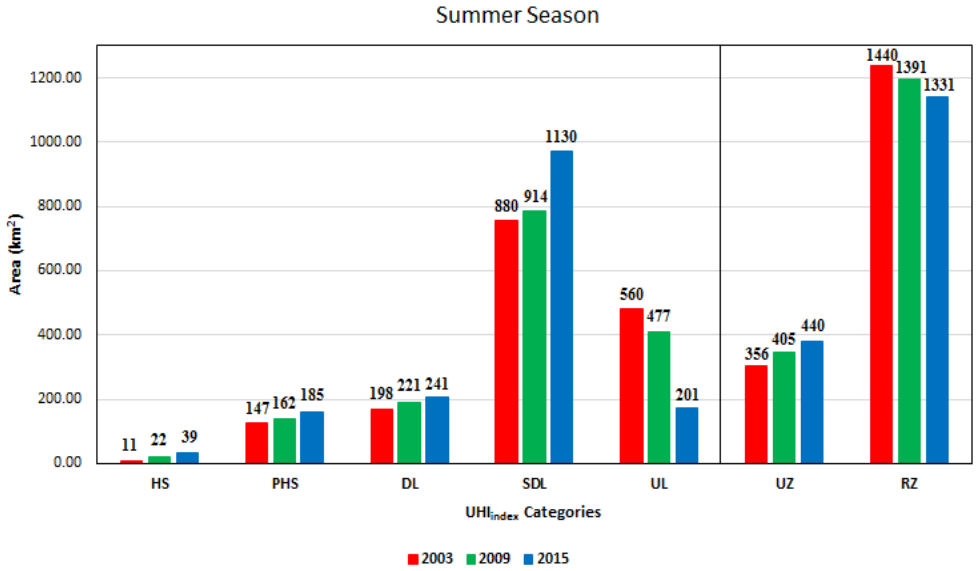

Fig. 4.16. SUHI Growth during Summer Season (Ahmedabad)

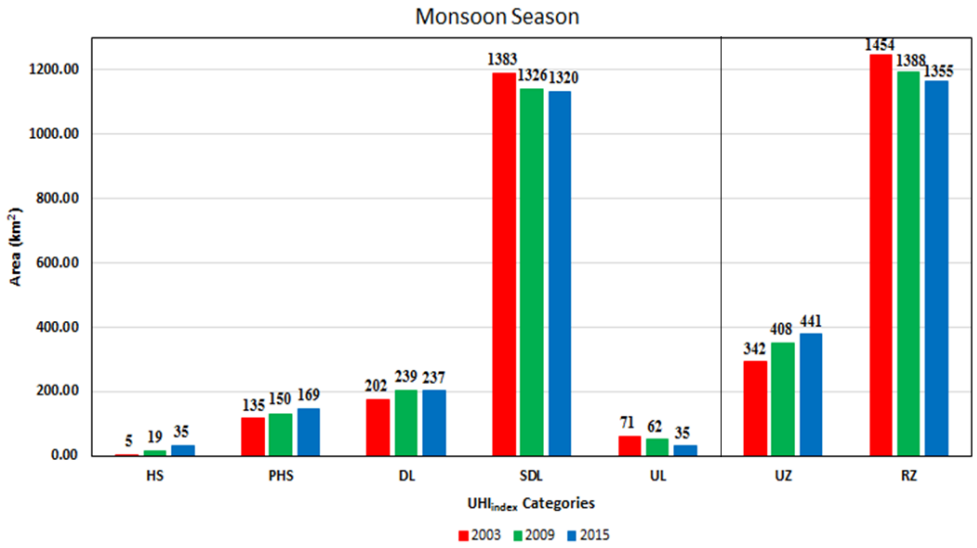

Fig. 4.17. SUHI Growth during Monsoon Season (Ahmedabad)

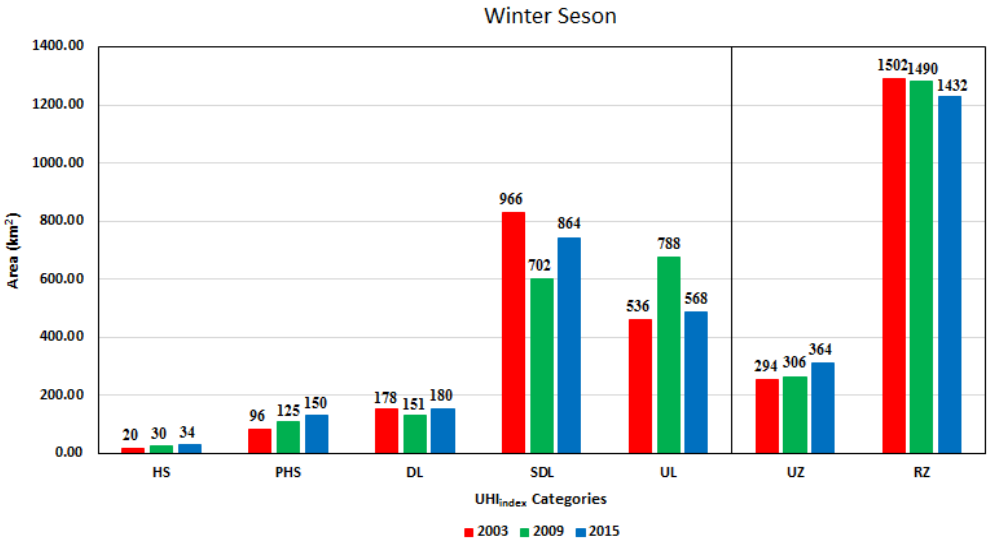

Fig. 4.18. SUHI Growth during Winter Season (Ahmedabad)

4.2.2.2 SUHI Growth Analysis using Transect Method

Mean LST for summer, monsoon and winter seasons of 2003, 2009, and 2015 has been calculated by considering the images of same season and average LST of each pixels for the season has been calculated. Mean LST images have been shown in Figs. 4.19, 4.20 and 4.21, respectively. HS pixels of Ahmedabad are distributed on other sides of Sabarmati river which runs in North-East to South-West direction. One transect is drawn by joining the CHS of both the HS and is extended up to the study area boundary. Two transects have been drawn at 90^{o} from this transect, one each from both the CHS. These transects are almost parallel to the Sabarmati river and these along with the transect passing through CHS of both the HS divide the space on both side of Sabarmati river in two direction each. These spaces have been then subdivided by drawing transects at 45^{0} each and extending from CHS up to study area boundary. This makes a total of five transects and ten directions from both the HS locations. Average of mean LST of all pixels falling under HS has been considered to be the temperature at the CHS at the base of transects. Pixels corresponding to every 1^{o} C fall in temperature with respect to the CHS are marked along each transect. Lines passing through these pixels corresponding to each 1^{o} C fall in LST with respect to the LST at CHS i.e. isothermal lines of fall in LST have been marked as -1^{o} C, -2^{o} C, -3^{o} C, -4^{o} C, and -5^{o} C in Figs. 4.19, 4.20 and 4.21.

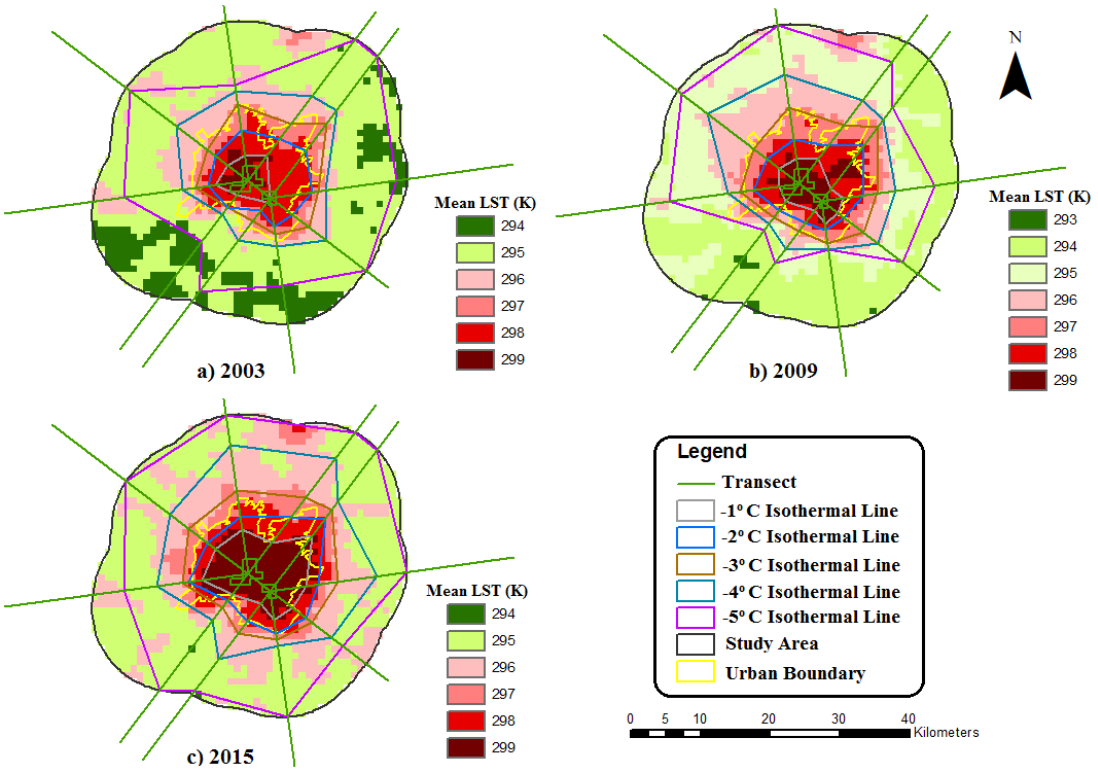

Fig. 4.19. Mean LST Images and Isothermal Lines for Summer Season (Ahmedabad)

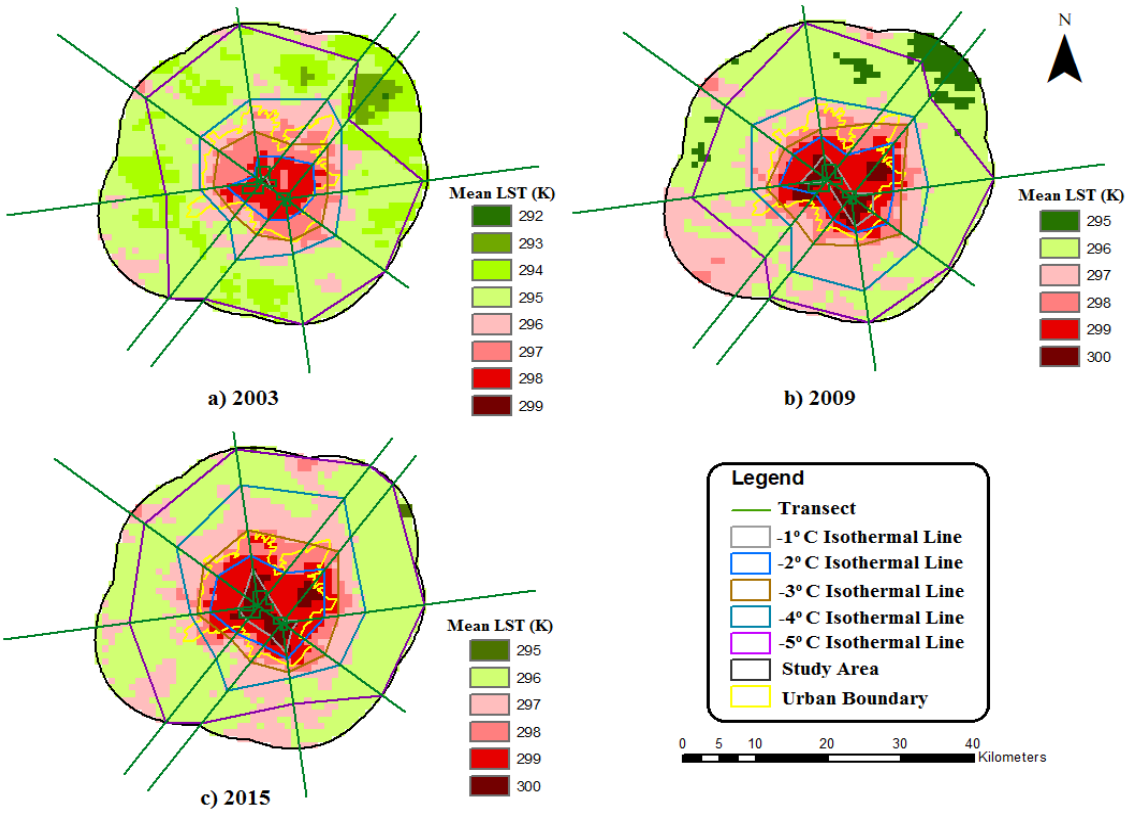

Fig. 4.20. Mean LST Images and Isothermal Lines for Monsoon Season (Ahmedabad)

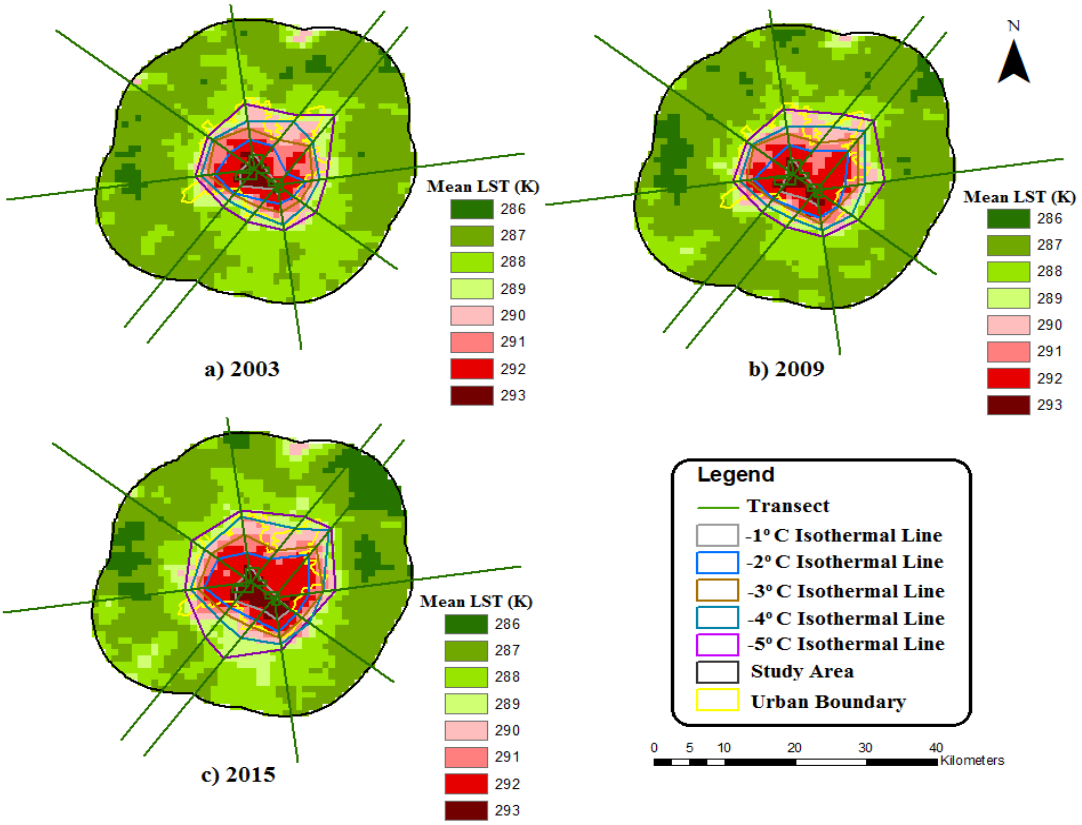

Fig. 4.21. Mean LST Images and Isothermal Lines for Winter Season (Ahmedabad)

A clear increase in the area enclosed by -1° C isothermal line, can be seen from images of the same season, corresponding to each six year time period. This represents an increase in area where the LST is within 1° C of the LST of CHS. Images corresponding to each season show similar patterns but the pattern shown by images of different seasons is quite different. Spacing between different isothermal lines of an image is not uniform and it is different in different directions. Summer images show a spread in different directions. Monsoon images also show a spread in different directions whereas winter images are very compact. Five isothermal lines cover urban and semi urban areas during winter season. i.e. one degree fall in LST from HS is in a very compact manner. The difference in the images is due to the development of different parts of the city during different times and also due to different extent of development of these areas.

Mean UHI intensity corresponding to summer seasons is 5° C for 2003 and 2015 while it is 6° C for 2009. For monsoon seasons the mean UHI intensity is 7° C for 2003 and 5° C for 2009 and 2015. The mean UHI intensity for winter seasons is uniformly 7° C. As the mean UHI intensity, for a season, does not vary by large extent, any increase in area enclosed by isothermal line shall be a clear signature of increase in LST over some area and hence

growth in SUHI effect. Total area enclosed within each isothermal line has been calculated and has been given in Table 4.6. It can be seen from the table that the area within each isothermal line of fall in LST steadily increases from 2003 to 2015. The area enclosed by -1^{o} C isothermal lines, during monsoon season of 2015, is about 30 times of area enclosed by the corresponding isothermal line of 2003. The increase in total area of other isothermal lines between different time periods is also significant and is up to 40% between 2003 and 2009 and above 200% between 2003 and 2015, for summer season. The corresponding increase for winter season is up to 34% between 2003 and 2009 and above 70% between 2003 and 2015. It can be interpreted from the Table 4.6 that there is a continuous increase in LST of the Ahmedabad city and the temperature gradient between HS and area surrounding it is falling i.e. more and more area is noticing temperatures which are moving close to the temperature of HS.

Table 4.6: Total Area Enclosed within Various Isothermal Lines (Ahmedabad)

Legend/ Category	**Summer**			**Monsoon**			**Winter**		
	2003	**2009**	**2015**	**2003**	**2009**	**2015**	**2003**	**2009**	**2015**
Area of pixels within 1^{o}C isothermal line	36.74	51.38	126.45	1.23	32.05	36.96	17.01	18.63	28.77
Area of pixels within 2^{o}C isothermal line	138.48	146.01	228.54	73.23	139.21	156.5	74.29	99.7	122.9
Area of pixels within 3^{o}C isothermal line	236.88	274.09	355.93	188.76	263.67	296.33	134.14	151.99	184.04
Area of pixels within 4^{o}C isothermal line	397.16	491.91	660.66	370.73	503.64	571.85	189.59	211.96	271.64
Area of pixels within 5^{o}C isothermal line	1013.6	905.42	1301.1	1122.48	1137.2	1242.6	273.63	303.25	367.23
Total area of all the pixels of study area	1537	1537	1537	1536.98	1537	1537	1537	1537	1537

Area enclosed between adjacent isothermal lines has been given in Table 4.7. It can be seen from the table that there is no clear pattern of change in area between different isothermal lines. Change in areas enclosed between consecutive isothermal lines of first four categories (higher LST than the outer/rural/suburban area) show rising pattern in most of the cases which clearly shows the significant SUHI growth over the area. Summer season

shows decrease in area between 1° C and 2° C isothermal lines and the decrease in area is also observed during winter season between 2° C and 3° C isothermal lines. The small decrease in these two cases may be due to movement of more area from those categories than the area added into these categories. There is decrease in area between 4° C and 5° C isothermal lines especially during monsoon and summer seasons which indicates that there is a decrease in the area of different parts of the city that are encountering lower LSTs with the passage of each six year time interval. There is a consistent increase in area between different isothermal lines which indicates that there is an increase in the area of different parts of the city that are encountering higher LSTs with the passage of each six year time interval. Increase in percentage of area between higher order isothermal lines (representing lower difference in LST between HS and area under consideration) is multiple times that of corresponding increase between lower order isothermal lines (representing higher difference in LST between HS and area under consideration). The change in area is higher during summer and monsoon season as compared to during winter season. Increase in the area between isothermal lines of low order can also be observed during few time intervals. This can be due to lesser addition in the area in this interval from further lower order lines, compared to the more shift of area from this interval to the next interval corresponding to higher order isothermal lines.

Table 4.7: Total Area Enclosed between Consecutive Isothermal Lines (Ahmedabad)

Difference in temperature with respect to LST of HS	Summer			Monsoon			Winter		
	2003	2009	2015	2003	2009	2015	2003	2009	2015
Up to 1° C	36.74	51.38	126.45	1.23	32.05	36.96	17.01	18.63	28.77
Between 1° C and 2° C	101.73	94.63	102.10	72.00	107.16	119.54	57.28	81.07	94.13
Between 2° C and 3° C	98.40	128.08	127.39	115.53	124.46	139.83	59.85	52.29	61.14
Between 3° C and 4° C	160.28	217.82	304.73	181.97	239.97	275.52	55.45	59.97	87.60
Between 4° C and 5° C	616.45	413.51	640.47	751.75	633.61	670.69	84.03	91.29	95.58
More than 5° C	523.37	631.56	235.85	414.5	399.74	294.43	1263.35	1233.73	1169.75

There is a consistent change in the position of different parts of the city with respect to the isothermal lines. There is a gradual shift of area from low order isothermal lines towards higher order isothermal lines. This indicates an increase in the LST of this area signified

by lower difference from LST of HS. The area falling outside 5° C isothermal line is reducing in each consecutive time interval indicating that some part of the area that was relatively cooler earlier, compared to the HS, has undergone some modifications that have resulted into increase in its LST indicated by the lower difference between the LST of this part and that of HS.

4.2.3 Spatio-Temporal SUHI Growth Pattern and Variations over Chandigarh

4.2.3.1. SUHI Growth Analysis using UHI_{index} Method

A comparative plot of the area of pixels falling in different categories, framed on the basis of UHI_{index} and explained above, during different years has been given in Figs. 4.22, 4.23 and 4.24 for summer, monsoon and winter seasons, respectively. The number of LST pixels corresponding to area is shown on the top of each bar. The number of pixels having annual mean UHI_{index} value more than 0.85, for the year 2003, is 4, 2 and 9 for summer, monsoon and winter season, respectively. These pixels have been designated as HS and the HS area, in 2003, is about 3.43 km^2, 1.72 km^2, and 7.73 km^2 in summer, monsoon and winter seasons, respectively. The corresponding area increases to 6.01 km^2, 5.15 km^2, and 12.02 km^2, respectively in 2009 and further increases to 9.44 km^2, 18.03 km^2, and 18.89 km^2, respectively in 2015. Consistent increase in area under HS has been observed during the two 6 year intervals. Overall, a large increase from144% to 950% can be observed in the HS area, during different seasons between 2003 and 2015. Similar observation has been made for Jaipur and Ahmedabad also. Total number of pixels under HS in 2015 (11, 21 and 22 pixels for summer, monsoon and winter seasons, respectively) is more than the number of pixels under HS as observed from mean UHI_{index} in Fig. 4.9 (12 pixels).

Similar trend has been observed for the other category representing PHS as well. The increase in area under category PHS, during different seasons between 2003 and 2015, has been observed to be between 17 and 59 km^2. Area of pixels under the category PHS has increased from 9% to 87% during different seasons between 2003 and 2009 whereas this increase is from 39% to 111% during different seasons between 2003 and 2015. Area under category DL shows increasing trend during winter season, but during summer season decreasing trend has been noticed between 2003 and 2015 and no difference between 2003 and 2009. However, when the analysis is extended using UZ, it can be seen that total area under UZ increases by up to 41% for the period from 2003 to 2009 and the increase is up

to 28% for the period from 2003 to 2015. This indicates that area of urban zone is increasing consistently with time. Some reduction in area under DL especially during summer and monsoon seasons is due to shifting of more area from DL to higher LST categories of HS/PHS as compared to shifting to DL category from lower LST category of SDL/UL. Overall growth in SUHI, represented by increase in area under different categories, has been observed over Chandigarh city during the period from 2003 to 2015 which indicates the clear picture of heat island growth in the study area.

Categories SDL and UL that represent rural area also show different pattern than that by the HS/PHS categories. It can be seen from Figs. 4.22, 4.23 and 4.24 that mixed trend with large variations is observed for categories SDL and UL. Chandigarh rural area mainly comprises of various land surfaces like Shivangi hill ranges in Eastern part of the city; Sukhna lake in the North-Eastern part of the city; and agricultural lands in North-Western and Southern part of the city. The contribution of various land surfaces on LST may vary depending on the season. Shift of various surfaces may happen to DL or in between SDL and UL resulting in mixed trend and season has an important role in these variations. Also, changes in LU-LC over rural areas also play a significant role in variations in SUHI growth over rural areas. Mixed geographical features and topography influence the LST of a particular area. In addition to that Chandigarh city has sub-tropical humid climate and encounters lower temperatures compared to Jaipur and Ahmedabad. Between 2003 and 2009, area under SDL increases during summer season but reduces during monsoon and winter seasons, whereas the area under UL decreases during summer season but increases during monsoon and winter seasons. Similarly, the trend between 2009 and 2015 is also mixed. The change in area under category SDL is absolutely different to that of the category UL during different seasons of all the periods. However, when the total area under categories SDL and UL is considered, a consistent decrease in the total area can be observed. The total area represented by rural categories is 852.63 km^2, 873.23 km^2, and 880.96 km^2 during summer, monsoon and winter seasons, respectively, of 2003. The corresponding area reduces to 832.88 km^2, 716.96 km^2, and 868.94 km^2, respectively, during 2009 and further reduces to 828.58 km^2, 765.04 km^2, and 813.99 km^2, respectively, during 2015.

In urban areas, especially around the CBD of the city, built-up density is higher than the sub-urban and rural areas and this causes higher surface and air temperatures at and around

the CBD of the city. The increase in area of UZ has been due to increase in LST and hence movement of some area from lower UHI_{index} category to higher UHI_{index} category. However, the categories representing rural zone have reduced area under them as development has been undertaken in this area resulting in the migration of a part of that land from lower temperature to higher temperature categories and movement of some area of these categories to category SDL. This can be interpreted that there is an increase in the urban area and reduction in rural/undeveloped land especially during summer and winter season and this is causing increase in LST of some parts of the city and continuous growth in SUHI is happening over Chandigarh city.

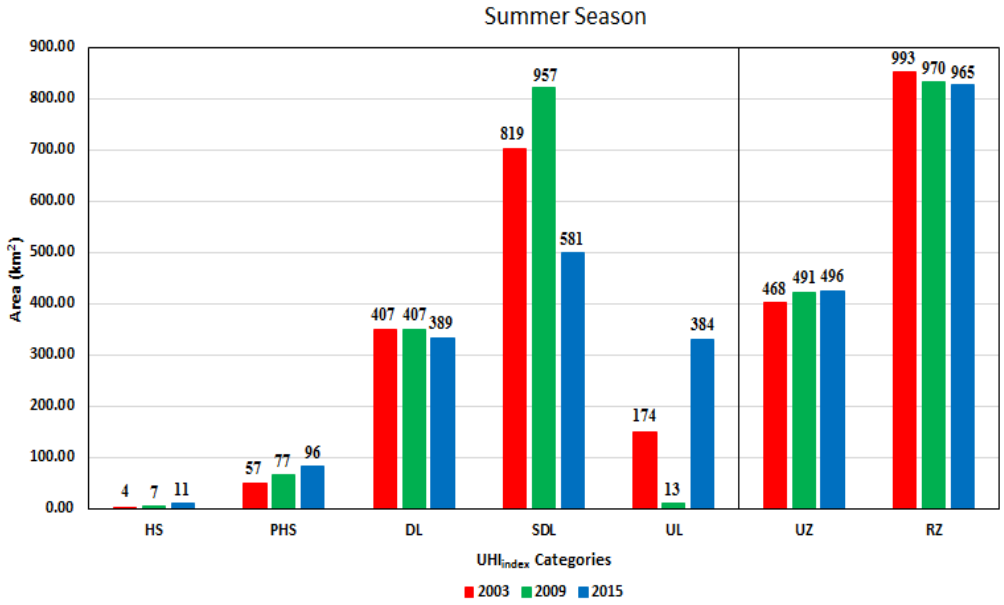

Fig. 4.22. SUHI Growth during Summer Season (Chandigarh)

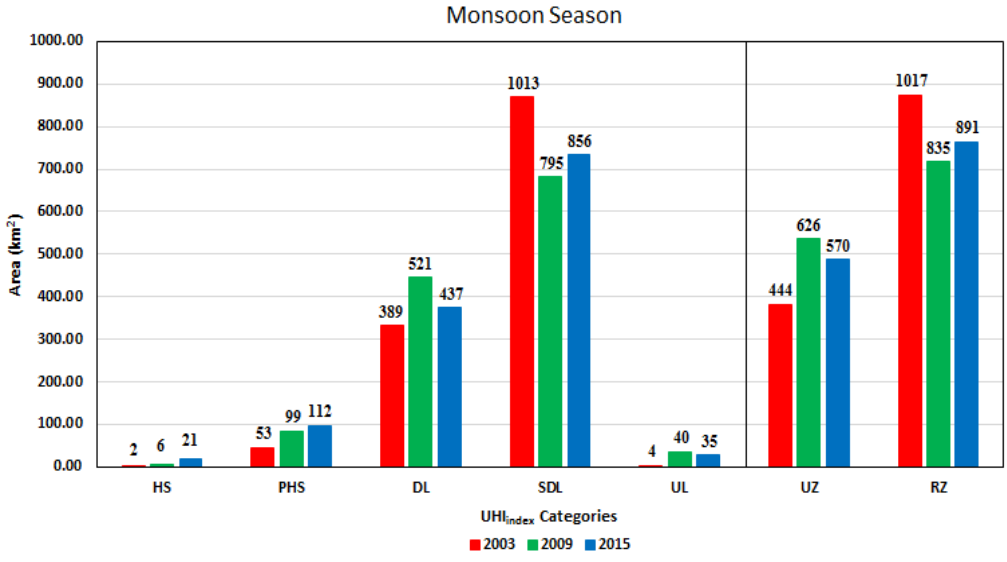

Fig. 4.23. SUHI Growth during Monsoon Season (Chandigarh)

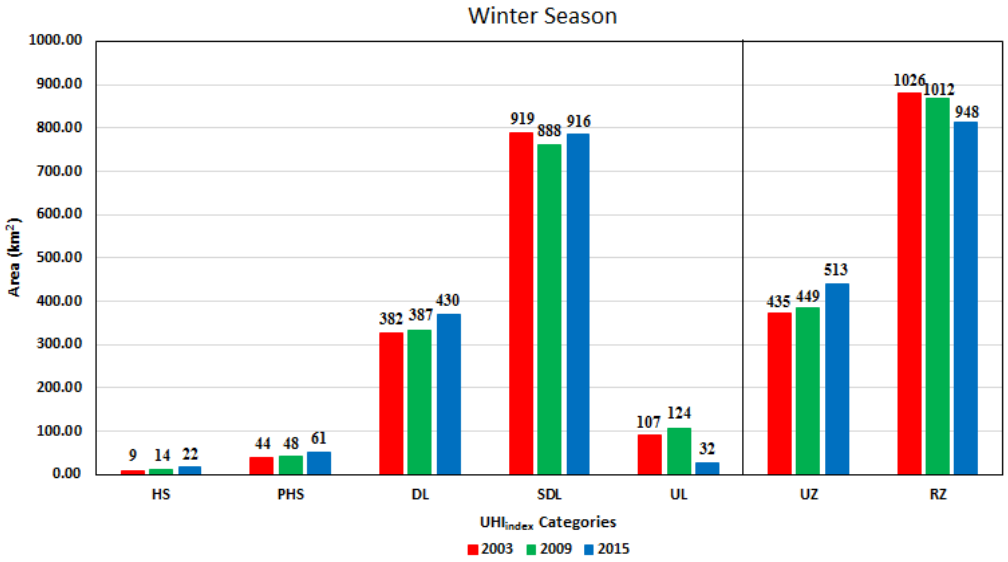

Fig. 4.24. SUHI Growth during Winter Season (Chandigarh)

4.2.3.2 SUHI Growth Analysis Using Transect Method

Mean LST images for summer, monsoon and winter seasons have been shown in Figs. 4.25, 4.26 and 4.27, respectively. CHS has been marked on the mean LST image and transects have been run in different directions through the CHS. Average of mean LST of all pixels falling under HS has been considered to be the temperature at the CHS. Isothermal lines corresponding to every 1^{o} C fall in temperature with respect to the CHS, as discussed earlier, have been marked along each transect and marked as -1^{o} C, -2^{o} C, -3^{o} C, -4^{o} C, and -5^{o} C in Figs. 4.25, 4.26 and 4.27.

The average maximum SUHI intensity of the Chandigarh study area is about 5.17 K which is low compared to Jaipur and Ahmedabad cities. Hence the number of isothermal lines is limited for different seasons. Summer season shows maximum of five isothermal lines; whereas monsoon and winter seasons show three and four isothermal lines, respectively.

A clear increase in the area enclosed by different isothermal lines up to 3^{o} C fall from LST of CHS, can be seen from images of the summer season. Increase in the area enclosed by isothermal line of -2^{o} C fall can also be seen from images of the monsoon and winter seasons. No significant SUHI growth is observed in the rural area where large variations in LST can be noticed. Spacing between different isothermal lines of an image is not uniform and it is different in different directions. Summer images show a spread in both directions. The spread of monsoon and winter images is more towards the West as compared to the East direction which means that the temperature gradient is steeper in East direction.

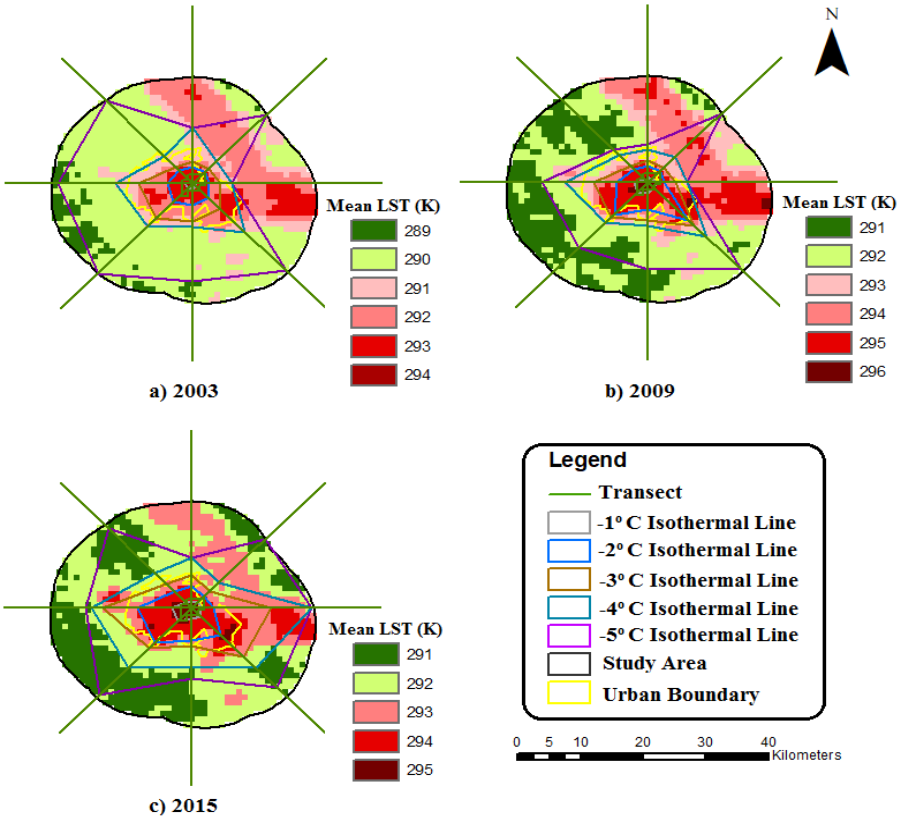

Fig. 4.25. Mean LST Images and Isothermal Lines for Summer Season (Chandigarh)

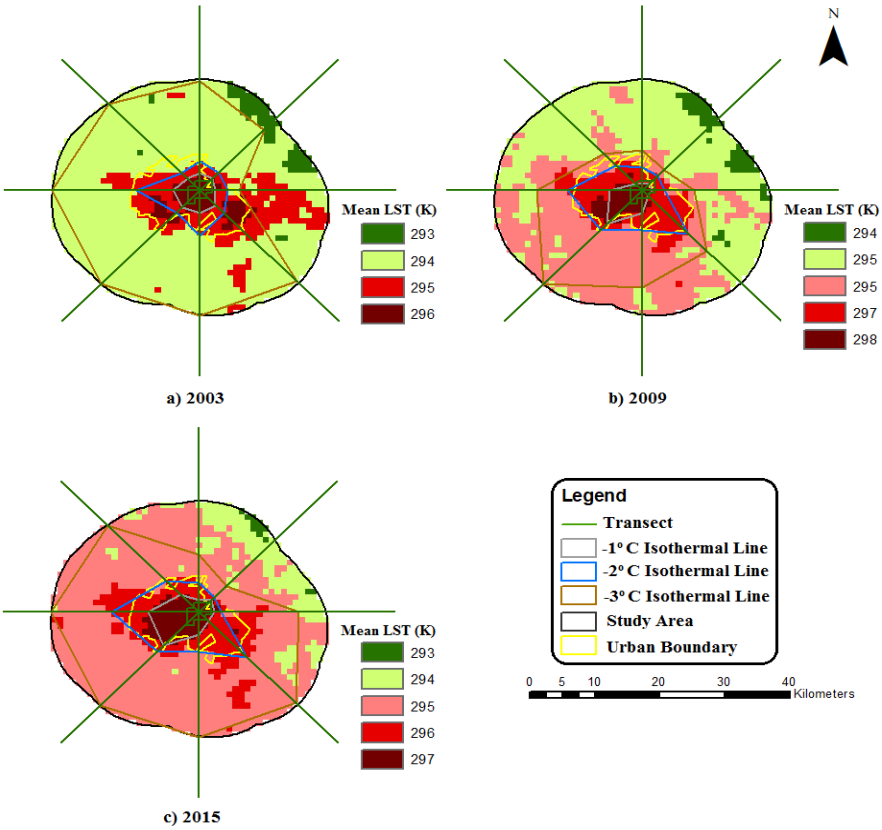

Fig. 4.26. Mean LST Images and Isothermal Lines for Monsoon Season (Chandigarh)

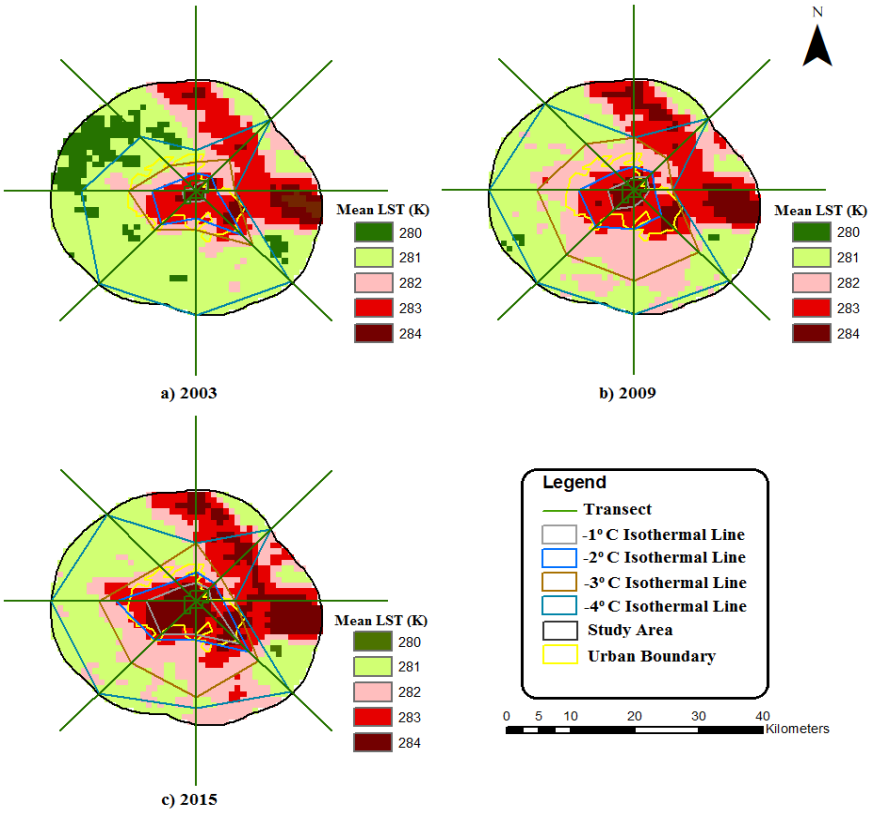

Fig. 4.27. Mean LST Images and Isothermal Lines for Winter Season (Chandigarh)

Consistent SUHI growth pattern has not been observed in Chandigarh study area compared to Ahmedabad and Jaipur because of the existence of lower SUHI intensity compared to those cities. Eastern part of the study area comprises of Shivangi hill ranges show higher LSTs due to the exposed surface rocks especially during summer and winter seasons resulting varying and higher thermal pattern over those areas. But during monsoon season, Shivangi hill ranges show low LSTs compared to other seasons because monsoon rainfall favours high vegetation density over those areas resulting lower LSTs.

The pattern in variations in temperature growth for each one degree fall in temperatures from the HS is entirely varying for different seasons. SUHI growth for each one degree fall in temperatures from the HS is in a discrete manner over the study area for different seasons. UHI has significant seasonal dependence and it shows considerable variations across the city.

Mean UHI intensity corresponding to summer seasons is 5^{o} C for 2003 and 2009 while it is 4^{o} C for 2015. For monsoon seasons the mean UHI intensity is 3^{o} C for 2003 and 4^{o} C for 2009 and 2015. The mean UHI intensity for winter season is uniformly 4^{o} C. As the mean UHI intensity, for a season, does not vary by large extent, any increase in area enclosed by

isothermal line shall be a clear signature of increase in LST over some area and hence growth in SUHI effect. Total area enclosed within each isothermal line has been calculated and has been given in Table 4.8. It can be seen from the table that the area within each isothermal line of fall in LST steadily increases from 2003 to 2015. Area enclosed by the isothermal line of -3^{o} C fall increases between each time period (there is a minor deviation for monsoon season which is due to very low UHI intensity during this season) It can be interpreted from the Table 4.8 that there is a continuous increase in LST of the Chandigarh city and the temperature gradient between HS and area surrounding it is falling i.e. more and more area is noticing temperatures which are moving close to the temperature of HS in a discrete manner.

Table 4.8: Total Area Enclosed within Various Isothermal Lines (Chandigarh)

Legend/ Category	Summer			Monsoon			Winter		
	2003	2009	2015	2003	2009	2015	2003	2009	2015
Area of pixels within 1^{o}C isothermal line	1.35	6.09	11.32	29.48	30.02	53.86	8.91	22.65	80.84
Area of pixels within 2^{o}C isothermal line	32.33	62.24	87.03	85.17	131.09	153.75	76.81	93.79	144.34
Area of pixels within 3^{o}C isothermal line	95.03	111.42	216.34	918.99	448.46	864.47	168.79	389.74	361.59
Area of pixels within 4^{o}C isothermal line	207.69	202.40	411.39	-	-	-	666.78	822.92	793.53
Area of pixels within 5^{o}C isothermal line	765.13	470.17	753.80	-	-	-	-	-	-
Total area of all the pixels of study area	1249.99	1249.99	1249.99	1249.99	1249.99	1249.99	1249.99	1249.99	1249.99

Area falling between two consecutive isothermal lines has been calculated by subtracting area under inner isothermal line from the area under next isothermal line of fall, and is given in Table 4.9. It can be seen from the table that there is a consistent increase in area of first isothermal line for all seasons. There is an increase in area between 1^{o} C and 2^{o} C isothermal lines during summer season, but no clear pattern of change in area can be observed for other seasons. Clear pattern of increase in area enclosed between consecutive isothermal lines has not been observed over Chandigarh compared to Jaipur and Ahmedabad. The surface coverage varies greatly at different times which may affect the alterations in area enclosed between consecutive isothermal lines. Sub-tropical climate of the city, less population, higher vegetation density over rural and urban areas, various land features such as Shivangi hill ranges, Dahriya reserved forest between Chandigarh and

Puchkula, Sukhna lake contain the SUHI growth over the city.

Table 4.9: Total Area Enclosed between Consecutive Isothermal Lines (Chandigarh)

Difference in temperature with respect to LST of HS	Summer			Monsoon			Winter		
	2003	2009	2015	2003	2009	2015	2003	2009	2015
Up to 1° C	1.35	6.09	11.32	29.48	30.02	53.86	8.91	22.65	80.84
Between 1° C and 2° C	30.98	56.15	75.71	55.69	101.07	99.89	67.89	71.14	63.50
Between 2° C and 3° C	62.69	49.18	129.31	833.82	317.37	710.72	91.98	295.95	217.25
Between 3° C and 4° C	112.67	90.98	195.05	-	-	-	497.99	433.18	431.95
Between 4° C and 5° C	557.43	267.76	342.41	-	-	-	-	-	-
More than 5° C/ 4° C/3° C	484.86	779.82	496.19	331.00	801.53	385.52	583.21	427.07	456.46

4.3 Diurnal LST Pattern and Comparison over Indian Cities

The efficacy of remote sensing data of different times during the day/night for SUHI studies has been discussed in this section in order to understand the importance of time of observation. Transit of a number of satellites over different places is at different times and therefore the remote sensing data is available with different times of observation. Application of the remote sensing data for SUHI studies has been analyzed using Aqua-Terra MODIS data The pass of Aqua and Terra satellites over the study cities has a lag of about 3 hours. Day and night LST images area available corresponding to both the satellites which have on-board MODIS sensor.

The temporal and spatial digital image capturing capability available from remote sensing helps in retrieving LST data of any desired location on Earth's surface. The LST data of the three cities from day time and night time images has been retrieved. The current section also attempts to explain diurnal variation of LST on the basis of NDVI values.

4.3.1 Diurnal LST Pattern and Comparison of Jaipur Study Area

Jaipur has mixed topography, mostly plain but surrounded by Aravalli hills on the North, North-East and East side. It has a semi-arid climate, receives low rainfall, and encounters extreme diurnal temperatures and high variations in the temperatures throughout the year. Due to extreme temperature conditions prevailing most part of the year as well as low water availability, the city has sparse vegetation.

a) Day Time Images

LSTs over the study area undergo significant variations during the day time, especially in rural areas. It is observed that the area outside the urban boundary, referred hereafter as the rural area, show higher LSTs than the urban area for all seasons. Fig. 4.28 shows the spatial variations of day and night LST images (1-Day LST derived from data of Aqua and Terra sensors) of Jaipur city. Southern and Eastern parts of the rural area have maximum temperature pixels. Most part of the area falling in this zone is barren land. North Western parts of rural areas show lower LSTs than other parts of the rural area, but higher LSTs than the urban area. This is due to the presence of agricultural fields over those areas. Aravalli hill ranges in rural areas exhibit low LSTs compared to other parts of the rural area for most of the seasons due to the effect of vegetation over the hills. The area falling within the urban boundary referred hereafter as an urban area mostly comprises of built-up surfaces. The effect of these surfaces is to store short wave radiations during the day time, and therefore the urban area shows lower surface temperature. The comparative temperature profile over the rural area vis-à-vis urban area clearly exhibits inverse or negative SUHI effect over the study area.

b) Night Time Images

The night time LST images show distinctly different thermal pattern as compared to the day time images. It can be seen from the images that there is a clear contrast in temperature of the urban area and the rural area and the LST of urban area is higher than the LST of rural area. The urban area near the Eastern side of urban boundary encounters maximum LST. This part of the urban area has predominantly built-up and paved areas, and consequently, the LST of this area is the highest during all the months when seen in nighttime LST images. Some high-temperature pixels are also visible near this part but outside the urban boundary which is the Aravalli hills region. The Aravalli hills exhibit different LST behavior during day and night. The reason may be the dominating elevation factor and the presence of rocks, which emit stored heat waves during night when there is no light source. The heat stored during day time reflects back to atmosphere during night without any obstruction. The overall LST profile over the study area can be used to convincingly explain that there is clear SUHI effect over the study area, when night time LST images are used.

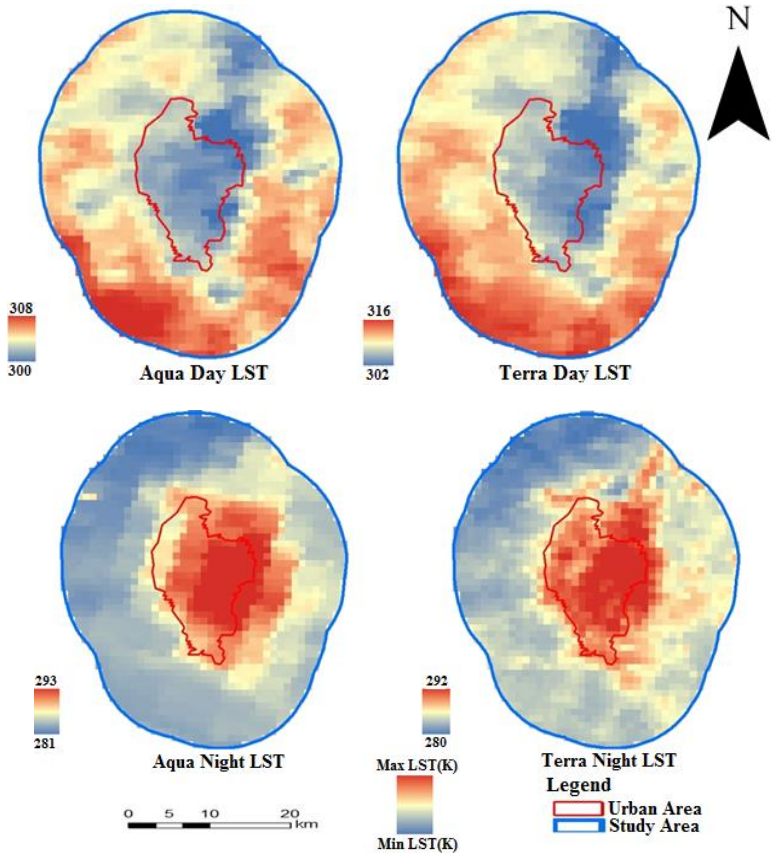

Fig. 4.28. Day and Night LST Images from Aqua-Terra 1-Day Data of Jaipur Study Area (315th Day of the Year 2004)

A close study of Fig. 4.28 reveals that though both the day time images show almost similar temperature profile over the study area, yet there are some variations between these images also. For example, the rural area just outside the urban boundary on the North and South-west directions have different temperature range when compared with other parts of the rural area. Similarly, the Eastern and Southern parts of the rural area show different temperature ranges when compared from night time images. This means that the LST profile over the study area undergoes diurnal variations and it does not remain same throughout the diurnal cycle. This can also be interpreted from existence of negative SUHI effect during day time and clear SUHI effect during night time. The day time and night time images from Aqua and Terra satellites are captured at different times during the day/night (Terra Day: 10.30 AM; Terra Night: 10.30 PM; Aqua Day: 1.30 AM; Aqua Night: 1.30 PM).

The relationship between temperatures of a pixel as observed in a particular image with the temperature of the corresponding pixel as observed in another image has been studied using scatterplots as given in Fig. 4.29. These scatterplots have been prepared to check if the

diurnal variation in LST of all the pixels of the study area undergoes similar change i.e. if the LST of all pixels either increase or decrease in resonance with each other.

It can be seen from Fig. 4.29 that the scatterplot of day vs. night images show inverse relationship indicating that the variation in temperature during day time and night time is different. The coefficient of correlation between these relationships is also very poor, which indicate that the relationship between day and night LSTs are almost insignificant. Inverse correlation between day vs. night scatterplots clearly depict the very poor spatial correlation between night and day time LST data in the study area. However, positive relationship exists between day vs. day and night vs night images which indicate that LST of all the pixels either increase or decrease depending on time of observation of the remote sensing data. The coefficient of correlation of day vs. day images is lower compared to night vs. night images. Hence it can be interpreted that surface temperature variations are more uniform during night time compared to day time. Positive relationship of day-day and night-night LSTs show that spatial variations of LSTs is almost similar during day and night periods uniquely.

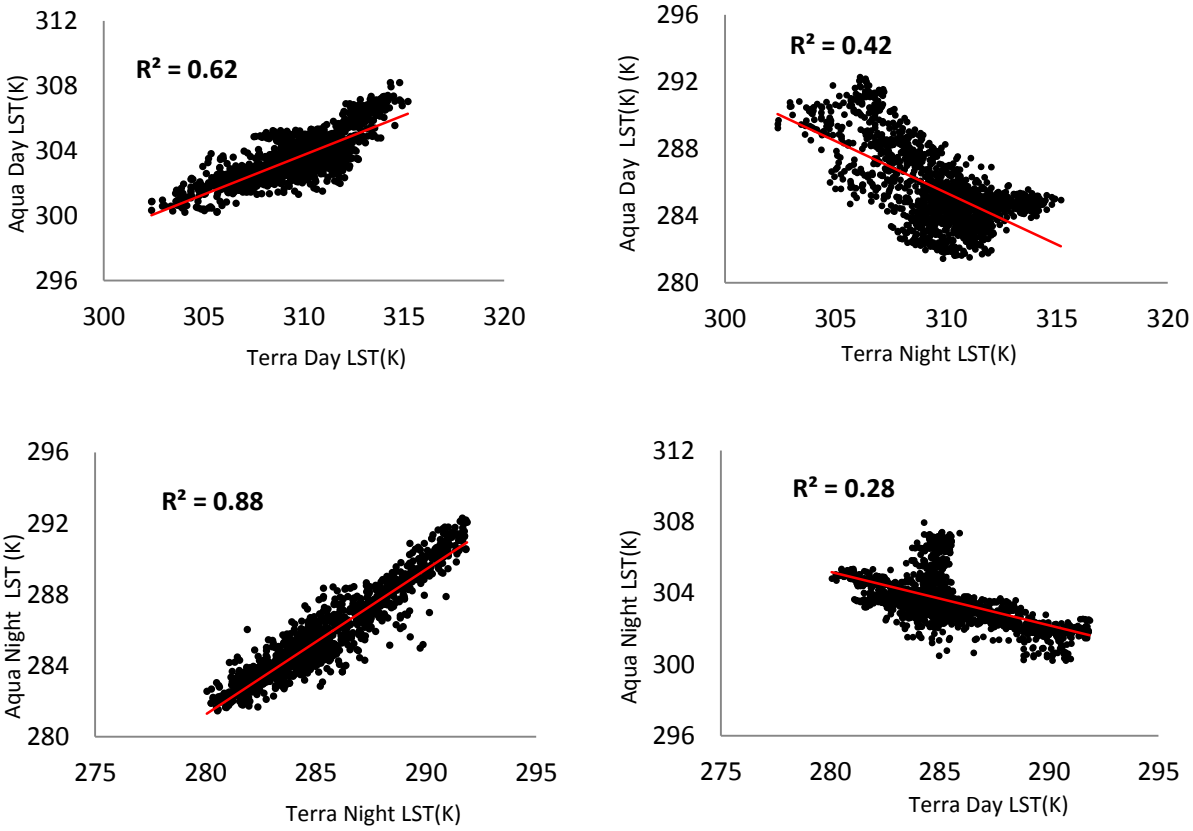

Fig. 4.29. Scatter Plots between Aqua and Terra Derived LST of Jaipur Study Area for Year 2004

The analysis of relationship of various images of same day but with different time of observation/sensor has been extended by considering images of different days of a year so as to cover different seasons also. The images have been randomly selected between the study period and quality criteria has been applied to include only best quality data for analysis. Table 4.10 shows the R^2 values of temporal and diurnal Aqua vs. Terra LST relationship for Jaipur study area. From the table, it can be observed that R^2 values for Aqua night vs. Terra night varies from 0.77 to 0.92 and show better coefficient of correlation compared to other Aqua-Terra LST relationships. R^2 values for Aqua day vs. Terra day LST vary from 0.02 to 0.79. Poor to moderate relationship can be observed between Aqua day and Terra day LST relationship. The between day vs. night LST relationship is poor with low R^2 values ranging from 0.00 to 0.59. The overall average of day to day and night to night relationships are 0.61 and 0.85, respectively.

Table 4.10: Comparisons of Coefficient of Correlation between Aqua and Terra 1-Day LST Data over Jaipur Study Area for Different Periods

Year	Day No. (Julian)	Coefficient of Correlation Between Aqua vs. Terra LST Data			
		ADVTD	ADVTN	ANVTD	ANVTN
2003	313	0.62	0.10	0.43	0.84
2004	315	0.62	0.42	0.28	0.88
2005	276	0.74	0.17	0.06	0.92
2006	276	0.79	0.32	0.41	0.86
2007	274	0.36	0.14	0.28	0.88
2008	062	0.53	0.20	0.01	0.77
2009	060	0.78	0.05	0.01	0.80
2010	141	0.56	0.21	0.59	0.83
2011	081	0.79	0.08	0.06	0.82
2012	089	0.70	0.11	0.04	0.84
2013	065	0.76	0.06	0.25	0.89
2014	072	0.68	0.06	0.00	0.84
2015	120	0.02	0.00	0.32	0.80

ADVTD-Aqua day LST VS. Terra day LST; ADVTN-Aqua day LST VS. Terra night LST; ANVTN-Aqua night LST VS. Terra night LST; ANVTD-Aqua night LST VS. Terra day LST

4.3.2 Diurnal LST Pattern and Comparison of Ahmedabad Study Area

Fig. 4.30 shows the LST images which clearly depicts SUHI effect existence during night, whereas weak or no such effect during daytime.

a) Day Time Images

Northern, Western and North Western parts of the rural area exhibit higher surface temperatures than other parts of rural areas especially during summer and winter seasons and Eastern part of the urban area shows higher LSTs than Western part of the urban area. Southern and Eastern parts of the rural areas show low LSTs compared to other rural areas. During day time, the central part of the city also exhibits low surface temperatures due to the presence of Sabarmati river. It can be seen from the images that LST of some parts of the rural area is higher than the LST of the urban area, thus indicating the nonexistence of SUHI effect or existence of negative SUHI effect over Ahmedabad city during day period.

b) Night Time Images

SUHI effect can be seen with higher LSTs over urban areas than the rural area. Most of the pixels representing high temperature are within the urban boundary. Few high-temperature pixels, scattered throughout the rural area, can also be observed from night-time LST images. The LST of these places may be higher than the nearby places due to some local conditions. High level of vegetation reduces the temperature of rural land.

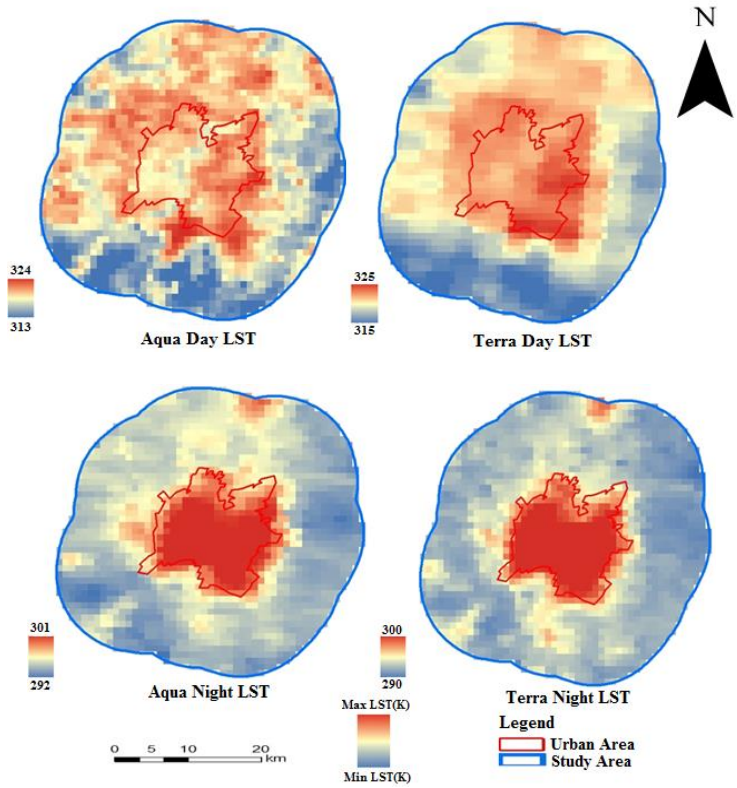

Fig. 4.30. Day and Night LST Images from Aqua-Terra 1-Day Data of Ahmedabad Study Area (90th Day of the Year 2004)

Fig. 4.31 shows the scatterplots between Aqua and Terra, day and night-time LST data of Ahmedabad study area. A positive correlation has been observed between Aqua night and Terra night LSTs. Aqua day and Terra day LSTs also shows a positive relationship. However, Aqua night vs. Terra night LSTs shows the better coefficient of correlation compared to Aqua day vs. Terra day LSTs. Hence, surface temperature variations are observed to be more uniform during night time compared day time. Day vs. night scatterplots does not show any relationship and a random scatterplot can be observed for day and night relationship. The coefficient of correlation is very low which also indicates that the relationship between day and night LSTs is insignificant.

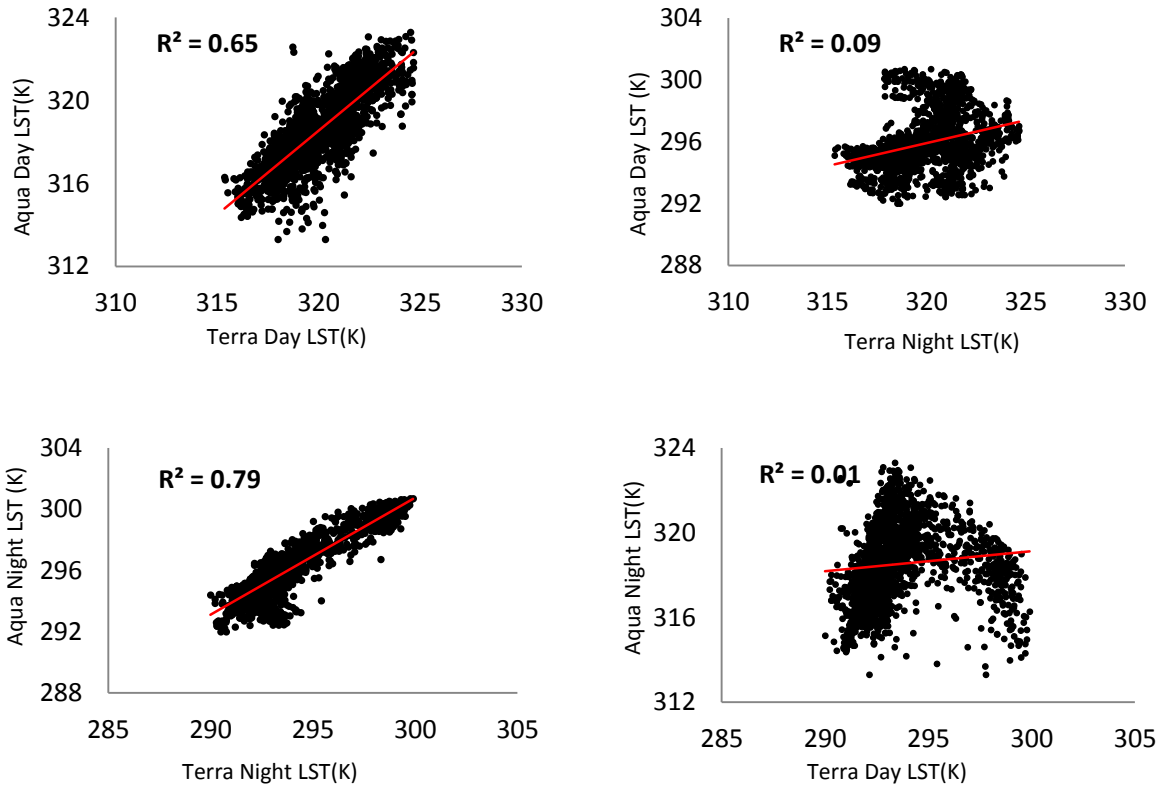

Fig. 4.31. Scatter Plots between Aqua and Terra Derived LST of Ahmedabad Study Area for Year 2004

Table 4.11 shows the R^2 values of temporal and diurnal Aqua vs. Terra LST relationship for Ahmedabad study area. Day vs. night LST relationship is poor with low R^2 values ranging from 0.01 to 0.42. R^2 values for day vs. day LST vary from 0.58 to 0.82 indicating a moderate relationship. However, R^2 values for night vs. night relationship is better compared to other Aqua-Terra LST relationships and R^2varies from 0.71 to 0.89 indicating

a good relationship. The overall average of day to day and night to night relationships are 0.70 and 0.83, respectively.

Table 4.11: Comparisons of Coefficient of Correlation between Aqua and Terra 1-Day LST Data over Ahmedabad Study Area for Different Periods

Year	Day No. (Julian)	Coefficient of Correlation Between Aqua vs. Terra LST Data			
		ADVTD	ADVTN	ANVTD	ANVTN
2003	014	0.68	0.15	0.00	0.80
2004	090	0.65	0.09	0.01	0.79
2005	089	0.71	0.19	0.18	0.88
2006	088	0.66	0.07	0.05	0.88
2007	056	0.70	0.06	0.17	0.84
2008	062	0.67	0.29	0.08	0.83
2009	060	0.68	0.13	0.08	0.79
2010	087	0.82	0.14	0.10	0.82
2011	081	0.80	0.26	0.27	0.88
2012	089	0.72	0.33	0.09	0.78
2013	065	0.72	0.17	0.42	0.89
2014	070	0.58	0.01	0.00	0.77
2015	113	0.71	0.13	0.00	0.81

4.3.3 Diurnal LST Pattern and Comparison of Ludhiana Study Area

The relationship of day LST with night LST has very low R^2 value, indicating different variation of LST of a location during day and night. The day to day and night to night LSTs have positive relationship with higher R^2 values than day-night relationship. This indicates that the variation in LST of a location during day or night is similar and the relationship is better for night to night LST. To explain this varying behavior, the study has been extended for Ludhiana city of India.

Ludhiana is one of the greenest cities of Punjab state, situated in the central part of the state in Malwa region. Population of Ludhiana city is about 1.62 million (Census, 2011). The topography of the city is alluvial plain. It is the most advanced agricultural district of Punjab. Ludhiana features a humid subtropical climate (Cwa) under the Köppen climate classification, with three defined seasons; summer, monsoon and winter. The average annual rainfall is approximately 730 mm.

Fig. 4.32 shows the Day-Night LST images of Aqua-Terra for Ludhiana study area. The pattern of LST for the entire study area, as a whole, does not change significantly. It can be seen from the images that LST of the urban area is higher than the LST of rural area, thus indicating the SUHI effect over Ludhiana city. It is evident from the LST images that a thermal gradient exists from these high-temperature pixels towards the rural area or other parts of the urban area. Most of the high-temperature pixels fall within the urban boundary and LSTs of the urban area are higher as compared to LSTs of the area outside the urban boundary. Minimum LSTs are observed over the area at the boundary of the study area.

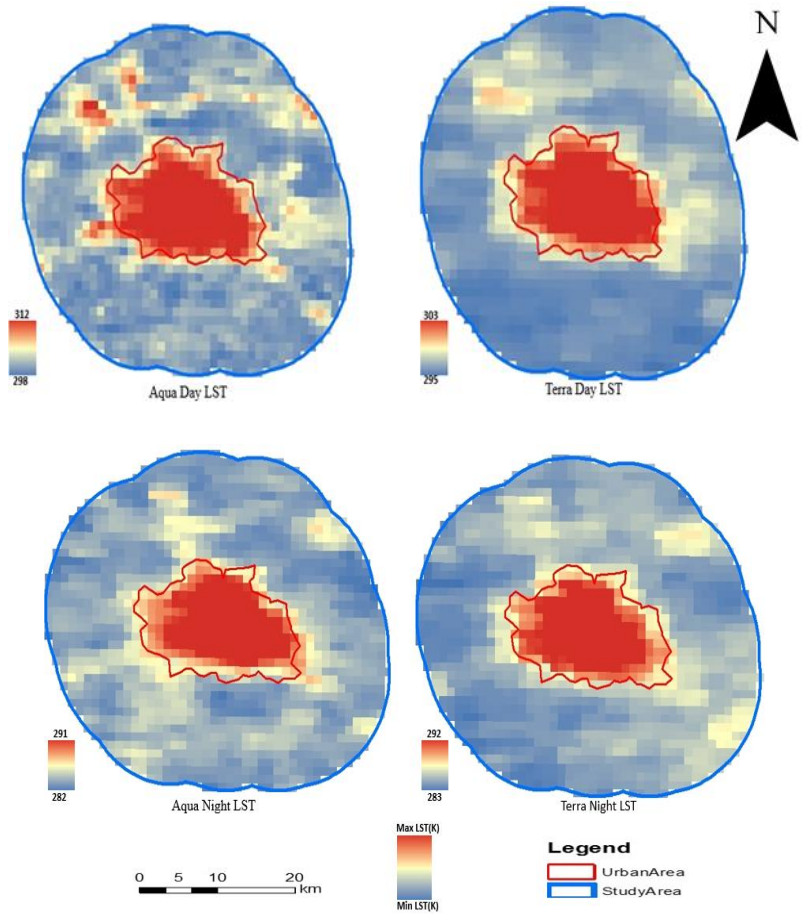

Fig. 4.32. Day And Night LST Images from Aqua-Terra 1-Day Data of Ludhiana Study Area (66th Day of the Year 2004)

Fig. 4.33 shows the scatterplots for the relationship between Aqua and Terra day and night-time LST data of Ludhiana study area. A positive relationship has been observed between all the LSTs of different observation times. The R^2 value for these relationships is also high. Though, the night to night relationship is better compared to other relationship (similar to Jaipur and Ahmedabad), other relationships have higher R^2 values close to night to night relationship and much better than the corresponding relationships to Jaipur and

Ahmedabad. Hence surface temperature variations are observed to be more uniform during both night and daytime. The coefficient of correlation for Ludhiana study area for day vs. night LST images is very good as compared to the corresponding coefficient of correlation for Ahmadabad and Jaipur. This means that the relationship between day and night LSTs of Ludhiana is very good. Good coefficient of correlation indicates that the LST of different places of the Ludhiana study area undergoes corresponding changes during different time periods.

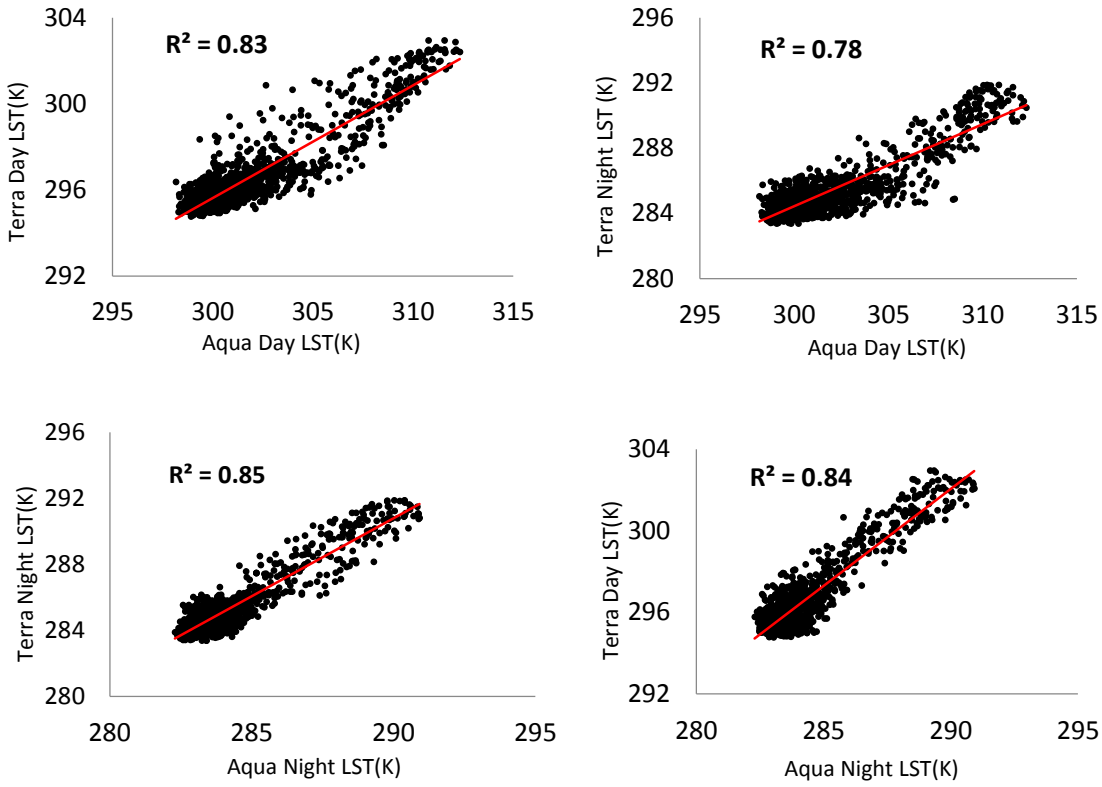

Fig. 4.33. Scatter Plots between Aqua and Terra Derived LST of Ludhiana Study Area for Year 2004

Table 4.12 shows the R^2 values of temporal and diurnal Aqua vs. Terra LST relationship for Ludhiana study area. From the table, it can be seen that R^2 values for Aqua night vs. Terra night varies from 0.63 to 0.88 and is similar to R^2 values for Aqua day vs. Terra day LST that varies from 0.59 to 0.88. Day vs. night LST relationship with R^2 values ranging from 0.20 to 0.84 are also reasonably good for most of the periods. The overall average of day to day and night to night relationships are 0.77 and 0.83, respectively.

Table 4.12: Comparisons of Coefficient of Correlation between Aqua and Terra 1-Day LST Data over Ludhiana Study Area for Different Periods

Year	Day No. (Julian)	Coefficient of Correlation Between Aqua vs. Terra LST Data			
		ADVTD	ADVTN	ANVTD	ANVTN
2003	090	0.82	0.64	0.60	0.83
2004	066	0.83	0.78	0.84	0.85
2005	289	0.84	0.82	0.68	0.86
2006	288	0.59	0.57	0.46	0.79
2007	285	0.80	0.73	0.50	0.78
2008	291	0.78	0.42	0.20	0.82
2009	069	0.88	0.77	0.65	0.81
2010	288	0.68	0.71	0.60	0.87
2011	288	0.66	0.60	0.28	0.83
2012	069	0.79	0.69	0.65	0.88
2013	289	0.70	0.73	0.52	0.80
2014	292	0.81	0.63	0.49	0.84
2015	065	0.78	0.73	0.69	0.80

4.3.4 Discussions

General LST profile over the Jaipur and Ahmadabad study areas, during the daytime, is similar throughout the year. However, the LST profile over these cities, during night time, is different than that observed during day time. The Ludhiana city also shows SUHI effect during night time, but it shows the same effect during day time as well.

The urban area surface comprises of mainly built up and anthropogenic material, whereas the area surrounding the city comprises of agricultural fields, barren soil, and forest. Thus the material property may be considered as one of the primary reasons behind the difference in SUHI pattern. Also, the concentration of dark colored object in urban area also has the role behind this effect. Night time images exhibit a clear pattern of SUHI in the study area, where urban areas exhibit higher surface temperatures than rural areas.

Different surface materials have certain internal thermal properties, like heat capacity, thermal conductivity and thermal inertia which play significant roles in prevailing the temperature of a body at equilibrium with its surroundings (Campbell, 2002). These surface thermal properties differ with the condition of soil type and its moisture content (Sandholt et al., 2002). Dry, bare, and low-density soils have been associated to high LST as a result of relatively low thermal inertia (Carnahan and Larson, 1990; Larson and Carnahan, 1997). The emissivity of soils has been considered as a function of soil moisture conditions, and soil density (Larson and Carnahan, 1997). Therefore, for areas mainly characterized by

limited vegetation cover, surface thermal properties can mostly affect the measurement of LST through the various thermal processes such as conduction, convection, and radiation.

During day time, various land covers exhibit thermal pattern depending on the thermal properties of various land surface materials in the presence of solar source. The thermal pattern of different surfaces is dependent on the solar radiation. Large variations in the thermal profile of different materials, in the presence of solar radiation, result in the varying diurnal thermal pattern for various land covers. This ultimately results in large variations in LSTs during different times of the day. However, due to the absence of external energy source (solar energy) during night time, the thermal behavior of the surface materials is dependent on their temperature only, and hence different temperature profile is visible during night time. The seasonal variations in LST profile of urban area are very less as compared to the rural area as the characteristics of the urban area remain similar throughout the year whereas the characteristics of rural area undergo reasonable seasonal changes due to various agricultural practices, thereby modifying the energy interactions in those areas. Energy interactions of barren land and vegetated ground are known to be different as no moisture is available at barren land and the rate of cooling of two types of land is also different, and these cause different temperature profiles over different parts of the rural area, where impervious surfaces are very less. The interaction of barren land with solar radiation during daytime results in the high surface temperature of the bare soil. The temperature of the bare soil is maximum around noon, and it is lower at sunset and sunrise and much less during night time. The effect of higher temperature of the bare soil is more pronounced in summer season as compared to the winter season as the temperature during the winter season is lower than during summer season and the effect of differential cooling rate is also not high. Thermal characteristics of various land surfaces during solar peak time may also affect alterations in LSTs in different areas. Hence the thermal behavior of various land use/ land covers may considerably influence the variations in surface temperatures.

4.3.5 Spatial NDVI Variations and Comparison

The radiative temperature difference between vegetation cover and the Earth's surface influence the measurement of LST (Sandholt et al., 2002). LST measurement is greatly influenced by the lower atmosphere and the temperature difference between the vegetation canopy and the soil background (Friedl, 2002). Thermal responses for vegetation cover can be greatly varied as a function of the different biophysical properties of the vegetation itself

(Quattrochi and Ridd, 1998). Diurnal and spatial variation of LSTs are significantly influenced by the vegetation in a particular area.

4.3.5.1 Spatial NDVI Variations and Comparison of Jaipur Study Area

Table 4.13 shows the statistical details of NDVI images of the Jaipur study area for different time periods. Mean NDVI values of rural area is higher than the urban area for all the corresponding periods. Plant species, leaf area, soil background, and shadow can all contribute to the NDVI variability (Jasinski, 1990). The mean NDVI for the entire study area varies from 0.18 to 0.39, whereas the mean NDVI for the urban and rural areas ranges from 0.17 to 0.34 and 0.18 to 0.40, respectively. For summer season, the mean NDVI values of rural and urban areas are nearly same. This is due to the reason that the vegetation cover over the study area is very low during summer season. Some patches have high NDVI values as groundwater is used to water these patches. Mean NDVI values of the rural area, during post monsoon period, are much higher than the corresponding values of urban area. The only exception to this can be observed for the year 2010 when the rainfall over the study area was deficient and hence the agriculture and vegetation in the rural area was very less due to scarcity of water. During winter season also the mean NDVI values of rural area are higher than the mean NDVI values of the urban area. A large part of the study area show low NDVI values for all seasons. Low NDVI values usually correspond to built-up area, barren land and sparse vegetation (Holme et al., 1987).

Table 4.13: Statistical Details of NDVI Images of the Jaipur Study Area for Different Seasons

Years	Common Day	Urban Area Only				Rural Area Only				Complete Study Area			
		Maximum	Minimum	Mean	SD	Maximum	Minimum	Mean	SD	Maximum	Minimum	Mean	SD
2003	313	0.53	0.16	0.27	0.06	0.56	0.19	0.28	0.05	0.56	0.16	0.28	0.05
2004	315	0.59	0.19	0.30	0.07	0.63	0.21	0.30	0.07	0.63	0.19	0.30	0.07
2005	276	0.68	0.17	0.34	0.08	0.72	0.23	0.40	0.09	0.72	0.17	0.39	0.09
2006	276	0.55	0.16	0.30	0.06	0.61	0.21	0.34	0.07	0.61	0.16	0.34	0.07
2007	274	0.64	0.16	0.32	0.08	0.67	0.24	0.39	0.07	0.67	0.16	0.38	0.08
2008	62	0.47	0.14	0.22	0.05	0.68	0.17	0.33	0.11	0.68	0.14	0.31	0.11
2009	60	0.40	0.13	0.20	0.04	0.57	0.17	0.28	0.08	0.57	0.13	0.27	0.08
2010	141	0.32	0.11	0.17	0.03	0.37	0.12	0.18	0.03	0.37	0.11	0.18	0.03
2011	81	0.41	0.13	0.23	0.05	0.59	0.19	0.33	0.08	0.59	0.13	0.31	0.08
2012	89	0.40	0.12	0.20	0.04	0.54	0.16	0.26	0.07	0.54	0.12	0.26	0.07
2013	65	0.50	0.14	0.23	0.06	0.69	0.19	0.35	0.12	0.69	0.14	0.33	0.12
2014	72	0.44	0.14	0.23	0.06	0.65	0.19	0.35	0.10	0.65	0.14	0.33	0.10
2015	120	0.37	0.13	0.22	0.05	0.39	0.18	0.25	0.03	0.39	0.13	0.25	0.04

4.3.5.2 Spatial NDVI Variations and Comparison of Ahmedabad Study Area

Table 4.14 shows the statistical details of NDVI images of the Ahmedabad study area for different images corresponding to different seasons. The mean NDVI values of rural area are significantly higher than the corresponding mean NDVI values of urban areas for all periods. The mean NDVI for the entire study area varies from 0.30 to 0.41, whereas the mean NDVI for the urban and rural areas ranges from 0.21 to 0.24 and 0.31 to 0.44, respectively. The variation of the NDVI for different parts of the urban area appear to be very limited throughout the year. The limited variation also indicate limited dependence on the amount of rainfall. The maximum and minimum NDVI values over the rural area ranges from 0.53 to 0.85 and -0.09 to 0.14, respectively during all periods. Very high values of NDVI are observed in some parts of the rural area especially during post monsoon periods. Some parts of the rural area show negative NDVI values indicating presence of water pixels at some locations. Rural area of Ahmedabad show higher mean NDVI value than Jaipur which clearly indicate the higher vegetation density in Ahmedabad compared to Jaipur rural areas. On the contrary the mean NDVI value of urban area of Jaipur is more than the mean NDVI values of urban area of Ahmedabad.

Table 4.14: Statistical Details of NDVI Images of the Ahmedabad Study Area for Different Seasons

Years		Urban Area Only				Rural Area Only				Complete Study Area			
	Common Day	Maximum	Minimum	Mean	SD	Maximum	Minimum	Mean	SD	Maximum	Minimum	Mean	SD
2003	14	0.50	0.13	0.24	0.06	0.79	-0.09	0.44	0.12	0.80	-0.09	0.41	0.14
2004	90	0.40	0.14	0.23	0.05	0.53	0.17	0.31	0.04	0.53	0.14	0.30	0.05
2005	89	0.42	0.13	0.22	0.05	0.55	0.16	0.32	0.05	0.55	0.13	0.30	0.06
2006	88	0.41	0.13	0.24	0.05	0.63	0.18	0.33	0.05	0.63	0.13	0.32	0.06
2007	56	0.49	0.14	0.24	0.06	0.75	0.17	0.42	0.10	0.78	0.14	0.39	0.11
2008	62	0.48	0.13	0.22	0.05	0.69	0.17	0.37	0.08	0.70	0.13	0.35	0.09
2009	60	0.39	0.14	0.22	0.05	0.80	0.15	0.34	0.07	0.80	0.14	0.33	0.08
2010	87	0.42	0.14	0.21	0.05	0.71	0.15	0.33	0.07	0.71	0.14	0.31	0.08
2011	81	0.43	0.12	0.22	0.05	0.85	0.15	0.36	0.07	0.85	0.12	0.34	0.09
2012	89	0.45	0.12	0.21	0.05	0.78	0.13	0.33	0.07	0.78	0.12	0.31	0.08
2013	65	0.42	0.13	0.21	0.05	0.62	0.14	0.38	0.08	0.62	0.13	0.35	0.10
2014	70	0.46	0.12	0.22	0.06	0.78	0.15	0.39	0.08	0.78	0.12	0.37	0.10
2015	113	0.43	0.11	0.22	0.06	0.61	0.14	0.33	0.06	0.61	0.11	0.32	0.07

4.3.5.3 Spatial NDVI Variations and Comparison of Ludhiana Study Area

Table 4.15 shows the statistical details of NDVI images of the Ludhiana study area for different time periods. The mean NDVI for the entire study area varies from 0.31 to 0.69, whereas the mean NDVI for the urban and rural areas ranges from 0.24 to 0.38 and 0.32 to 0.75, respectively. The maximum and minimum NDVI values over the urban area ranges from 0.41 to 0.76 and 0.00 to 0.17, respectively whereas the maximum and minimum NDVI values over the rural area ranges from 0.59 to 0.88 and 0.08 to 0.37, respectively during all periods. High NDVI values can be observed both in the urban and rural areas. Similarly, some parts of the rural area has built-up surfaces or soil cover, as represented by the presence of low NDVI pixels in these areas. However, high mean NDVI values for the entire study area indicate good vegetation cover over the study area.

Table 4.15: Statistical Details of NDVI Images of the Ludhiana Study Area for Different Seasons

Year	Common Day	Urban Area Only				Rural Area Only				Composite Study Area			
		Maximum	minimum	mean	SD	Maximum	minimum	mean	SD	Maximum	minimum	mean	SD
2003	90	0.61	0.15	0.32	0.09	0.70	0.21	0.45	0.06	0.70	0.15	0.43	0.08
2004	66	0.76	0.15	0.38	0.15	0.88	0.37	0.74	0.09	0.88	0.15	0.69	0.16
2005	289	0.45	0.00	0.28	0.07	0.65	0.18	0.37	0.05	0.65	0.00	0.36	0.06
2006	288	0.45	0.14	0.29	0.06	0.67	0.22	0.38	0.05	0.67	0.14	0.37	0.06
2007	285	0.41	0.12	0.24	0.06	0.59	0.19	0.32	0.04	0.59	0.12	0.31	0.05
2008	291	0.56	0.17	0.36	0.08	0.76	0.08	0.50	0.08	0.76	0.08	0.48	0.09
2009	69	0.68	0.13	0.31	0.11	0.81	0.28	0.66	0.10	0.81	0.13	0.61	0.16
2010	288	0.49	0.16	0.31	0.07	0.73	0.08	0.37	0.05	0.73	0.08	0.36	0.06
2011	288	0.50	0.14	0.28	0.08	0.71	0.12	0.41	0.08	0.71	0.12	0.39	0.09
2012	69	0.68	0.13	0.31	0.12	0.83	0.33	0.68	0.10	0.85	0.13	0.63	0.17
2013	289	0.50	0.14	0.31	0.08	0.73	0.18	0.45	0.05	0.73	0.14	0.43	0.08
2014	292	0.53	0.14	0.28	0.07	0.65	0.21	0.37	0.06	0.65	0.14	0.35	0.06
2015	65	0.73	0.15	0.38	0.14	0.87	0.34	0.75	0.09	0.87	0.15	0.69	0.16

Ludhiana city shows UHI effect both in day and night (refer Fig. 4.32). The day-night LST scatterplots show better relationship than other two cities. NDVI values in higher range is observed in the rural areas of Ludhiana city which indicates higher vegetation density in the rural area. This vegetation maintains a uniformity in temperature variations. The good vegetation density indicated by high range of NDVI values causes suppressed LST variations and hence Ludhiana city shows better day-night LST correlation throughout the year and especially for 2004, 2009, 2012 and 2015.

Many factors contribute to the diurnal and spatial variations of spectral radiance and texture in LST. The spatial arrangement and areal extent of various LC types is fundamental to the

spatial and temporal patterns of UHI. NDVI not only measures the amount of vegetation, but also its values are highly influenced by many factors external to the plant leaf, including viewing angle, soil background, and differences in the row direction and spacing in the case of crops (Weng et al., 2004). The NDVI values for three cities show variations in vegetation density for both urban and rural areas. The range of NDVI values in urban areas of the three cities has been found to be almost similar, but large variation in the NDVI range can be observed in the rural areas of three cities. Ludhiana shows higher range of NDVI values in rural areas compared to Jaipur and Ahmedabad where the range is almost similar. Ludhiana exhibits lower temperature in rural areas due to higher vegetation density which causes SUHI effect in the urban area. Conversely, Jaipur and Ahmedabad study areas show low NDVI values in rural areas which results in large variations in LSTs.

The mean NDVI for the urban area of Ludhiana is higher than the mean NDVI for urban area of Ahmedabad whereas it is slightly higher to the mean NDVI for the urban area of Jaipur. However, the mean NDVI of rural area of Ludhiana is much higher than the corresponding mean NDVI of rural areas of Jaipur and Ahmedabad. The standard deviation of NDVI for urban area of Jaipur, Ahmedabad and Ludhiana varies from 0.03 to 0.08, 0.05 to 0.06 and 0.06 to 0.15, respectively, whereas the corresponding values for rural area of these cities varies from 0.03 to 0.12, 0.04 to 0.12 and 0.04 to 0.10, respectively. The urban area of Jaipur and Ahmedabad show little variation compared to the urban area of Ludhiana thereby indicating high variation in the vegetation patches. Low standard deviation and high mean NDVI for rural area of Ludhiana indicate more or less complete range of vegetation. Further, the standard deviation for rural area of Ludhiana is lower than the standard deviation of urban area of Ludhiana which is in contrast to the trend observed in the other two cities. These values can be used to interpret that the vegetation over the Ludhiana study area is more dense as well as it is spread over a large part of the study area.

The natural land cover of the surface of Earth can be soil, vegetation of varying intensity or rocks. These surfaces are modified due to urbanization and converted into a variety of built-up surfaces like roads, parking lots, buildings, etc. The LST of the surface of Earth is determined on the basis of the composite effect of all of these surfaces over the pixel/location under consideration. The energy interaction of all the natural and modified surfaces is different. The energy interaction of various surfaces depend on the properties of the surface which are highly variable. The interaction of various surfaces is not constant

during different times of the day, and it changes in the presence of the active solar radiation. The amount of energy stored by any surface varies throughout the day. This energy is then released during the period when the active source is absent.

The change in temperature of different surfaces due to change in the solar radiation is different. At noon, when the solar radiation is at its peak, the barren soil surface temperature are somewhat higher than the temperature observed for even built-up surface like roads or concrete surfaces. When the remote sensing imageries are used, which have the satellite pass time close to the time corresponding to peak solar radiation, the barren soil surface temperature of the rural area is observed to be higher than built up surface temperature of urban areas. This has been proposed as the Surface Cool Island Effect by some investigators. This effect has been observed from day time images of the Jaipur and Ahmedabad cities. But this effect is reversed when night time images are used for analysis. As can be seen from the night time images of the Jaipur and Ahmedabad cities, the night time images show clear SUHI effect. The main reason of this change is due to the low thermal inertia of the soil surface which makes it to heat very fast and at the same time it cools very fast too. Hence, when the day time images are used to determine the LST, this behaviour of soil surface show the temperature of the surface which is highly dependent on the solar radiation. However, when the night time images are used for determining the LST inverse behaviour of that observed from day time images is found for Jaipur and Ahmedabad. As can be seen from the statistical values of the NDVI for Jaipur and Ahmedabad cities, the rural area has limited pixels of high vegetation, which can be interpreted as the presence of large patches of soil cover or land having sparse vegetation. In such cases the LST of the surface has a large fraction of LST of soil cover. The soil surfaces show different behaviour during day and night as compared to other surface and hence the coefficient of correlation between the different day-night images of Jaipur and Ahmedabad study areas is very low. However, this correlation is better for day-day images which is the result of solar radiation in presence of which the soil behaviour does not vary by a large extent. Further, the correlation is best for night-night images, when the soil behaviour is similar to that shown by other surfaces.

On the other hand, both the day and night images show clear SUHI effect over Ludhiana. Similarly the correlation coefficient for different day-night or day-day images is also fairly good. This is due to the presence of vegetation over the entire study area thereby meaning

the low distribution of barren land/soil surface. The temperature profile of all other materials/surfaces is similar and hence there is not much difference in the day and night images. However, for Ludhiana city also, the night-night images show maximum coefficient of correlation. This indicates that the time of observation of remote sensing observations is very important when the remote sensing imagery is to be used for analysis of UHI effect over a city. If the city has good vegetation cover, then the day/night LST pattern do not vary by a large extent. However, when the city has low/moderate vegetation cover and has large areas of barren land/soil cover, the day LST images show different pattern as compared to the night LST images. The pattern during different times of the day is also highly variable owing to the interactions in the presence of solar radiation. But the pattern during night time is more or less similar thereby making the night time images best suited for analysis of UHI effects.

4.4 Diurnal Variations of SUHI and AUHI Effect using In-Situ Temperature Measurements

For the analysis of diurnal variations in the temperature of different surfaces as well as to compare the AUHI and SUHI effects, in-situ field survey has been conducted at seven locations spread around the Jaipur study area.

4.4.1 Diurnal Variations of Temperatures of Different Surfaces for Different Seasons at Seven Locations of Jaipur

The diurnal analysis of LST for Jaipur, Ahmedabad and Chandigarh shows different thermal pattern during daytime and nighttime. Nocturnal SUHI effect has been observed in these cities and most part of the urban areas shows higher LSTs than rural areas. The mean LST of the entire urban area is about 3 K higher than the mean LST of the entire rural area. The maximum UHI intensity corresponding to maximum LST of the urban area and minimum LST of rural area is 12 K. However, the daytime LST pattern has been observed to be different than the nocturnal LST pattern. The daytime LST profile shows a negative SUHI effect at Jaipur whereas the SUHI effect at Ahmedabad is of very low intensity. The LST spatial profiles show a thermal pattern with a large extent of surface temperature variations. Many previous SUHI studies have reported the existence of SUHI effect in various cities during day time. Also, day SUHI intensity has been observed to be higher than the night SUHI intensity. But in the present study, it has been observed that there is

no existence of SUHI effect during day time. Negative or inverse SUHI effect has been observed over the study area during day period during which rural area shows higher LSTs than urban area. But during night time, clear SUHI effect has been observed over the study area.

Thermal profile of various land surfaces has been plotted from in-situ field data, and thermal behavior of various surface materials has been investigated in this section.

a) Monsoon Season

Fig. 4.34 shows the thermal profile of various land surfaces at seven locations during monsoon season.

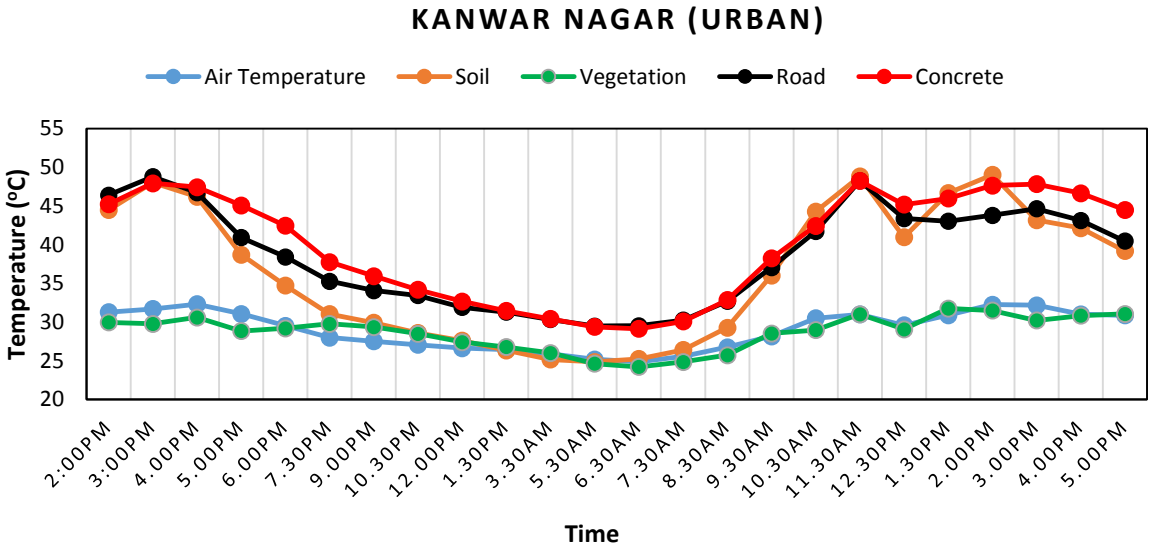

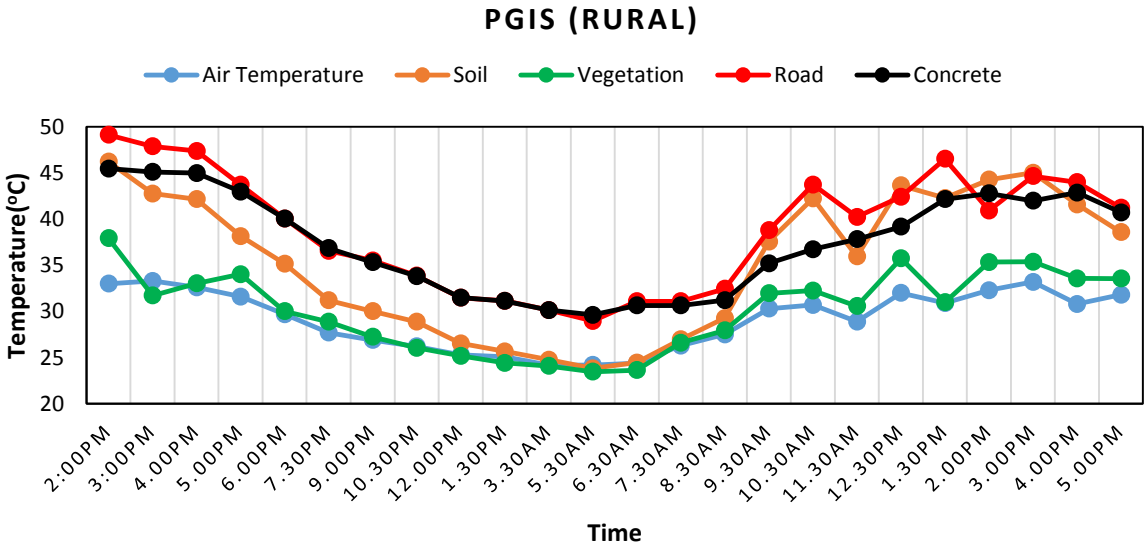

SITAPURA (SEMI-URBAN)

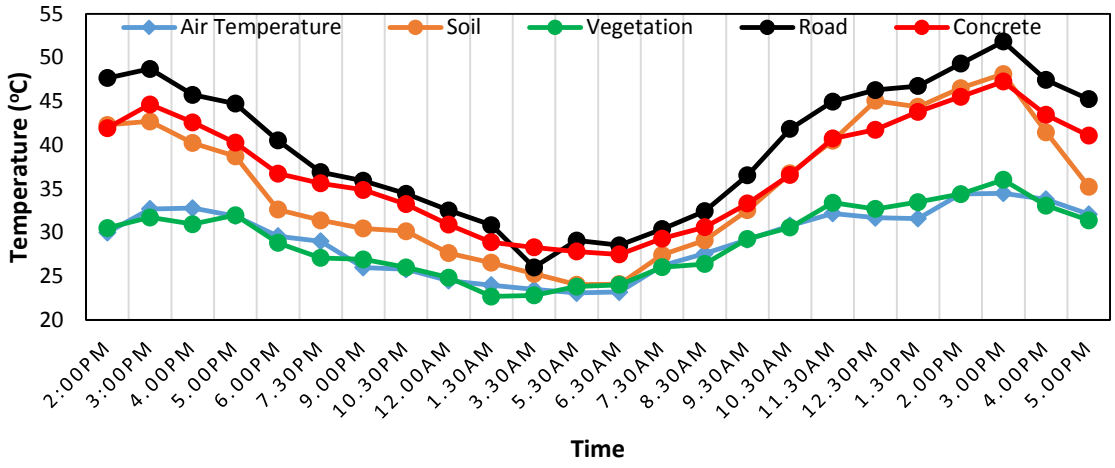

VAISHALI NAGAR (URBAN)

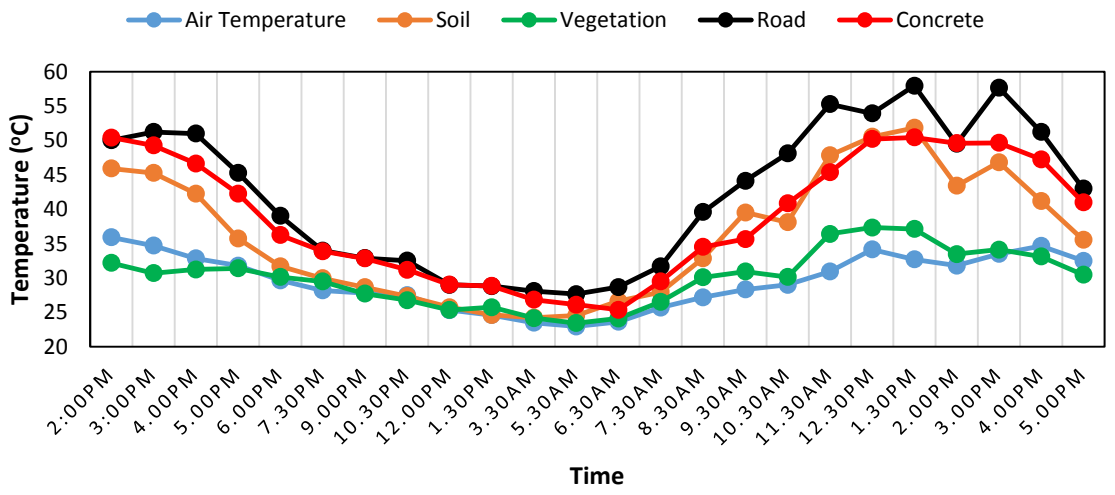

BENAD (RURAL)

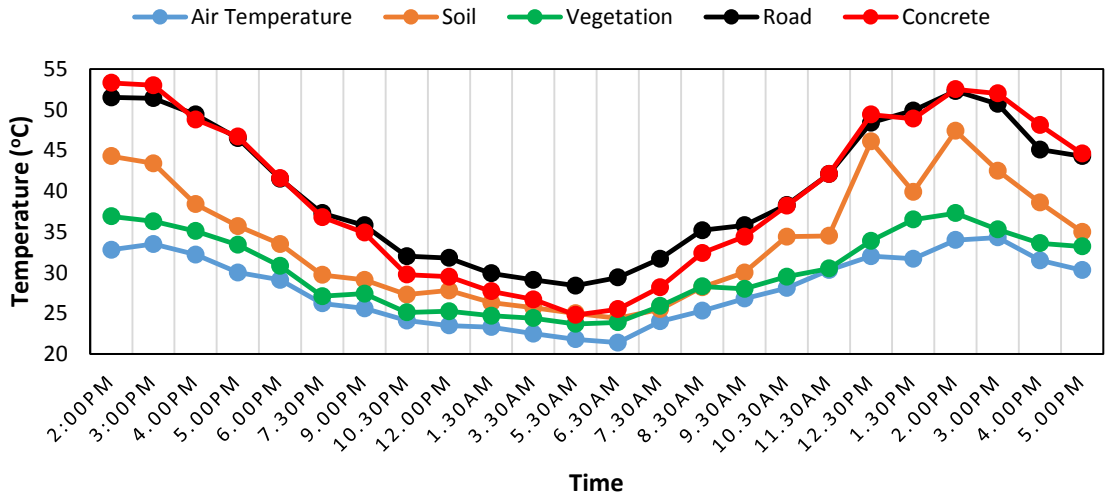

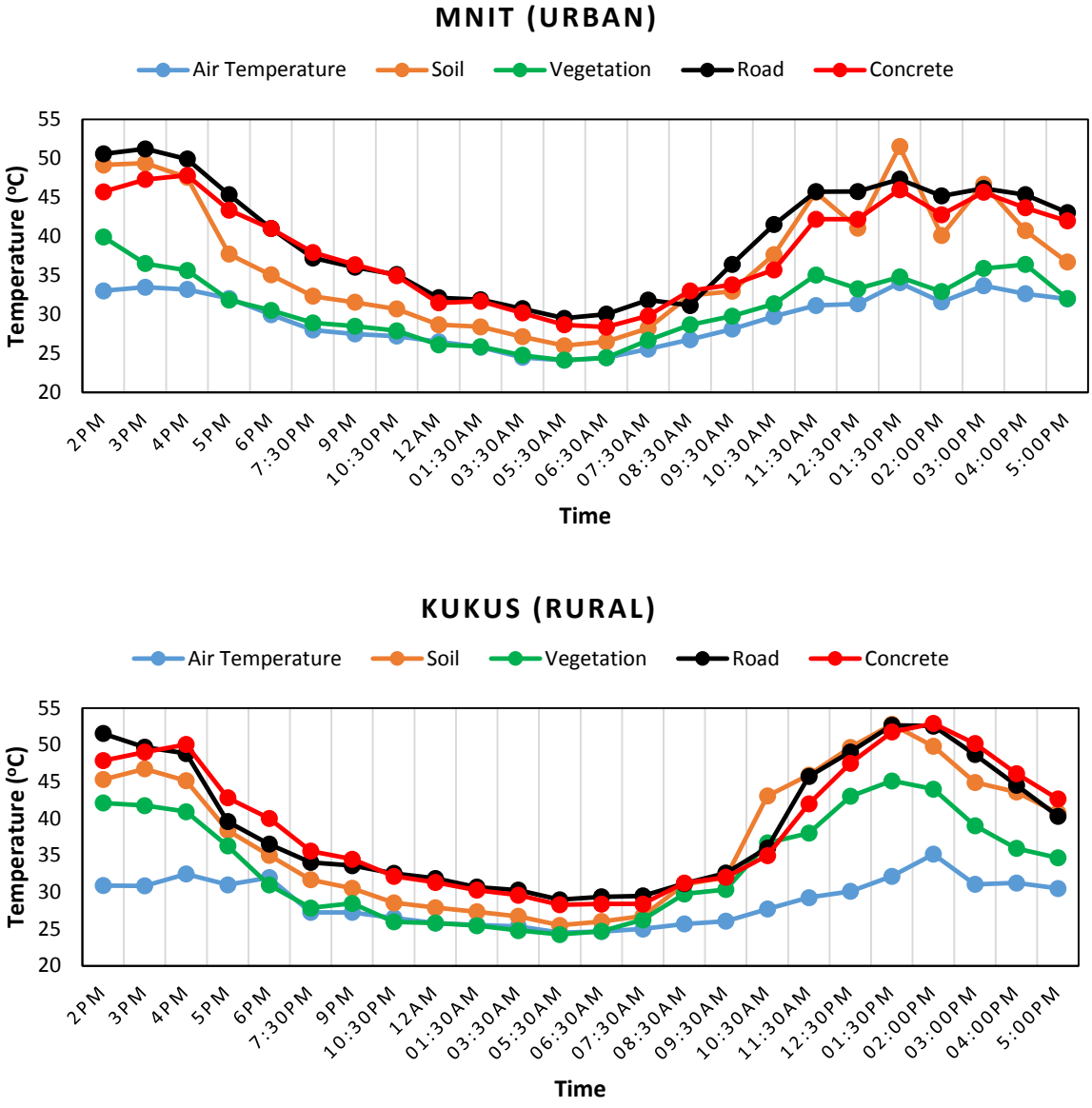

Fig. 4.34. Diurnal Variations of Surface and Air Temperatures at Different Locations of Jaipur (Monsoon Season)

It can be observed from the diurnal surface temperature measurements of different materials, that there are significant variations in the surface temperatures during day time. However, variation in surface temperatures during night time is comparatively lower than during day time. Scattered clouds during monsoon season can cause significant variations in temperatures of different land surfaces usually during day time as these can interrupt the solar radiation over some pixels resulting in shadow over these pixels. LST of similar surfaces, which have different solar radiations at the same time due to shadow effect will be different.

It has been observed that soil exhibits higher surface temperatures than urban materials like concrete and bitumen, especially during clear sky condition at peak solar time. At Kanwar Nager, PGIS, MNIT and Kukas, higher soil surface temperature has been observed for some observations especially during day time as compared to concrete and road. Road temperature at Sitapura and Vaishali Nagar locations has been observed to be higher than soil and concrete temperatures during day time. In Benad, road and concrete show higher temperatures than soil because of the cloud cover during the whole day. Thermal inertia, one of the important surface properties which determines the surface characteristics has been observed to be effectively affecting the surface temperature variations especially during monsoon season due to scattered cloud cover. Drastic changes in temperatures of different surfaces have been observed at some locations where cloud interrupts the solar radiation. Cooling of soil happens suddenly compared to concrete and road, when cloud cover appears. Built-up materials like concrete, bitumen etc. take long time to get cooled compared to soil. Soil has low thermal inertia as compared to concrete and bitumen. This explains large variations in soil temperatures in the figures at Kanwar Nager, PGIS, MNIT and Kukas locations. Large variations in surface temperatures for different surfaces have been observed during day time which are much more than those observed during night time. In addition to the cloud cover, effect of shade, geographic location and wind speed can also be the reasons for variations of temperatures for different land surfaces. However, in the present study, all the observations have been carried out at locations open to sky and at a distance from other buildings/objects of height and hence effect of shade on surface temperature measurements has been eliminated except shade due to cloud effects.

It can be seen from the charts that out of all the surfaces considered, minimum peak temperature as well as overall minimum temperature is recorded for vegetation. The difference in maximum and minimum temperatures of vegetation varies by about 7.53 to 20.84 ^{o}C in monsoon season, during the observation period for seven locations. The temperature difference between maximum and minimum of other surfaces, on the other hand, undergo much higher variations and it varies by about 15.84 to 28.5 ^{o}C and 19.28 to 30.31 ^{o}C, respectively for concrete and road surfaces in monsoon season, during a period of 27 hours. The difference in maximum and minimum temperatures of soil varies by about 22.39 to 27.62 ^{o}C in monsoon season, during the observation period for seven locations. This means that the effect of vegetation is to moderate the temperature changes and the

places having good vegetation cover must have a lower temperature than the places having no vegetation or sparse vegetation or any other built-up surface.

Absolute maximum surface temperatures of soil, vegetation, road, and concrete have been observed to be 52.78 ^{o}C, 45.10 ^{o}C, 57.96 ^{o}C, and 53.3 ^{o}C, respectively. The absolute minimum surface temperatures of soil, vegetation, road, and concrete have been observed to be 23.83 ^{o}C, 22.70 ^{o}C, 26.03 ^{o}C, and 24.80 ^{o}C, respectively. The absolute maximum and minimum temperature of different surfaces has been observed in the order, road > concrete > soil > vegetation during monsoon season.

It can be seen from the chart corresponding to monsoon season (Fig. 4.34) that the peak road temperature of 57.96 ^{o}C is recorded at about 1:30 PM at Vaishali Nagar and the road temperature is about 6 ^{o}C and 7.5 ^{o}C higher than the corresponding temperature of soil and concrete surfaces, respectively and it is about 20 ^{o}C higher than the corresponding temperature of vegetation. The peak concrete temperature of 53.30 ^{o}C is recorded at about 2:00 PM at Benad and the concrete temperature is about 1 ^{o}C and 6 ^{o}C higher than the corresponding temperature of road and soil surfaces, respectively and it is about 16 ^{o}C higher than the corresponding temperature of vegetation. The peak soil temperature of 52.78 ^{o}C is recorded at about 1:30 PM at Kukus and the soil temperature is comparable with corresponding temperature of road and soil surfaces with less difference and it is about 18 ^{o}C higher than the corresponding temperature of vegetation.

The temperature of all the surfaces starts increasing in the morning as the sun rises and this rise continues till the time of peak solar radiation. The temperature of all the surfaces, except vegetation, changes in tandem with each other during the observation period and temperature of all the surfaces is much higher than that of vegetation. The peak temperature of all the surfaces is observed around the time of peak solar radiation i.e. between 12:00 Noon to 3:00 PM. The temperature of all the surfaces starts falling after the peak solar radiation. The temperature fall continues during the night also and it starts increasing again after sunrise next day.

The in-situ temperature study observes that soil gets heated quickly in the presence of solar radiation and it also cool down quickly when solar radiation is not present. The temperature of soil is even higher than the temperature of road surface/concrete surface during peak sunshine hours of the season. The higher temperature of soil as compared to other materials

is observed up to about 3:00 PM and then the temperature starts falling under clear sky conditions. The rate of cooling of soil is maximum as compared to other materials. The crossing time of soil temperature with respect to concrete and road is insignificant during monsoon season due to the undulations in soil thermal profile due to cloud cover.

During night time, it has been observed that concrete and road show higher surface temperatures compared to soil for all locations. Concrete and road exhibit almost same surface temperatures with less variations for all locations. Also, soil and vegetation show similar surface temperature pattern with less variations during night time for all locations. Hence during night time all land surfaces show similar thermal pattern with less variations. So thermal variations of all land covers are almost consistent during night time. From the figures, it is clear that during night time comparative variations in surface temperatures seems to be constant for all surfaces.

Table 4.16: In-Situ Air Temperature Readings at Various Locations (Monsoon)

Time	Kanwar	MNIT	PGIS	Sitapura	Vaishali	Benad	Kukas
2:00 PM	31.3	33.0	33.0	30.0	35.9	32.8	30.9
3:00 PM	31.7	33.5	33.3	32.7	34.7	33.5	30.9
4.00 PM	32.3	33.2	32.6	32.8	32.7	32.2	32.5
5.00 PM	31.1	32.1	31.6	31.9	31.8	30.0	31.0
6.00 PM	29.5	29.9	29.7	29.6	29.67	29.1	31.9
7.30 PM	28.0	28.0	27.7	29.0	28.2	26.2	27.3
9.00 PM	27.5	27.5	26.9	26.0	27.8	25.6	27.3
10.30 PM	27.1	27.2	26.2	25.8	27.5	24.1	26.5
12.00 AM	26.6	26.5	25.3	24.5	25.3	23.5	25.8
1.30 AM	26.4	25.8	25.1	24	24.6	23.3	25.6
3.30 AM	25.9	24.5	24.2	23.5	23.5	22.5	25.4
5.30 AM	25.2	24.2	24.2	23.1	22.9	21.8	24.5
6.30 AM	24.9	24.5	24.4	23.2	23.63	21.4	24.7
7.30 AM	25.6	25.6	26.3	26.2	25.7	24.0	25.0
8.30 AM	26.8	26.8	27.5	27.6	27.2	25.3	25.7
9.30 AM	28.2	28.1	30.3	29.2	28.3	26.8	26.1
10.30 AM	30.5	29.7	30.7	30.8	29.0	28.1	27.7
11.30 AM	31.0	31.2	28.9	32.2	30.9	30.3	29.3
12.30 PM	29.6	31.4	32.0	31.7	34.2	32.0	30.1
1.30 PM	30.9	34.1	30.9	31.6	32.7	31.7	32.2
2.00 PM	32.3	31.6	32.3	34.4	31.8	34	35.2
3.00 PM	32.2	33.7	33.2	34.5	33.5	34.3	31.1
4.00 PM	31.0	32.7	30.8	33.8	34.7	31.5	31.3
5.00 PM	30.9	32.0	31.8	32.1	32.5	30.3	30.5

Maximum and minimum air temperatures during the time period of observation (monsoon season) are 35.93 ºC and 21.4 ºC in Vaishali Nagar and Benad, respectively. Tables 4.16 shows air temperatures at different time observations of seven locations. Red color and green color indicate the highest and lowest air temperatures, respectively at any timeout of the seven locations. During night time, Vaishali Nagar and Kanwar Nagar show higher air temperatures and Benad shows the lowest air temperatures. During day time, Vaishali Nagar and Sitapura locations mainly show higher air temperatures and Benad, Kukas and PGIS (locations in rural areas) mainly show lower air temperatures.

b) Winter Season

Fig. 4.35 shows the thermal profile of various land surfaces of seven locations during winter season.

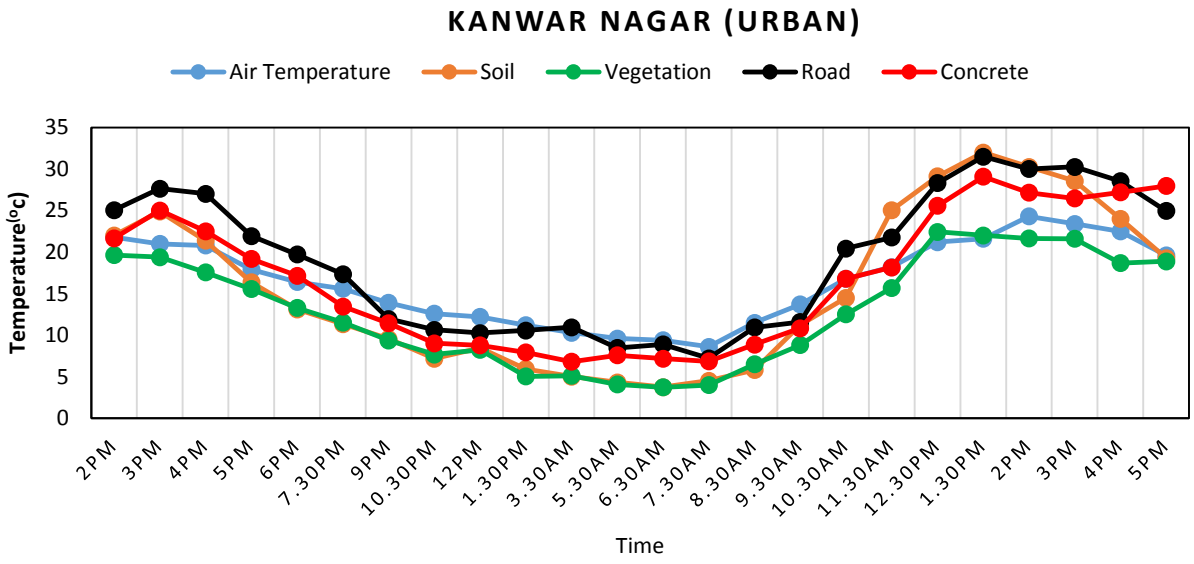

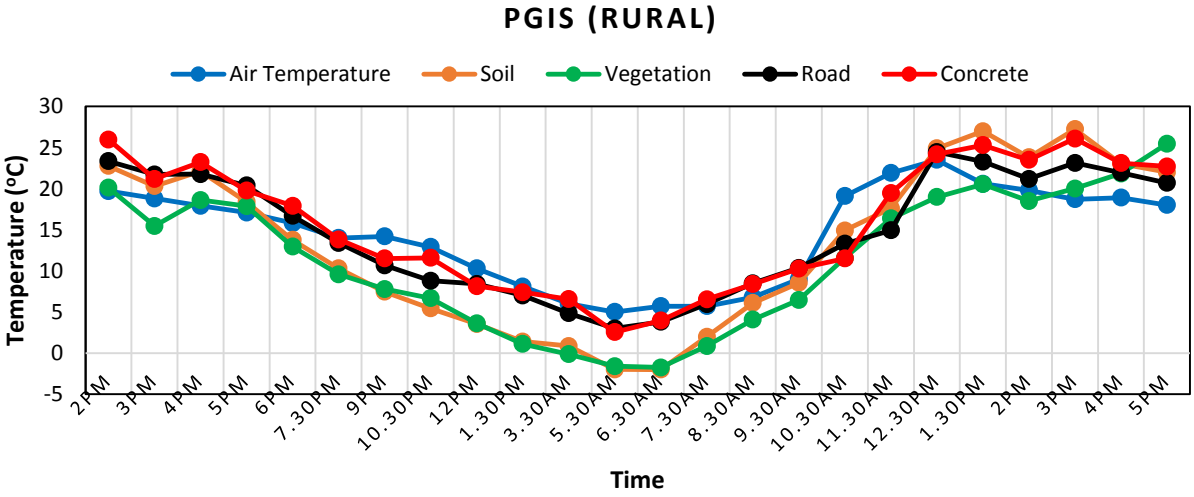

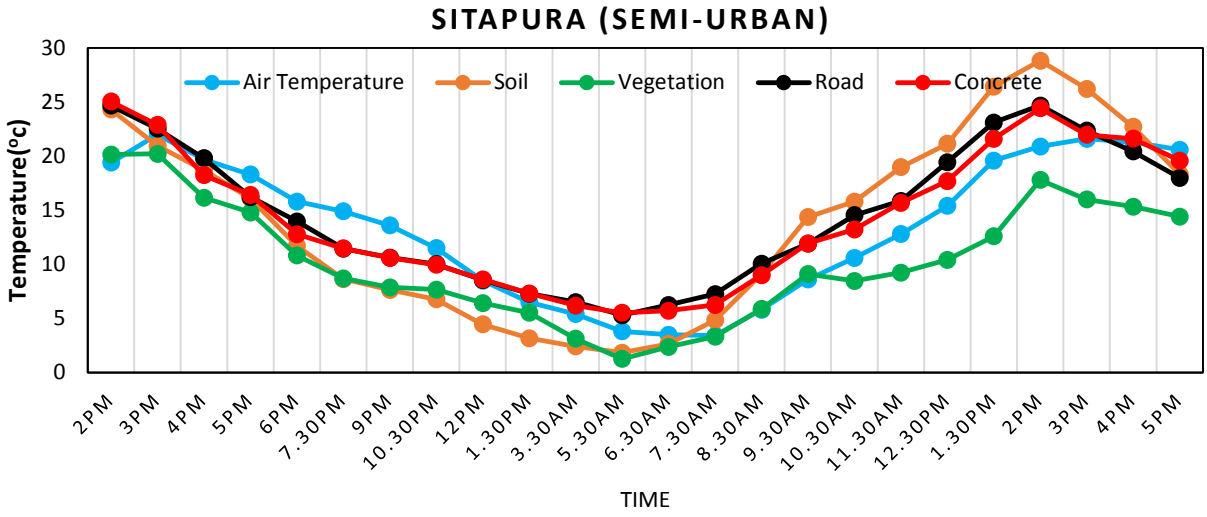
SITAPURA (SEMI-URBAN)
Air Temperature
Soil
Vegetation
Road
Concrete
Temperature(°c)
30
25
20
15
10
5
0
2PM
3PM
4PM
5PM
6PM
7.30PM
9PM
10.30PM
12PM
1.30PM
3.30AM
5.30AM
6.30AM
7.30AM
8.30AM
9.30AM
10.30AM
11.30AM
12.30PM
1.30PM
2PM
3PM
4PM
5PM
TIME

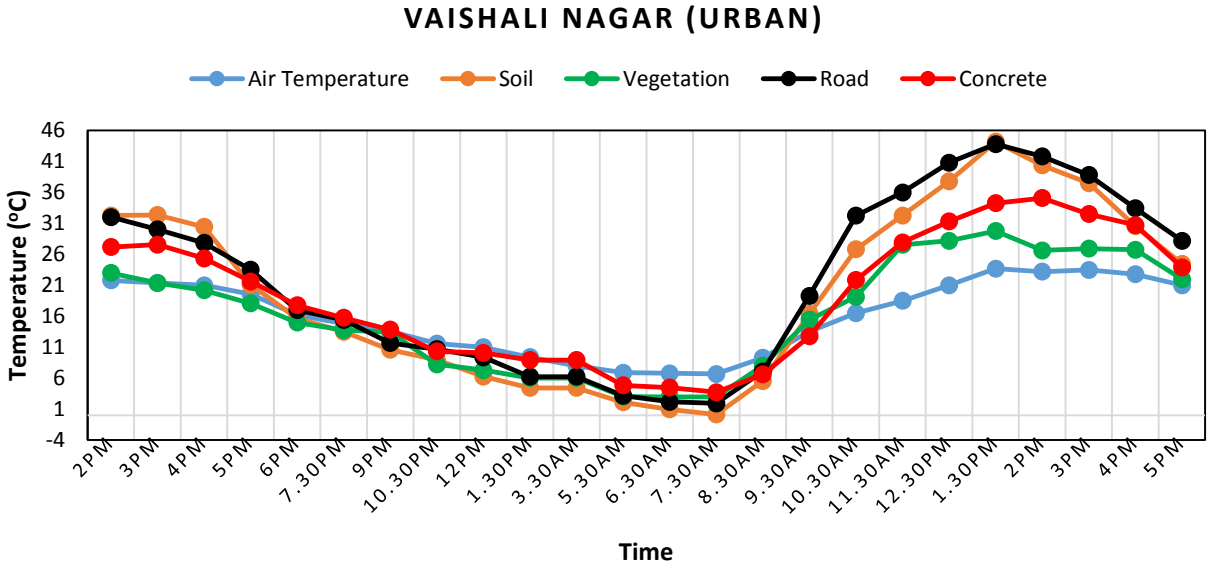
VAISHALI NAGAR (URBAN)
Air Temperature
Soil
Vegetation
Road
Concrete
Temperature (°C)
46
41
36
31
26
21
16
11
6
1
-4
2PM
3PM
4PM
5PM
6PM
7.30PM
9PM
10.30PM
12PM
1.30PM
3.30AM
5.30AM
6.30AM
7.30AM
8.30AM
9.30AM
10.30AM
11.30AM
12.30PM
1.30PM
2PM
3PM
4PM
5PM
Time

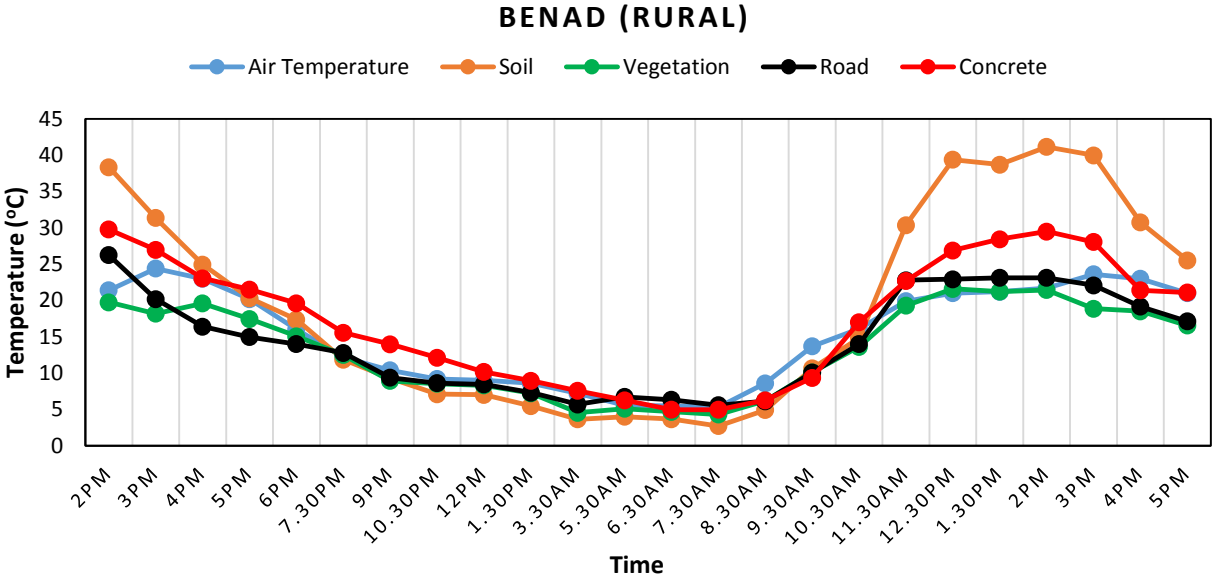
BENAD (RURAL)
Air Temperature
Soil
Vegetation
Road
Concrete
Temperature (°C)
45
40
35
30
25
20
15
10
5
0
2PM
3PM
4PM
5PM
6PM
7.30PM
9PM
10.30PM
12PM
1.30PM
3.30AM
5.30AM
6.30AM
7.30AM
8.30AM
9.30AM
10.30AM
11.30AM
12.30PM
1.30PM
2PM
3PM
4PM
5PM
Time

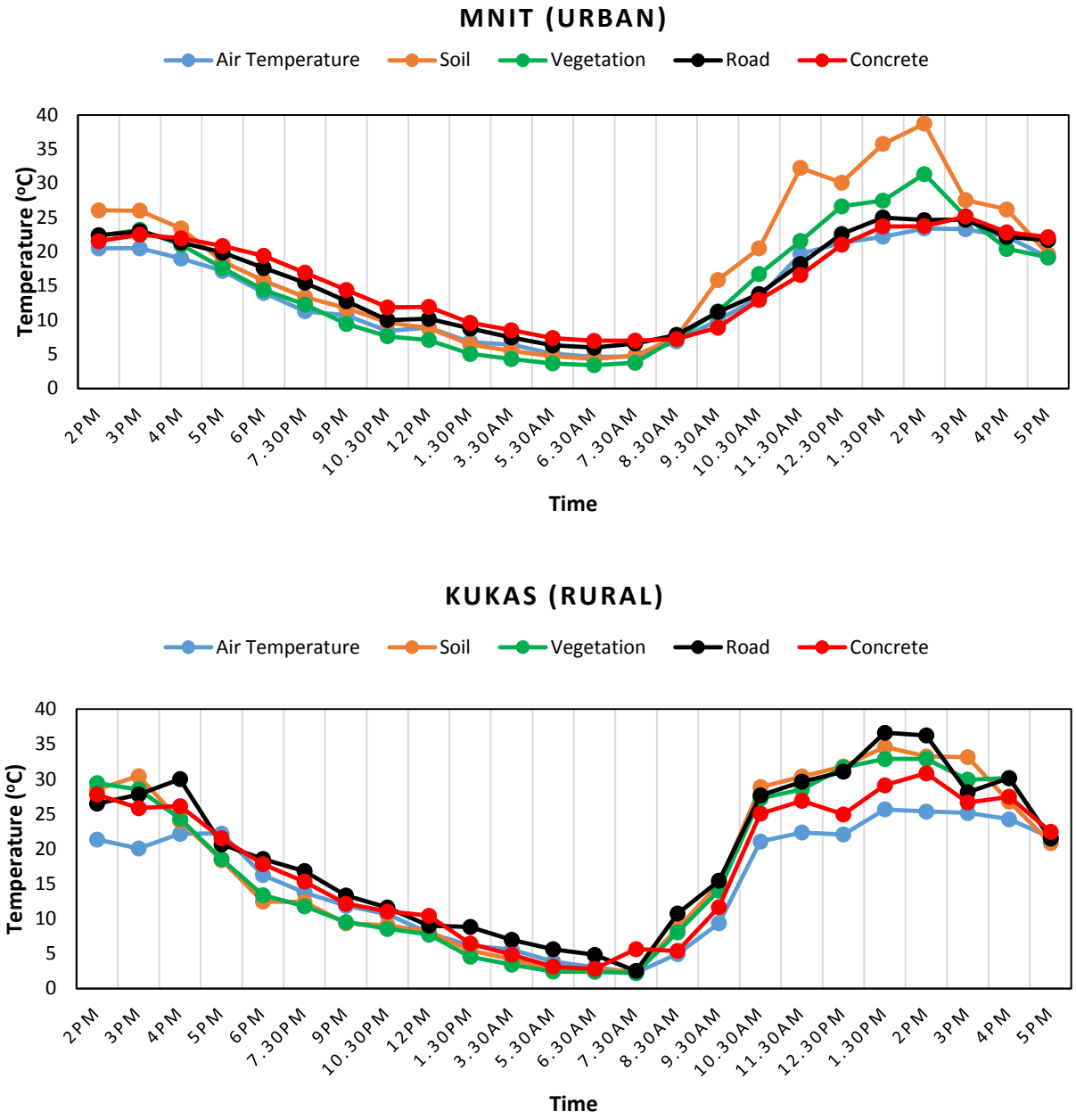

Fig. 4.35. Diurnal Variations of Surface and Air Temperatures at Different Locations of Jaipur (Winter Season)

Higher surface and air temperature variations are observed during daytime compared to night time during winter season also. Soil temperature has been observed to be higher than road and concrete in clear sky conditions during most of the day period when sun is at high altitude at almost all locations. It has also been observed that newly built-up roads exhibit higher surface temperatures than old roads, because new black bitumen absorbs and stores more heat than old black brown bitumen. In Kukas and MNIT during day time, it has been observed that temperatures of vegetation is almost same to soil temperatures, because the

vegetation is drier/ sparse vegetation. It shows the similar spectral reflectance pattern of bare soil. Hence surface properties of different materials are different and affect the surface temperature variations significantly.

The difference between maximum and minimum temperatures of vegetation varies by about 17.28 to 30.70 ^{o}C in winter season, during the observation period for seven locations. The difference between maximum and minimum temperatures of other surfaces undergoes large variations and it varies by about 18.18 to 31.35 ^{o}C, 19.00 to 41.89 ^{o}C and 27.00 to 44.04 ^{o}C, respectively for concrete, road and soil surfaces in winter season, during the period of observation.

Absolute maximum surface temperatures of soil, vegetation, road, and concrete during the observation period have been observed to be 44.20 ^{o}C, 32.9 ^{o}C, 43.82 ^{o}C, and 35.1 ^{o}C, respectively. The absolute minimum surface temperatures of soil, vegetation, road, and concrete have been observed to be -2.0 ^{o}C, -1.73 ^{o}C, 1.93 ^{o}C, and 2.55 ^{o}C, respectively. Soil shows the maximum absolute temperature during day period and minimum absolute temperature during night period compared to other surfaces during winter season.

The higher temperature of soil as compared to other materials is observed up to about 4:00 PM and then the temperature starts falling under clear sky conditions.

It can be seen from the chart corresponding to winter season (Fig. 4.35) that the peak road temperature of 43.82 ^{o}C is recorded at about 1:30 PM at Vaishali Nagar and the road temperature is about 14.04 ^{o}C and 8.72 ^{o}C higher than the corresponding temperature of vegetation and concrete surfaces, respectively and it is about 0.38 ^{o}C lower than the corresponding temperature of soil. The peak concrete temperature of 35.10 ^{o}C is recorded at about 2:00 PM at Vaishali Nagar and the concrete temperature is about 8.72 ^{o}C and 9.1 ^{o}C lower than the corresponding temperature of road and soil surfaces, respectively and it is about 5.32 ^{o}C higher than the corresponding temperature of vegetation. The peak soil temperature of 44.20 ^{o}C is recorded at about 1:30 PM at Vaishali Nagar and the soil temperature is about 0.38 ^{o}C and 9.1 ^{o}C higher than the corresponding temperature of road and concrete surfaces, respectively and it is about 14.04 ^{o}C higher than the corresponding temperature of vegetation.

Table 4.17: In-Situ Air Temperature Readings at Various Locations (Winter)

Time	Kanwar	MNIT	PGIS	Sitapura	Vaishali	Benad	Kukas
2:00 PM	21.8	**20.5**	19.7	19.4	21.8	21.4	21.4
3:00 PM	21.0	**20.5**	18.8	22.0	21.4	24.4	20.1
4.00 PM	20.8	**19.0**	17.9	19.7	21.0	23.0	22.2
5.00 PM	17.9	**17.2**	17.1	18.3	19.6	20.2	22.2
6.00 PM	16.4	**14.0**	15.8	15.8	16.2	16.0	16.3
7.30 PM	15.6	**11.3**	14.0	14.9	14.8	12.2	13.8
9.00 PM	13.9	**10.7**	14.2	13.6	13.6	10.4	11.9
10.30 PM	12.6	**8.4**	12.9	11.5	11.6	9.2	10.7
12.00AM	12.2	**8.9**	10.3	8.5	11.0	9.0	7.9
1.30 AM	11.2	**6.8**	8.1	6.5	9.4	8.6	6.2
3.30 AM	10.3	**6.4**	6.0	5.4	8.0	7.2	5.6
5.30 AM	9.6	**5.1**	5.0	3.8	6.9	5.6	3.9
6.30 AM	9.4	**4.6**	5.7	3.5	6.8	5.5	3.1
7.30 AM	8.6	**4.7**	5.7	3.4	6.7	5.3	2.3
8.30 AM	11.5	**6.9**	6.8	5.8	9.3	8.6	4.9
9.30 AM	13.7	**10.0**	9.0	8.6	13.5	13.7	9.4
10.30 AM	16.8	**13.3**	19.1	10.6	16.5	16.1	21.1
11.30 AM	18.2	**19.7**	21.9	12.8	18.5	19.9	22.4
12.30 PM	21.2	**21.3**	23.5	15.4	21.0	21.0	22.1
1.30 PM	21.6	**22.2**	20.6	19.6	23.7	21.2	25.7
2.00 PM	24.3	**23.4**	19.8	20.9	23.2	21.7	25.4
3.00 PM	23.4	**23.3**	18.7	21.6	23.5	23.6	25.2
4.00 PM	22.5	**22.2**	18.9	21.3	22.8	23.0	24.3
5.00 PM	19.6	**19.2**	18.0	20.6	21.0	21.0	21.7

Tables 4.17 shows air temperatures at different time observations of seven locations. During winter season, maximum and minimum air temperatures of 25.65 ^{o}C and 2.25 ^{o}C are observed at Kukus. During night time, thermal pattern of different materials varies consistently. Road and concrete show higher surface temperatures than the soil and vegetation. During night, it has been observed that surface temperatures of both soil and vegetation are almost same. In PGIS location, surface temperatures of both soil and vegetation has been observed to be negative. Air temperature during night has been found to be higher compared to soil and vegetation temperatures. Concrete and road show almost similar temperature pattern with less variations during night time. Temperatures has been found to be decreasing till 6.30 AM constantly with less variations during night.

The temperature of soil surface is much lower than the temperature of other built-up surfaces after sunset and it is comparable to the temperature of vegetation. The soil temperature is even lower than the temperature of vegetation during the period of winter season. Thus it can be deduced that soil shows typical behaviour of quickly heating up

during the peak hours of the day when the sun shines brightly above the horizon and also quickly cools down during the latter part of the day.

c) Summer Season

Fig. 4.36 shows the thermal profile of various land surfaces of seven locations during summer season.

The charts in Fig. 4.36 can be studied by dividing them into two parts. The first part is to be considered between about 8:00 AM in the morning to about 5:00 PM in the evening. This time corresponds to sunshine hours. The second part can be considered after 5:00 PM in the evening and before 8:00 AM in the morning. The temperature of all the surfaces starts increasing in the morning as the sun rises and this rise continues till the time of peak solar radiation. The peak temperature of all the surfaces is observed around the time of peak solar radiation i.e. between 12:00 Noon to 3:00 PM. The temperature of all the surfaces starts falling after the peak solar radiation. The temperature fall continues during the night also and it starts increasing again after sunrise next day.

From the in-situ temperature study of different materials during 27 hours period, it has been observed that soil becomes warmer than the urban materials like cement concrete, bitumen, etc. during day and urban materials show higher temperatures compared to soil and vegetation during night.

The temperature of different land covers has been observed in the order, soil > road > concrete > vegetation during day time of summer season. The corresponding order during night time has been observed as road and concrete > soil > vegetation during summer season. During monsoon and winter seasons this order modifies to concrete > road > soil > vegetation during daytime and road > concrete > soil > vegetation during nighttime.

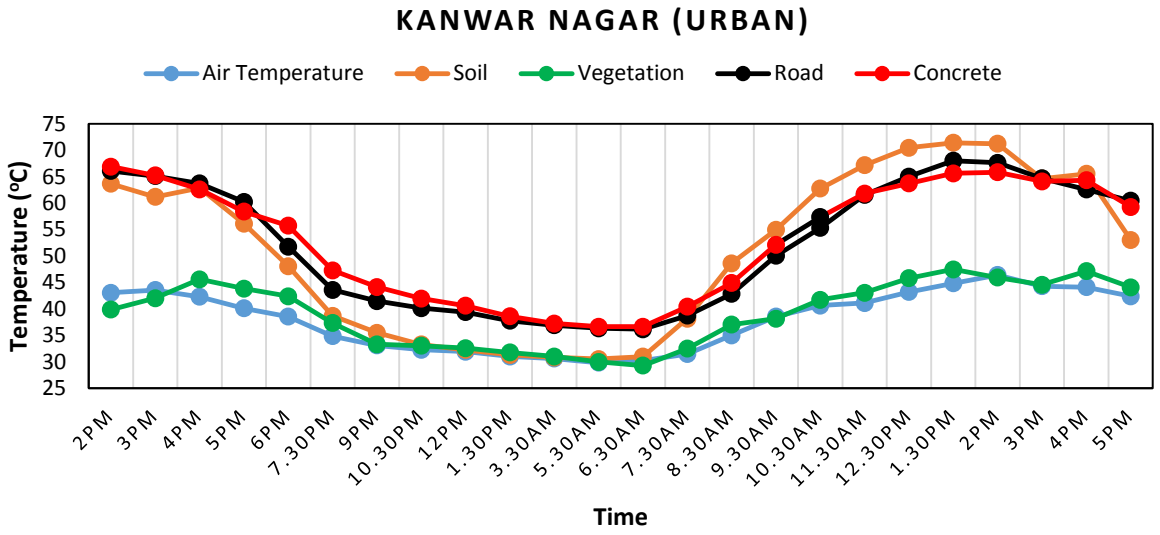
KANWAR NAGAR (URBAN)
Air Temperature
Soil
Vegetation
Road
Concrete
Temperature (°C)
75
70
65
60
55
50
45
40
35
30
25
2PM
3PM
4PM
5PM
6PM
7.30PM
9PM
10.30PM
12PM
1.30PM
3.30AM
5.30AM
6.30AM
7.30AM
8.30AM
9.30AM
10.30AM
11.30AM
12.30PM
1.30PM
2PM
3PM
4PM
5PM
Time

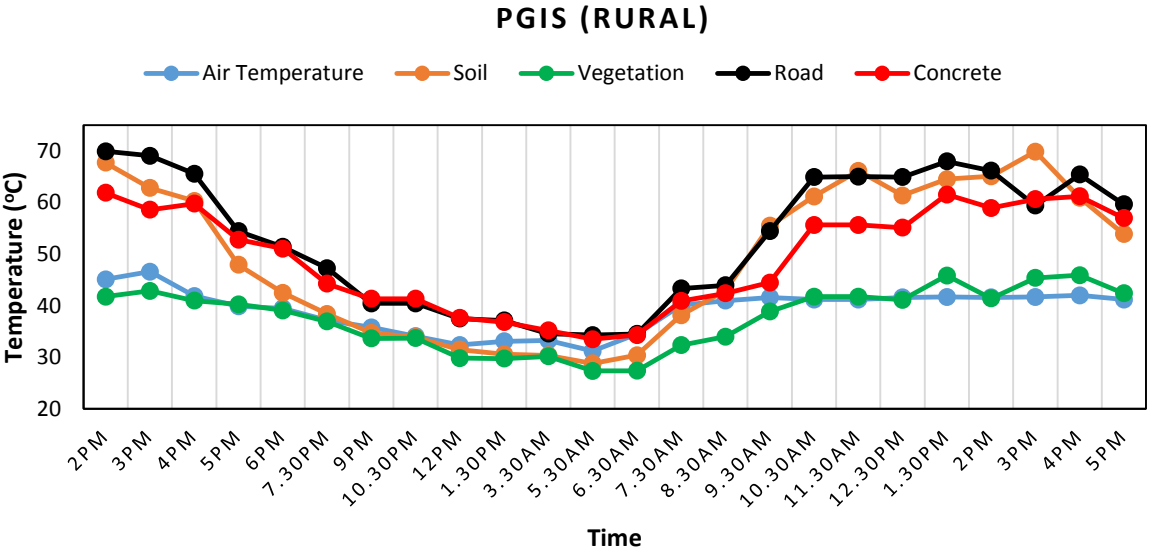
PGIS (RURAL)
Air Temperature
Soil
Vegetation
Road
Concrete
Temperature (°C)
70
60
50
40
30
20
2PM
3PM
4PM
5PM
6PM
7.30PM
9PM
10.30PM
12PM
1.30PM
3.30AM
5.30AM
6.30AM
7.30AM
8.30AM
9.30AM
10.30AM
11.30AM
12.30PM
1.30PM
2PM
3PM
4PM
5PM
Time

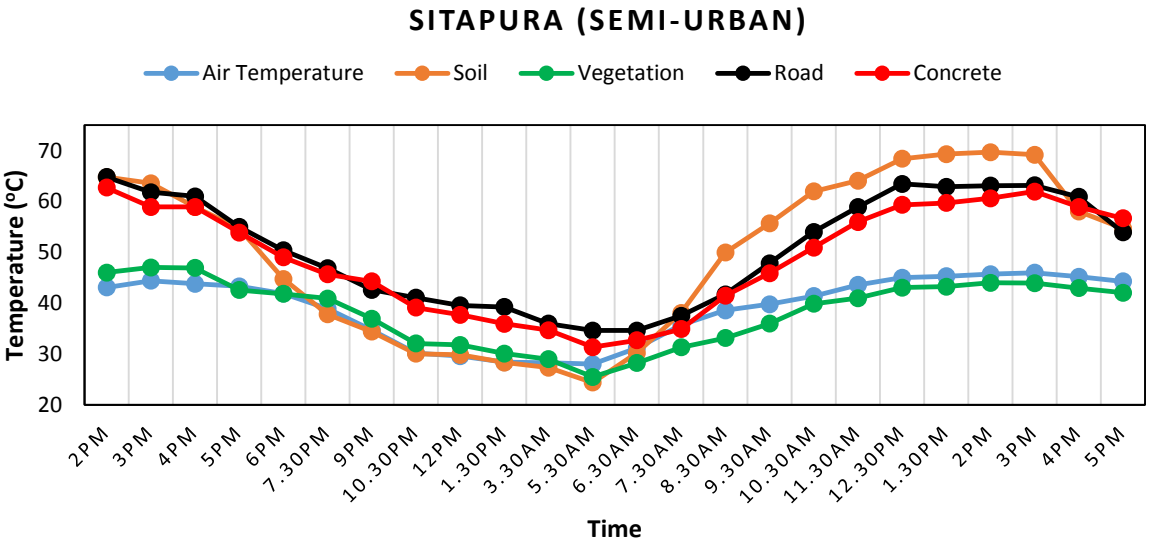
SITAPURA (SEMI-URBAN)
Air Temperature
Soil
Vegetation
Road
Concrete
Temperature (°C)
70
60
50
40
30
20
2PM
3PM
4PM
5PM
6PM
7.30PM
9PM
10.30PM
12PM
1.30PM
3.30AM
5.30AM
6.30AM
7.30AM
8.30AM
9.30AM
10.30AM
11.30AM
12.30PM
1.30PM
2PM
3PM
4PM
5PM
Time

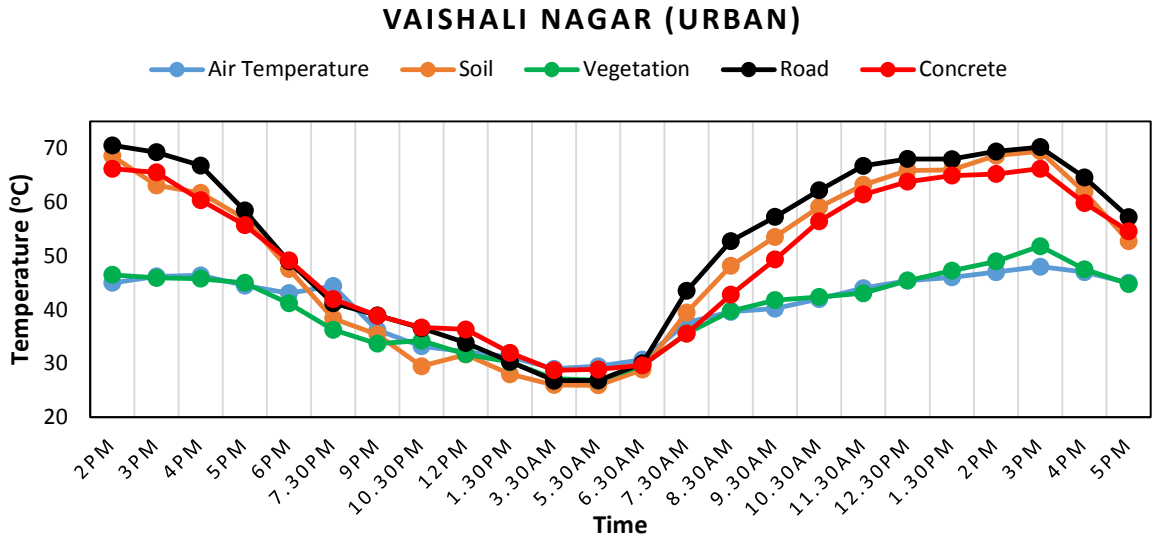
VAISHALI NAGAR (URBAN)
Air Temperature
Soil
Vegetation
Road
Concrete
Temperature (°C)
70
60
50
40
30
20
2PM
3PM
4PM
5PM
6PM
7.30PM
9PM
10.30PM
12PM
1.30PM
3.30AM
5.30AM
6.30AM
7.30AM
8.30AM
9.30AM
10.30AM
11.30AM
12.30PM
1.30PM
2PM
3PM
4PM
5PM
Time

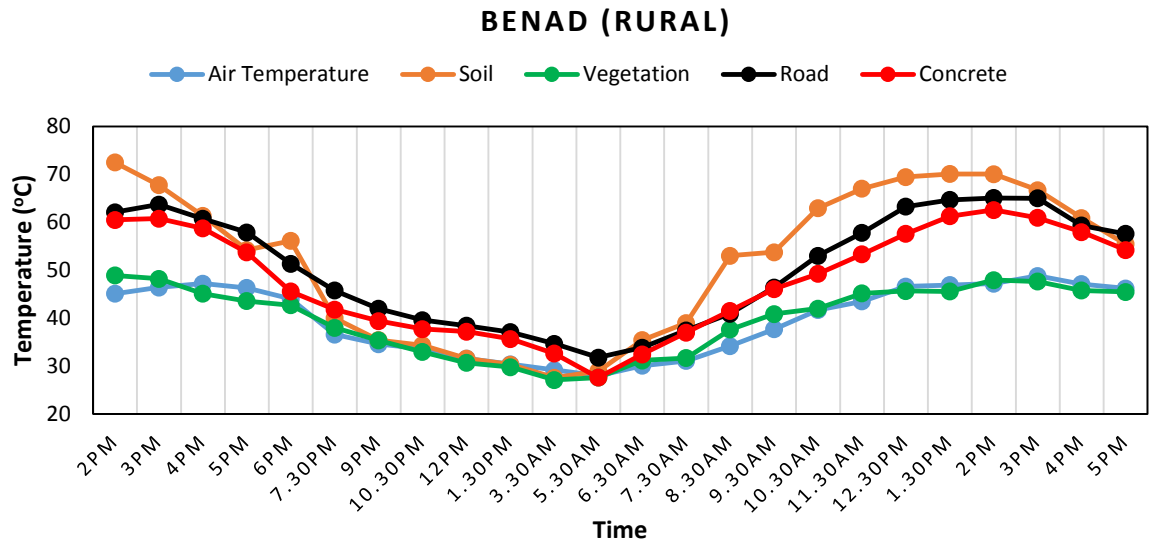
BENAD (RURAL)
Air Temperature
Soil
Vegetation
Road
Concrete
Temperature (°C)
80
70
60
50
40
30
20
2PM
3PM
4PM
5PM
6PM
7.30PM
9PM
10.30PM
12PM
1.30PM
3.30AM
5.30AM
6.30AM
7.30AM
8.30AM
9.30AM
10.30AM
11.30AM
12.30PM
1.30PM
2PM
3PM
4PM
5PM
Time

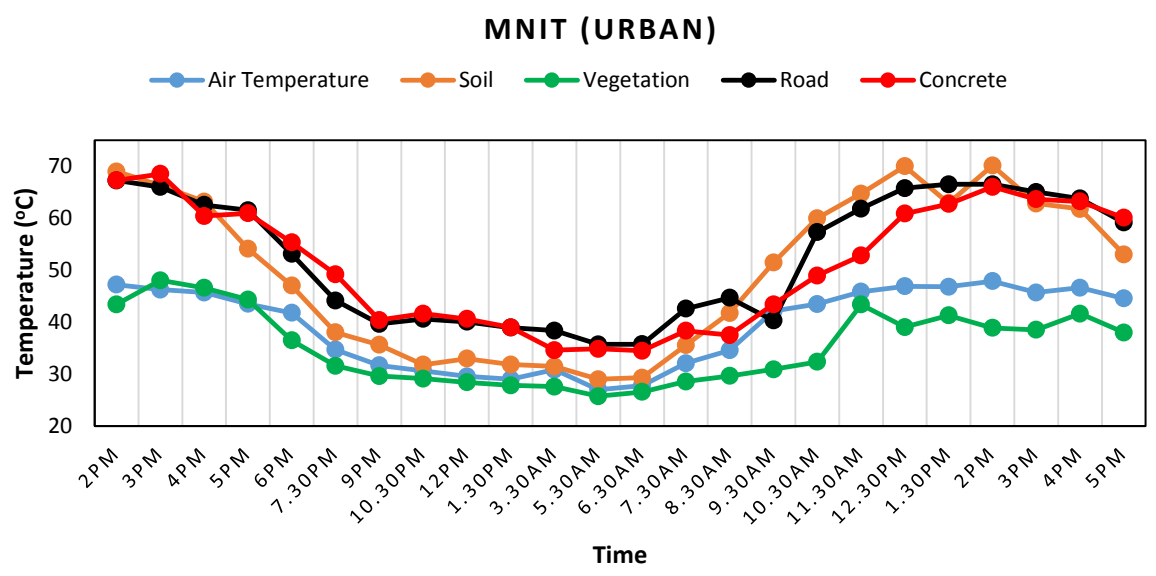
MNIT (URBAN)
Air Temperature
Soil
Vegetation
Road
Concrete
Temperature (°C)
70
60
50
40
30
20
2PM
3PM
4PM
5PM
6PM
7.30PM
9PM
10.30PM
12PM
1.30PM
3.30AM
5.30AM
6.30AM
7.30AM
8.30AM
9.30AM
10.30AM
11.30AM
12.30PM
1.30PM
2PM
3PM
4PM
5PM
Time

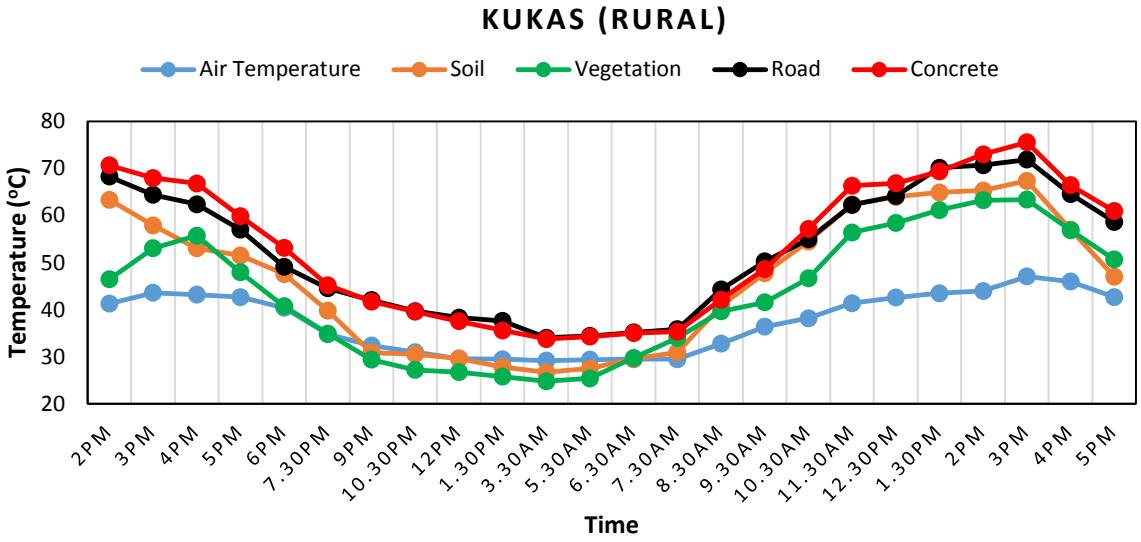

Fig. 4.36. Diurnal Variations of Surface and Air Temperatures at Different Locations of Jaipur (Summer Season)

The difference between maximum and minimum temperatures of vegetation varies by about 18.2 to 24.92 ^{o}C in summer season, during the observation period for seven locations. The temperature difference between maximum and minimum of other surfaces undergoes large variations and it varies by about 28.40 to 37.48 ^{o}C, 30.20 to 43.78 ^{o}C and 40.94 to 45.29 ^{o}C, respectively for concrete, road and soil surfaces in summer season, during the period of observation. Summer season shows large variations in temperatures of various surfaces compared to other seasons.

Absolute maximum surface temperatures of soil, vegetation, road, and concrete during the observation period have been observed to be 72.48 ^{o}C, 51.80 ^{o}C, 70.58 ^{o}C, and 68.50 ^{o}C, respectively. The absolute minimum surface temperatures of soil, vegetation, road, and concrete have been observed to be 24.40 ^{o}C, 24.80 ^{o}C, 26.80 ^{o}C, and 36.64 ^{o}C, respectively. Soil shows the maximum absolute temperature during day period and minimum absolute temperature during night period compared to other surfaces during summer season.

The higher temperature of soil as compared to other materials is observed up to about 4:00 PM and then the temperature starts falling under clear sky conditions.

It can be seen from the chart corresponding to summer season (Fig. 4.36) that the peak road temperature of 70.58 ^{o}C is recorded at about 2:00 PM at Vaishali Nagar and the road temperature is about 18.78 ^{o}C and 4.35 ^{o}C higher than the corresponding temperature of vegetation and concrete surfaces, respectively and it is about 1.11 ^{o}C higher than the

corresponding temperature of soil. The peak concrete temperature of 68.5 ^{o}C is recorded at about 3:00 PM at MNIT and the concrete temperature is about 1.62 ^{o}C lower than the corresponding temperature of soil surface and it is about 20.48 ^{o}C and 1.26 ^{o}C higher than the corresponding temperature of vegetation and road surfaces. The peak soil temperature of 72.48 ^{o}C is recorded at about 2:00 PM at Benad and the soil temperature is about 23.56 ^{o}C, 7.41 ^{o}C and 9.9 ^{o}C higher than the corresponding temperature of vegetation, road and concrete surfaces, respectively.

Table 4.18: In-Situ Air Temperature Readings at Various Locations (Summer)

Time	Kanwar	MNIT	PGIS	Sitapura	Vaishali	Benad	Kukas
2:00 PM	43.1	47.2	45.1	43.1	45	45.1	41.3
3:00 PM	43.6	46.2	46.6	44.4	46.2	46.4	43.6
4.00 PM	42.3	45.7	41.9	43.8	46.4	47.2	43.2
5.00 PM	40.1	43.5	39.9	43.3	44.5	46.3	42.7
6.00 PM	38.6	41.8	39.5	41.9	43.1	44.0	40.4
7.30 PM	34.8	34.7	37.2	38.9	44.4	36.6	34.8
9.00 PM	33.1	31.7	35.8	34.7	36.2	34.6	32.4
10.30 PM	32.3	30.6	34.1	30.2	33.2	33.6	31.0
12.00 AM	31.9	29.6	32.4	29.6	32.2	31.6	29.6
1.30 AM	31.0	29.0	33.1	28.4	31.2	30.4	29.5
3.30 AM	30.6	30.9	33.3	28.3	29.0	29.2	29.2
5.30 AM	29.8	27.0	31.2	28.0	29.5	28.0	29.4
6.30 AM	30.3	27.8	34.5	31.2	30.7	30.1	29.5
7.30 AM	31.5	32.1	40.1	35.7	37.6	31.1	29.5
8.30 AM	35.0	34.6	41.0	38.6	39.6	34.2	32.8
9.30 AM	38.6	42.1	41.6	39.8	40.2	37.7	36.4
10.30 AM	40.6	43.5	41.2	41.4	42.0	41.7	38.2
11.30 AM	41.1	45.8	41.2	43.6	44.0	43.5	41.4
12.30 PM	43.2	46.9	41.6	45.0	45.4	46.6	42.6
1.30 PM	44.9	46.8	41.7	45.3	46.0	46.9	43.5
2.00 PM	46.4	47.9	41.6	45.7	47.0	47.2	44.0
3.00 PM	44.3	45.7	41.7	46.0	48.0	48.8	47.1
4.00 PM	44.1	46.6	42.0	45.2	47.0	47.1	46.0
5.00 PM	42.4	44.5	41.2	44.3	45.0	46.2	42.7

Tables 4.18 shows air temperatures at different times at seven locations. The absolute maximum and minimum air temperatures of 48.8 ^{o}C and 27.00 ^{o}C are observed at Benad and MNIT, respectively. At all locations, during night time concrete and road temperatures have been observed to be higher than the soil temperatures. The thermal pattern of road and concrete surfaces, during night time, has been observed to be similar and the temperature of road and concrete surfaces is almost same. Air temperature has been observed to be very

close to soil and vegetation temperatures during nighttime. Vegetation shows lowest temperature during night time, but in most of the cases it is very close to the soil temperature as well. The soil temperature is less than road and concrete temperature up to about 7.30 AM. After this time, soil surfaces has higher temperature than other land covers like road, concrete, vegetation etc. till the solar radiation starts decreasing at about 4 PM. During summer season, due to prolonged day time clear sky conditions, and intense solar radiations, exposed soil surfaces show higher surface temperatures than other land covers for a prolonged time compared to other seasons.

4.4.1.1 Discussions on In-Situ Temperature Measurements for Different Seasons

Large variations in temperatures of different land covers has been observed predominantly during day time. Soil absorbs more heat and shows higher temperature than built-up materials like concrete and bitumen during day time. Hence rural areas (where soil/sparse/drier vegetation surfaces are more) show higher land surface temperatures than the urban areas where concrete buildings and roads are predominant. Urban materials like concrete, roads, stone etc. absorb and store heat during daytime. These materials gradually release this heat after sunset, in order to maintain the environmental thermal equilibrium, resulting in SUHI effect during night time. Hence SUHI can be considered as a nocturnal phenomenon.

From the seasonal analysis, it has been observed that surface temperature variations of various land covers are affected by the season. During monsoon season, thermal profile of soil varies inconsistently due to the presence of cloud cover. When the cloud cover appears, soil cools immediately compared to other land covers because of the lower thermal inertia. Similarly, in absence of cloud cover, soil gets warm faster compared to other land surfaces. During winter season, the surface and air temperatures observed are lower than monsoon season observations.

During night time, irrespective of the season, thermal profiles of various land covers show less variations. In all seasons during night time built-up materials like road and concrete show higher surface temperatures than soil and vegetation. The urban surfaces, compared to rural surfaces, have higher solar radiation absorption, greater thermal conductivity and capacity to release the heat stored during day, at night. The difference in thermal properties of the radiating surfaces lead to an increase in sensible heat stored in the fabric of the city.

Hence night time data is best suitable for SUHI studies than day time data. Though, there are many advantages of using remote sensing techniques for SUHI studies, it must be kept in mind that the derived temperatures are the surface temperatures of the emitted materials and these are much different than the in situ measured air temperatures. Due to the abundance of varying surface types in the urban environment, the surface temperatures exhibit a much greater spatial variation than the concurrent air temperatures (Streutker, 2002).

Vegetation always show similar thermal profile at all time observations and provides cooling effect during day and night time and exhibit lowest surface temperatures diurnally. Soil exhibits contradictory thermal pattern during day and night time. During day time with clear sky conditions, soil exhibit higher surface temperatures than built-up and vegetation. During night time, built-up surfaces have higher surface temperatures and soil and vegetation show lower temperatures.

4.4.2 Relationship of Difference in Temperatures of Various Surfaces with Respect to Time

Difference in soil and road or concrete temperatures at different times have been plotted for different seasons (Figs. 4.37 and 4.38). Difference in soil and road temperature of study locations ranges from -6.6 to 18 ^{o}C for winter season and the corresponding difference in soil and concrete temperature ranges from -8.68 to 15.65 ^{o}C. Positive difference shows higher soil temperature than other surfaces and negative difference shows lower soil temperature than these surfaces. For monsoon season, difference in soil and road temperature ranges from -11.52 to 7.04 ^{o}C and the corresponding difference in soil and concrete temperature ranges from -15 to 8.09 ^{o}C. Difference in soil and road temperature ranges from -11.64 to 12.1 ^{o}C for summer season and the corresponding difference in soil and concrete temperature ranges from -13.92 to 13.69 ^{o}C.

The maximum positive difference between soil and concrete temperature for all study locations ranges from 5.37 to 13.69 K, 0.2 to 8.09 K, and 3.4 to 15.65 K for summer, monsoon and winter seasons, respectively. The maximum positive difference between soil and road or concrete temperature has been observed between 12.30 PM to 3.00 PM.

The maximum negative difference between soil and road temperature ranges from -11.64 to -6.82 K, -11.52 to -5.15 K, and -6.6 to -2.32 K for summer, monsoon and winter seasons, respectively.

Negative difference between soil and road or concrete temperature has been observed especially during solar off periods. The maximum negative difference between soil and road and concrete temperature has been observed between 1.30 AM and 6.30 AM.

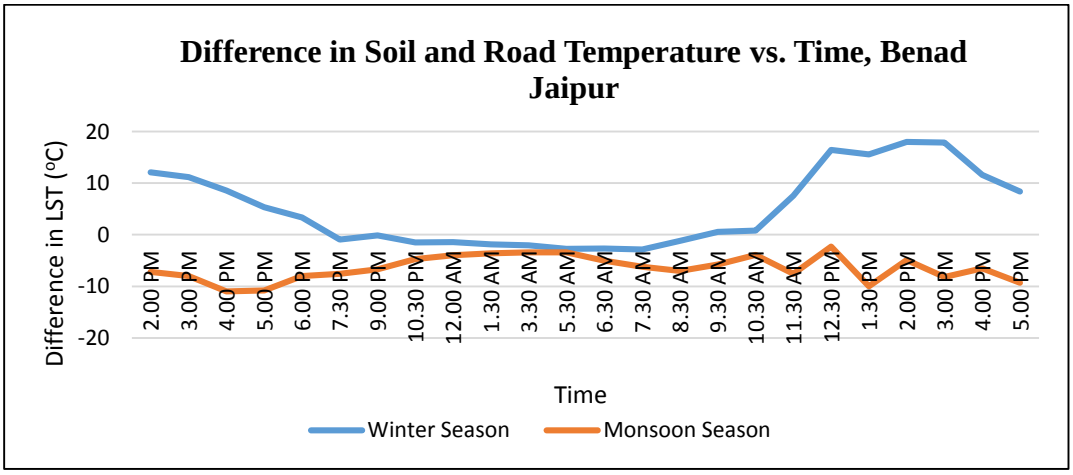

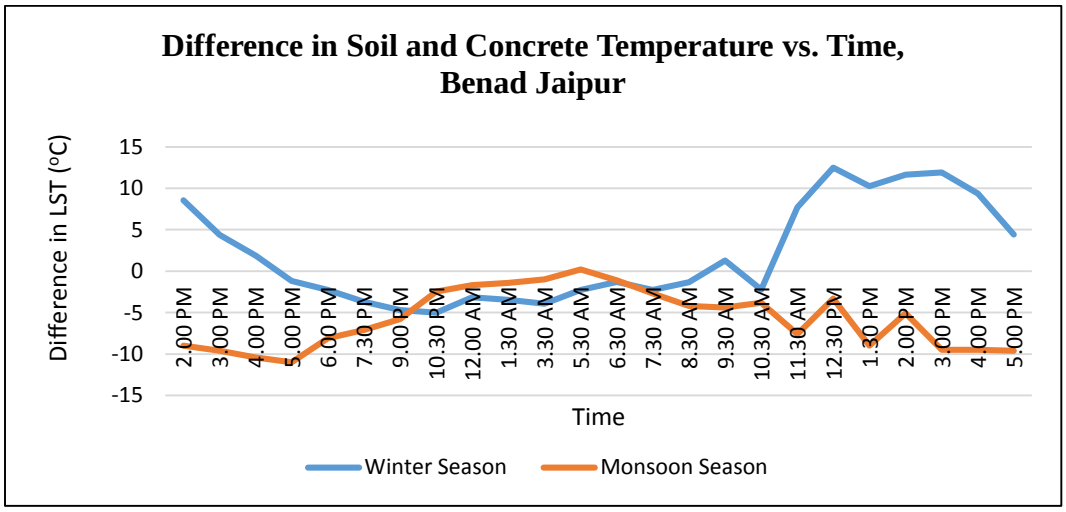

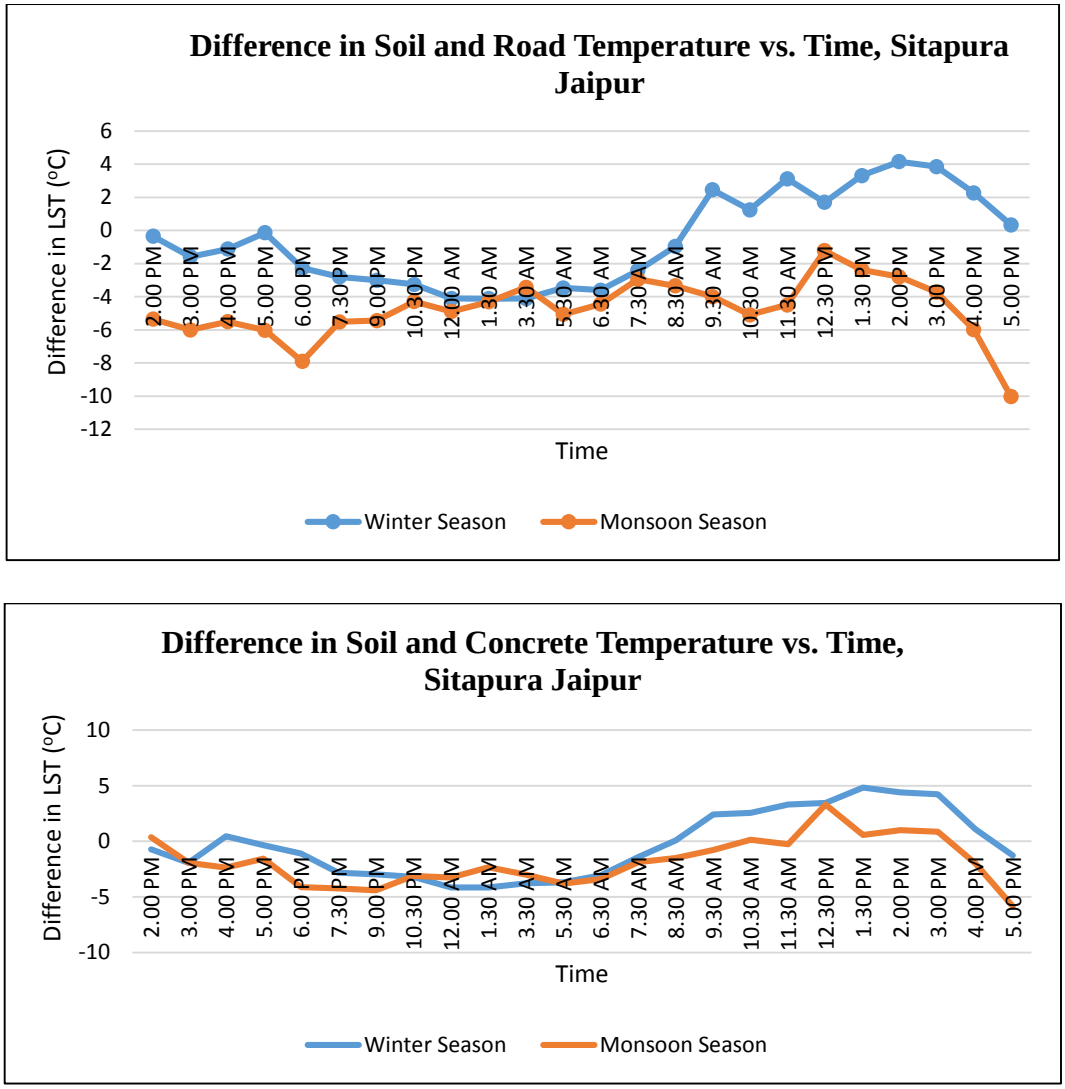

Fig. 4.37. Difference in Temperature vs. Time between Winter and Monsoon Seasons

This can be seen from Figs. 4.37 and 4.38 that difference in surface temperatures of soil and concrete or road is mainly dependent on time. During nighttime at most of the locations difference in LST of soil with urban surfaces is almost consistent with less variations. But during daytime, large variations in difference in LST of natural and built-up surfaces has been observed. During solar peak time, thermal behavior of different land surfaces is different as compared to the behavior in the absence of solar radiations during nighttime. During summer and winter seasons, it has been observed that during daytime soil shows high temperature profile than urban materials like cement concrete, etc. and during night time urban materials show higher temperature profile compared to soil and vegetation. Soil and road or concrete temperature difference for monsoon and winter season has been observed to be more uniform during night time compared to day time. i.e. soil and road or concrete temperature difference shows higher variations during day time. From the winter

and summer in-situ surface temperature study for different land surface materials, it has been observed that the crossing time when the soil temperature starts decreasing, gets extended during summer season compared to winter season.

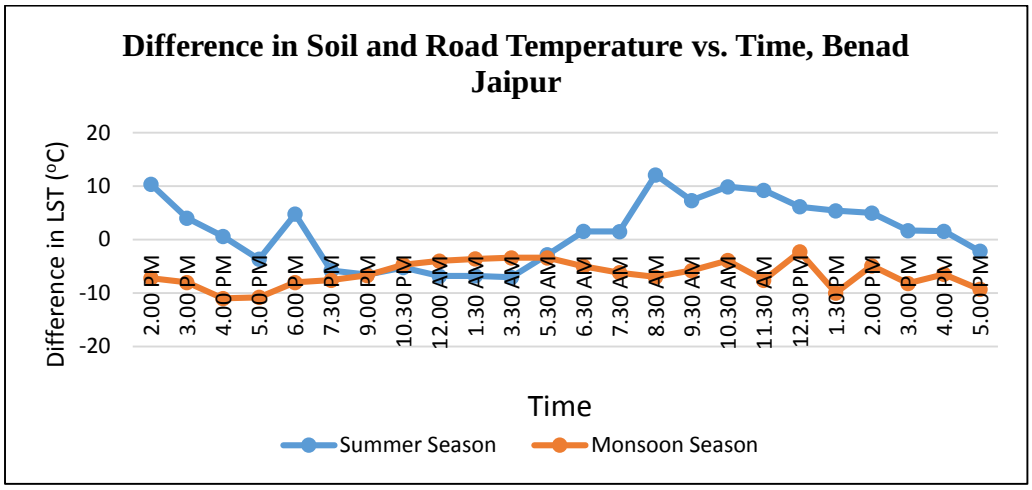

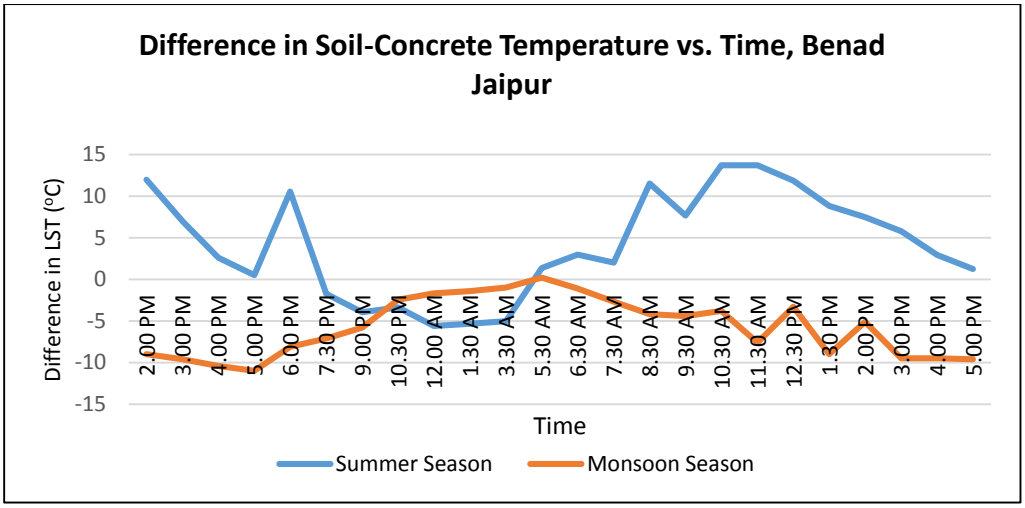

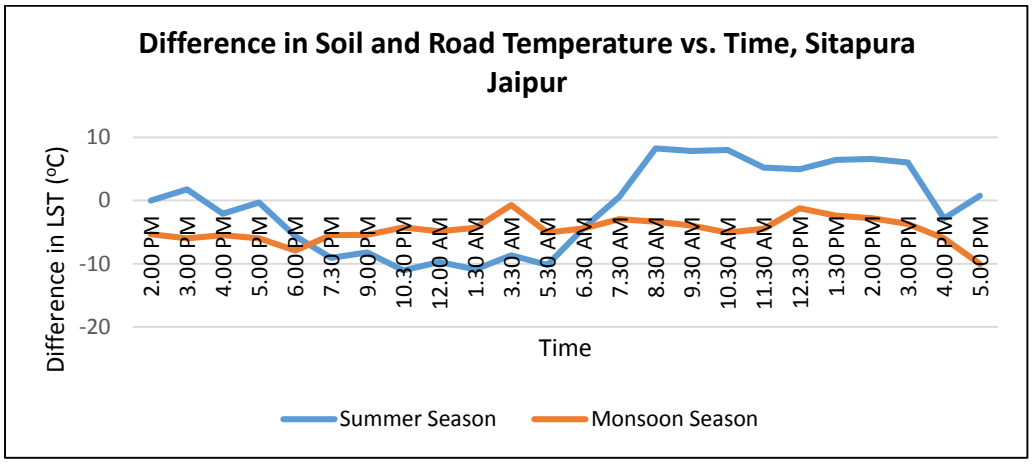

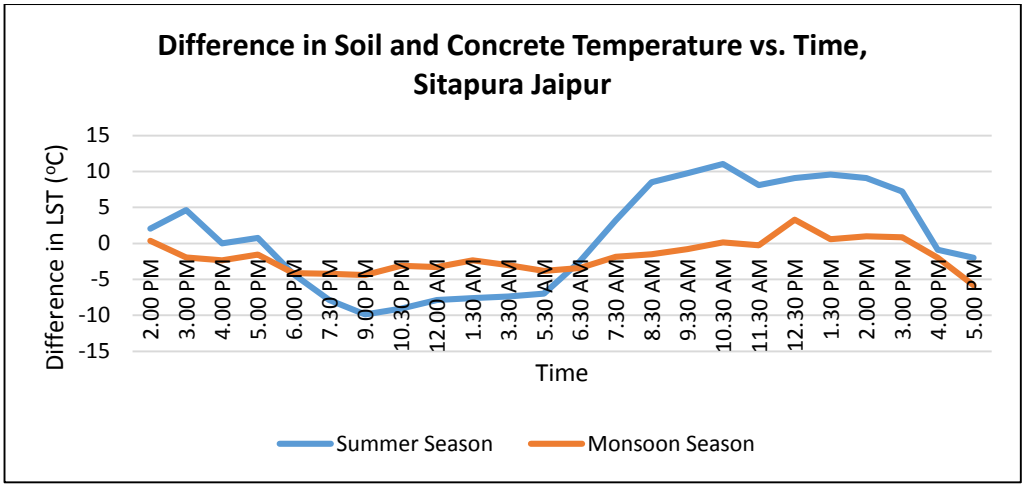

Fig. 4.38. Difference in Temperature vs. Time between Summer and Monsoon Season

Bituminous road shows higher surface temperatures than concrete and less temperatures than bare soil especially during day time. At almost all the locations soil shows slightly higher surface temperatures than road especially during daytime. In Vaishali Nagar, difference in soil and road LST during both seasons observed to be negative, i.e. bituminous road shows slightly higher surface temperatures than soil. Freshly built roads exhibit higher temperatures than old roads. All other locations difference in soil and road LST observed to be positive during summer season with clear sky conditions and at some times of observations, it is observed to be negative especially during monsoon season with cloud cover conditions. During night time, it has been observed that all locations exhibit negative values for difference in soil and road LST in both seasons which means that soil shows very less temperatures compared to road. Hence diurnal thermal behavior of soil can be clearly identified from the above graphs.

4.4.3 Comparison of AUHI and SUHI Effect over Jaipur City

Existence of SUHI and AUHI over Jaipur has been analyzed using in-situ air temperature and satellite derived LST data of seven locations. SUHI and AUHI intensity have been estimated at 10.30 AM and 10.30 PM which is the Terra satellite pass time over the study area. UHI intensity has been calculated as the difference between maximum and minimum temperatures at two points. The location where the air temperature is minimum at 10.30 PM has been considered as the reference temperature and for UHI intensity at all other locations has been calculated with respect to this reference temperature. AUHI intensities have been calculated using in-situ air temperature readings And SUHI intensities have been calculated using MODIS Terra LST data.

4.4.3.1 Summer Season

Table 4.19 shows air and surface temperature values at the time of satellite pass of different locations during summer season. Minimum air temperature of 30.2 ^{o}C has been observed at Sitapura and UHI intensity has been calculated with reference to the temperature at Sitapura. The MODIS derived day and night LSTs observed at 10:30 AM (318.9 K) and 10:30 PM (300.9 K), respectively have been considered as the base LSTs for calculation of SUHI intensity. Air temperature recorded at Sitapura at 10:30 AM (40.4 ^{o}C) and 10:30 PM (30.2 ^{o}C) has been considered for day and night AUHI intensity calculations, respectively.

Table 4.19: Estimation of Atmospheric and Surface Urban Heat Island Effect over Jaipur City during Summer Season

	Day				Night			
Location	**Air Temperature** (^{o}C)	**LST(K)**	**AUHI intensity (K)**	**SUHI Intensity (K)**	**Air Temperature** (^{o}C)	**LST (K)**	**AUHI intensity (K)**	**SUHI Intensity (K)**
Kanwar	40.6	317.0	0.2	-1.9	32.3	304.7	2.1	3.8
MNIT	43.5	317.2	3.1	-1.8	30.6	303.1	0.4	2.2
PGIS	41.2	318.0	0.8	-0.9	34.1	300.8	3.9	0.1
Sitapura	40.4	318.9	0.0	0.0	**30.2**	300.9	0.0	0.0
Vaishali	42.0	317.4	1.6	-1.6	33.2	303.6	3.0	2.7
Benad	41.7	317.2	1.3	-1.7	33.6	302.7	3.4	1.8
Kukas	38.2	318.8	-2.2	-0.1	31.0	302.4	0.8	1.5

a) Day Period

Kanwar Nagar shows minimum SUHI intensity -1.9 K during day period which clearly shows the existence of negative SUHI effect over the area. Similarly, most of the study locations show negative SUHI intensity ranges from -0.1 K to -1.9 K while using MODIS day LST data. This clearly shows that inverse or negative SUHI exists over the study area during day period if LST is used for study of UHI effect. Conversely, most of the study locations show positive AUHI intensity ranging from 0.2 K to 3.1 K while using air temperature which clearly shows the existence AUHI effect over the study area during day period. The AUHI intensity at urban locations is higher than those observed at rural locations. Negative AUHI intensity of -2.2 K at Kukas indicates that the air temperature at Kukas is lower than the corresponding temperature at Sitapura.

b) Night Period

Maximum AUHI intensity of 3.9 K has been observed at PGIS location, whereas Kanwar Nagar shows maximum SUHI intensity of 3.8 K while using Terra LST data. AUHI intensity ranges from 0 to 3.9 K, whereas SUHI intensity ranges from 0 to 3.8 K for Terra LST data. Both the AUHI and SUHI intensities are higher for urban locations than the rural locations.

4.4.3.2 Monsoon Season

Table 4.20 shows air and surface temperature values at the time of satellite pass of different locations during monsoon season. Minimum air temperature of 24.1 ^{o}C has been observed at Benad and UHI intensity has been calculated with reference to the temperature at Benad. The MODIS derived day and night LSTs observed at 10:30 AM (307.2 K) and 10:30 PM (296.3 K), respectively have been considered as the base LSTs for calculation of SUHI intensity. Air temperature recorded at Benad at 10:30 AM (28.1 ^{o}C) and 10:30 PM (24.1 ^{o}C) has been considered for day and night AUHI intensity calculations, respectively.

Table 4.20: Estimation of Atmospheric and Surface Urban Heat Island Effect over Jaipur City during Monsoon Season

	Day				**Night**			
Location	**Air Temperature (^{o}C)**	**LST(K)**	**AUHI intensity (K)**	**SUHI Intensity (K)**	**Air Temperature (^{o}C)**	**LST (K)**	**AUHI intensity (K)**	**SUHI Intensity (K)**
Kanwar	30.5	304.8	2.4	-2.4	27.1	298.9	3.0	2.6
MNIT	29.7	305.9	1.6	-1.3	27.2	297.7	3.1	1.4
PGIS	30.7	305.3	2.6	-1.9	26.2	296.1	2.1	-0.2
Sitapura	30.8	306.4	2.7	-0.8	25.8	297.0	1.7	0.7
Vaishali	29.0	308.7	0.9	1.5	27.5	297.4	3.4	1.1
Benad	28.1	307.2	0.0	0.0	**24.1**	296.3	0.0	0.0
Kukas	27.7	306.8	-0.4	-0.4	26.5	297.1	2.4	0.8

a) Day Period

Kanwar Nagar shows minimum SUHI intensity of -2.4 K during day period which clearly shows the existence of negative SUHI effect over the area. Similarly, most of the study locations show negative SUHI intensity ranges from -0.4 K to -2.4 K while using MODIS day LST data. This clearly shows that inverse or negative SUHI exists over the study area during day period while LST is used. Conversely, most of the study locations show positive AUHI intensity ranges from 0.9 K to 2.7 K while using air temperature day data which clearly shows the existence AUHI effect over the study area during day period. Most of the

locations show positive AUHI effect except Kukus showing AUHI intensity of -0.4 K which is also a rural location.

b) Night Period

Maximum AUHI intensity of 3.4 K has been observed at Vaishali location, whereas Kanwar Nagar shows maximum SUHI intensity of 2.6 K while using Terra LST data. AUHI intensity ranges from 0 to 3.4 K, whereas SUHI intensity ranges from -0.2 to 2.6 K for Terra data. Both the SUHI and AUHI intensities at the three urban locations are much more than the corresponding SUHI and AUHI intensities at the rural locations. The only exception is PGIS, where the AUHI intensity is high but the SUHI intensity is nearly zero. This can be due to the effect of prevailing wind direction.

4.4.3.3 Winter Season

Table 4.21 shows air and surface temperature values at the time of satellite pass of different locations during winter season. Minimum air temperature of 9.2 ^{o}C has been observed at Benad and UHI intensity has been calculated with reference to the temperature at Benad. The MODIS derived day and night LSTs observed at 10:30 AM (297.8 K) and 10:30 PM (281.2 K), respectively have been considered as the base LSTs for calculation of SUHI intensity. Air temperature recorded at Benad at 10:30 AM (16.1 ^{o}C) and 10:30 PM (9.2 ^{o}C) has been considered for day and night AUHI intensity calculations, respectively.

Table 4.21: Estimation of Atmospheric and Surface Urban Heat Island Effect over Jaipur City during Winter Season

	Day				**Night**			
Location	**Air Temperature** (^{o}C)	**LST(K)**	**AUHI intensity (K)**	**SUHI Intensity (K)**	**Air Temperature** (^{o}C)	**LST (K)**	**AUHI intensity (K)**	**SUHI Intensity (K)**
Kanwar	16.8	295.4	0.7	-2.4	12.6	286.4	3.4	5.3
MNIT	13.3	293.8	-2.8	-4.0	8.4	284.1	-0.8	2.9
PGIS	19.1	299.7	3.0	1.9	12.9	280.2	3.7	-0.9
Sitapura	16.6	296.2	0.5	-1.6	11.5	281.5	2.3	0.4
Vaishali	16.5	296.4	0.4	-1.4	11.6	283.3	2.4	2.1
Benad	16.1	297.8	0.0	0.0	**9.2**	281.2	0.0	0.0
Kukas	21.1	296.5	5.0	-1.3	10.7	281.3	1.5	0.2

a) Day Period

MNIT shows minimum SUHI intensity of -4 K while using MODIS data during day period which clearly shows the existence of negative SUHI effect over the area. Similarly, most of the study locations show negative SUHI intensity ranges from -1.3 K to -4 K while using

MODIS day LST data. This clearly shows that inverse or negative SUHI exists over the study area during day period while LST is used. Conversely, most of the study locations show positive AUHI intensity ranges from 0 K to 5 K while using air temperature day data which clearly shows the existence AUHI effect over the study area during day period.

b) Night Period

Most of the study locations show positive SUHI and AUHI intensity during both periods. Maximum AUHI intensity of 3.7 K has been observed at PGIS location, whereas Kanwar Nagar shows maximum SUHI intensity of 5.3 K while using Terra LST data. AUHI intensity ranges from -0.8 to 3.7 K, whereas SUHI intensity ranges from -0.9 to 5.3 K for Terra LST data. Kanwar Nagar, which falls in the CBD of Jaipur city observes maximum SUHI and AUHI intensities during nighttime.

It can be seen from above tables that the SUHI intensity, during daytime, at the urban locations is negative as the LST of rural locations is higher than the LST of urban locations. This shall mean a cool island effect. However, the same cool island effect shall have been observed from AUHI intensity as well. But the AUHI intensity is different from SUHI intensity during daytime and the air temperatures at urban locations are higher than the corresponding air temperatures at rural locations. When the nighttime data is considered both the SUHI and AUHI intensities for urban locations are higher than the rural locations. Maximum AUHI and SUHI intensities are observed at one or other urban locations (mostly at the location that is at the CBD of the city). AUHI and SUHI intensities at other urban locations are also high. All three seasons show similar observations of AUHI and SUHI effect for both day and night period. SUHI is more apparent at night, i.e. SUHI has been considered as a nocturnal phenomenon and not prominent during day period. AUHI has been observed during both day and night. Clear existence of AUHI and non-existence of SUHI has been observed over the study area during day period through the field survey analysis, whereas clear existence of both AUHI and SUHI has been observed during the night. Significant diurnal AUHI effect has been observed over the study area which depicts that urban area is warmer compared to rural area. Inverse or negative SUHI effect has been observed over some cities due to the variations in thermal behavior of various land surfaces. In general, SUHI is not apparent at daytime. Daytime LST data have been used in many SUHI studies. SUHI varies during the day and it is more significant during the evening/night.

4.5 Diurnal Relationship of LST with Various Parameters

This section documents the comprehensive results and discussion of the effects of various parameters on LST. Parameters considered include NDVI to represent vegetation; MNDWI to represent water; NDBaI to represent soil; %ISA, RD, NDBI to represent urbanization; and DEM to represent terrain;. It is possible that the utilization of NDVI, MNDWI, NDBaI, ISA, RD and NDBI could represent land-cover types quantitatively so that the diurnal relationships between different indices and LST can be established in UHI studies.

Diurnal trends of various surface and topographical parameters with LST for three Indian cities have been discussed in the following sections.

4.5.1 Vegetation Pattern

NDVI can be used to represent the intensity of vegetation over an area. The study areas of Jaipur and Ahmedabad have semi-arid climate and rainfall during monsoon season and groundwater are the primary sources of fulfilling water demand. Vegetation and agriculture, throughout the study areas, mainly depend on monsoon rainfall, and hence vegetation density is different during same periods of different years. Landsat derived NDVI images of different periods, representing three seasons of the years 2003, 2009 and 2015 have been shown in Fig. 4.39. Frequent spalls of rainfall during monsoon results in the growth of vegetation of variable density over the entire study area. Poorly vegetated areas have lower NDVI values and appear purple while highly vegetated areas appear green in the figures. Rural area has few purple spots and different intensity green spots indicating varying vegetation growth. The center of the urban area appear much darker and represent much lower NDVI values, in comparison to other parts of the urban area which appear light purple. Large part of the urban area appears purple as there is less scope of vegetation growth due to urbanization. A large percentage of these areas comprises of impervious built-up surfaces, and there is very little (almost insignificant) vegetation on these regions. The range of NDVI values is more during monsoon season than the winter season. The range of NDVI values is lowest during summer season. There is a continuous reduction of green color throughout the study area from March to May, and very few isolated patches of vegetation can be seen. High temperature and low supply of water during summer season cause degradation in the density of vegetation of the study area. Large part of the study

areas is purple during summer season and NDVI values are typically for barren land. Varying vegetation pattern of three study areas has been observed for different seasons, which clearly depicts that NDVI is a season dependent parameter.

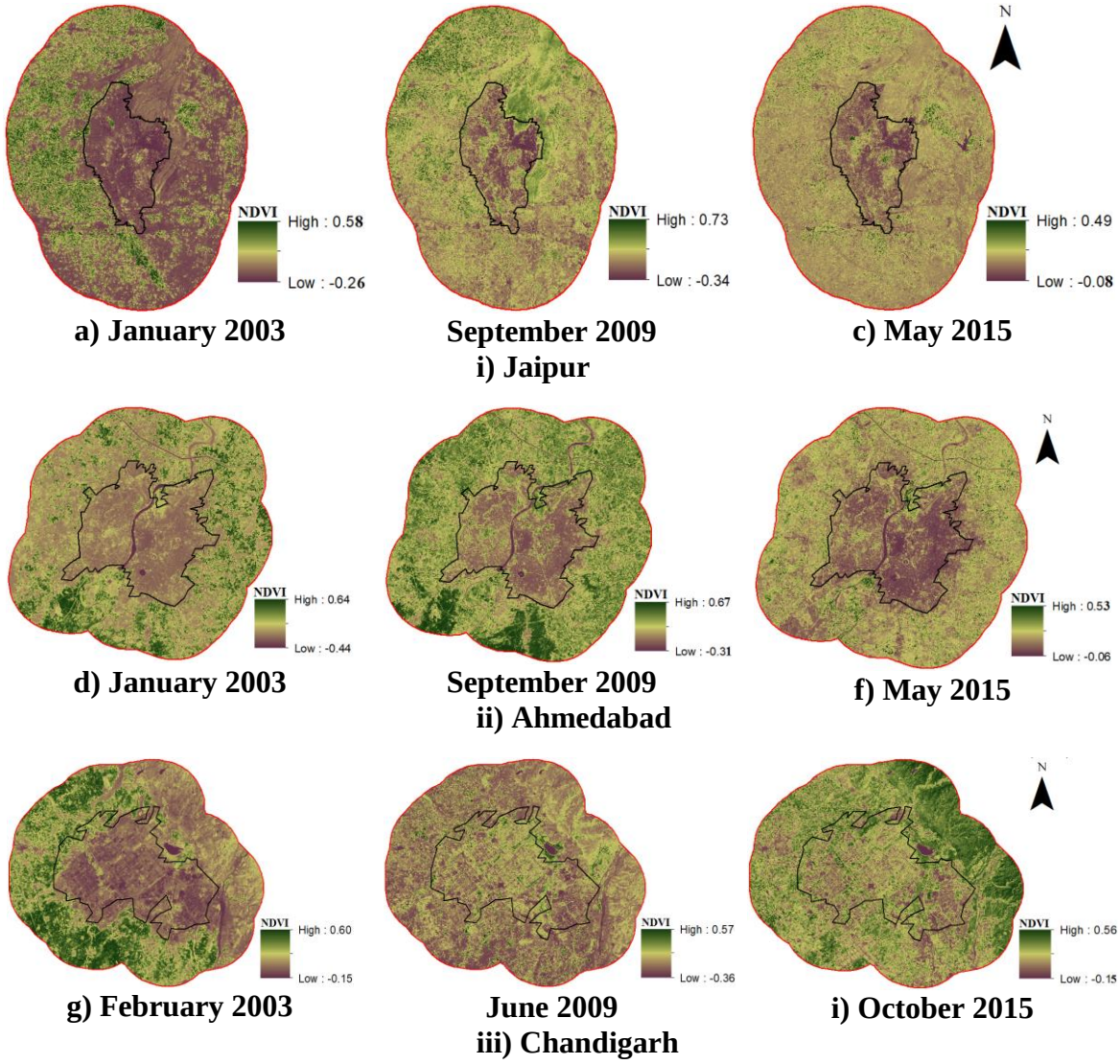

Fig. 4.39. Landsat Derived NDVI Images of the Study Areas for Different Seasons

The contrast between vegetation in urban and rural areas is more prominent with the advance of monsoon and the entire rural area is under vegetation cover (can be seen from monsoon NDVI image), whereas the vegetation over urban area is in the form of few localized spots (Fig. 4.39). North Western part of the Jaipur study area appears dark green in color indicating high NDVI values. Few pixels of low NDVI values are visible at the Eastern boundary of the urban area which are at the foot of Aravalli hills. Rainfall during monsoon season results in higher vegetation density compared to other season over hill

ranges. Aravalli hill ranges appear light purple color during summer season; light green color during winter season; and green color during monsoon season.

Ahmedabad also shows large seasonal variations in vegetation pattern especially in rural areas. Central part of Ahmedabad city and water bodies like Sabarmati River, Kankaria Lake, etc. show very low NDVI values. Rural areas shows different vegetation pattern depending on various seasonal agricultural practices.

Shivangi hill ranges of Chandigarh show very low NDVI values especially during winter and summer season due to the low vegetation density. Rainfall during monsoon season results in higher vegetation density over hill ranges, compared to other seasons. Shivangi hill ranges appear light purple color during summer season; light green color during winter season; and green color during monsoon season. Pixels of high NDVI values have been observed inside the Chandigarh urban boundary due to the higher vegetation spots inside the city like parks, Dahriya reserved forest, etc. Sukhna Lake located near the North Eastern urban boundary which appear in dark purple show very low NDVI Values.

4.5.1.1 Diurnal LST vs. NDVI Relationship

Diurnal relationship between mean LST and NDVI has been analyzed. Figs. 4.40, 4.41 and 4.42 show the relationship between mean LST and NDVI for different seasons for Jaipur, Ahmedabad and Chandigarh study areas. Tables 4.22, 4.23 and 4.24 show the coefficient of correlation (linear and polynomial, respectively) of Jaipur, Ahmedabad and Chandigarh for mean LST vs. NDVI relationship.

a) Jaipur

Table 4.22: Coefficient of Correlation (Linear and Polynomial) for Mean LST and NDVI Relationship (Jaipur)

	Periods	January 2003	May 2003	May 2009	September 2009	November 2009	January 2015	May 2015	September 2015
Linear	Day	0.74	0.35	0.05	0.34	0.01	0.22	0.27	0.04
	Night	0.56	0.36	0.47	0.68	0.33	0.78	0.54	0.70
Polynomial	Day	0.74	0.41	0.10	0.36	0.01	0.75	0.67	0.54
	Night	0.80	0.54	0.56	0.73	0.78	0.86	0.60	0.70

During day time, the regression co-efficient (R^2 values) ranges from 0.01 to 0.75 (polynomial) and 0.01 to 0.74 (linear). During night time, the regression co-efficient ranges from 0.54 to 0.86 (polynomial) and 0.33 to 0.78 (linear). Winter season shows good

relationship between LST and NDVI, whereas summer season shows moderate relationship.

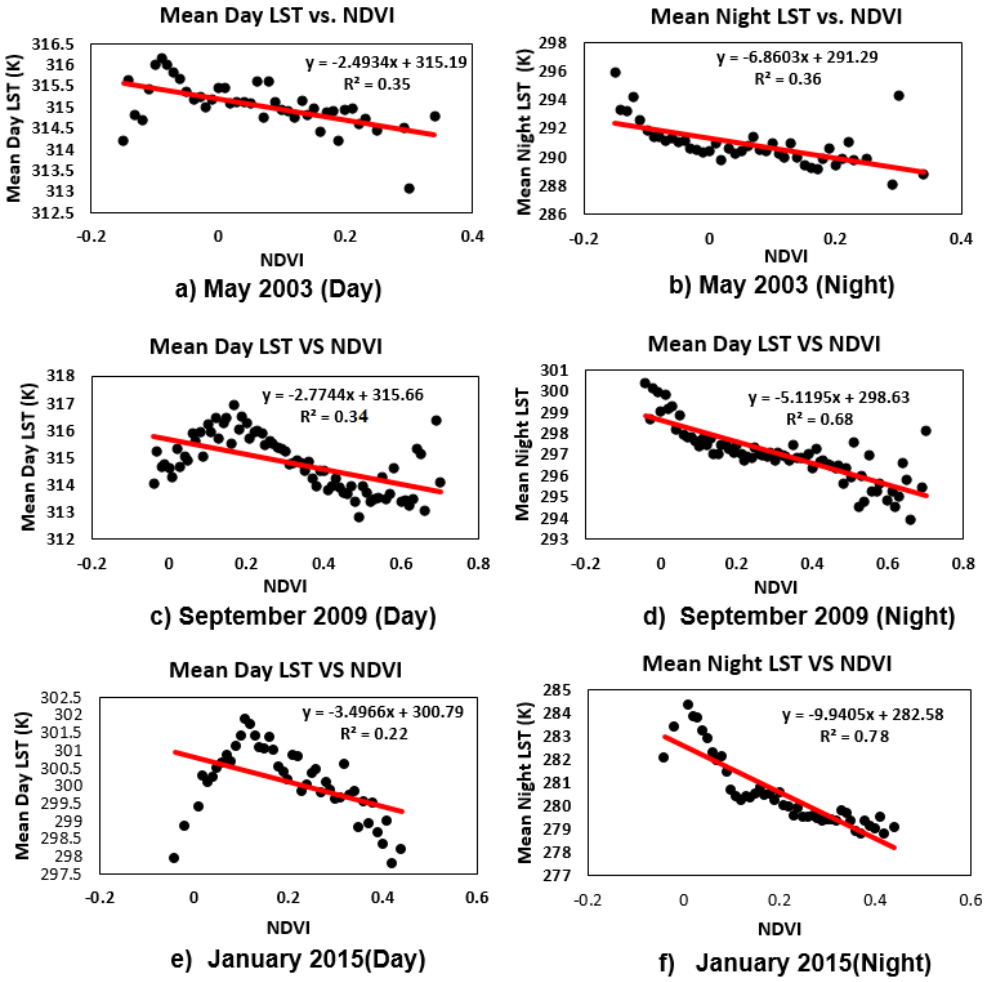

Fig. 4.40. Diurnal Mean LST and NDVI Relationship for Different Seasons (Jaipur)

b) Ahmedabad

Table 4.23: Coefficient of Correlation (Linear and Polynomial) for Mean LST and NDVI Relationship (Ahmedabad)

	Periods	January 2003	June 2009	2009 September	2009 December	2015 May	2015 October	2015 December
Linear	Day	0.41	0.36	0.76	0.02	0.01	0.62	0.19
	Night	0.46	0.42	0.78	0.62	0.19	0.59	0.52
Polynomial	Day	0.56	0.38	0.86	0.02	0.32	0.69	0.50
	Night	0.48	0.58	0.80	0.72	0.49	0.64	0.53

During day time, the R^2 values vary from 0.02 to 0.86 and 0.01 to 0.76, respectively for polynomial and linear correlation. During night period, the R^2 values range from 0.48 to 0.80 and 0.19 to 0.78, respectively for polynomial and linear correlation. Monsoon season

shows good relationship between LST and NDVI, whereas summer and winter seasons show moderate relationship.

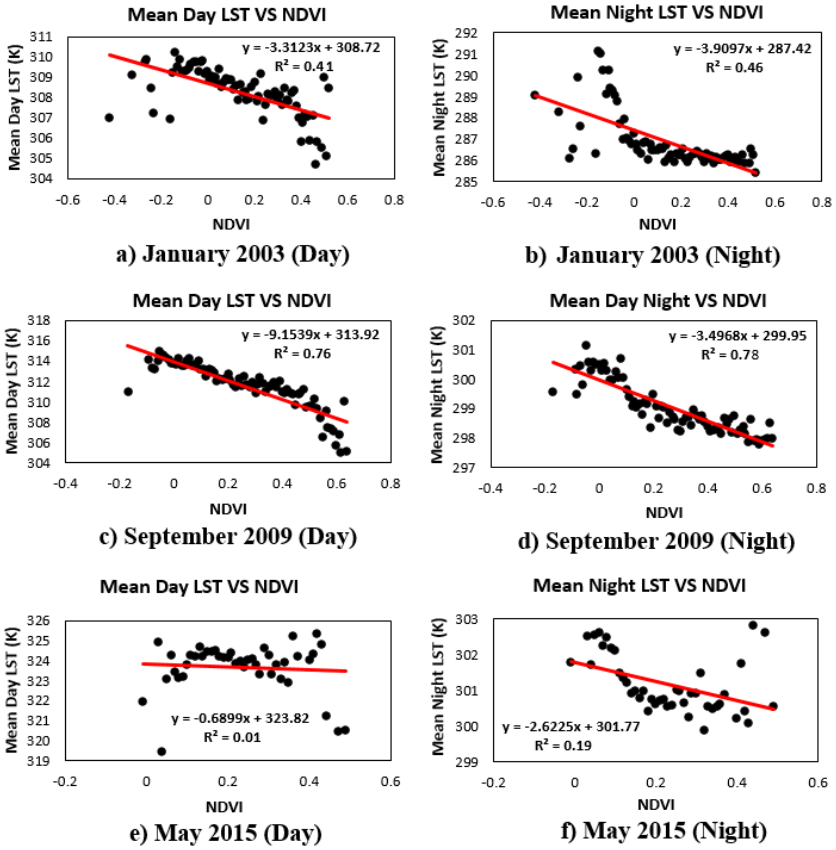

Fig. 4.41. Diurnal Mean LST and NDVI Relationship for Different Seasons (Ahmedabad)

c) Chandigarh

Table 4.24: Coefficient of Correlation (Linear and Polynomial) for Mean LST and NDVI Relationship (Chandigarh)

	Periods	2003 February	2009 June	2009 October	2009 December	2015 May	2015 October	2015 December
Linear	Day	0.59	0.02	0.38	0.09	0.16	0.20	0.07
	Night	0.72	0.17	0.09	0.04	0.10	0.46	0.33
Polynomial	Day	0.64	0.03	0.82	0.18	0.16	0.71	0.13
	Night	0.72	0.23	0.14	0.10	0.10	0.59	0.34

The regression co-efficient ranges from 0.03 to 0.82 (polynomial) and 0.02 to 0.59 (linear) during day time, whereas during night period, the regression co-efficient ranges from 0.10 to 0.72 (polynomial) and 0.04 to 0.72 (linear). Large variations in LSTs during day period is clearly evident from the analysis. Diurnal LST-NDVI relationship is not much strong in Chandigarh city as compared to other cities and the effect LST is minimized over the city

due to the sub-tropical climate of the city which favours higher vegetation density over the area.

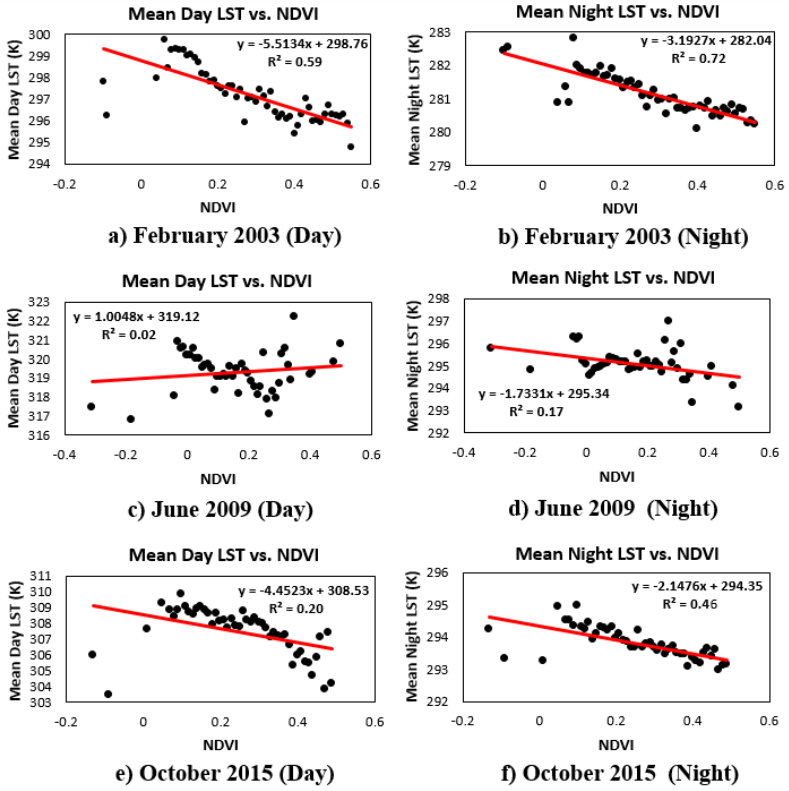

Fig. 4.42. Diurnal Mean LST and NDVI Relationship for Different Seasons (Chandigarh)

4.5.1.2 Discussions

From Tables 4.22-4.24, it can be noted that the correlation of mean LST with NDVI is better represented by non-linear (polynomial) relationship. This may be due to the fact that though the vegetation has an effect on LST yet this effect cannot be same for the entire range of vegetation. It can be expected that as the vegetation density increases, the rate of decrease of LST would reduce beyond a level of vegetation. The cooling effect of vegetation on the LST of an area is due to the reason that vegetation increases moisture availability of the area, and it also provides a shadow effect which is due to the shadow of vegetation falling on the nearby surface and thereby modifying the energy interactions which otherwise would have been different in the absence of the vegetation. This is the main reason of reduction in LST due to the introduction of vegetation at a particular place.

From the diurnal LST vs. NDVI relationship, inverse or negative relationship can be observed between LST and NDVI for both day and night periods. The relationship has been observed to be more significant and stronger during night than the day. Inverse convex

polynomial trend line has been obtained during night period, whereas during day period, inverse concave polynomial trend line has been obtained for most of the time periods. The inverse effect of NDVI on LST has been noticed for both periods from the analysis, but the effect of vegetation is more prominent during night. The effect of other parameters may dominate the effect of vegetation on LST during day period, which may result in the weak correlation of NDVI on LST during the day time. The diurnal effect of other parameters has been discussed in the following subsections.

High variation in LST of non-vegetated/low-vegetated locations is observed which is due to variable LU over such areas whereas these variations for densely vegetated areas are much lower. It is seen that the LST and VIs relationship scatterplots show different trends during different seasons thus indicating that their relationship is dependent on season, which is similar to the findings of many previous studies. From the overall analysis, it is observed that vegetation always shows inverse or negative relationship with LST irrespective of time periods. LST-NDVI relationship is mainly dependent on climate of the study area that governs the significance of NDVI and LST relationship for a particular season.

4.5.2 Pattern of Percent Impervious Surface Area (%ISA)

Imperviousness gives an objective measurement of the areal extent and intensity of urban development. The resulting classification gives a continuous range of %ISA from 0 to 100%. %ISA is a parameter representing urbanization and is independent of season. In order to analyze the spatial pattern of impervious surfaces of the study area, %ISA images (30 m resolution) for different periods of the study areas are shown in Fig. 4.43.

The values of %ISA have been calculated at the Landsat TM/OLI resolution of 30 m and at the aggregated resolution of 926.6 m. Even after aggregation, the general %ISA profile remains the same. The overall absolute maximum and minimum %ISA values of the study area are 0 and 100, respectively. The overall average of the %ISA of the study area varies from 10.13 % to 49.76 % during the study period between 2003 and 2015.

Urban areas have higher %ISA values and appear green while highly vegetated areas appear brown in the figure. Very limited green spots have been observed in the rural area especially in the western parts of the study areas of Ahmedabad and Chandigarh, which indicate low imperviousness in the rural area. Most of the green spots representing higher %ISA values

are observed within the urban boundary, especially CBD of the cities. The %ISA pattern in the urban area has been found to be almost same during different seasons with a similar trend. Rural areas show changes in %ISA pattern during different seasons due to the LU-LC changes which are almost insignificant, because of vegetation and bare land exhibit very low %ISA values which are almost equal to zero. During summer season, exposed rock surfaces over hilly areas of Jaipur and Chandigarh over dominating vegetation resulting in higher ISA values over those areas. Consistent ISA pattern has been observed over urban areas than rural areas for three cities.

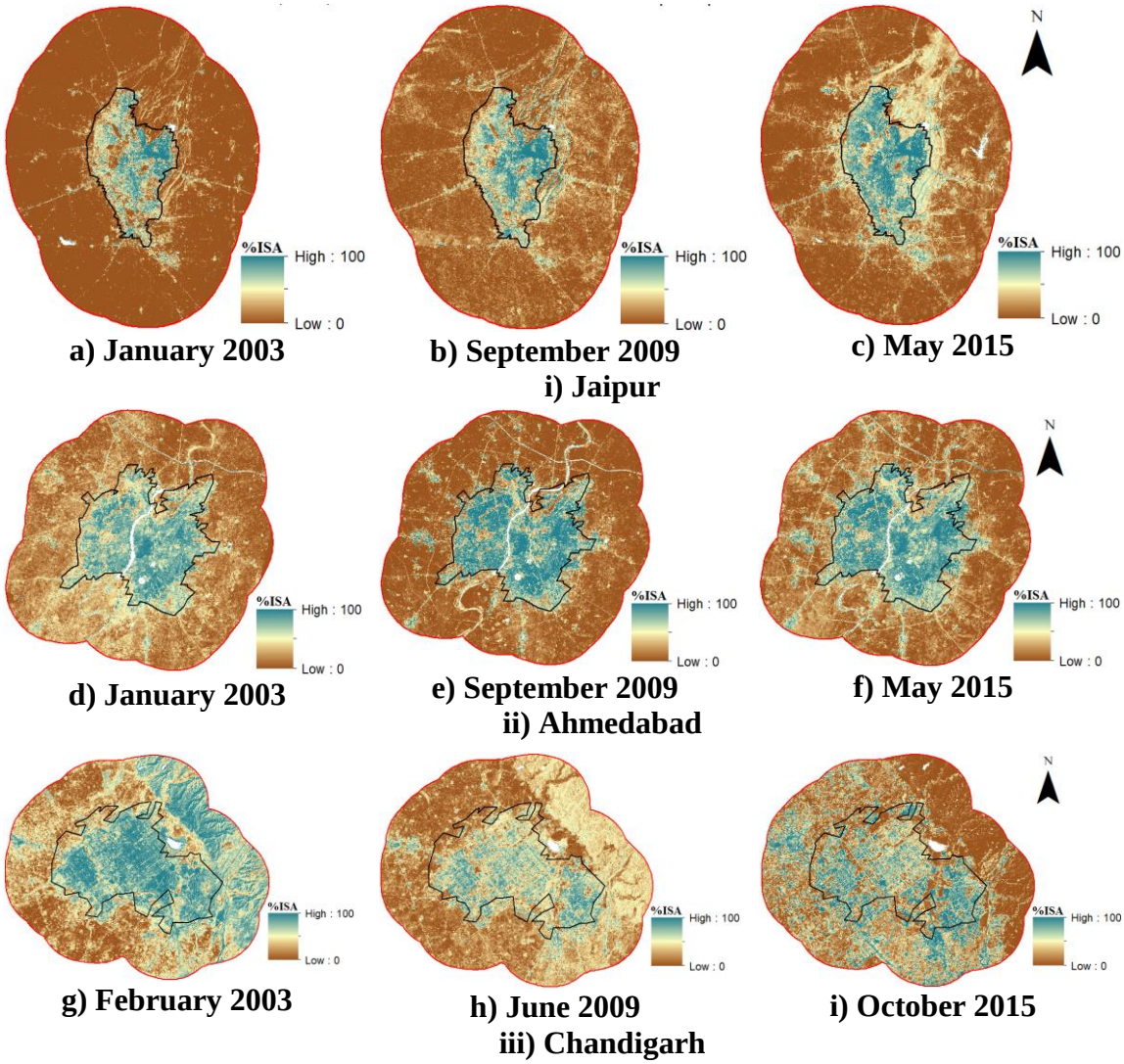

Fig. 4.43. %ISA Images of the Study Area for Different Seasons

Urban areas show higher values of %ISA compared to rural areas due to the presence of impervious surfaces like buildings, pavements, parking lots, etc. Agricultural land and vegetated areas in rural areas show zero %ISA. Bare soil in rural areas shows very low

values of %ISA compared to urban areas. Aravalli hill ranges of Jaipur and Shivangi hill ranges of Chandigarh, show varying ISA pattern depending on season.

4.5.2.1 Diurnal LST vs. %ISA Relationship

Figs. 4.44, 4.45 and 4.46 show the correlation between mean LST and ISA for different seasons. Linear and second order polynomial relationship have been used to estimate the correlation. Tables 4.25, 4.26 and 4.27 represent the coefficient of correlation (linear and polynomial, respectively) of Jaipur, Ahmedabad and Chandigarh for mean LST and ISA relationship.

a) Jaipur

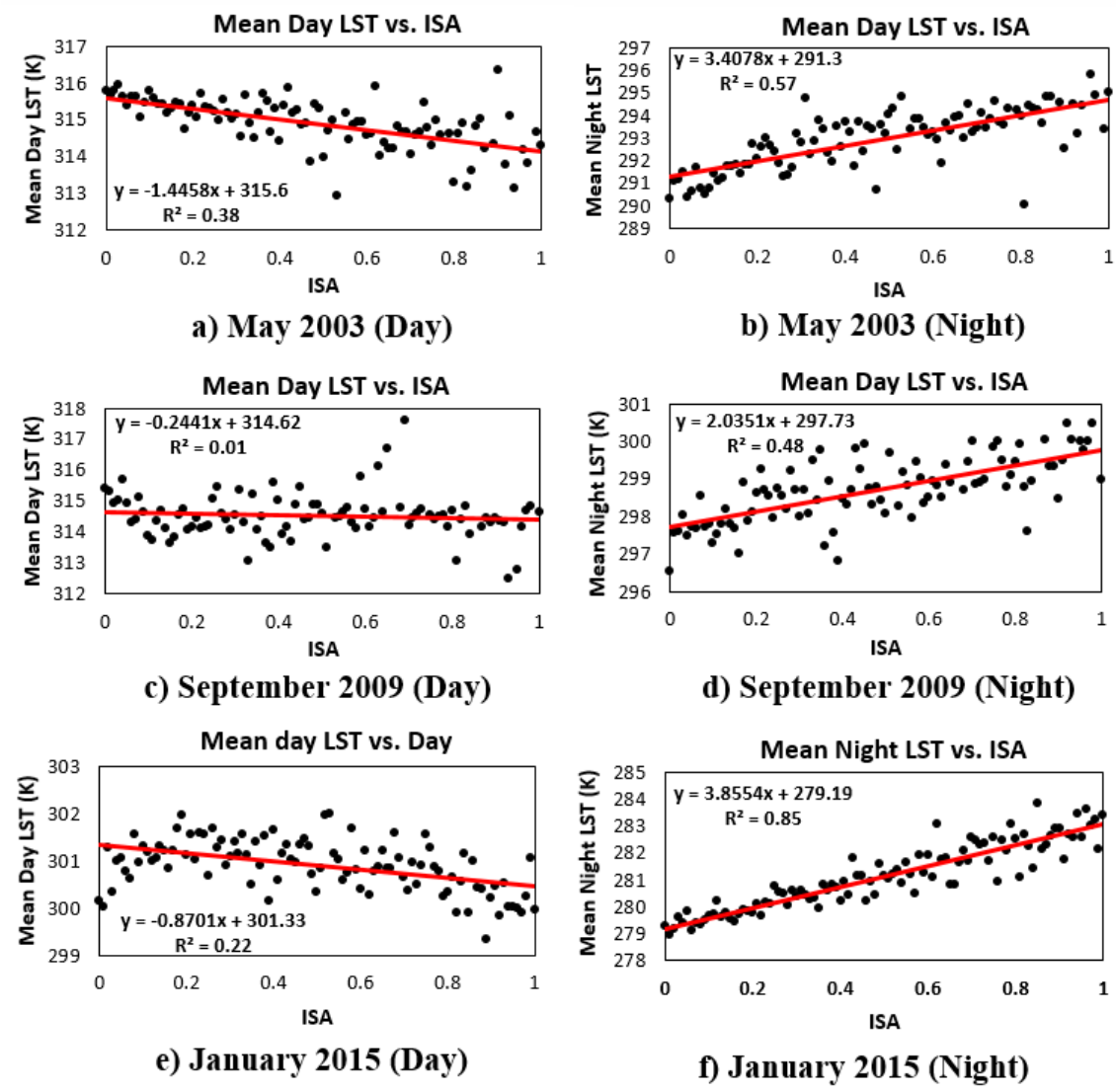

Fig. 4.44. Diurnal Mean LST and ISA Relationship for Different Seasons (Jaipur)

Table 4.25: Coefficient of Correlation (Linear and Polynomial) for Mean LST and ISA Relationship (Jaipur)

	Periods	January 2003	May 2003	May 2009	September 2009	November 2009	January 2015	May 2015	September 2015
Linear	Day	0.01	0.38	0.59	0.01	0.54	0.22	0.60	0.06
	Night	0.75	0.57	0.68	0.48	0.85	0.85	0.66	0.51
Polynomial	Day	0.25	0.39	0.60	0.02	0.54	0.39	0.60	0.12
	Night	0.75	0.60	0.74	0.48	0.85	0.85	0.68	0.52

Co-efficient of correlation of different time periods vary from 0.02 to 0.60 (polynomial) and 0.01 to 0.60 (linear) during day time. During night time, R^2 values vary from 0.48 to 0.85 (polynomial) and 0.48 to 0.58 (linear). Winter season shows better relationship between mean LST and ISA than summer and monsoon seasons. Jaipur shows good relationship between mean LST and ISA during night period and comparatively poor relationship during day period.

b) Ahmedabad

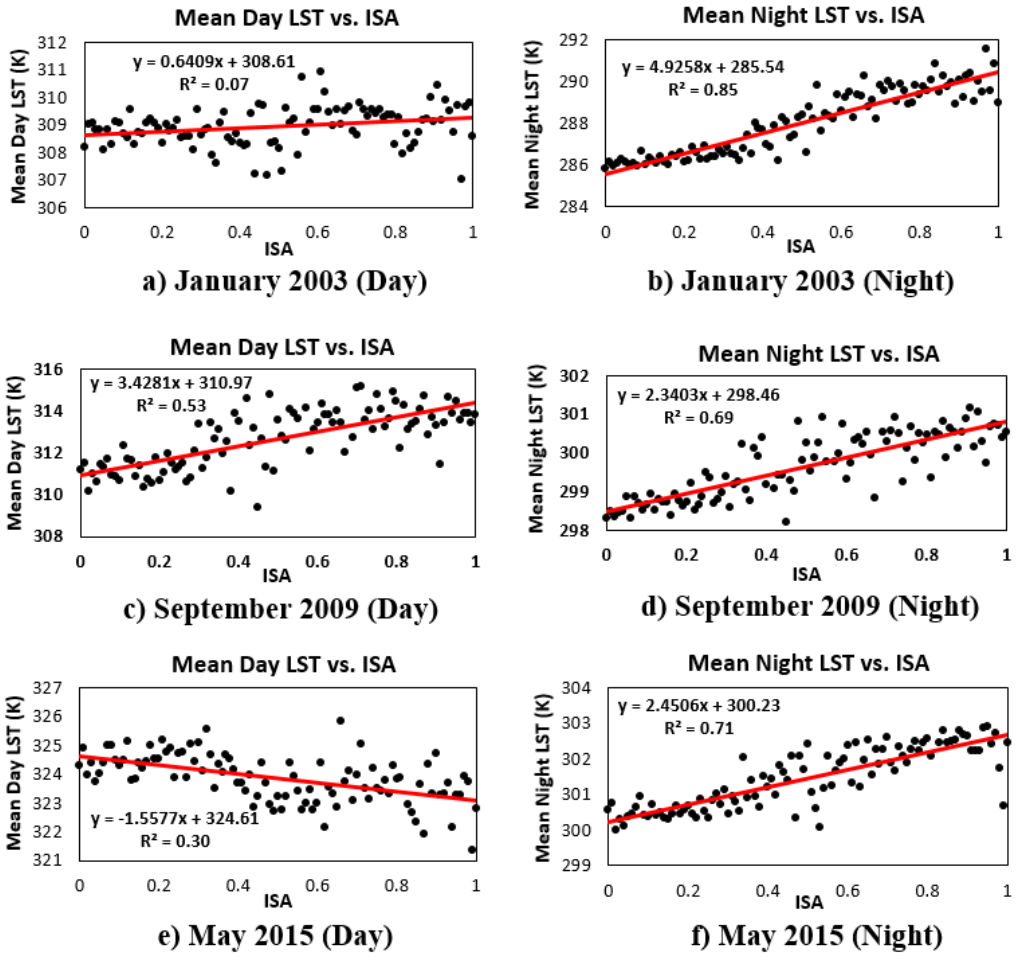

Fig. 4.45. Diurnal Mean LST and ISA Relationship for Different Seasons (Ahmedabad)

Table 4.26: Coefficient of Correlation (Linear and Polynomial) for Mean LST and ISA Relationship (Ahmedabad)

	Periods	January 2003	June 2009	2009 September	2009 December	2015 May	2015 October	2015 December
Linear	Day	0.07	0.43	0.53	0.01	0.30	0.67	0.07
	Night	0.85	0.47	0.69	0.73	0.71	0.76	0.33
Polynomial	Day	0.07	0.43	0.56	0.01	0.31	0.69	0.07
	Night	0.85	0.48	0.70	0.74	0.72	0.78	0.33

Co-efficient of correlation of different time periods vary from 0.01 to 0.69 (polynomial) and 0.01 to 0.67 (linear) during day time. Co-efficient of correlation range from 0.33 to 0.85 (polynomial and linear, respectively) during night time. Monsoon season shows better relationship between mean LST and ISA than summer and winter seasons. Ahmedabad shows good relationship between mean LST and ISA during night period and poor relationship during day period.

c) Chandigarh

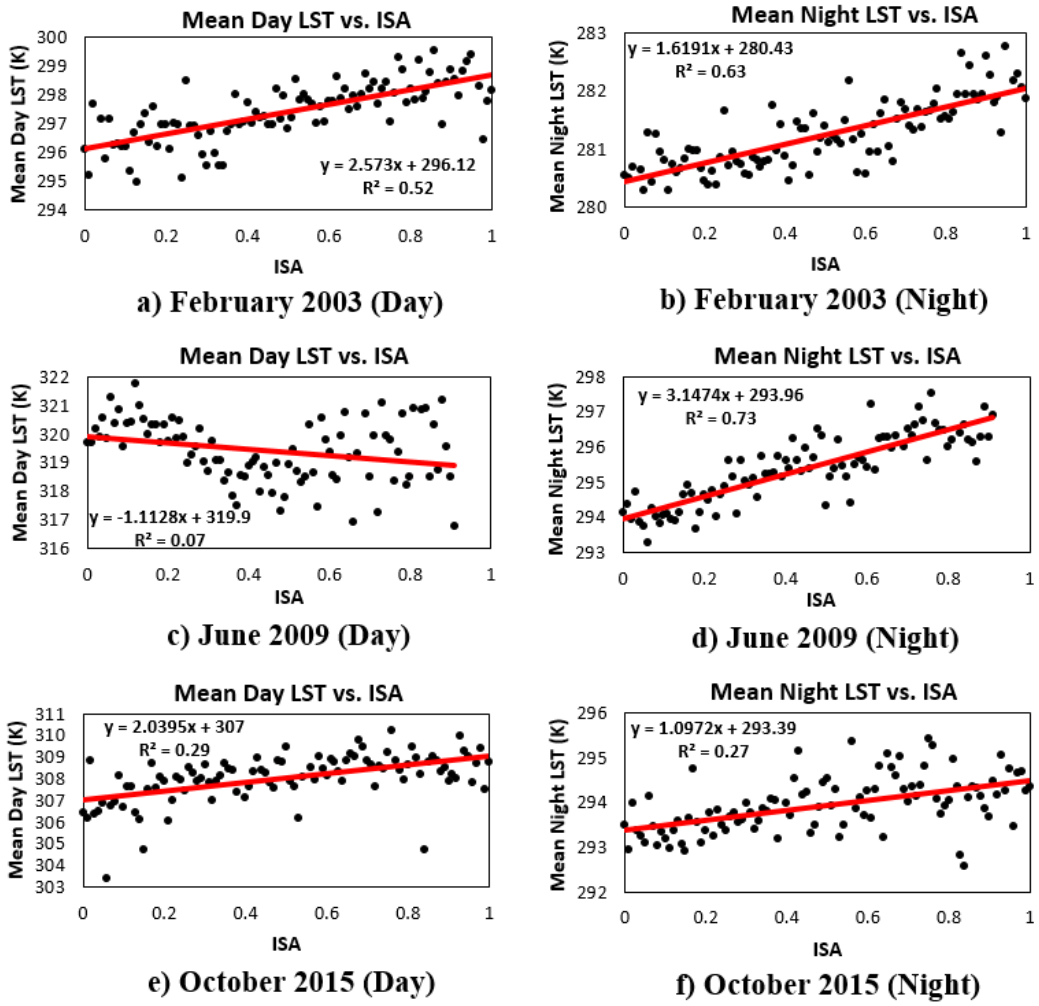

Fig. 4.46. Diurnal Mean LST and ISA Relationship for Different Seasons (Chandigarh)

Table 4.27: Coefficient of Correlation (Linear and Polynomial) for Mean LST and ISA Relationship (Chandigarh)

	Periods	2003 February	2009 June	2009 October	2009 December	2015 May	2015 October	2015 December
Linear	Day	0.52	0.07	0.44	0.00	0.28	0.29	0.10
	Night	0.63	0.73	0.35	0.23	0.52	0.27	0.03
Polynomial	Day	0.53	0.22	0.49	0.03	0.34	0.36	0.1
	Night	0.66	0.74	0.36	0.26	0.52	0.30	0.05

R^2 values of different time periods vary from 0.03 to 0.53 (polynomial) and 0.00 to 0.52 (linear) during day time. During night time, R^2 values vary from 0.05 to 0.74 (polynomial) and 0.03 to 0.73 (linear). Chandigarh shows moderate relationship between mean LST and ISA during night period and poor relationship during day period. Varying land covers over the area like Shivangi hill ranges, Dahriya reserved forest etc. show different ISA pattern and its relationship with LST varies significantly depending on season except built-up areas.

4.5.2.2 Discussions

The relationship between %ISA and LST is similar for all three seasons with a consistent rising trend during night period, whereas falling trend during day period. Though high variation can be observed in the plots showing a weak trend for low %ISA values, but the trend is strong for high %ISA values. Normally %ISA values are very less in rural areas compared to urban areas due to the lack of impervious surfaces like roads, built-up areas, etc. which results in weak trend and also the presence of bare land, vegetation cover and agricultural field show very low %ISA values in rural areas which lead to low LST. The weak trend may be due to the fact that for low %ISA values, the effect of urbanization is insignificant and hence LST variations are governed by the combined effect of several other parameters such as vegetation cover and its disposition, type and extent of surface imperviousness, the condition of nearby pixels, etc. The improved trend for higher %ISA values indicates that for an urbanized area, %ISA, compared to other parameters, has more effect on LST. Similar trend for different seasons indicates that unlike NDVI the relationship of %ISA with LST is independent of season.

Yuan and Bauer (2007) have documented a strong linear relationship between the amount of impervious surface area and LST or the UHI effect in the field of urban climate which is also validated by the present study only during night period. During day period, opposite

correlation has been observed. It has been observed that the graph between mean LST and %ISA shows rising trend in all seasons during night period. The correlation between mean LST and %ISA is better during winter season than summer and monsoon seasons.

From the diurnal analysis, it is observed that during day period, inverse or negative relationship has been observed between mean LST and %ISA for most of the time periods, whereas direct or positive relationship has been observed between mean LST and %ISA during night period. Positive convex polynomial trend line has been obtained during night period, whereas negative concave polynomial trend line has been obtained during night period for most of the time periods. Most of the previous studies show a positive relationship of LST with ISA during day period (Yuan and Baur, 2007). This study depicts the opposite relationship between LST and ISA during day period, which clearly indicates the non-existence of SUHI effect over the study area. i.e. urban surfaces show low LSTs than the rural regions. The higher temperature in rural surfaces has been affected by some other factors. But direct or positive relationship between mean LST and %ISA during night period shows the clear existence of nocturnal SUHI effect over the area.

4.5.3 Pattern of Normalized Difference Built-up Index (NDBI)

NDBI is used to automate the process of built-up mapping. It takes use of the unique spectral response of built-up areas and other land covers (Xu, 2006). Wu et al. (2005) have also used NDBI as an urban parameter to extract urban built-up features. NDBI can be used to characterize the LU-LC types and to explore the quantitative relationships between LU-LC types and UHI over the study area. The assumption underlying the NDBI method is the spectral reflectance of urban areas in SWIR band exceeding that in NIR band. Because the reflectance of urban areas exhibits little seasonality, this method is not prone to its impact. NDBI images of different periods, representing different seasons are shown in Fig. 4.47.

The values of NDBI have been calculated at the Landsat TM resolution of 30 m and the aggregated resolution of 926.6 m. The overall absolute maximum and minimum NDBI values of the study area are 0.64 and -0.97, respectively.

High values in NDBI image represent built-up areas and low values represent vegetation and water. Summer NDBI images show higher values in rural areas than urban areas. During monsoon and winter seasons, urban area shows higher NDBI values compared to rural areas. Vegetated areas show very low NDBI values in every season. Water bodies in

these cities also show very low NDBI values. In the summer season, it has been found that rural areas show high NDBI values than urban areas because bare soil and sparse vegetation in rural areas show higher spectral reflectance compared to urban areas. Hence from Fig. 4.47, it is clear that NDBI images show contrast pattern during different seasons mainly due to the ambiguity in LU-LC changes.

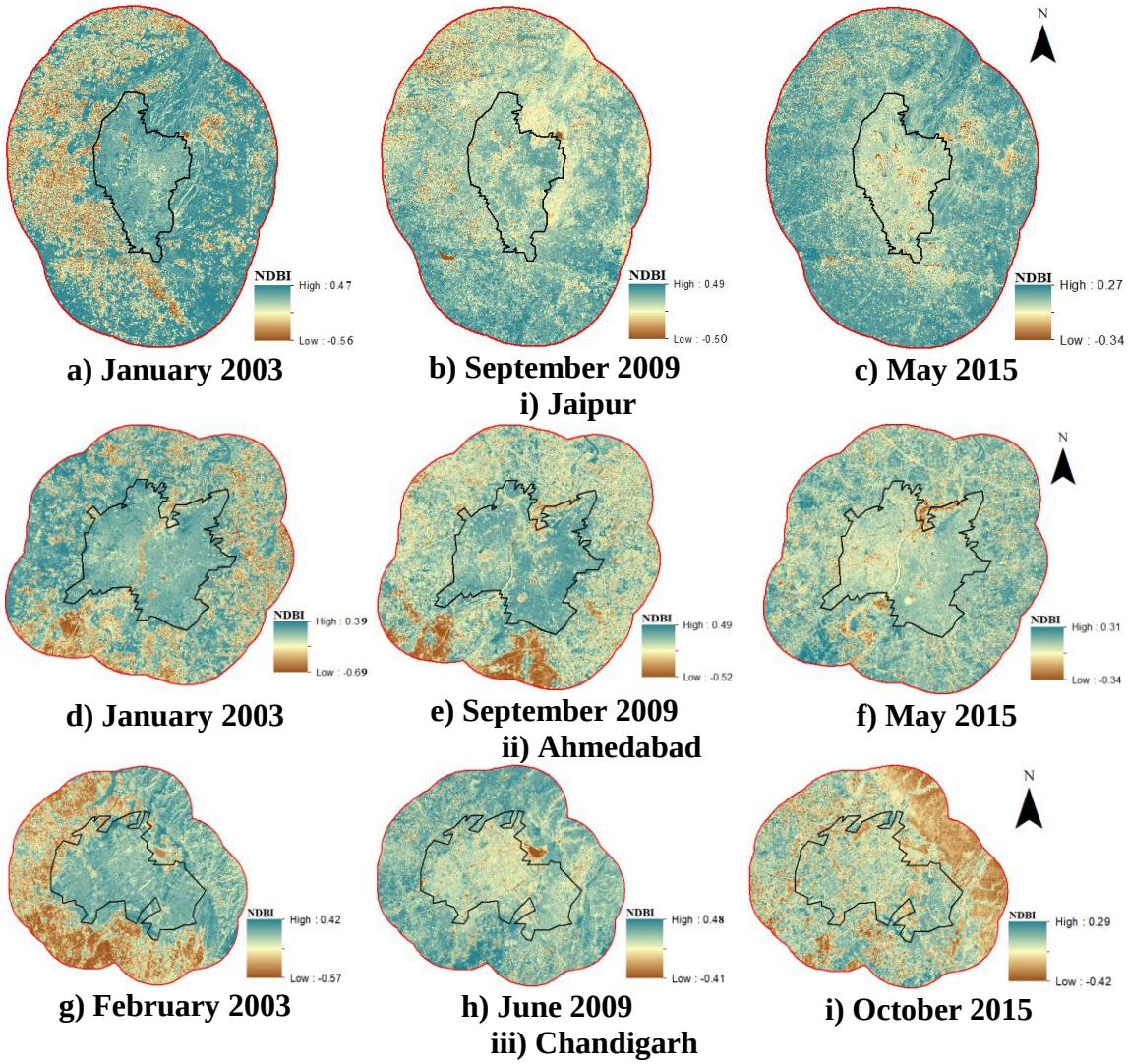

Fig. 4.47. NDBI Images of the Study Areas for Different Seasons

4.5.3.1 LST vs. NDBI Relationship

The NDBI has been developed for the identification of urban and built-up areas (Zha et al., 2003). The graphs representing mean LST vs. NDBI relationship for different seasons are shown in Figs. 4.48, 4.49 and 4.50. Mean LST vs. NDBI plots show different patterns and a varying trend can be observed for all seasons. Linear and second order polynomial relationship have been used for the correlation analysis. Tables 4.28, 4.29 and 4.30

represent the coefficient of correlation (linear and polynomial, respectively) of the study areas for mean LST and NDBI relationship.

a) Jaipur

Table 4.28: Coefficient of Correlation (Linear and Polynomial) for Mean LST and NDBI Relationship (Jaipur)

	Periods	January 2003	May 2003	May 2009	September 2009	November 2009	January 2015	May 2015	September 2015
Linear	Day	0.45	0.38	0.51	0.52	0.20	0.69	0.51	0.58
	Night	0.42	0.00	0.05	0.12	0.05	0.33	0.004	0.37
Polynomial	Day	0.58	0.45	0.53	0.67	0.26	0.70	0.52	0.66
	Night	0.45	0.04	0.09	0.12	0.05	0.47	0.005	0.40

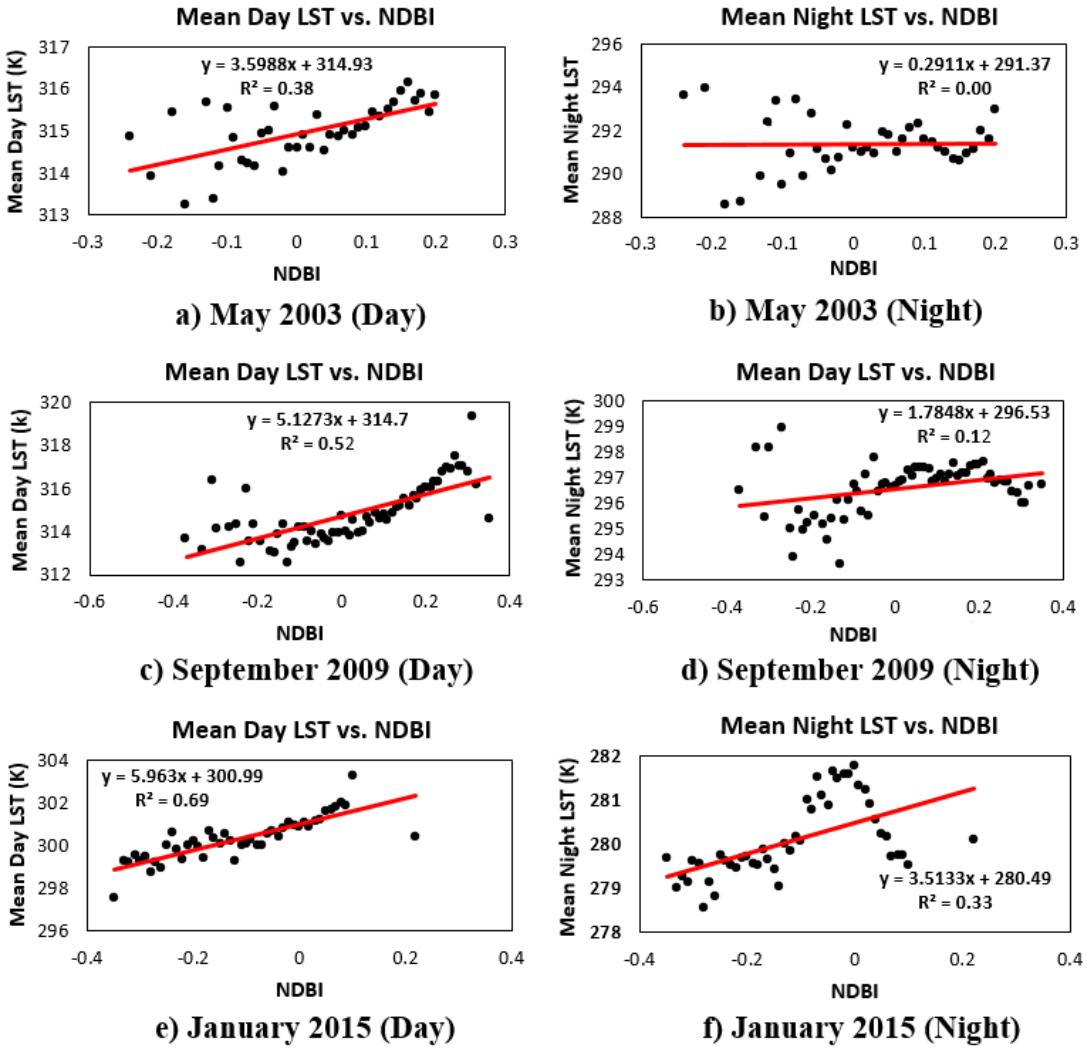

Fig. 4.48. Diurnal Mean LST and NDBI Relationship for Different Seasons (Jaipur)

R^2 values of different time periods vary from 0.26 to 0.70 (polynomial) and 0.20 to 0.69 during day period. R^2 values of different time periods vary from 0.00 to 0.47 (polynomial) and 0.00 to 0.42 (linear) during night period. During summer season, very low inverse or negative or no such correlation between mean LST and NDBI has been noticed during night period. Winter and monsoon season shows poor positive correlation between mean LST and NDBI during night period. The relationship between mean LST and NDBI shows better correlation during day period than night period.

b) Ahmedabad

Table 4.29: Coefficient of Correlation (Linear and Polynomial) for Mean LST and NDBI Relationship (Ahmedabad)

	Periods	January 2003	June 2009	2009 September	2009 December	2015 May	2015 October	2015 December
Linear	Day	0.53	0.08	0.77	0.18	0.62	0.66	0.50
	Night	0.25	0.02	0.55	0.04	0.25	0.43	0.00
Polynomial	Day	0.56	0.30	0.85	0.23	0.62	0.88	0.77
	Night	0.32	0.45	0.56	0.05	0.25	0.51	0.43

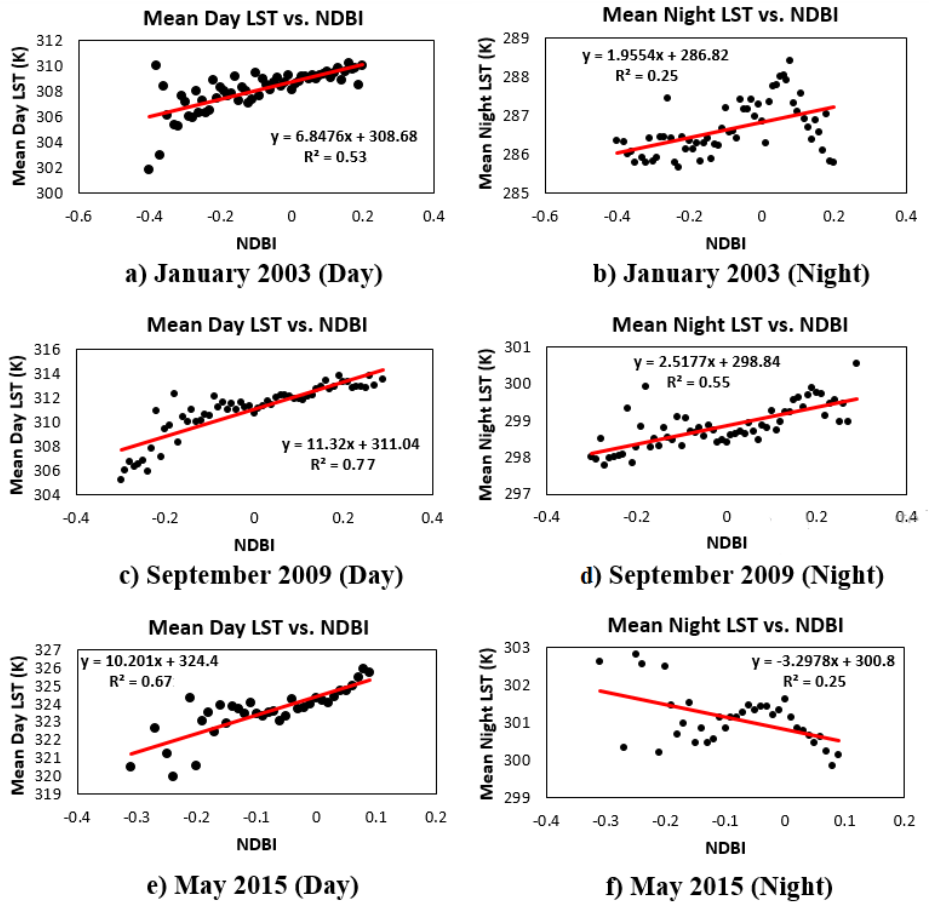

Fig. 4.49. Diurnal Mean LST and NDBI Relationship for Different Seasons (Ahmedabad)

Co-efficient of correlation of different time periods vary from 0.23 to 0.88 (polynomial) and 0.08 to 0.66 (linear) during day period. Co-efficient of correlation during night period vary from 0.05 to 0.56 (polynomial) and 0.00 to 0.55 (linear). During night period of summer season, no clear correlation between mean LST and NDBI can be noticed. Winter and monsoon season shows low or moderate positive correlation between mean LST and NDBI during night period.

c) Chandigarh

Table 4.30: Coefficient of Correlation (Linear and Polynomial) for Mean LST and NDBI Relationship (Chandigarh)

	Periods	2003 February	2009 June	2009 October	2009 December	2015 May	2015 October	2015 December
Linear	Day	0.61	0.22	0.57	0.21	0.10	0.74	0.01
	Night	0.68	0.00	0.27	0.03	0.08	0.09	0.05
Polynomial	Day	0.64	0.24	0.57	0.37	0.80	0.77	0.41
	Night	0.69	0.01	0.28	0.25	0.30	0.46	0.10

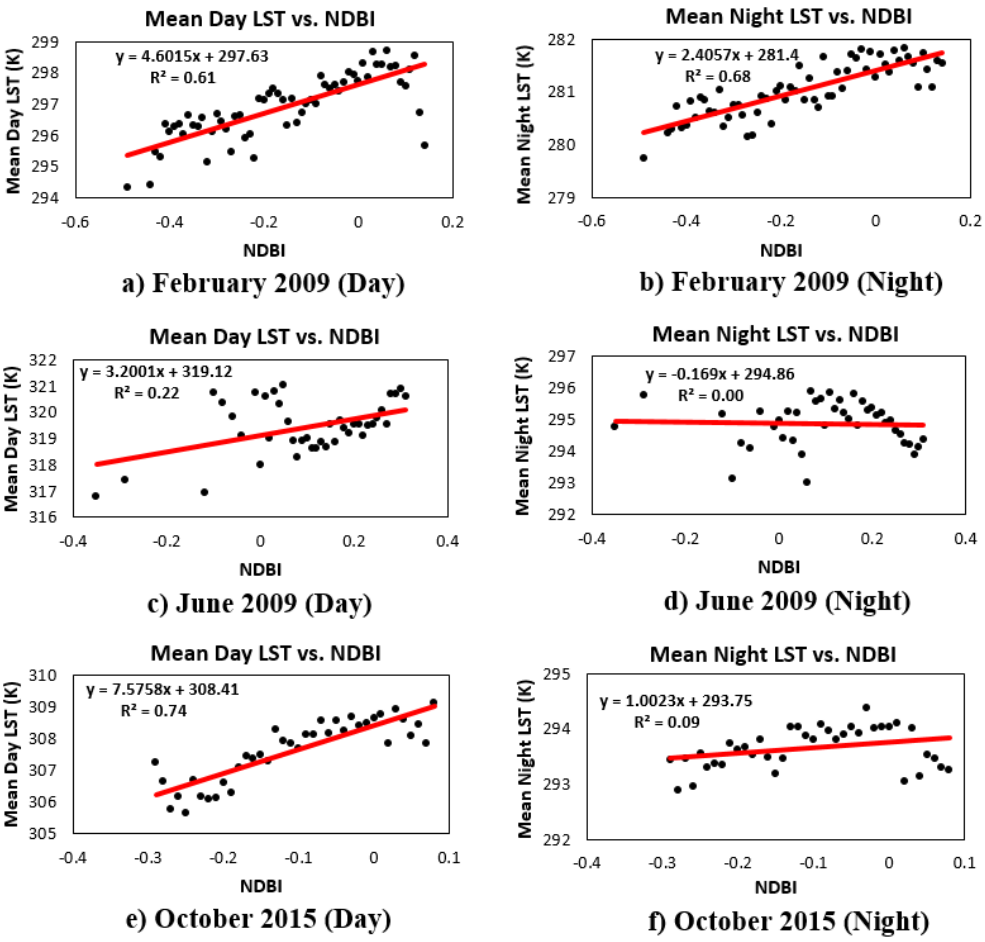

Fig. 4.50. Diurnal Mean LST and NDBI Relationship for Different Seasons (Chandigarh)

Co-efficient of correlation of different time periods vary from 0.24 to 0.80 (polynomial) and 0.01 to 0.61 (linear) during day time, whereas during night period Co-efficient of correlation vary from 0.01 to 0.69 (polynomial) and 0.00 to 0.68 (linear). Winter and monsoon season shows poor positive correlation between mean LST and NDBI during night period.

4.5.3.2 Discussions

Generally, bare soil in rural areas shows higher spectral reflectance in SWIR band compared to urban built-up areas. Drier or sparse vegetation can even show higher reflectance in SWIR wavelength range than in NIR range (Gao, 1996), resulting in positive NDBI values in NDBI images for drier vegetation. So during the summer season, the soil in rural areas shows higher NDBI values as compared to urban areas. Rural areas show higher NDBI values than urban areas and urban areas show higher LSTs which causes low correlation between LST and NDBI during night period. Hence NDBI can not be used as a good indicator for SUHI studies where bare land, includes soil and drier vegetation, is predominant in rural areas. The graphs show positive trend line during monsoon and winter season. The trend of LST-NDBI relationship during different season is different, which clearly indicates that the relationship between mean LST and NDBI is linear and is season dependent. NDBI performance may be adversely affected indirectly by the presence of other covers whose reflectance is seasonal, such as vegetation.

Significant variations have been observed in the diurnal relationship between LST and NDBI. Direct relationship has been observed between LST and NDBI during day period. Conversely, mixed relationships have been observed during night period for different seasons. Significant correlation between LST and NDBI has been observed during daytime than during night. Season which affects various agricultural practices over the area has an important role in the variations of diurnal relationship between LST and NDBI.

For Jaipur study area, the correlation between mean LST and NDBI is better during monsoon season than summer and winter seasons. The disadvantage of NDBI method is that NDBI is unable to distinct urban areas from barren land like sandy regions because both of them have a similar pattern of spectral response in all TM/OLI bands. So especially in summer season, bare soil in rural areas shows higher reflectance in SWIR than NIR resulting in higher values of NDBI at rural areas. The overall analysis of the relationship of LST with different parameters indicates that the relationship of %ISA with LST is better

than the corresponding relationship of LST with NDBI. %ISA can be used to reflect the seasonal and temporal fluctuations in similar linear patterns, but with different governing relationship equations. Hence, %ISA is a better indicator for the analysis of SUHI effect, with no dependence on the season.

4.5.4 Road Density (RD)

Figs. 4.51, 4.52 and 4.53 show the final road network and RD maps of the Jaipur, Ahmedabad and Chandigarh study areas. All the roads, major or minor have been digitized within the study area. The total length of roads in Jaipur, Ahmedabad and Chandigarh study areas are around 4579, 7085 and 3918 kms, respectively. The effect of urbanization can be clearly understood from the road network map, and it can be seen that the urban area has extensive road network. The length of roads in rural and semi-urban areas is very less as compared to that in the urban area. Table 4.31 shows the statistical details of RD of the study areas.

Table 4.31: Statistical Details of RD (Km/Sq. Km) of the Study Areas

Study Areas	Urban Area Only			Rural Area Only			Composite Study Area		
	Maximum	minimum	mean	Maximum	minimum	mean	Maximum	minimum	mean
Jaipur	27.74	0.84	14.18	22.20	0.00	1.61	27.74	0.00	3.34
Ahmedabad	39.44	2.09	18.64	32.68	0.00	6.27	39.44	0.00	10.27
Chandigarh	27.54	1.03	14.41	25.78	0.00	4.93	27.54	0.00	7.60

RD is also an indicator of urbanization which increases with growth of the city. Mean RD of the Jaipur, Ahmedabad and Chandigarh rural areas is only about 11%, 30%, 34%, respectively of the mean RD of the corresponding urban areas. RD of the suburban area is much lower than the RD of the urban area.

Some signs of development in the form of an increase in road network can also be seen outside the West and North-Western part of the Ahmedabad urban boundary. The length of roads is minimum in the Southern zone as most of the area of this zone comprises of agricultural fields. Within the urban area also some patches of lower road network can be seen corresponding to central parts of the city due to water bodies like Sabarmati river. Kankaria and Chandola lakes in Sothern part of the city and parks in different parts of the city resulting lower road network in some parts of the urban area.

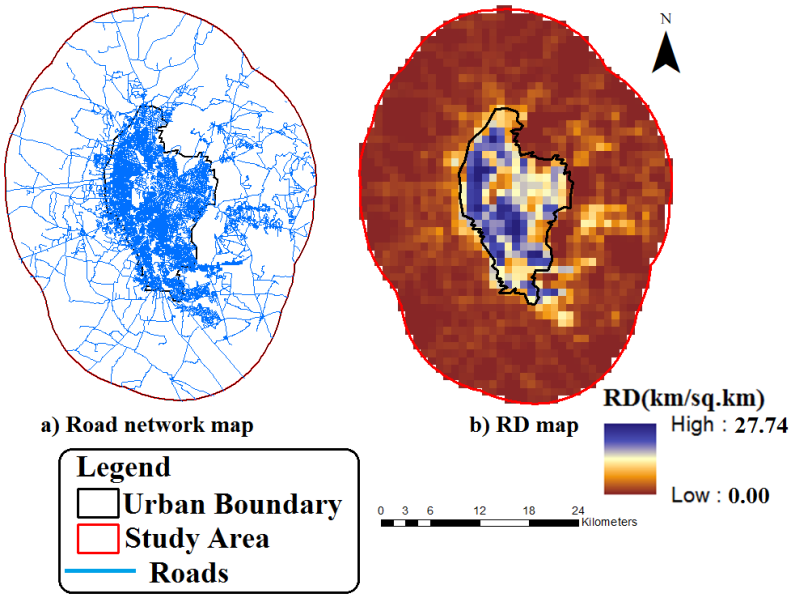

Fig. 4.51. Road network and RD map of the Jaipur study area

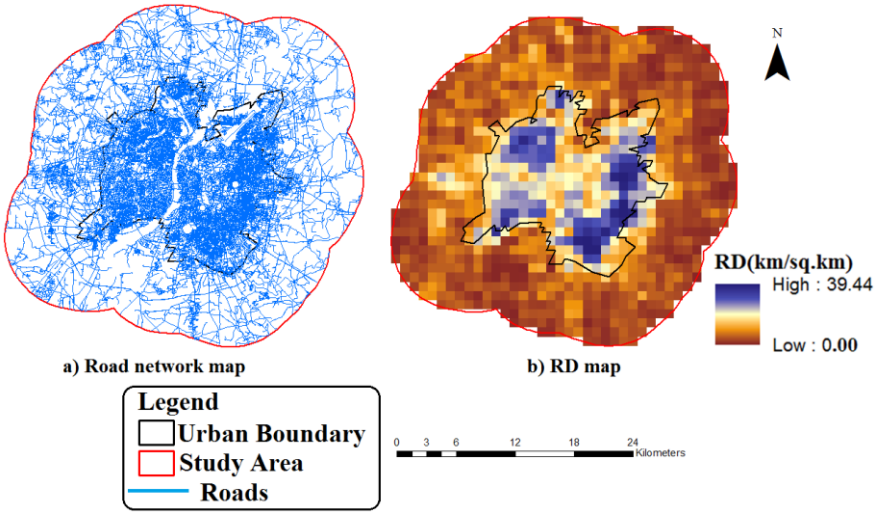

Fig. 4.52. Road Network and RD Map of the Ahmedabad Study Area

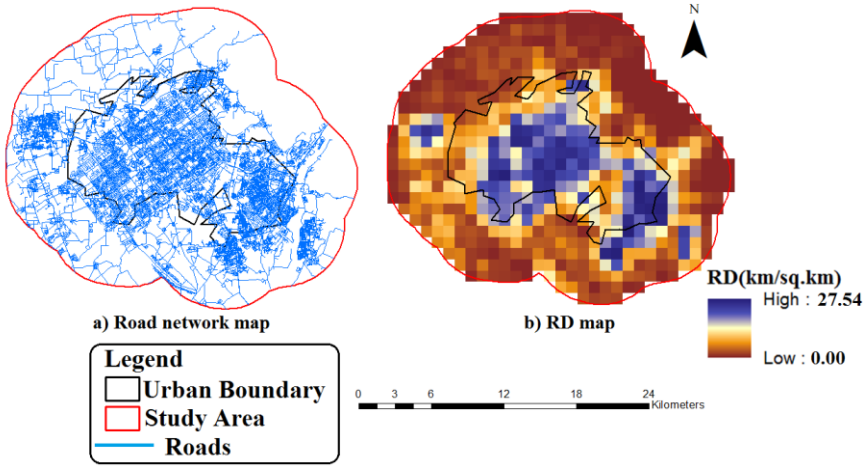

Fig. 4.53. Road Network and RD Map of the Chandigarh Study Area

4.5.4.1 Diurnal LST vs. RD Relationship

Figs. 4.54, 4.55 and 4.56 show the correlation between mean LST and RD for different seasons of study areas. The relationship between RD and LST is similar for all three seasons with a consistent rising trend during night period. Tables 4.32, 4.33 and 4.34 represent the coefficient of correlation (linear and polynomial, respectively) of the study areas for mean LST and RD relationship.

a) Jaipur

Table 4.32: Coefficient of Correlation (Linear and Polynomial) for Mean LST and RD Relationship (Jaipur)

	Periods	January 2003	May 2003	May 2009	September 2009	November 2009	January 2015	May 2015	September 2015
Linear	Day	0.02	0.16	0.23	0.08	0.32	0.11	0.32	0.08
	Night	0.51	0.38	0.59	0.33	0.59	0.54	0.55	0.52
Polynomial	Day	0.04	0.16	0.24	0.1	0.32	0.11	0.34	0.08
	Night	0.55	0.45	0.66	0.41	0.65	0.62	0.61	0.62

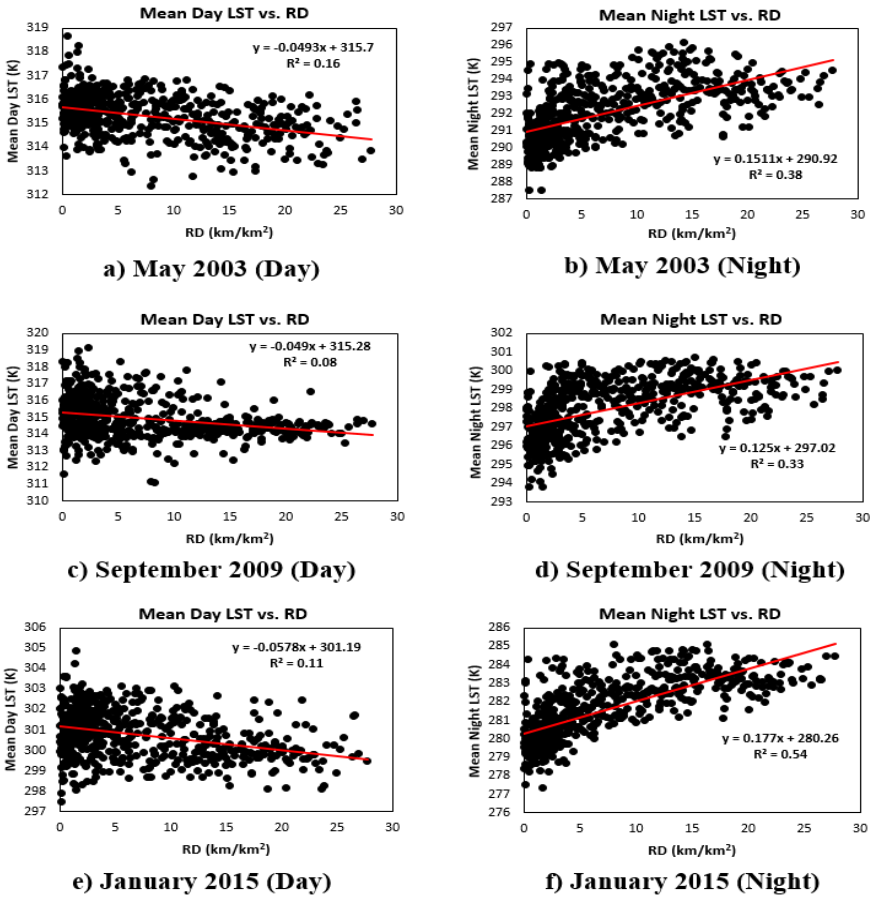

Fig. 4.54. LST vs. RD scatterplots for different seasons (Jaipur)

Co-efficient of correlation of different time periods range from 0.04 to 0.32 (polynomial) and 0.02 to 0.32 (linear) during day period, whereas during night period R^2 values vary from 0.41 to 0.66 (polynomial) and 0.33 to 0.59 (linear).

b) Ahmedabad

Table 4.33: Coefficient of Correlation (Linear and Polynomial) for Mean LST and RD Relationship (Ahmedabad)

	Periods	Periods	January 2003	June 2009	2009 September	2009 December	2015 May	2015 October
Linear	Day	0.07	0.37	0.34	0.00	0.11	0.42	0.01
	Night	0.64	0.58	0.62	0.66	0.54	0.65	0.61
Polynomial	Day	0.12	0.37	0.36	0.00	0.12	0.45	0.01
	Night	0.66	0.63	0.65	0.67	0.58	0.68	0.63

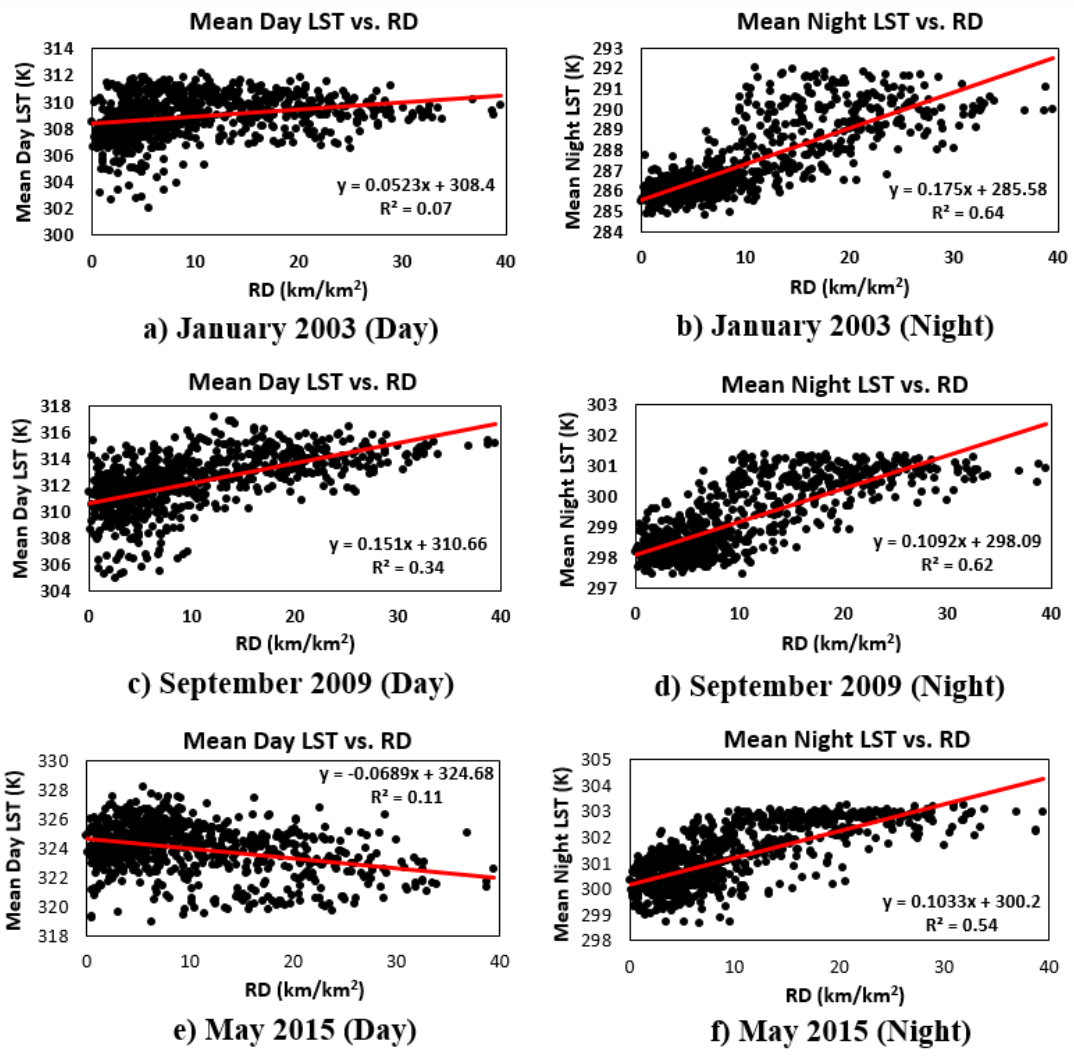

Fig. 4.55. LST vs. RD Scatterplots for Different Seasons (Ahmedabad)

Co-efficient of correlation of different time periods vary from 0.00 to 0.45 (polynomial) and 0.00 to 0.42 (linear) during day period. Co-efficient of correlation vary from 0.58 to 0.68 (polynomial) and 0.54 to 0.66 (linear) during night period.

c) Chandigarh

Table 4.34: Coefficient of Correlation (Linear and Polynomial) for Mean LST and RD Relationship (Chandigarh)

	Periods	2003 February	2009 June	2009 October	2009 December	2015 May	2015 October	2015 December
Linear	Day	0.39	0.03	0.24	0.03	0.00	0.23	0.00
	Night	0.26	0.52	0.60	0.28	0.39	0.66	0.23
Polynomial	Day	0.41	0.03	0.26	0.03	0.00	0.24	0.00
	Night	0.27	0.52	0.60	0.29	0.40	0.66	0.23

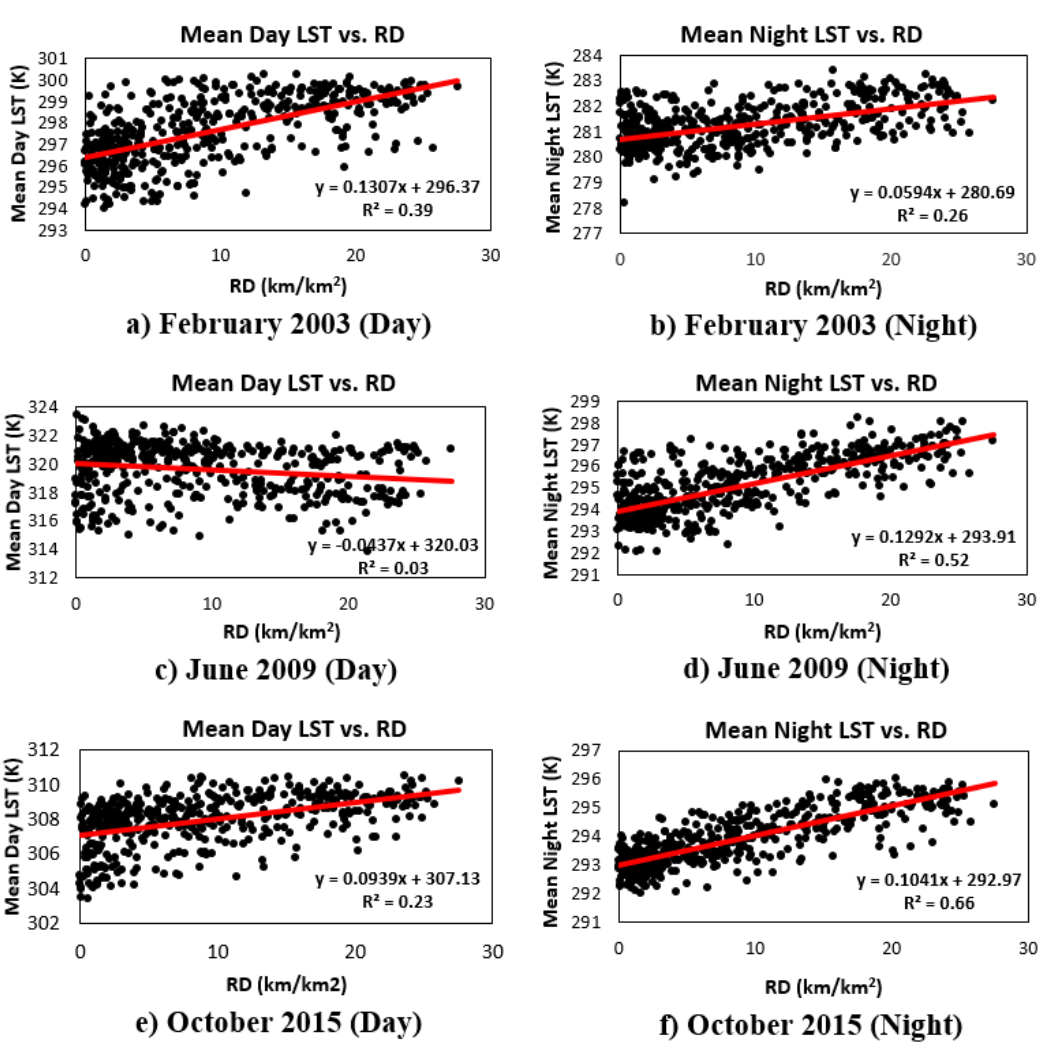

Fig. 4.56. LST vs. RD Scatterplots for Different Seasons (Chandigarh)

Co-efficient of correlation of different time periods vary from 0.00 to 0.41 (polynomial) and 0.00 to 0.39 (linear) during day time. Co-efficient of correlation during night time vary from 0.23 to 0.66 (polynomial) and 0.23 to 0.66 (linear) for different time periods. Chandigarh shows less diurnal correlation between LST and RD compared to Ahmedabad for all seasons.

4.5..4.2 Discussions

From the diurnal analysis, it is observed that during day period, inverse or negative or no relationship has been observed between mean LST and RD for most of the time periods, whereas direct or positive relationship has been observed between mean LST and RD during night period for the study areas. Better mean LST-RD relationship can be observed during the night period compared to day period. Similar to ISA, contrast diurnal LST-RD relationship has been observed for both study areas. The significance of RD on SUHI effect is more prominent during night period than the day. The contribution of RD is not much significant for higher LSTs during day period, whereas more significant during night period. This study depicts the opposite relationship between LST and RD during day period, which clearly indicates the non-existence of SUHI effect over the study area. Some other land surfaces primarily bare soil attribute higher LSTs than road surface during day period which predominantly cover rural areas resulting in weak correlation between LST and RD. But direct or positive relationship between mean LST and RD during night period shows the clear existence of nocturnal SUHI effect over the area.

A positive relationship has been found between LST and RD during night period, and this relationship has been found to be consistently similar during all the three seasons. Though high variation can be observed in the plots showing a weak trend for low RD values, but the trend is strong for high RD values. The weak trend may be due to the fact that for low RD values, urbanization does not have a significant effect and hence LST variations are governed by the combined effect of several other parameters such as vegetation cover and its disposition, type, and extent of surface imperviousness, condition of nearby pixels, etc. The improved trend for higher RD values indicates that for an urbanized area, RD, has good effect on LST. Similar trend for different seasons indicates that relationship of RD with LST is independent of season. RD has been considered to include the indirect effect on the rise in temperature due to anthropogenic heat in addition to the direct effect due to the imperviousness of urban surfaces. The relationship between mean LST and RD is good for

all the three seasons (Figs. 15 and 16). High R^2 values for the relationship between mean LST and RD for different periods and different seasons of the entire study period indicate that the relationship between LST and RD is not only independent of the season, but the variations in LST can be accounted for very well by RD.

4.5.5 NDBaI Pattern of Jaipur City

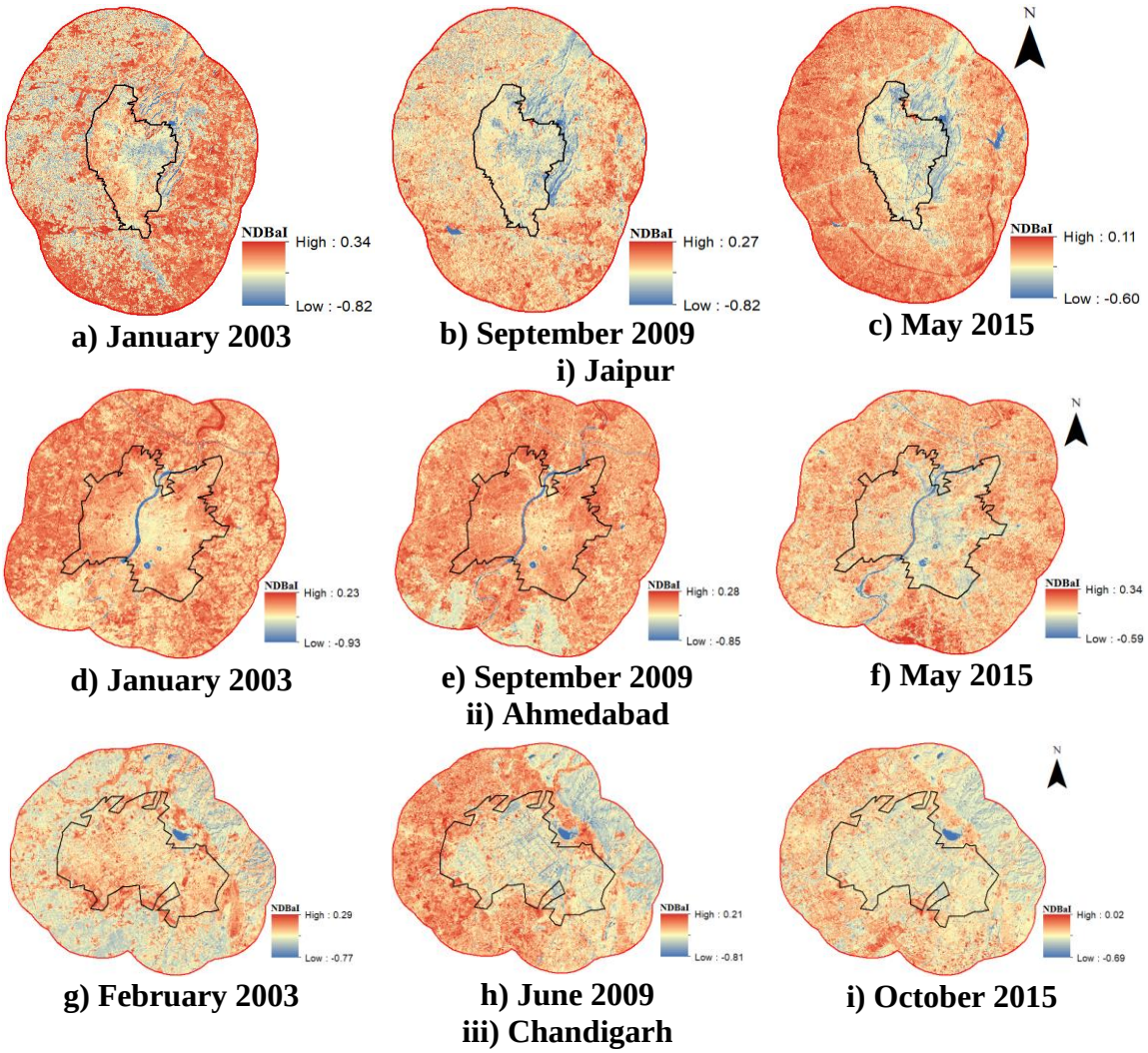

Fig. 4.57. Landsat Derived NDBaI Images of the Study Area for Different Seasons

NDBaI has been used for analyzing the spectral and spatial characteristics of bare land. Spectral characteristic of MIR− TIR> 0 is highly consistent with bare land. So bare land (Including beach, bare land, and land under development) could be distinguished by images with NDBaI> 0, which also refers to primary bare land (Zhao and Chen, 2005; Chen et al., 2006). At the same time, NDBaI could be used to classify different bare lands (e.g. primary bare land and secondary bare land) according to different values of NDBaI. Urban areas show low NDBaI values as compared to rural areas. Semi-arid climate of the Jaipur and

Ahmedabad cities favour higher bare land and sparse vegetation density over the rural area result in higher NDBaI values over the rural area. Water bodies show very low NDBaI values. Summer season favours higher bare land density over rural areas and results in higher NDBaI values over those areas. NDBaI images during monsoon season show varying pattern compared to summer season because of low bare land density over rural areas due to higher vegetation density. Hence NDBaI can also be considered as a season dependent parameter. Different seasons show different NDBaI pattern mainly depending on various agricultural practices and LU-LC changes. Fig. 4.57 shows the NDBaI images of the study areas for different periods.

4.5.5.1 LST vs. NDBaI Relationship

Diurnal relationship of LST with NDBaI of Jaipur, Ahmedabad and Chandigarh for different time periods has been analysed in the study. Figs. 4.58, 4.59 and 4.60 show the correlation between mean LST and NDBaI for different seasons of study areas. Linear and second order polynomial relationship have been used for the correlation analysis. Tables 4.35, 4.36 and 4.37 represent the coefficient of correlation (linear and polynomial, respectively) for mean LST and NDBaI relationship.

a) Jaipur

Table 4.35: Coefficient of Correlation (Linear and Polynomial) for Mean LST and NDBaI Relationship (Jaipur)

	Periods	**January 2003**	**May 2003**	**May 2009**	**September 2009**	**November 2009**	**January 2015**	**May 2015**	**September 2015**
Linear	Day	0.20	0.82	0.51	0.44	0.50	0.38	0.67	0.86
	Night	0.34	0.87	0.46	0.32	0.46	0.27	0.40	0.49
Polynomial	Day	0.23	0.82	0.78	0.46	0.53	0.60	0.67	0.87
	Night	0.5	0.9	0.73	0.51	0.49	0.38	0.43	0.5

Co-efficient of correlation of different time periods vary from 0.23 to 0.87 (polynomial) and 0.20 to 0.86 (linear) during day period. During night time, co-efficient of correlation vary from 0.38 to 0.90 (polynomial) and 0.27 to 0.87 (linear) for different time periods.

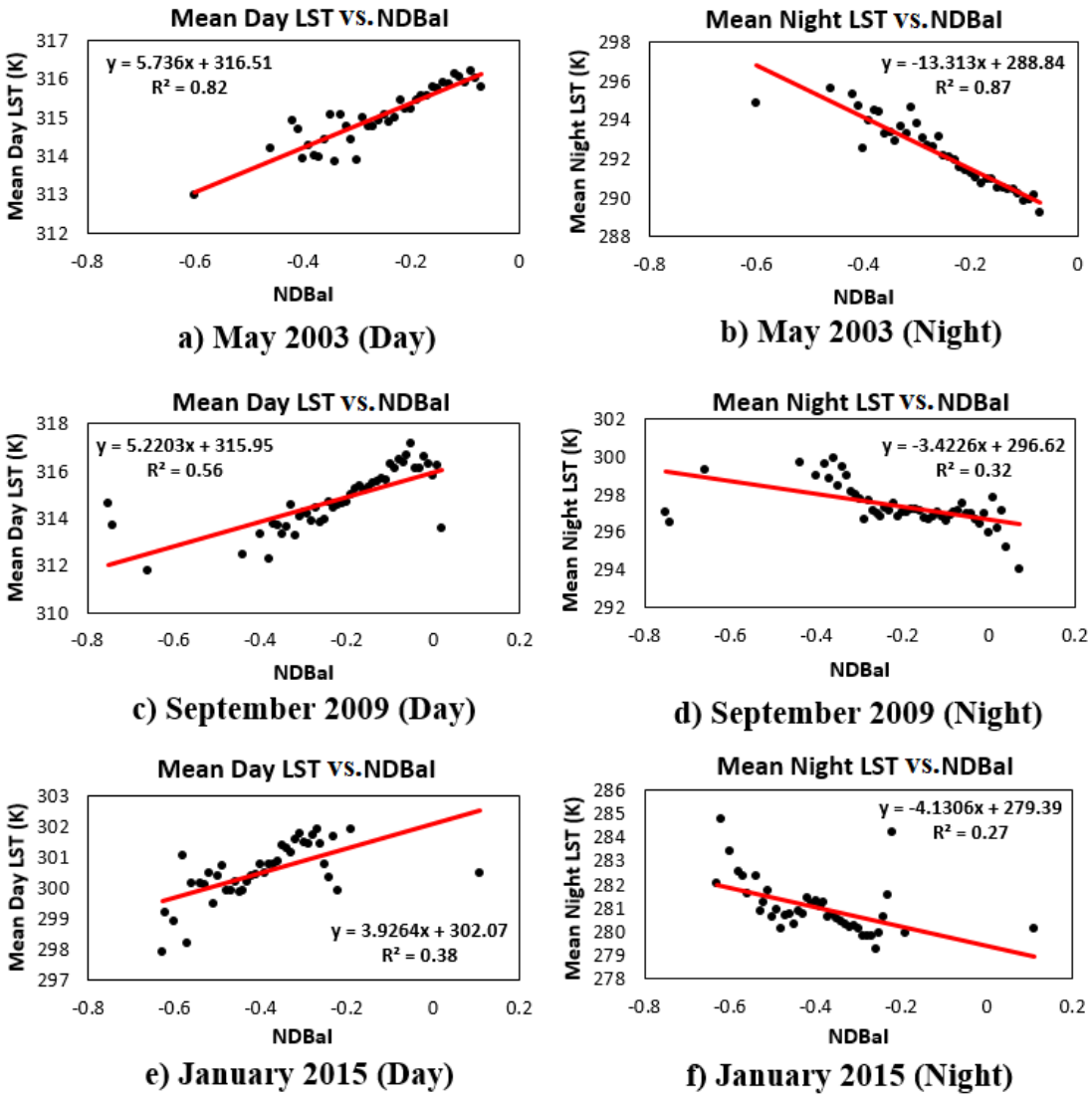

Fig. 4.58. LST vs. NDBaI Scatterplots for Different Seasons (Jaipur)

b) Ahmedabad

Table 4.36: Coefficient of Correlation (Linear and Polynomial) for Mean LST and NDBaI Relationship (Ahmedabad)

	Periods	January 2003	June 2009	2009 September	2009 December	2015 May	2015 October	2015 December
Linear	Day	0.26	0.61	0.26	0.49	0.35	0.03	0.09
	Night	0.20	0.00	0.01	0.09	0.33	0.05	0.37
Polynomial	Day	0.30	0.61	0.35	0.50	0.68	0.04	0.17
	Night	0.25	0.08	0.14	0.10	0.70	0.05	0.43

Co-efficient of correlation of different time periods vary from 0.04 to 0.68 (polynomial) and 0.03 to 0.61 (linear) during day time. Co-efficient of correlation vary from 0.05 to 0.70 (polynomial) and 0.00 to 0.37 (linear) during night period.

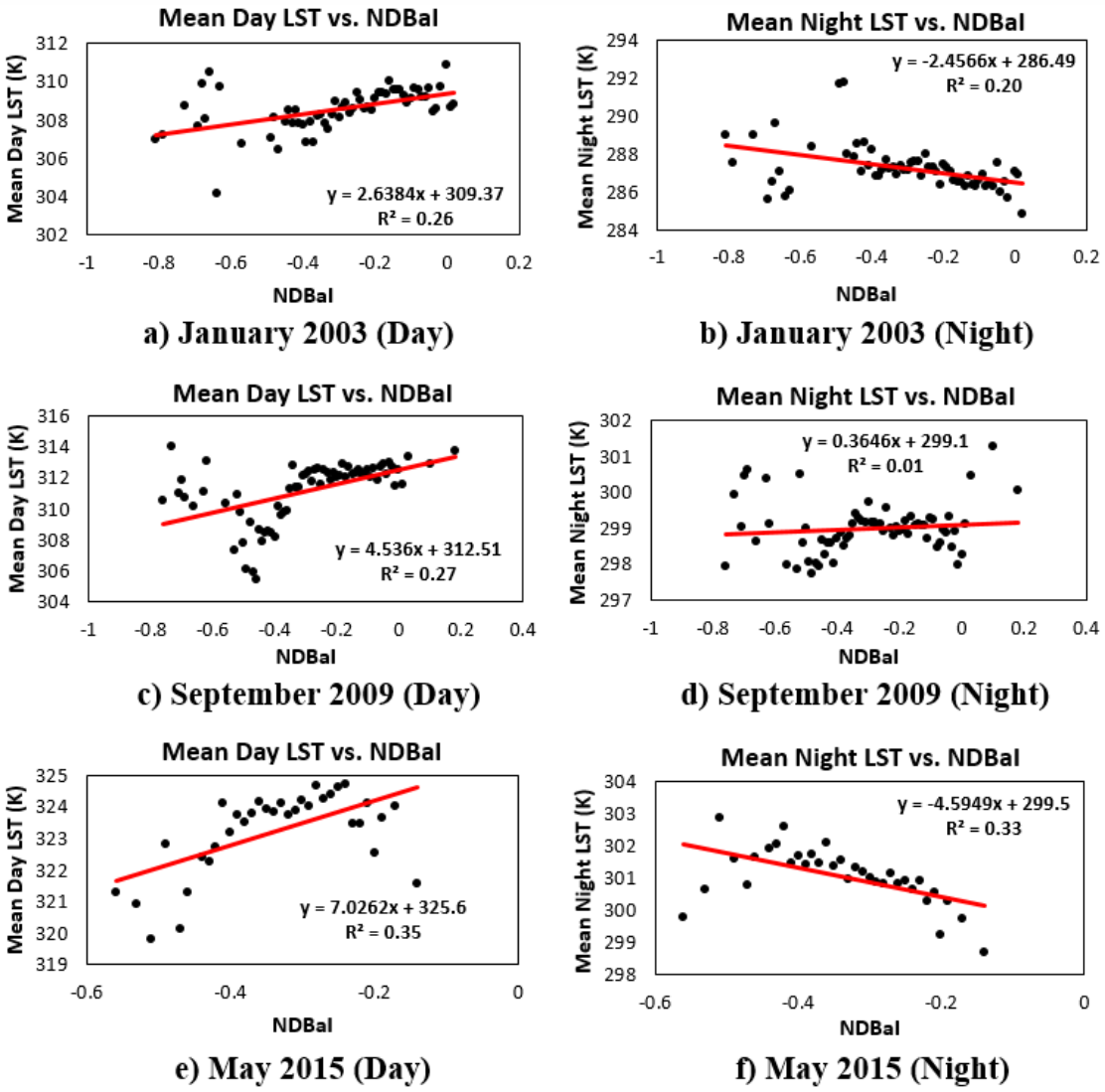

Fig. 4.59. LST vs. NDBaI Scatterplots for Different Seasons (Ahmedabad)

c) *Chandigarh*

Table 4.37: Coefficient of Correlation (Linear and Polynomial) for Mean LST and NDBaI Relationship (Chandigarh)

	Periods	2003 February	2009 June	2009 October	2009 December	2015 May	2015 October	2015 December
Linear	Day	0.53	0.60	0.42	0.50	0.72	0.40	0.75
	Night	0.01	0.28	0.35	0.68	0.48	0.02	0.06
Polynomial	Day	0.56	0.72	0.42	0.50	0.73	0.40	0.77
	Night	0.10	0.55	0.38	0.68	0.56	0.03	0.22

Co-efficient of correlation of different time periods vary from 0.40 to 0.77 (polynomial) and 0.40 to 0.75 (linear) during day period. Co-efficient of correlation vary from 0.03 to 0.68 (polynomial) and 0.01 to 0.68 (linear) during night period.

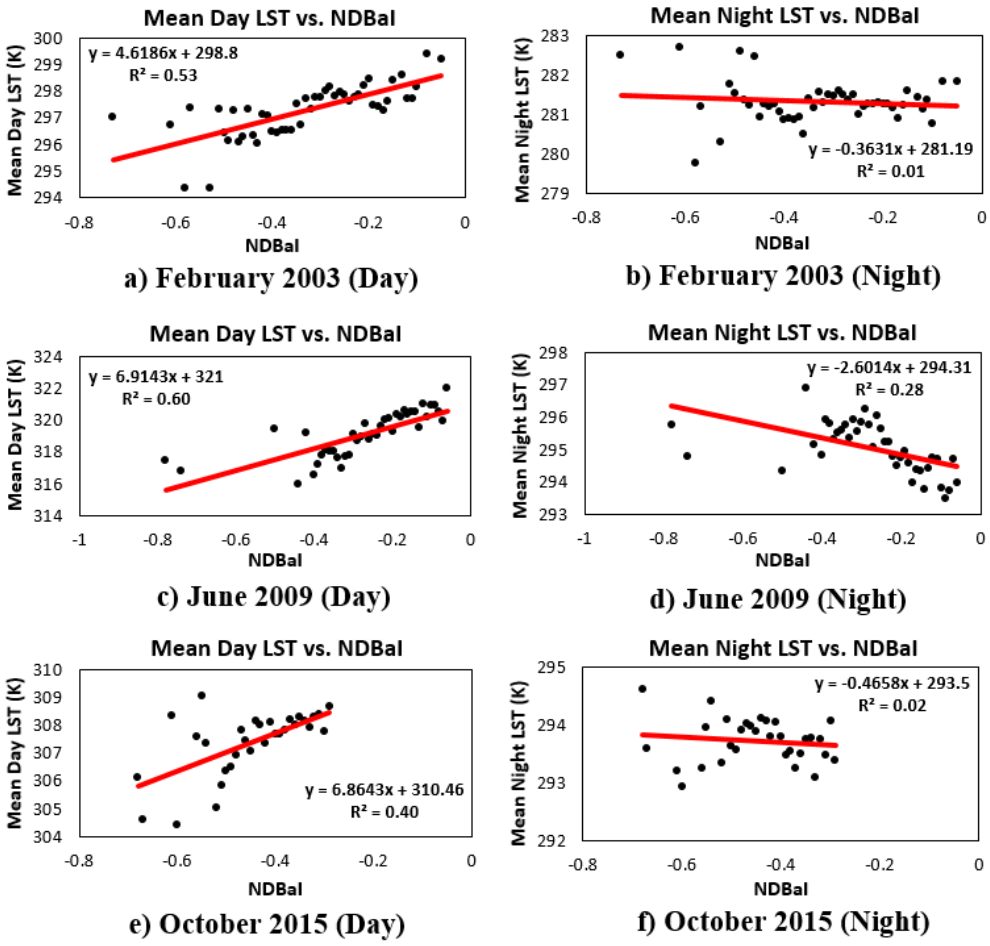

Fig. 4.60. LST vs. NDBaI Scatterplots for Different Seasons (Chandigarh)

4.5.5.2 Discussions

Price (1990) has found that bare soil locations experienced a wider variation in surface radiant temperature than densely vegetated locations. During day period, positive or direct correlation has been observed between LST and NDBaI. Soil has a positive effect on LST during day period which increase the rural LST resulting in high surface temperatures over rural areas than urban areas. This has resulted in the inverse or negative SUHI effect over the study area during day period. Hence barren soil has a significant role in the diurnal variations in the SUHI effect and it has been considered as the primary contributor of inverse or negative SUHI effect over semi-arid cities where bare land density is maximum.

The relationship between LST and NDBaI shows better correlation during day period than the night. Summer season shows good correlation between mean LST and NDBaI compared to winter season. Summer season favours higher bare land density resulting in higher NDBaI values over rural areas. Monsoon season shows very weak correlation

between mean LST and NDBaI compared to other seasons. Chandigarh and Ahmedabad show low diurnal correlation between LST and NDBaI compared to Jaipur because of the low bare land density over those areas due to higher vegetation density.

4.5.6 MNDWI Pattern of Jaipur City

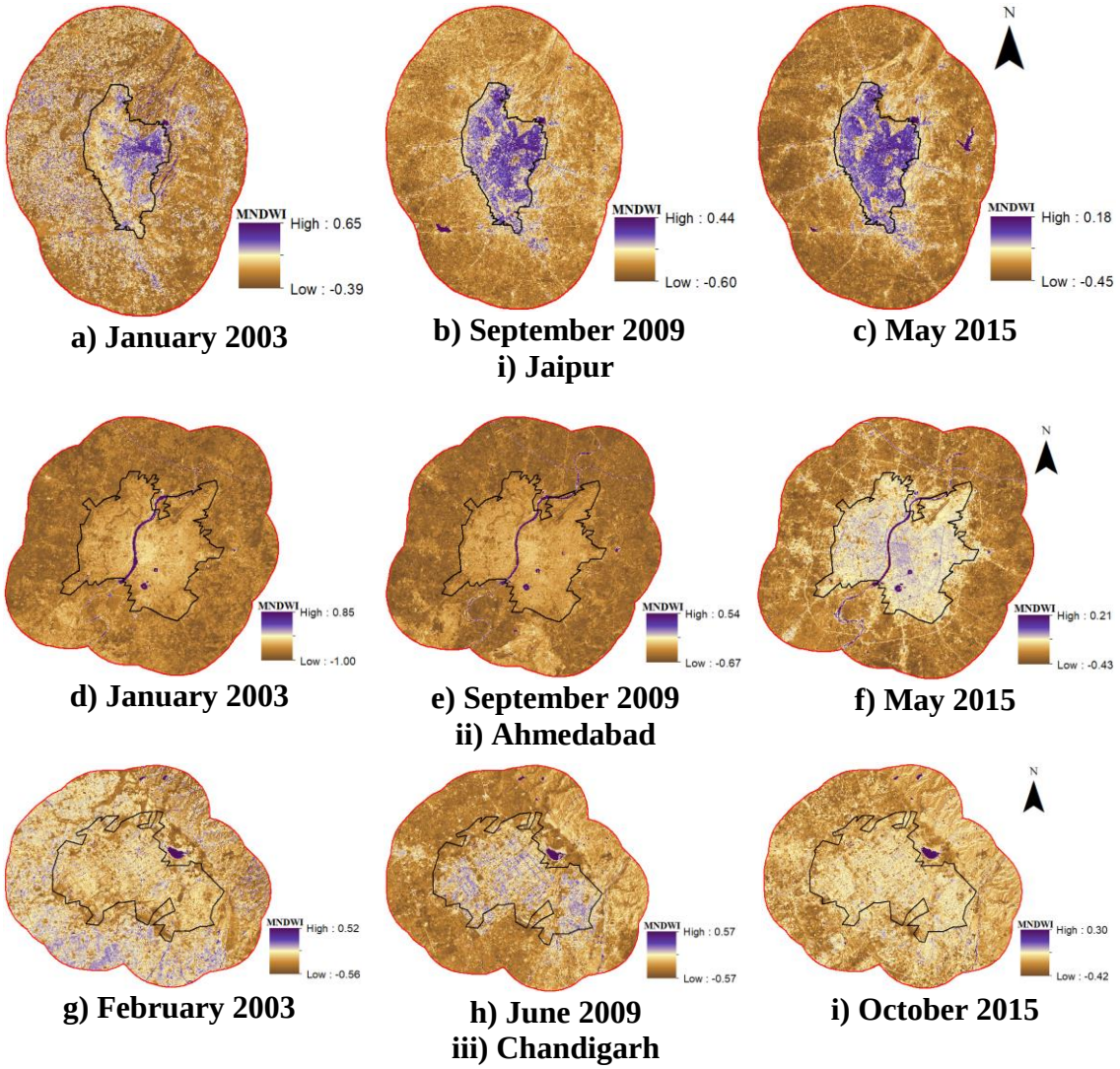

Fig. 4.61. Landsat Derived MNDWI Images of the Study Area for Different Seasons

MNDWI has been used to extract the water features over the study areas. The value of MNDWI ranges from -1 to +1. Water features show higher MNDWI values (appear dark blue) greater than zero. Soil and vegetation over the area show very low MNDWI values (appear brown). Sabarmati River and lakes in Ahmedabad, Sukhna Lake in Chandigarh are clearly highlighted with dark blue color in MNDWI images for different seasons. Fig. 4.61 shows the MNDWI images of the study areas for different periods.

4.5.6.1 LST vs. MNDWI relationship

Figs. 4.62, 4.63 and 4.64 show the correlation between mean LST and MNDWI for different seasons of study areas. Tables 4.38, 4.39 and 4.40 represent the coefficient of correlation (linear and polynomial, respectively) for mean LST and MNDWI relationship. Linear and second order polynomial relationship have been used for the correlation analysis.

a) Jaipur

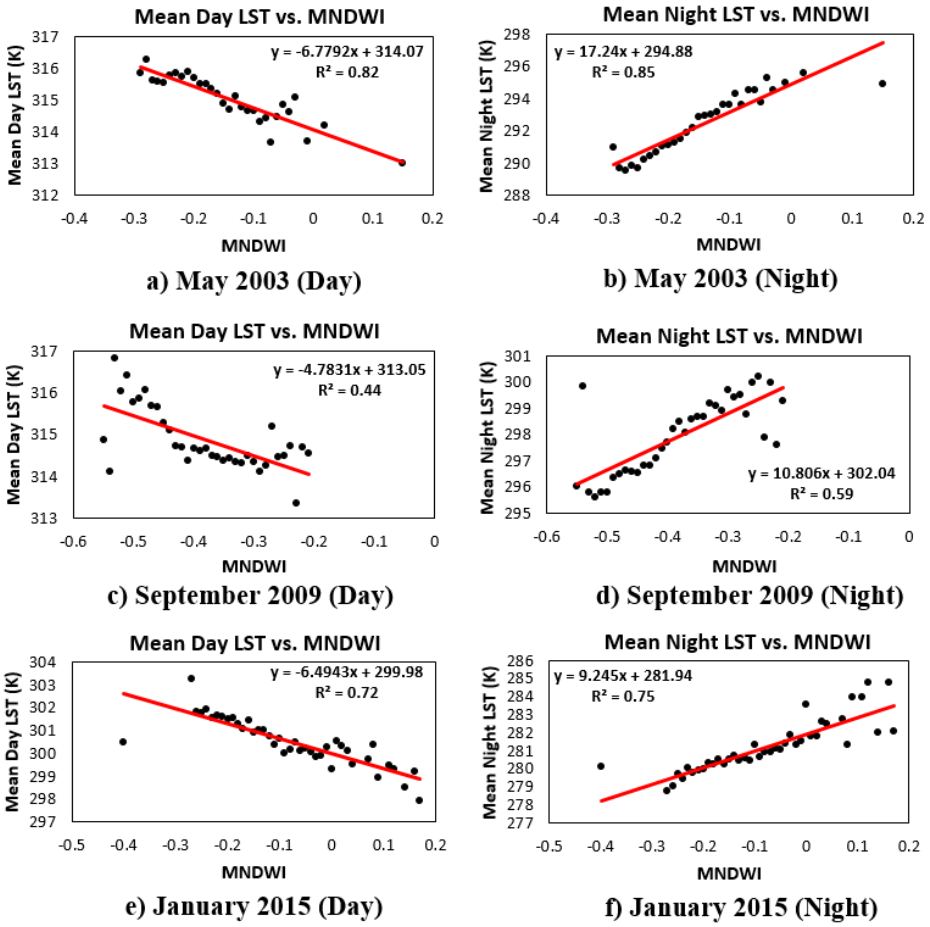

Fig. 4.62. LST vs. MNDWI Scatterplots for Different Seasons (Jaipur)

Table 4.38: Coefficient of Correlation (Linear and Polynomial) for Mean LST and MNDWI Relationship (Jaipur)

	Periods	**January 2003**	**May 2003**	**May 2009**	**September 2009**	**November 2009**	**January 2015**	**May 2015**	**September 2015**
Linear	Day	0.06	0.82	0.18	0.42	0.32	0.72	0.63	0.76
	Night	0.5	0.85	0.31	0.11	0.27	0.75	0.41	0.39
Polynomial	Day	0.06	0.82	0.38	0.51	0.47	0.76	0.64	0.82
	Night	0.5	0.93	0.96	0.6	0.74	0.77	0.61	0.63

Co-efficient of correlation of different time periods vary from 0.06 to 0.82 (polynomial and linear) during day time. Co-efficient of correlation vary from 0.50 to 0.96 (polynomial) and 0.11 to 0.85 (linear) during night period. The relationship between mean LST with MNDWI shows better correlation during night period than the day.

b) *Ahmedabad*

Table 4.39: Coefficient of Correlation (Linear and Polynomial) for Mean LST and MNDWI Relationship (Ahmedabad)

	Periods	January 2003	June 2009	2009 September	2009 December	2015 May	2015 October	2015 December
Linear	Day	0.05	0.44	0.00	0.47	0.51	0.03	0.05
	Night	0.18	0.06	0.26	0.13	0.22	0.14	0.31
Polynomial	Day	0.05	0.68	0.00	0.51	0.53	0.03	0.10
	Night	0.40	0.41	0.40	0.47	0.54	0.37	0.57

Co-efficient of correlation of different time periods vary from 0.00 to 0.68 (polynomial) and 0.00 to 0.51 (linear) during day period. Co-efficient of correlation vary from 0.37 to 0.57 (polynomial) and 0.06 to 0.31 (linear) during night period.

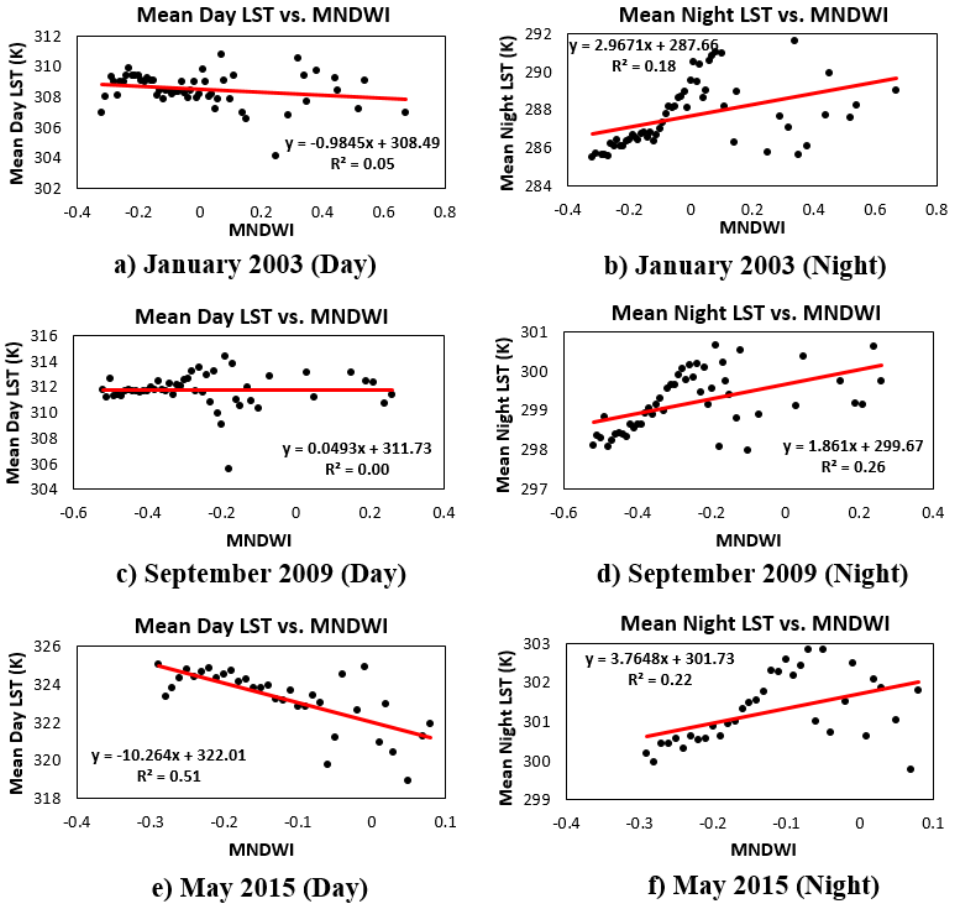

Fig. 4.63. LST vs. MNDWI Scatterplots for Different Seasons (Ahmedabad)

c) Chandigarh

Table 4.40: Coefficient of Correlation (Linear and Polynomial) for Mean LST and MNDWI Relationship (Chandigarh)

	Periods	2003 February	2009 June	2009 October	2009 December	2015 May	2015 October	2015 December
Linear	Day	0.09	0.23	0.09	0.12	0.67	0.28	0.43
	Night	0.01	0.01	0.18	0.27	0.13	0.01	0.02
Polynomial	Day	0.12	0.26	0.22	0.12	0.76	0.42	0.48
	Night	0.34	0.06	0.23	0.27	0.37	0.11	0.02

Co-efficient of correlation of different time periods vary from 0.12 to 0.76 (polynomial) and 0.09 to 0.67 (linear) during day period. Co-efficient of correlation vary from 0.02 to 0.37 (polynomial) and 0.01 to 0.27 (linear) during night period. For Chandigarh, very weak correlation has been observed between night LST and MNDWI compared to Jaipur and Ahmedabad. Moderate or weak correlation has been observed between LST and MNDWI during day period.

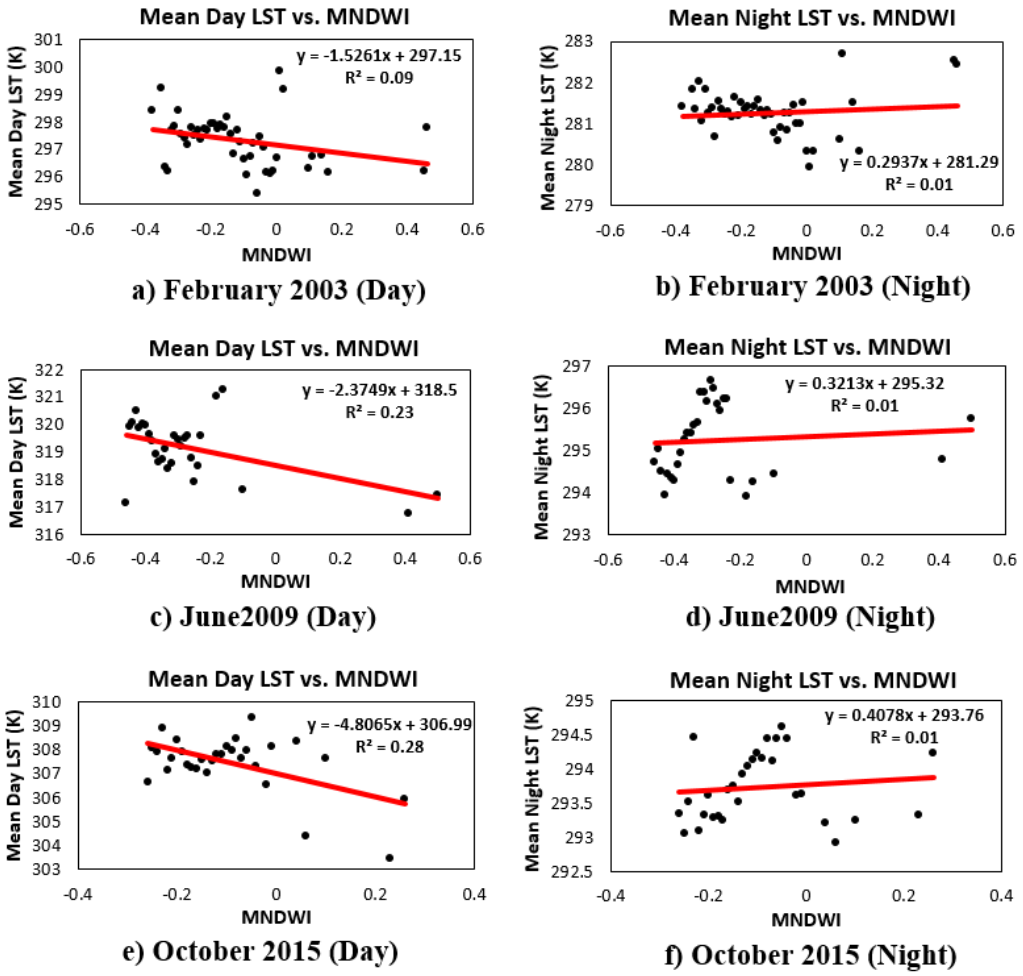

Fig. 4.64. LST vs. MNDWI Scatterplots for Different Seasons (Chandigarh)

4.5.6.2 Discussions

Inverse or negative correlation has been observed between mean LST and MNDWI during day period of all seasons. Conversely, Positive or direct correlation has been observed between mean LST and MNDWI during night period for all seasons. During night, water features favour SUHI effect due to the heat release which causes warmth of surrounding areas, whereas during day period, water features favour SUCI effect by providing cooling effect in nearby areas.

Thermal capacity of water is higher compared to other surfaces. During day period, it absorbs the solar radiation, and during night to maintain the thermal equilibrium, releasing the heat into the atmosphere resulting higher LSTs over the area. Water features show similar behavior of built-up areas during night period favoring heat island effect, whereas cooling effect of water features has been observed during day period.

4.5.7 Pattern of Elevation

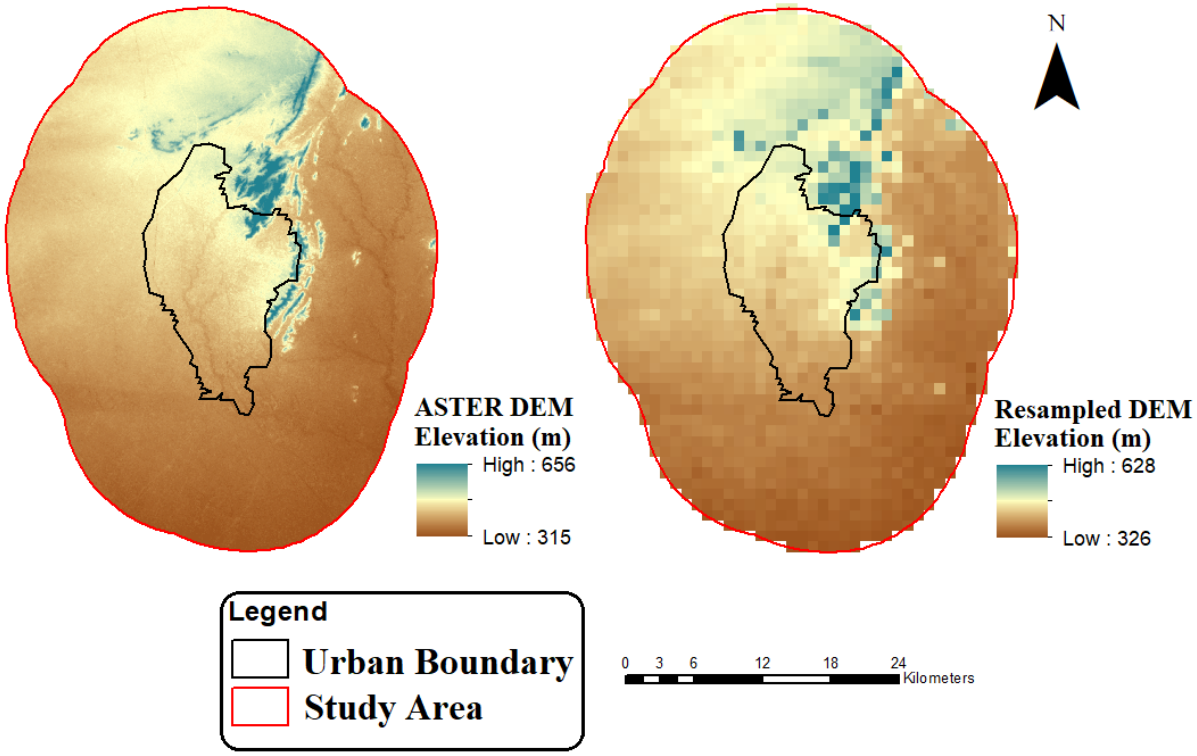

Fig. 4.65. Digital Elevation Model of the Jaipur Study Area

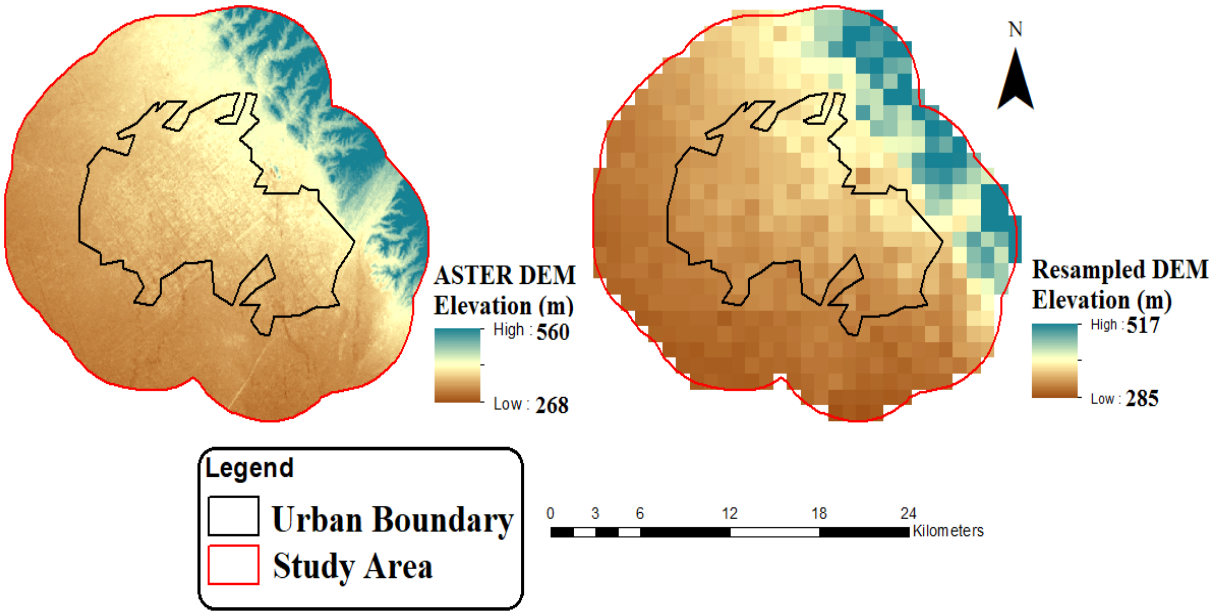

Fig. 4.66. Digital Elevation Model of the Chandigarh Study Area

There are some level differences throughout the study area. Fig. 4.65 shows the digital elevation model (DEM) of the Jaipur study area in which the hills of different elevation can be clearly seen. Some other isolated hills can also be observed within the study area. The study area is undulating with the minimum and maximum elevations as 315 m and 656 m, respectively. The general slope of the ground is from North-West to South-East. The Aravalli hill range, falling in the study area, extends in both the North and North-East directions. ASTER image has been resampled at the same resolution (926.6 m) as that of MODIS LST image. After resampling, the maximum elevation has reduced to 628 m from 656 m, and minimum elevation has increased to 326 m from 315 m due to averaging of neighbourhood pixels. Spatial variation of vegetation indices is not only subject to the impact of vegetation amount, but also to topography, elevation, availability of solar radiation, and other factors (Walsh et al., 1997). In remote sensing image of the mountainous regions, due to the effect of the ground slope, high density of vegetation is recorded over such regions. Hence ground terrain and topography of a particular area is an essential factor for UHI studies.

Fig. 4.66 shows the DEM of the Chandigarh study area produced from ASTER DEM data at 24.8 m resolution. Elevation is undulating with the lowest and highest elevations as 268 m and 560 m, respectively. The Shivalik hill range, falling in the study area, extends in both the North and North-East directions. In order to compare elevation values with LST,

ASTER image has been resampled at the same resolution as that of LST and Fig. 4.66 shows the resampled ASTER DEM image also. After resampling the highest elevation has reduced to 517 m from 560 m and lowest elevation has increased to 285 m from 268 m. The DEM image has also been snapped with LST image so that pixels of different images represent same area on ground.

4.5.7.1 LST vs. Elevation Relationship

Figs. 4.67 and 4.68 show the correlation between mean LST and elevation for different seasons of Jaipur and Chandigarh study areas. Tables 4.41 and 4.42 show the correlation (linear and polynomial, respectively) between mean LST and elevation for all three seasons along with the coefficient of correlation (R^2). Linear and second order polynomial relationship have been used for the correlation analysis.

a) Jaipur

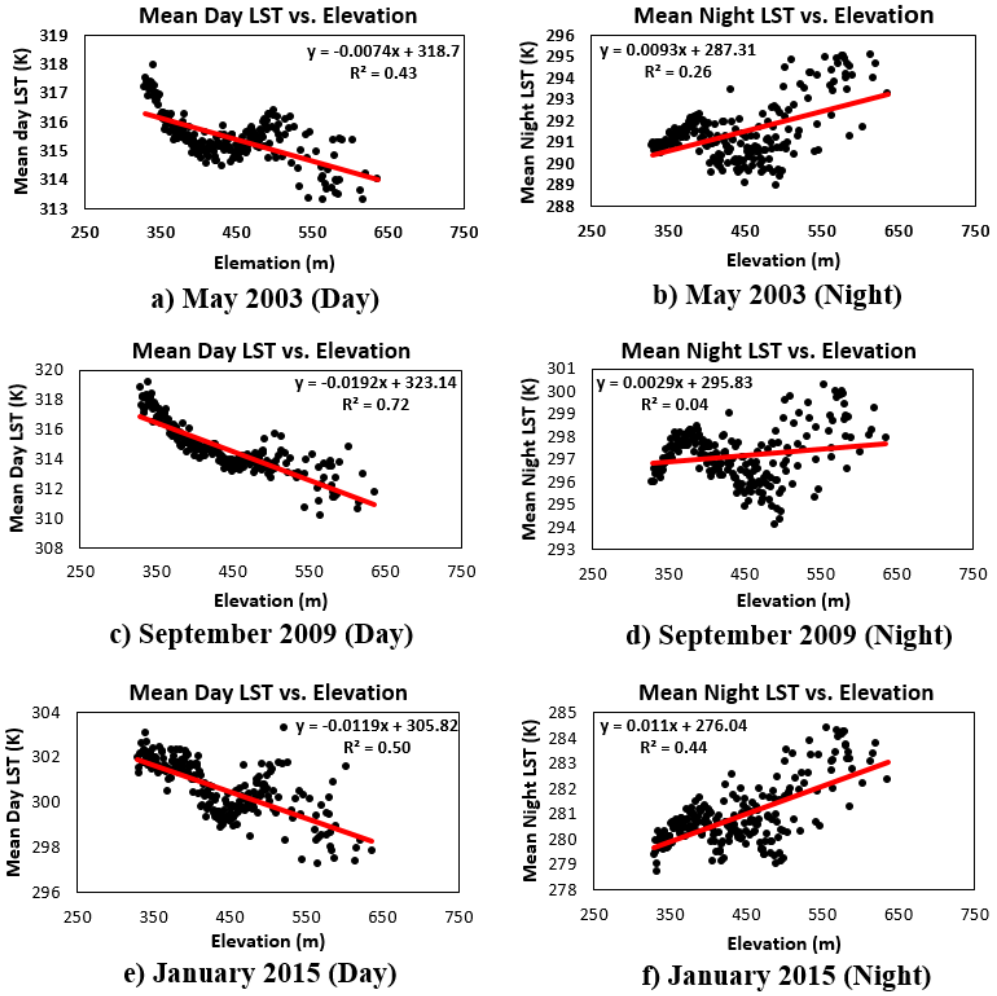

Fig. 4.67. LST vs. Elevation Scatterplots for Different Seasons (Jaipur)

Table 4.41: Coefficient of Correlation (Linear and Polynomial) for Mean LST and Elevation Relationship (Jaipur)

	Periods	January 2003	May 2003	May 2009	September 2009	November 2009	January 2015	May 2015	September 2015
Linear	Day	0.06	0.43	0.53	0.72	0.5	0.50	0.50	0.47
	Night	0.55	0.26	0.33	0.04	0.33	0.44	0.04	0.14
Polynomial	Day	0.29	0.45	0.55	0.81	0.65	0.51	0.52	0.53
	Night	0.60	0.45	0.35	0.19	0.42	0.51	0.17	0.28

Co-efficient of correlation of different time periods vary from 0.29 to 0.81 (polynomial) and 0.06 to 0.72 (linear) during day period. Co-efficient of correlation vary from 0.17 to 0.60 (polynomial) and 0.04 to 0.55 (linear) during night period. Positive or direct correlation has been observed between mean LST and elevation during night period of all seasons. Conversely, inverse or negative correlation has been observed between mean LST and elevation during day period of all seasons.

b) Chandigarh

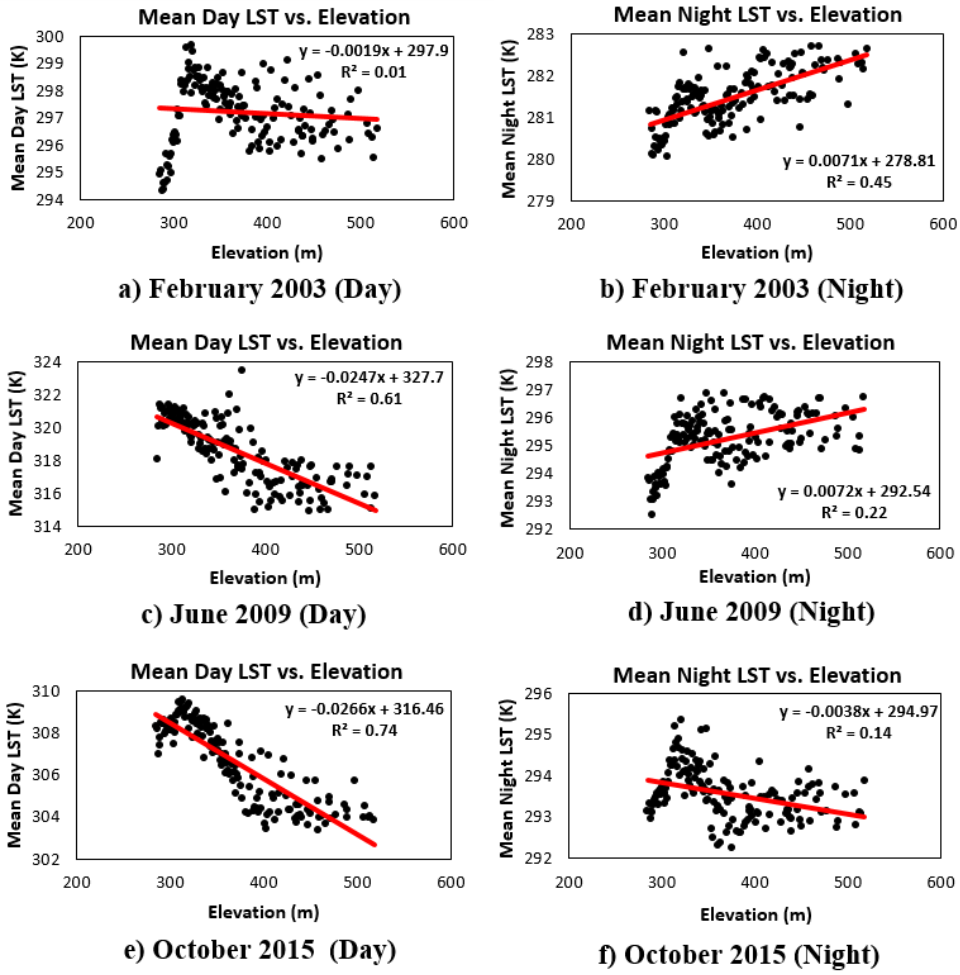

Fig. 4.68. LST vs. Elevation Scatterplots for Different Seasons (Chandigarh)

Table 4.42: Coefficient of Correlation (Linear and Polynomial) for Mean LST and Elevation Relationship (Chandigarh)

	Periods	2003 February	2009 June	2009 October	2009 December	2015 May	2015 October	2015 December
Linear	Day	0.01	0.61	0.76	0.69	0.61	0.74	0.69
	Night	0.45	0.22	0.06	0.66	0.23	0.14	0.19
Polynomial	Day	0.13	0.65	0.80	0.72	0.69	0.77	0.69
	Night	0.46	0.32	0.07	0.70	0.29	0.15	0.20

Co-efficient of correlation of different time periods vary from 0.13 to 0.80 (polynomial) and 0.01 to 0.76 (linear) during day period. Co-efficient of correlation of different time periods vary from 0.07 to 0.70 (polynomial) and 0.06 to 0.66 (linear) during night period. Positive or direct correlation has been observed between mean LST and elevation during night period of most of the seasons. During monsoon season, inverse or negative correlation has been observed between mean LST and elevation during night period due to over dominance of higher vegetation density. Conversely, inverse or negative correlation has been observed between mean LST and elevation during day period of all seasons.

4.5.7.2 Discussions

Inverse or negative relationship has been observed between LST and elevation during day period over the study areas, whereas direct or positive relationship has been noticed between LST and elevation during night period. A comparison of the LST vs. elevation correlation images of Jaipur and Chandigarh study areas indicates that during the monsoon season, less number of pixels fall in the higher temperature zone, followed by winter season and summer season has maximum pixels in the higher temperature zone. A consistent positive linear trend has been observed between LST and elevation for all the seasons during night period. It has been observed that LST-Elevation scatterplots show a negative relationship in high elevation areas during monsoon months compared to summer and winter months. This can be attributed to the fact that during the monsoon season the land is usually covered with green vegetation due to rainfall and therefore it produces a cooling effect on LST whereas during the summer season the vegetation cover is at its minimum and therefore the LST is high. It has been found out that the emissivity values of Aravalli and Shivangi rock samples are greater than dry soil samples of other areas within the study area boundary. So exposed rock surfaces would have higher LST, due to higher emissivity, as compared with dry soil and vegetation areas. The scatter plots show a consistent linear pattern between elevation and LST for all the three seasons. As the elevation increases,

normally LST has a falling trend (Kandelwal et al., 2017; Cheval et al., 2011). But in this study, as the elevation increases, rising trend of LST can be observed because of LST is influenced by many parameters such as solar incident radiation, angle of incidence of solar radiation, surface properties such as surface roughness, moisture content, extent of vegetation, etc. and these results in the different scattering during different seasons. It has also been observed that the variation in LST due to change in elevation is different from environmental lapse rate which is applicable when considering air temperatures along air column above the ground level. The fall in LST varies from 3.5 K to 4.6 K per 1000 m change in elevation when the change in elevation is associated with the horizontal distance between the points of interest. Hence the LST variations due to change in altitude of two locations are almost half that of the environmental lapse rate. This indicates that besides other factors elevation also plays a significant role in land surface temperature dynamics and in any study related with the spatial distribution of LST over a large area, the effect of a change in elevation should also be considered.

Overall analysis of the relationship of LST with all the different parameters indicates that a very complex relationship exists between them. There is direct relationship between LST and NDBI whereas inverse relationship exists between LST and NDVI. However, both these relationships are not similar during day and night time and the nighttime relationship is better than the corresponding relationship during daytime. On the other hand the relationship of LST with MNDWI, %ISA, RD and elevation is inverse during day and positive during night. The relationship of LST with different parameters undergoes both diurnal and seasonal variations. As can be seen from the results above, though the coefficient of correlation of the relationship of LST with different parameters is highly variable during different times and seasons and some parameters have better relationship with LST compared to others, yet there is no single parameter that can be used to completely express the variations in LST. Though NDVI, %ISA, NDBI, RD, NDBaI, MNDWI and elevation are independent parameters and uniquely affect the LST, but they are influenced, to some extent, by each other also. Most of the previous studies have analyzed the LST variations as an effect of single parameter individually and have not considered the simultaneous effect of several parameters. It may, therefore, be important to determine the effect of a combination of these parameters on LST.

4.6 Prediction of Surfaces Temperatures for the Assessment of SUHI Effect

This section documents the process to develop a model to predict the LST of any area on the basis of historical temperatures and parameters representing vegetation, impervious surface/roads and elevation of that area. Linear time series (LTS) model has been developed in the present study for the prediction of LST. The output of LTS model has been compared with output of artificial neural networks (ANN) model to find out the efficiency of LTS model. A Ten year LTS model has been developed to predict the LST at any location for the assessment of SUHI effect over, Ahmedabad, Chandigarh and Jaipur cities.

4.6.1 Methods for the Estimation of Error and Skill Scores

4.6.1.1 Error Estimation

The principal statistics used to evaluate the performance of the proposed model are mean absolute error (MAE), mean absolute percentage error (MAPE), and regression co-efficient (R^2). The model predicted LST has been compared with the observed LST and the error has been calculated. Absolute error in prediction of LST from the model E_A has been calculated by taking the difference between observed and predicted LST values for each pixel. MAE and MAPE have been calculated from equations 4.2 and 4.4, respectively. The regression co-efficient has been estimated by fit regression model using Minitab software.

$$E_A = \left| Y-Q \right| \tag{4.1}$$

where, Y and Q are the observed and predicted values for a pixel. Mean absolute error is calculated by taking the mean of absolute errors of all the pixels.

$$MAE = \Sigma E_A/n \tag{4.2}$$

$$E_A = E_{A1} + E_{A2} + E_{A3}\ldots\ldots\ldots E_{An} \tag{4.3}$$

where, E_{A1}, E_{A2}, $E_{A3}\ldots\ldots E_{An}$ are absolute errors at each pixel and n is the number of pixels in the study area. Percentage error (PE) is calculated by dividing absolute error (E_A) by corresponding observed LST value (Y). MAPE is the mean of absolute percentage errors,

$$MAPE = (1/N)\ \Sigma PE \tag{4.4}$$

4.6.1.2 Skill Matric and Skill Score Factor

The validation statistics have been based on skill scores, taking into consideration of reference prediction, since there will be inherent autocorrelation in the data. Skill score requires comparison of the proposed model with any other reference model to judge the suitability of the proposed model. Skill matric and skill score factor have been used to find out the efficacy of proposed model with respect to the reference model. Skill matric and skill score factor have been calculated by the following equations,

$$\text{Skill Matric} = MSE_{Forecast}/MSE_{Reference} \quad (4.5)$$

$$\text{Skill Score Factor} = 1 - (MSE_{Forecast}/MSE_{Reference}) \quad (4.6)$$

where, MSE = Mean Squared error

$MSE_{Forecast}$ = Mean Squared error of proposed model

$MSE_{Reference}$ = Mean Squared error of reference model

The skill score factor defined by equation (4.6) is one for perfect forecasts and zero (negative) for forecasts that are only as accurate as (less accurate than) the reference forecast (Roebber, 1998). The skill score is positive (negative) when the accuracy of forecast is greater (less) than the accuracy of the reference forecasts.

4.6.2 Ten Year Linear Time Series (LTS) Model for LST Prediction

LTS model has been developed to predict the LST at any location of three Indian cities for the assessment of SUHI effect. Ten year LTS model has been developed from LST values of 10 years from 2004 to 2013 along with other various parameters representing vegetation (NDVI), roads (RD), built-up or impervious surfaces (%ISA) and elevation to predict LST for the year subsequent to the 10 year data period and at the same time interval as the 10-year data. The results of the model have been validated using the observed data of year 2014. The performance of the proposed model has been evaluated using statistical parameters such as MAE, MAPE and R^2. Linear equations of LST derived from NDVI, RD, ISA and elevation as input parameters have been used for developing the LTS model in addition to the LST values. The LST values predicted by the model have been compared to the LST values of the corresponding period as calculated from the remote sensing data.

The various input parameters used for the model development have been described below.

a) LST: LST map as discussed in section 4.1 has been used to input LST value corresponding to each of the pixel of the study area. The number of pixels are 1053, 595, 1595, respectively for Ahmedabad, Chandigarh and Jaipur study areas;

b) NDVI: The land-surface or near-surface temperature is dependent on different parameters such as nature of land surface cover that ranges from bare land to vegetation of variable density. MODIS NDVI, used to represent vegetation, has been found to be a good indicator for SUHI studies. Hence, NDVI has been used as an input parameter to the model;

c) RD: RD map has been used to input RD value corresponding to all the pixels of the study area;

d) %ISA: ISA derived from linear spectral unmixing model has been used an input parameter to the model;

e) Elevation: Elevation of natural Earth surface remains the same over a period of time and does not undergo any major change, even after urbanization. Elevation of the study area pixels, taken from ASTER GDEM map has been used and entered as an input parameter;

Input parameters to the model, mentioned above are independent and are not directly related to each other and each parameter may affect the LST uniquely. It is therefore important to determine the combined effect of these parameters on LST. Thus, LTS model has been developed for predicting LST at any location, corresponding to a set of input parameters of NDVI, RD, ISA and elevation. Prediction of surface temperatures for the assessment of SUHI effect over Ahmedabad, Chandigarh and Jaipur cities using 10 year LTS model has been described below

a) Ahmedabad

LST images of Ahmedabad city for three different periods have been shown in Fig. 4.69. LST of area in urban boundary is higher as compared to the area outside the urban boundary and most of the pixels representing high temperature are within the urban boundary. The effect of built-up density of an area on LST can be clearly understood by analysing the area falling within the urban boundary (urban area) and area outside urban boundary (rural area), as the LST of rural area is lower as compared to the LST of urban area. The pattern of LST over the entire study area does not change significantly throughout the three periods. There

is an increasing trend of mean LST from the year 2004 to 2013 for all the three months of January, March and May.

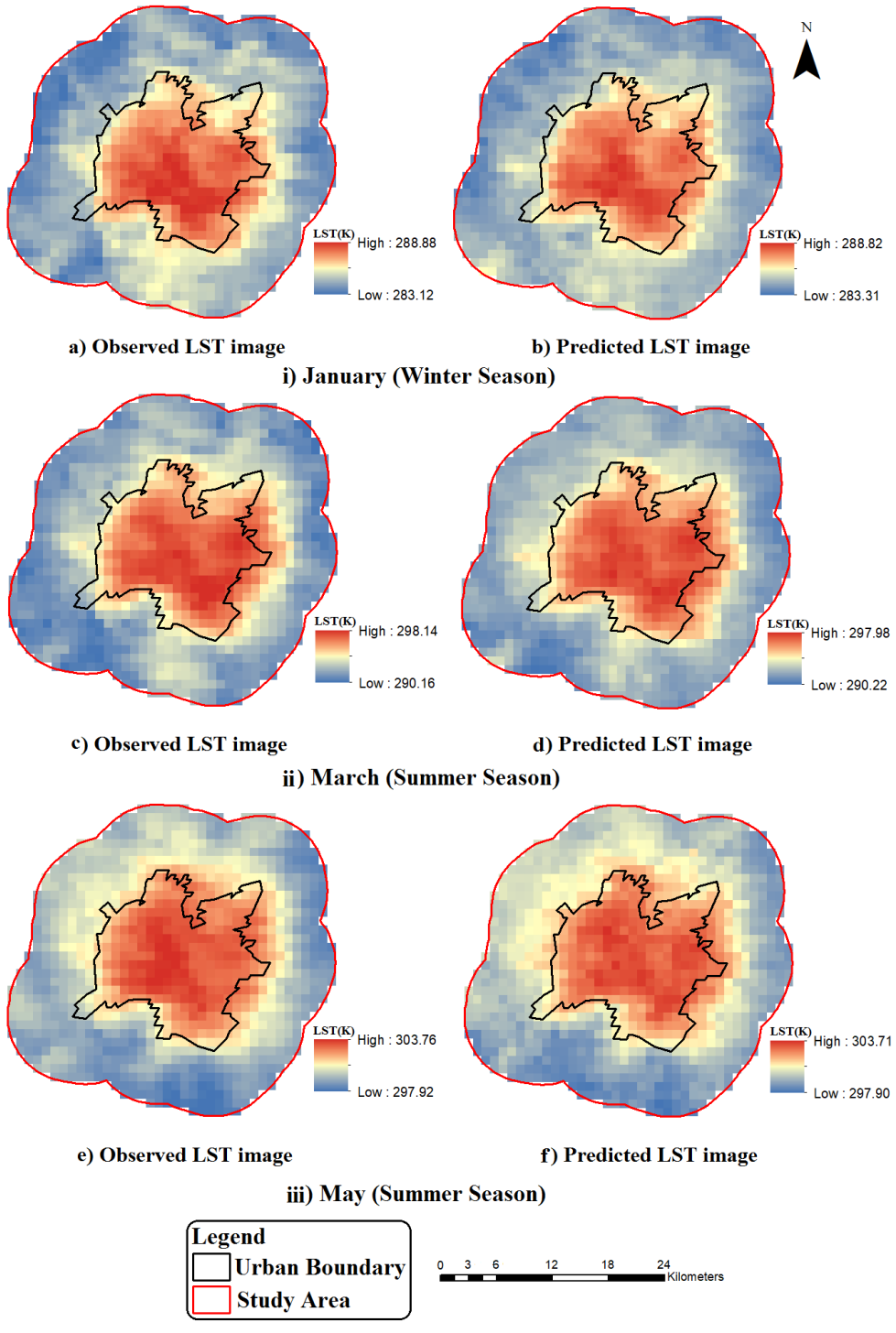

Fig. 4.69. Spatial Variation of Observed and Model Predicted LST for Different Seasons (Ahmedabad)

The output of the LTS model, estimated from MATLAB, is in the form of discrete data and has been converted into image format using ArcGIS software. The LST images derived

from MODIS data using ArcGIS software and corresponding LST images obtained from the LTS model are shown in the Fig. 4.69 which show comparison of spatial variation of model predicted and observed LST values for three periods of January (009-016 days), March (073-080 days) and May (137-144days) of 2014. It can be observed that within the urban boundary all the images show similar spatial patterns. Pixels having maximum LST range have similar spatial location and the pixels just outside the urban boundary also have similar pattern in the figures.

A comparison of observed and predicted maximum, minimum and mean LST values has been given in Table 4.43. It can be seen from the table that all the predicted and observed LST values are in close approximation and the standard deviation of the two values is also very close.

Table 4.43: Comparison of Model Predicted and Observed LST Values for Different Periods (Ahmedabad)

Day No:		**Maximum**	**Minimum**	**Mean**	**Standard Deviation**
009-016	**Observed**	288.88	283.12	285.47	1.43
	Predicted	288.82	283.31	285.32	1.39
073-080	**Observed**	298.14	290.160	293.47	2.12
	Predicted	297.98	290.22	293.54	2.10
137-144	**Observed**	303.76	297.92	300.57	1.54
	Predicted	303.71	297.90	300.38	1.51

LST values predicted from the model have been plotted along with the observed LST values for randomly selected 200 pixels over the study area. This has been done to compare the temporal and spatial variation of the model predicted and observed LST. Fig. 4.70 shows the model predicted and observed LST values for the month of January (009-016 days), March (073-080 days) and May (137-144 days). It is observed that there is close agreement between the model predicted and observed LST values for most of the measurements. It can also be seen that the model predicts both the higher and lower LSTs with great accuracy. Further, as the pixels have been randomly selected and are scattered throughout the study area, it can be understood that the model is able to predict correctly for the entire study area and it does not have any affinity towards any area within or outside the urban boundary.

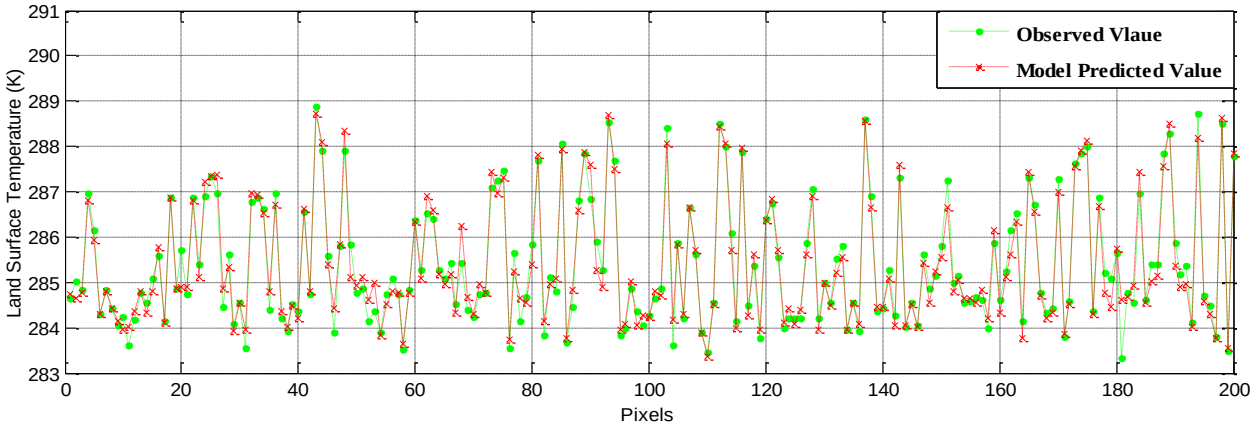

a) January (009-016 days)

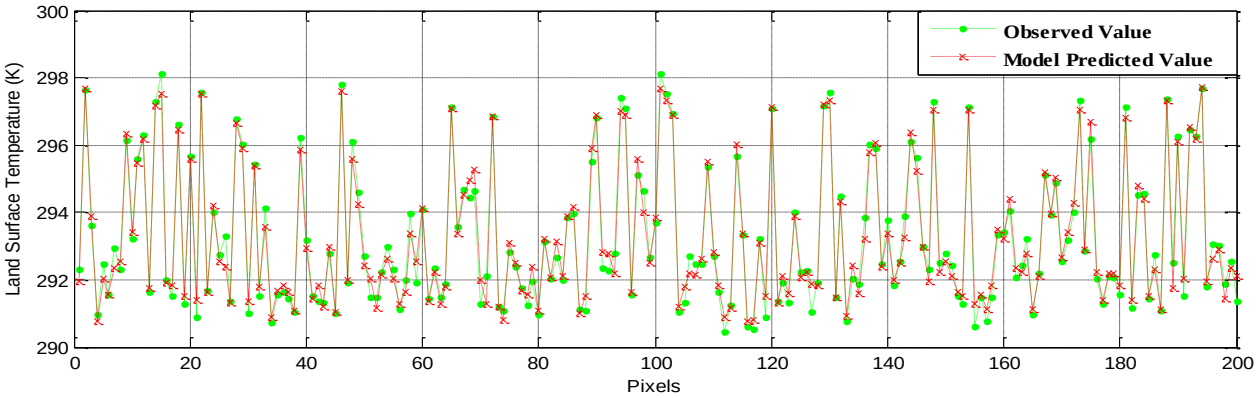

b) March (073-080 days)

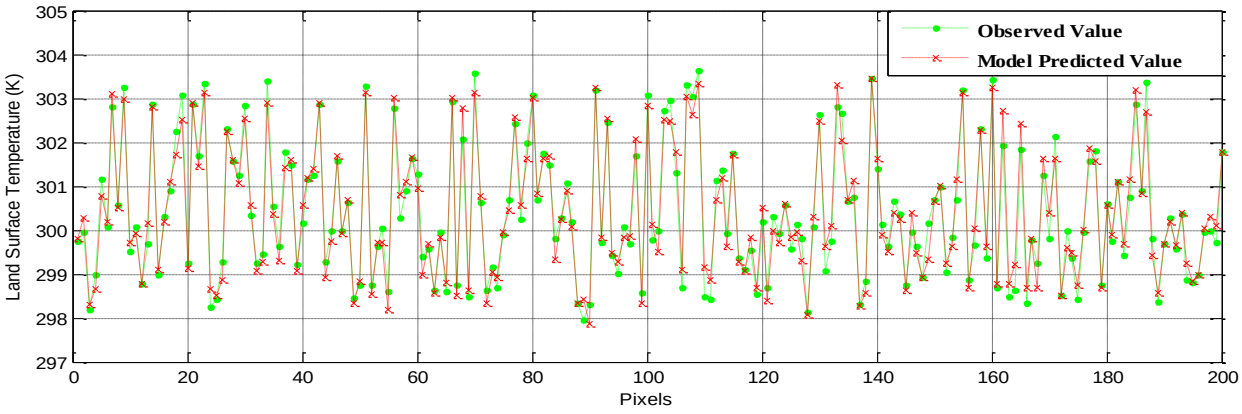

c) May (137-144 days)

Fig. 4.70. Comparison of Model Predicted and Observed LST for Randomly Selected Pixels of the Study Area for Different Periods (Ahmedabad)

Table 4.44 shows MAE, MAPE and R^2 for the three periods of 2014. The highest value of 1.45 K for maximum absolute error may be due to continuous changes occurring on the corresponding pixel in form of change in vegetation/road density/built-up or impervious

surfaces. The minimum value of absolute error is insignificant and almost equal to zero. The MAE is only 0.23 K, 0.26 K and 0.24 K for the three periods which means that there is very less variance between model predicted values and observed values and there is a good agreement between model predicted and observed values in LTS model. The maximum MAPE is only 0.09% thereby indicating that the model is able to predict the LST to a high accuracy. These observations can also be drawn from Fig. 4.71 that shows the scatterplots between the predicted LST values using LTS model and the observed ones for the study periods of 2014. It can be seen that there is a good agreement between predicted and observed LST values. The coefficient of determination (R^2) corresponding to these plots varies from 0.95 to 0.97 which means that there is a strong relationship between observed and model predicted values.

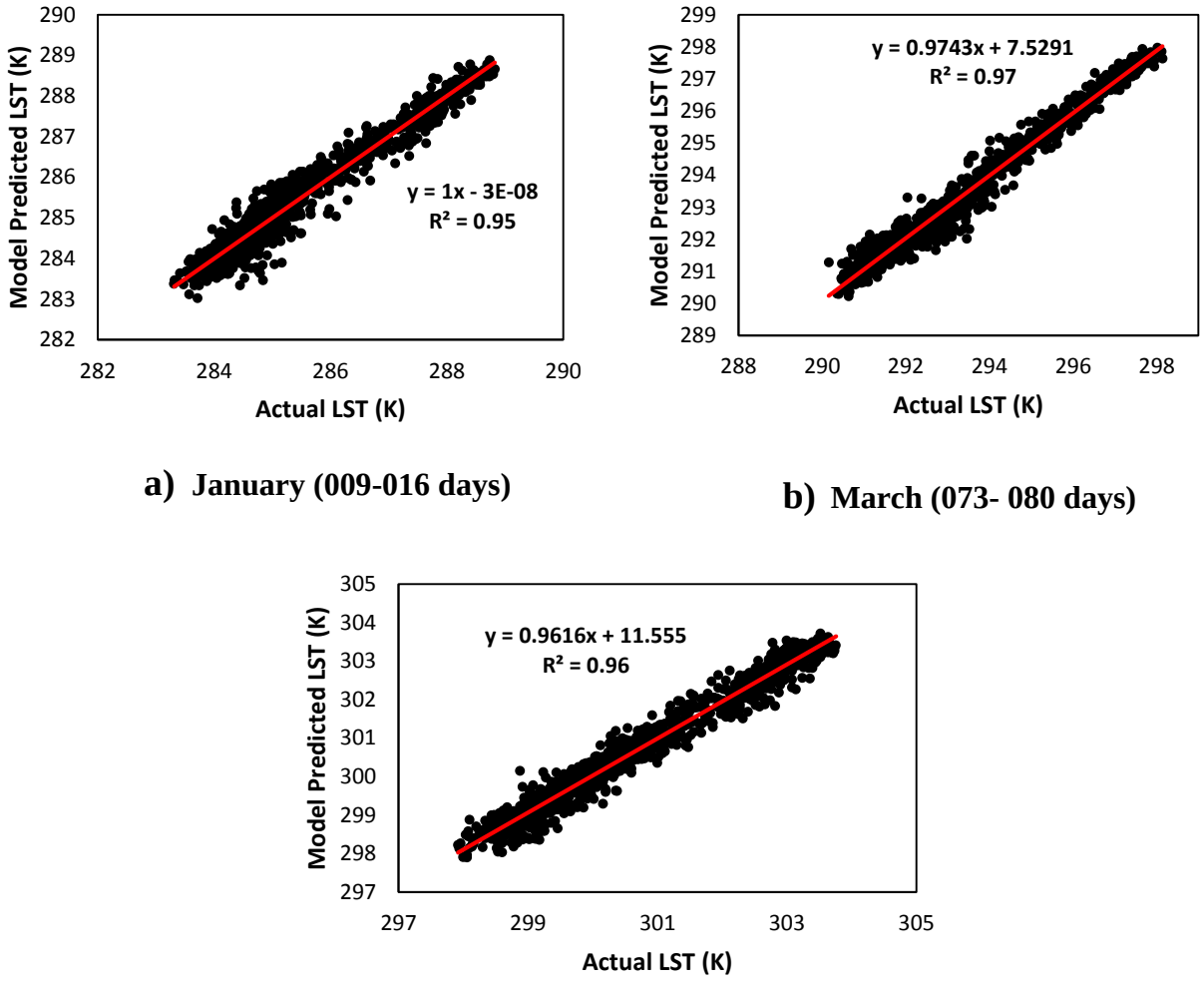

a) January (009-016 days)

b) March (073- 080 days)

c) May (137-144 days)

Fig. 4.71. Scatterplots between Model Predicted and Observed LST (Ahmedabad)

Table 4.44: Statistical Parameters for Performance Evaluation of the Model (Ahmedabad)

Month	January	March	May
Day No.	**009-016**	**073-080**	**137-144**
Maximum Absolute Error (K)	1.38	1.45	1.26
Minimum Absolute Error (K)	0.00	0.00	0.00
MAE (K)	0.23	0.26	0.24
MAPE (%)	0.08	0.09	0.08
R^2	0.95	0.97	0.96

The performance of the model has also been evaluated using Table 4.45 that shows the number of pixels of the study area, categorized on the basis of the error in prediction of LST. A negative error indicates that the model predicted LST value is higher than the observed value whereas the observed value is higher when the error is positive. It can be seen from the table that the model is able to predict the LST at different parts of the study area quite accurately as the error in prediction at about 90% pixels of the study area is within 0.5 K of the observed LST for all the study periods. The number of pixels where the error is beyond 1.0 K of the observed values is very small for all the three periods and it is only 9, 14 and 1 for the January, March and May months, respectively which is less than 2% of the total pixels in the study area.

Table 4.45: Number of Pixels in Different Error Ranges (% of Pixels in Study Area) (Ahmedabad)

Day No:	More than -1.0 K	Between -0.5 to -1.0 K	Between -0.5 to +0.5 K	Between +0.5 to +1.0 K	More than +1.0 K
009-016 (January)	9(0.85%)	49(4.65%)	951(90.31%)	44(4.18%)	0(0.00%)
073-080 (March)	6(0.57%)	51(4.84%)	929(88.22%)	59(5.60%)	8(0.76%)
137-144 (May)	1 (0.09%)	36(3.42%)	955(90.69%)	61(5.79%)	0(0.00%)

Spatial variation of error in prediction has been shown in Fig. 4.72 for the different periods. The pixels having error in prediction of LST are distributed over the entire study area. It can be seen from figure that the error between model predicted and observed LST is beyond 0.5 K for very few pixels of the study area which predominantly fall at or outside the urban boundary, whereas the prediction is very close to observed values in the urban region. This can be attributed to the fact that the values of NDVI of the urban area have lower variations compared to the NDVI of rural area. NDVI of the rural area changes significantly during

different seasons as well as undergoes annual changes due to variations in the rainfall intensity. Another reason of more error in the rural area may be due to the RD. For the present study one RD data has been used. It is possible that over the period of 10 years, the rural area has undergone some development during which some roads might have been constructed thus resulting into change in the RD. This problem is not expected in the urban area as the roads in the urban area are already present and usually no new roads are constructed in the area after development and only road widening is carried out during later years. There can be changes in %ISA of the pixels falling in the rural area which is a continuous process, i.e. the %ISA of few pixels may change which can happen over a period of time. This can also be a reason for little error in LST prediction. It can also be seen that the error in prediction is beyond 0.5 K at more pixels of the urban area during May month compared to other months. This can be due to the effect of season as the May month is during summer season and it is possible that extra high temperatures are observed in the urban area due to other factors like air pollution, anthropogenic heat etc. As mentioned earlier also, the error in prediction at most part of the study area is within 0.5 K of the observed values. It can also be seen that the error in prediction is beyond 0.5 K at more pixels of the rural area.

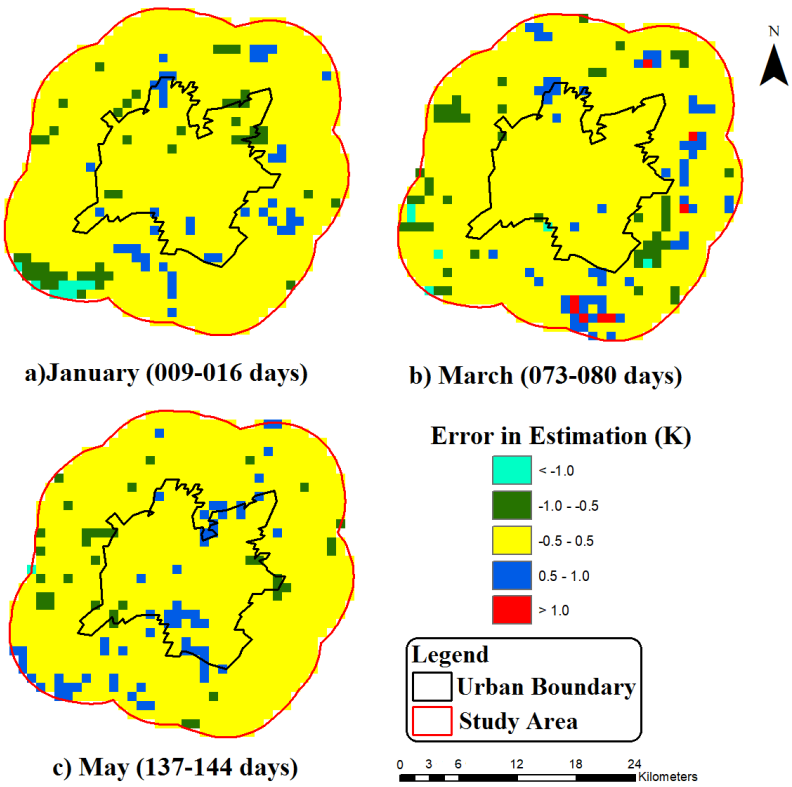

Fig. 4.72. Spatial Variation of Error between Observed and Model Predicted LST (Ahmedabad)

From the present study, it is clear that LTS model generated LST values closely approximate with the observed values and it can be concluded that the model can be used for highly accurate prediction of LST. Hence the model can be used for analysis of SUHI effects.

b) Chandigarh

Fig. 4.73 shows comparison of spatial variation of model predicted and actual LST values for the three study periods (2ndFebruary to 9th February, 23rd April to 30th April, and 2nd June to 9th June) of 2014. The LST images derived from MODIS data and corresponding LST images obtained from the LTS model are shown in the Fig. 4.73.

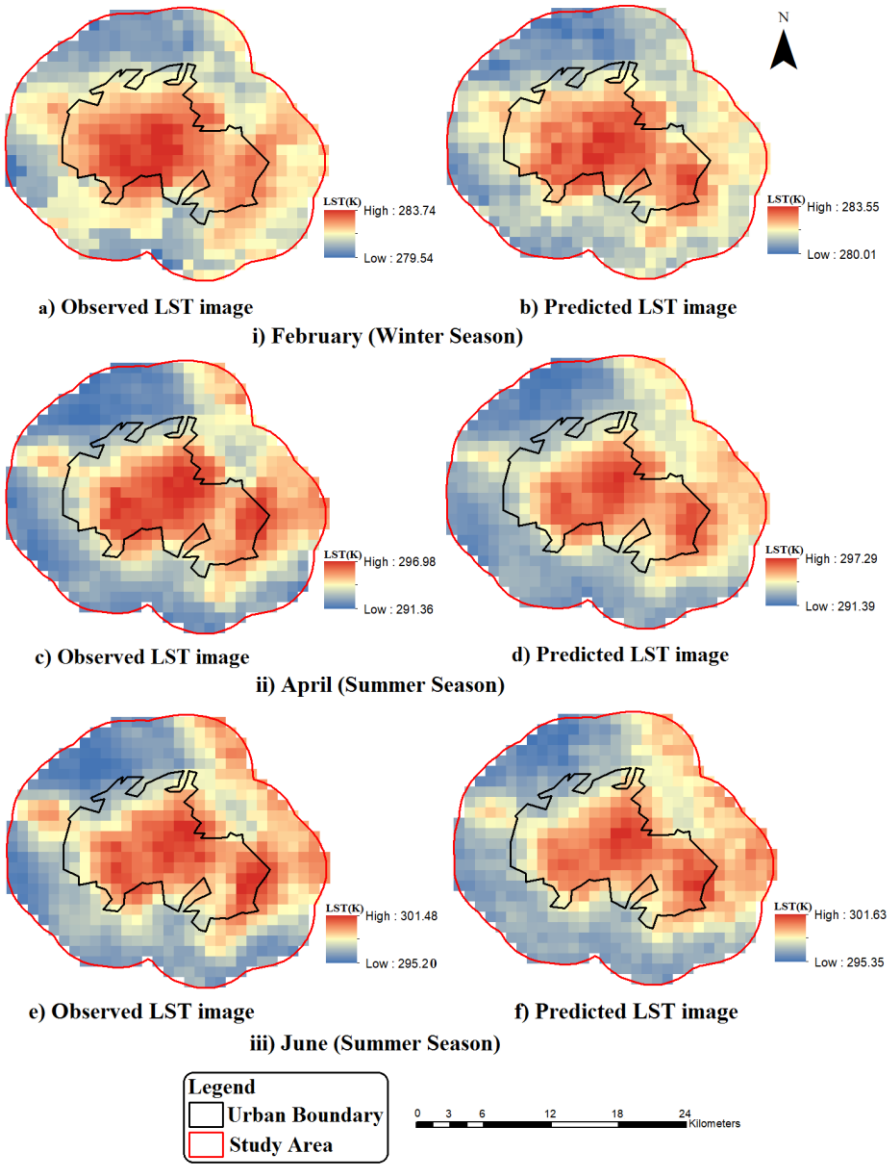

Fig. 4.73: Spatial Variation of Observed and Model Predicted LST for Different Seasons (Chandigarh)

It has been observed that within the urban boundary all the images show similar spatial variation. Pixels having maximum LST range have similar spatial location and the pixels just outside the urban boundary also have similar pattern in the images. These results show that the model has good capability of accounting the variations in the LST values at different pixels of the study area. The main difference between the model estimated and measured LSTs in the images can be observed mainly in some parts of rural areas because these areas undergo considerable seasonal and annual variations and show temporal variations in LSTs.

Table 4.46 shows the comparison of observed and predicted maximum, minimum and mean LST values for the three periods of 2014. The model predicted LST values are very close to the actual LST values and the mean values are also quite close. Almost similar standard deviation coupled with the similar range of maximum to minimum values and nearly same mean values indicate that the prediction from the model is good. The comparison shows that the predicted LST values perform well with the measured ones for the whole set of periods and pixels.

Table 4.46: Comparison of Model Predicted and Observed LST Values for Different Periods (Chandigarh)

Day No:		**Maximum**	**Minimum**	**Mean**	**Standard Deviation**
February (033-040 days)	**Actual**	283.74	279.54	281.68	0.92
	Predicted	283.55	280.01	281.41	0.85
April (113-120 days)	**Actual**	296.98	291.36	293.94	1.53
	Predicted	297.29	291.39	293.62	1.48
June (153-160 days)	**Actual**	301.48	295.20	298.21	1.61
	Predicted	301.63	295.35	298.57	1.55

LST values predicted from the model have been plotted along with the observed LST values for randomly selected 200 pixels over the study area. This has been done to compare the temporal and spatial variation of the model predicted and actual LST values. Fig. 4.74 shows the comparison of model predicted and actual LST values for the months of (2^{nd}February to 9^{th} February, 23^{rd} April to 30^{th} April, and 2^{nd} June to 9^{th} June) of 2014 for the selected 200 pixels. It can be observed that there is a good agreement between the model predicted and actual values for most of the measurements. It can also be seen that the model predicts both the higher and lower LSTs with good accuracy.

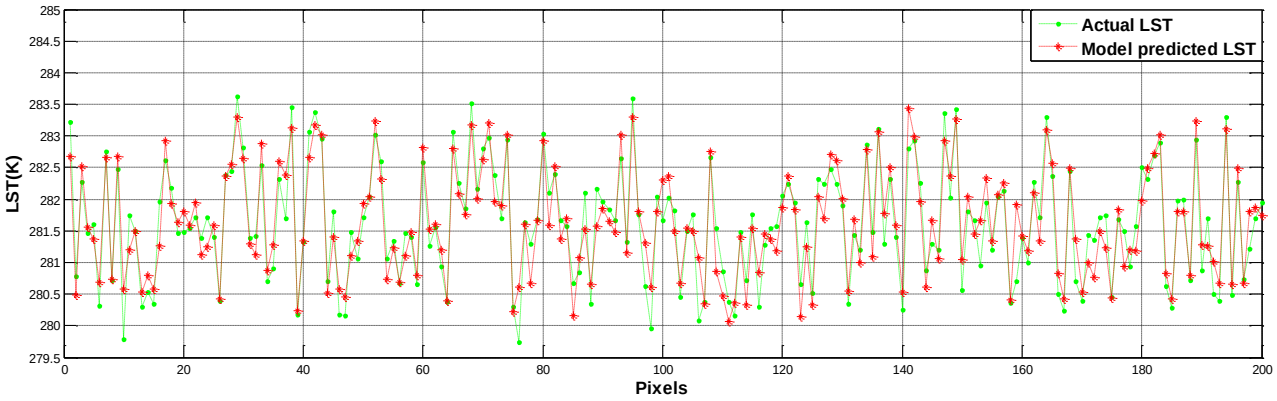

a) February (033-040 days) 2014

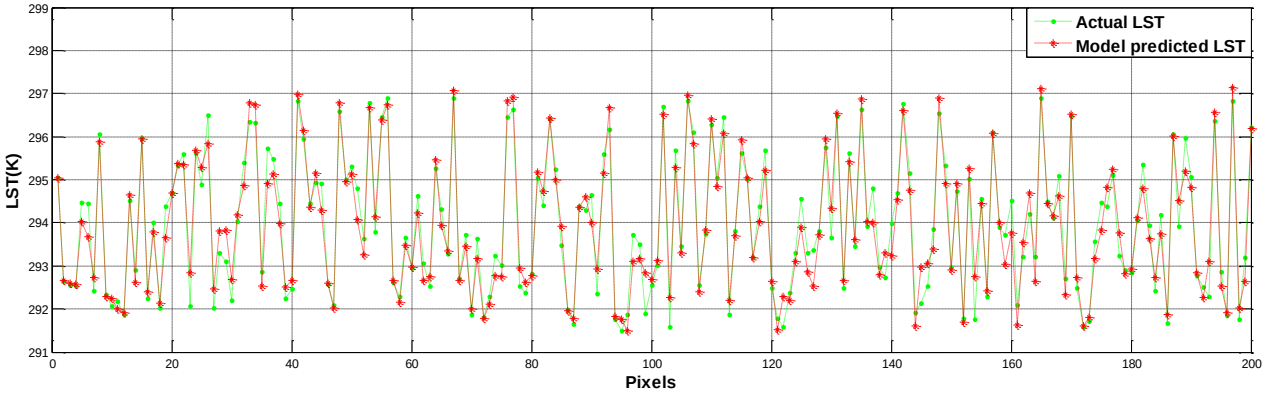

b) April (113-120 days) 2014

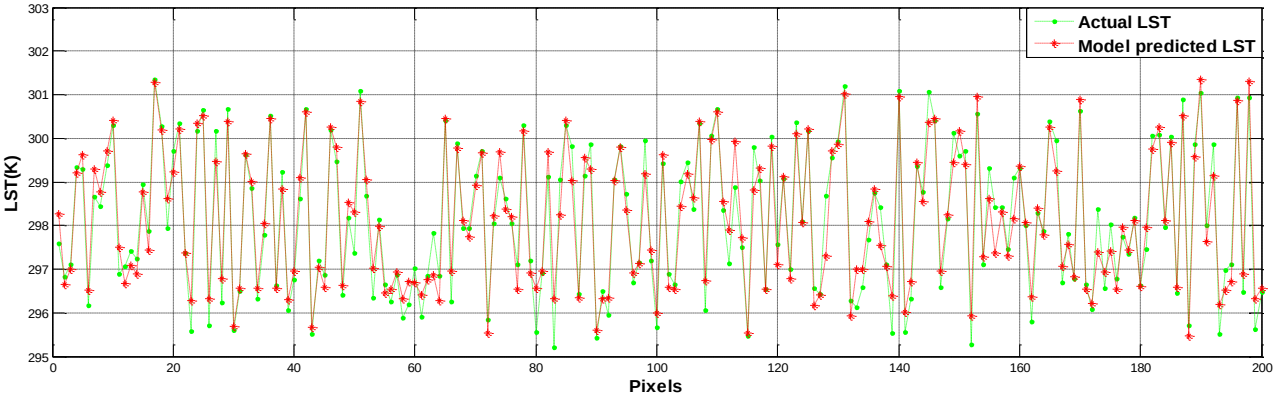

c) June (153-160 days)

Fig. 4.74. Comparison of Model Predicted and Observed LST for Randomly Selected Pixels of the Study Area for Different Periods (Chandigarh)

Table 4.47 shows MAE, MAPE and R^2 values for the three periods. MAE varies from 0.29 K to 0.36 K and MAPE varies from 0.10 % to 0.12 %, which indicates that there is a good agreement between LTS model predicted and actual LST values. Fig. 4.75 shows the

scatterplots for the comparison between the predicted LST values using LTS model and the observed LST values. Good agreement between predicted and actual LST values can be observed from these scatter plots. The coefficient of determination (R^2) corresponding to these scatter plots varies from 0.84 to 0.94 which means that there is a strong relationship between observed and model predicted values.

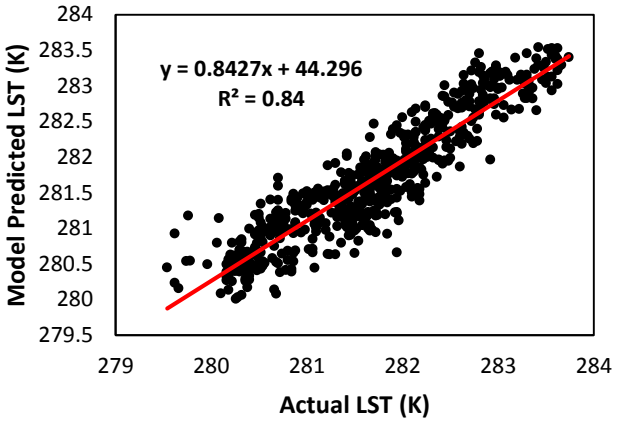

a) February (033-040 days) 2014

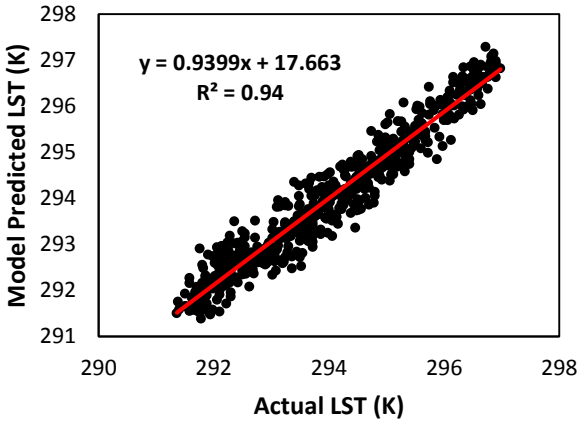

b) April (113-120 days) 2014

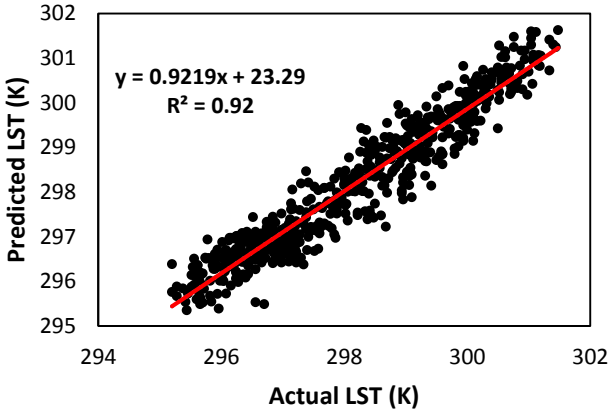

c) June (153-160 days) 2014

Fig. 4.75. Scatterplots between Model Predicted and Observed LST (Chandigarh)

Table 4.47: Statistical parameters for performance evaluation of the model (Chandigarh)

Month	February	April	June
Day No.	(033-040 days)	(113-120 days)	(153-160 days)
Maximum Absolute Error (K)	1.42	1.15	1.46
Minimum Absolute Error (K)	0.00	0.00	0.00
MAE (K)	0.30	0.29	0.36
MAPE (%)	0.10	0.10	0.12
R^2	0.84	0.94	0.92

The performance of the model has also been evaluated using Table 4.48 that shows the number of error pixels in different ranges for different periods, categorized on the basis of the error in prediction of LST. It can be seen from the table that the model is able to predict the LST at different parts of the study area quite accurately as the error in prediction at about 80% pixels of the study area is within 0.5 K of the observed LST for all the study periods. Error in most part of the urban area, especially the CBD, is within ±0.5 K, which indicates good agreement between measured and model estimated LST values. The number of pixels where the error is beyond 1.0 K of the observed values is very small for all the three periods and it is only 5, 4 and 15 for the February, April and June months, respectively which is less than 3 % of the total pixels in the study area.

Table 4.48: Number of Pixels in Different Error Ranges (% of Pixels in Study Area) (Chandigarh)

Day No:	<1	-1 to -0.5	-0.5 to +0.5	0.5 to 1	>1
033-040 (February)	4 (0.67%)	44 (7.39%)	495 (83.19%)	51 (8.57%)	1 (0.17%)
113-120 (April)	2 (0.34%)	54 (9.08%)	479 (80.50%)	58 (9.75%)	2 (0.34%)
153-160 (June)	6 (1.01%)	69 (11.60%)	442 (74.62%)	69 (11.60%)	9 (1.51%)

Fig. 4.76 shows the spatial variation of error calculated between the measured and model estimated LST values for the months of (2^{nd}February to 9^{th} February, 23^{rd} April to 30^{th} April, and 2^{nd} June to 9^{th} June) of 2014. Positive error may be a result of urbanization at these pixels during the later part of study period due to which the model could not account for the urbanization and its associated effects. Most of the negative error pixels are outside the urban boundary and very few are inside the urban boundary. This may be the effect of increase in vegetation/vegetation density over these pixels. The error between model estimated and measured LST is beyond ±1 K for very few pixels of the study area which predominantly fall in the rural area, whereas the prediction is close to actual values in the urban region. This can be attributed to the reasons of variations in NDVI, %ISA or the RD. As mentioned earlier also, error in most part of the study area, is within 0.5 K, which indicates observed and model predicted LST values are in good agreement.

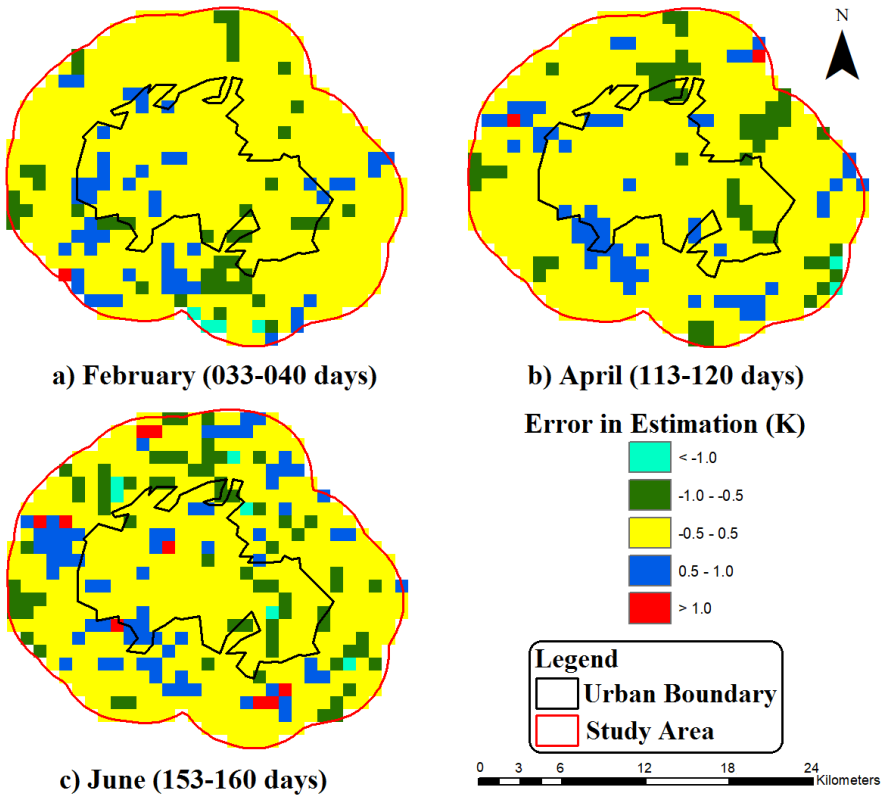

Fig. 4.76. Spatial Variation of Error between Observed and Model Predicted LST (Chandigarh)

Distinct characteristics can be observed in the error image corresponding to the range when the error between the observed and estimated LSTs is within ±0.5 K. The majority of this error correspond to the pixels which encounter the lower range of the LST. Lower LST range, usually, is over the pixels at the boundary of the study area, where there is no urbanization. Hence, pixels of these locations are influenced by local flows of wind, such as if the wind direction is towards urban area or the direction is from urban area and other local site-specific factors such as high vegetation and zero (or low) RD and building density. At the middle and higher range the model estimated values closely correspond to the measured LST values. This is due to the effect of combined effect of different parameters, which are able to consider the UHI effect in a very good manner. From the present study, it is clear that LTS model generated LST values closely approximate with the actual LST values and from the above graphs and scatter plots it can be concluded that the model can be used for highly accurate prediction of LST.

These results suggest that the model has good capability of accounting the variations in the LST at different locations of the study area. The model can be utilized for predicting the LST at any location of a city.

c) Jaipur

Fig. 4.77 shows comparison of spatial variation of model predicted and actual LST values for the three study periods (9thJanuaryto 16th January, 73rd March to 80th March, and 137th May to 144th May) of 2014. It is observed that within the urban boundary that all the corresponding figures show similar spatial variation. Pixels having maximum LST range have similar spatial location, and the pixels just outside the urban boundary also have similar pattern in the figures.

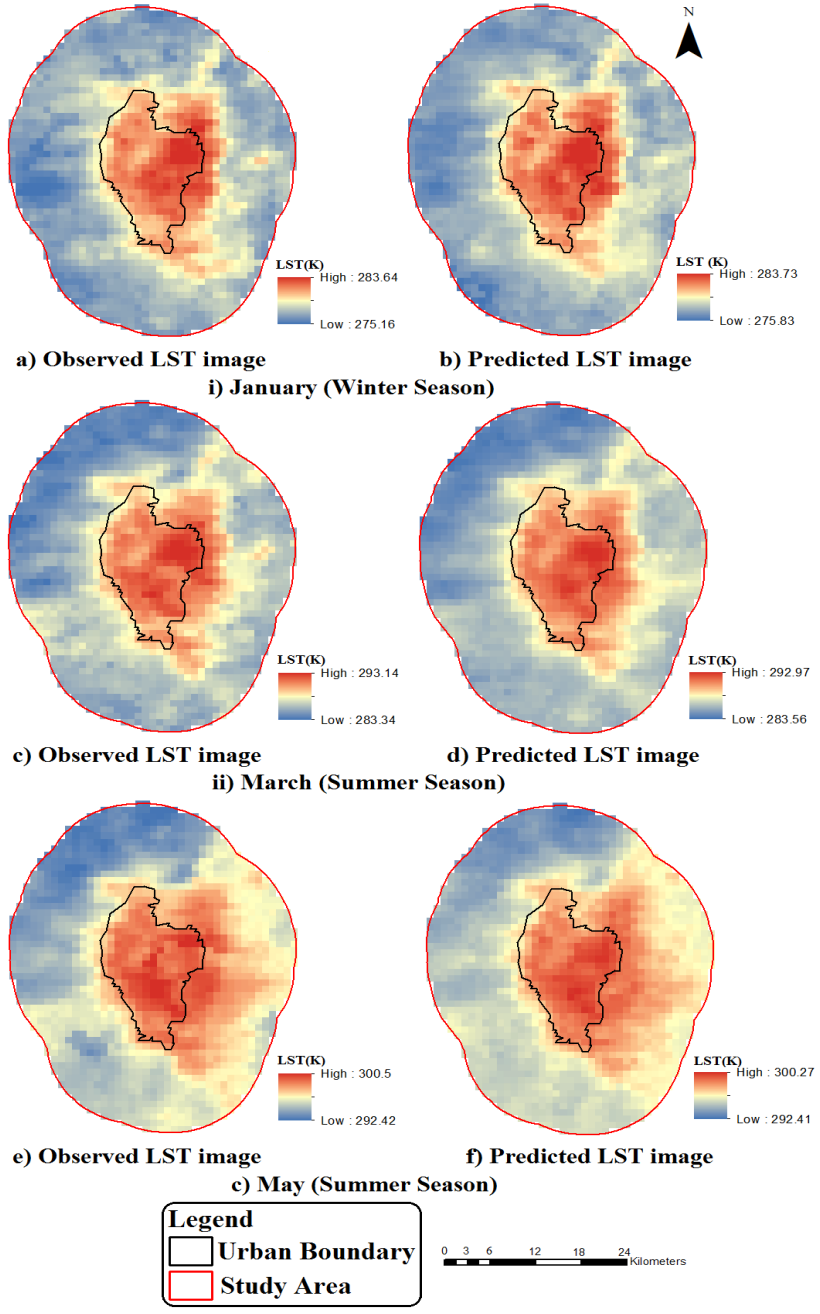

Fig. 4.77. Spatial Variation of Observed and Model Predicted LST for Different Seasons (Jaipur)

Table 4.49 shows the comparison between the maximum, minimum, and mean values of actual and predicted LST. The comparison shows that the estimated LST values perform well with the measured ones for the whole set of periods and pixels. These results show that the model has good capability of accounting the variations in the LST values at different parts of the study area. Figs. 4.78 show the variation of the model predicted and actual LST values at 200 randomly selected pixels from the study area for the three study periods. It can be seen that there is a close agreement between the model-predicted and actual LST.

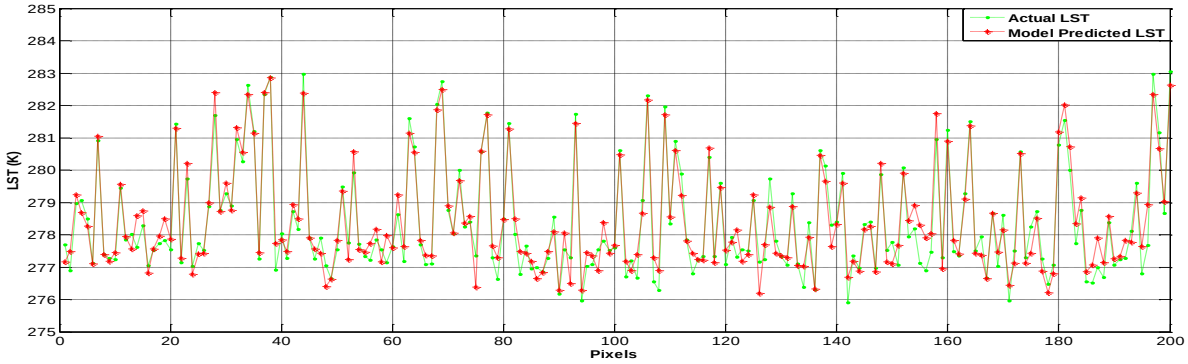

(a) January (009–016 days) 2014

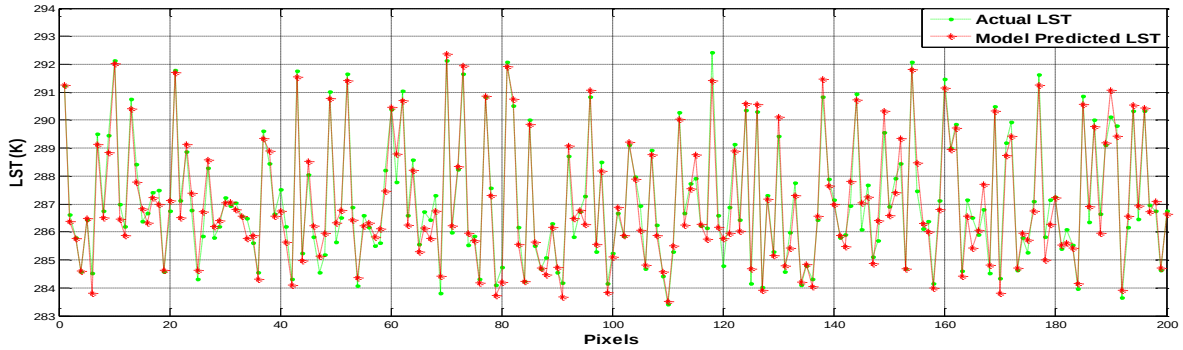

(b) March (073–080 days) 2014

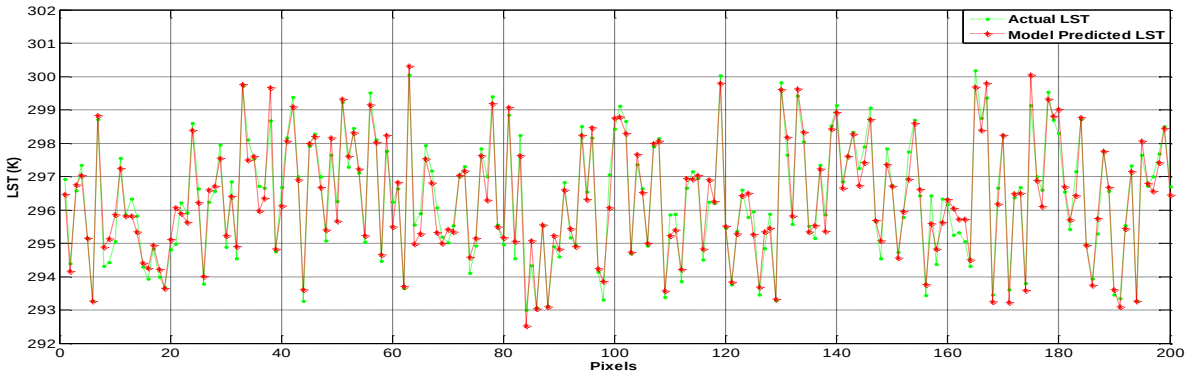

(c) May (137–144 days) 2014

Fig. 4.78. Comparison of Model Predicted and Observed LST for Randomly Selected Pixels of the Study Area for Different Periods (Jaipur)

Table 4.49: Comparison of Model Predicted and Observed LST Values for Different Periods (Jaipur)

Day No:		Maximum	Minimum	Mean	Standard Deviation
January (009-016 days)	**Actual**	283.64	275.16	278.59	1.81
	Predicted	283.73	275.83	278.67	1.76
March (073-080 days)	**Actual**	293.14	283.34	287.17	2.25
	Predicted	292.97	283.56	287.20	2.21
May (137-144 days)	**Actual**	300.50	292.42	296.26	1.80
	Predicted	300.27	292.41	296.24	1.76

Table 4.50 shows MAE, MAPE, and R^2 values for the three periods of 2014. MAE for the three periods varies from 0.29 to 0.35 K, while MAPE varies from 0.10 to 0.12. This indicates that there is good agreement between LTS model predicted and actual values. Fig. 4.79 shows the scatterplots for the comparison between the actual LST and estimated LST using the LTS model. The model-predicted and actual values show coefficient of determination (R^2) that ranges from 0.94 to 0.96, which means that there is a strong relationship between actual and model predicted values.

Table 4.50: Statistical Parameters for Performance Evaluation of the Model (Jaipur)

Month	January	March	May
Day No.	009-016	073-080	137-144
Maximum Absolute Error (K)	1.36	2.03	1.38
Minimum Absolute Error (K)	0.00	0.00	0.00
MAE (K)	0.34	0.35	0.29
MAPE (%)	0.12	0.12	0.10
R^2	0.94	0.96	0.96

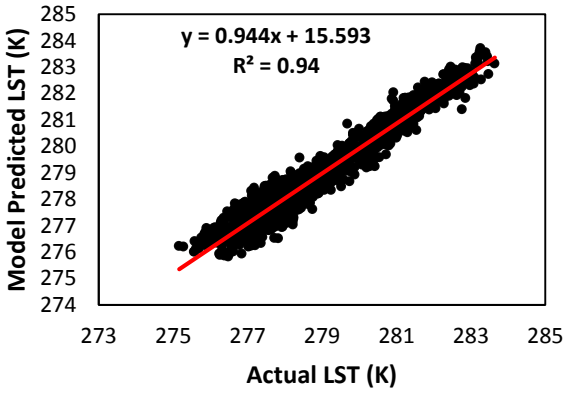

(a) January (009–016 days) 2014

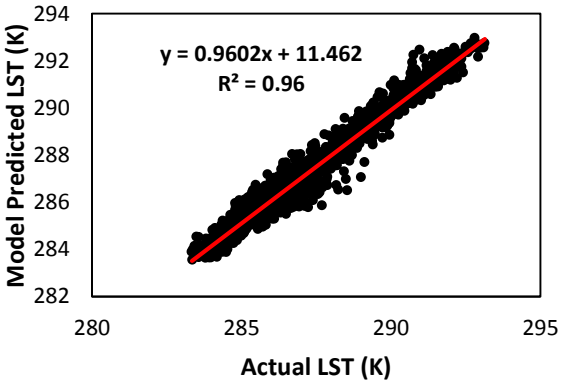

(b) March (073–080 days) 2014

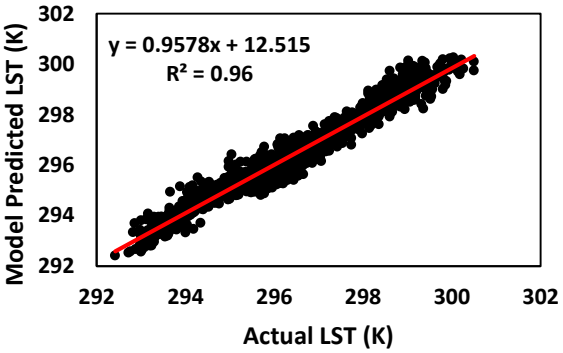

(c) May (137–144 days) 2014

Fig. 4.79. Scatterplots between Model Predicted and Observed LST (Jaipur)

The performance of the model has also been evaluated using Table 4.51 that shows the number of pixels of the study area, categorized on the basis of the error in prediction of LST. It can be seen from the table that the model is able to predict the LST at different parts of the study area quite accurately as the error in prediction at about 75% pixels of the study area is within 0.5 K of the observed LST for all the study periods. The number of pixels where the error is beyond 1.0 K of the observed values is very small for all the three periods and it is only 32, 13 and 56 for the January, March and May months, respectively which is about 3% of the total pixels in the study area.

Table 4.51: Number of Pixels in Different Error Ranges (% of Pixels in Study Area) (Jaipur)

Day No:	More than -1.0 K	Between -0.5 to -1.0 K	Between -0.5 to +0.5 K	Between +0.5 to +1.0 K	More than +1.0 K
009-016 (January)	17 (1.07%)	172 (10.78%)	1212 (75.99%)	179 (11.22%)	15 (0.94%)
073-080 (March)	10 (0.63%)	103 (6.46%)	1330 (83.39%)	149 (9.34%)	3 (0.19%)
137-144 (May)	33 (2.07%)	182 (11.41%)	1216 (76.24%)	141 (8.84%)	23 (1.44%)

Error in the estimation of LST values has been calculated. Fig. 4.80 shows the spatial variation of error calculated between the actual and model-estimated LST values, and close association between observed and model predicted LST values can be seen from this figure. It can be seen that the error is within ±0.5 K for most part of the study area, indicating that the LTS model has been able to accurately predict the LST for the study area. The error between model estimate and measured LST is beyond ±1 K for very few pixels of the study area that predominantly falls in the rural area, whereas the prediction is close to actual values in the urban region. This can be attributed to the fact that the NDVI of the urban area has lower variation compared to the NDVI of the rural area that undergoes great changes depending on rainfall and season.

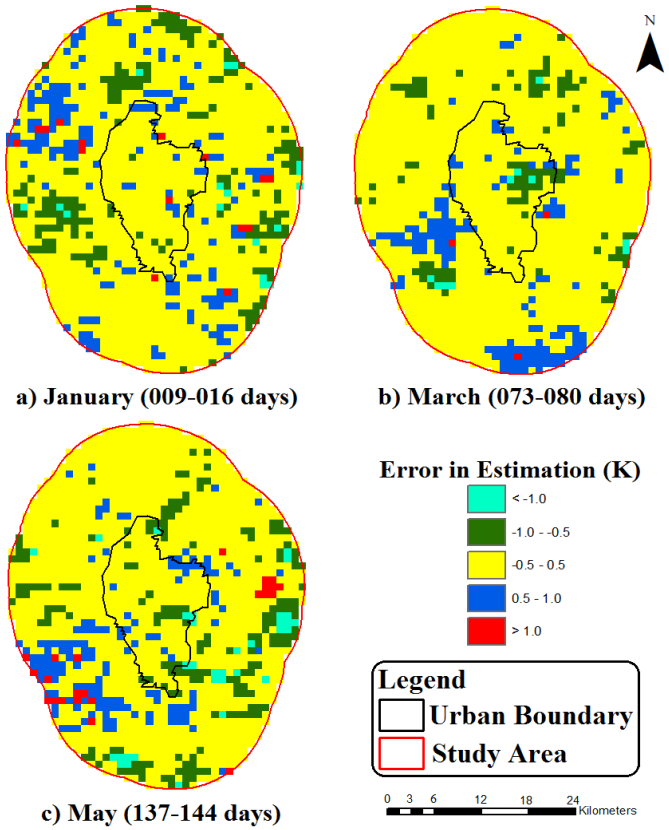

Fig. 4.80. Spatial Variation of Error between Observed and Model Predicted LST (Jaipur)

From the above graphs and scatter plots, it can be concluded that the model is capable of predicting LST values of high accuracy and the LTS model generates LST values approximately close with the actual values, and it can be concluded that the model can be used for highly accurate prediction of LST. Hence, the model can be used for analysis of SUHI effects. The model can be utilized for predicting the LST at any location of a city. Hence, if there is a requirement to develop some area within or outside a city, it is possible

to plan the development of the city in a scientific manner using the LTS model generated in the present study. For this purpose, some options of the proposed development may be prepared having desired road density, green areas, permissible ground coverage and parking lots etc. The LST over the proposed areas corresponding to different such options may be calculated using the model. It has been estimated that the peak urban electrical demand rises by about 2–4% for each 1°C rise in the daily maximum temperature above a threshold of 15–20°C (Akbari, 1995). Hence, the options with lowest LST may be adopted, which not only incorporates all the requirements of good planning principles but which may also include the scientific method to control the UHI effect and thereby help in lowering the electrical demand.

For planned development of a city master plan is prepared in which area for different type of activities are earmarked, but they are decided without taking into account the role of various parameters on UHI. If in addition to various principles of planning, the information available on UHI is also utilized during the process of development, it may enable the city planners to design the physical urban layout in such a manner that it helps to contain UHI associated with the development. It is very necessary to develop a model incorporating the parameters affecting UHI. This will serve as a tool for the city planners to help them in preparing the master plan of a city on scientific lines. Preparing master plan of a city, after considering the effect of various parameters in such a fashion that it can help to contain the UHI effect to a predetermined extent, can result that both the UHI effect and its consequent effects on environment can be reduced.

4.6.3 Inter comparison of Three year LTS model with ANN model (Jaipur)

A number of UHI prediction studies are based on the ANN technique (Gobakis et al., 2011; Lee et al., 2016). A neural network architecture has been developed to predict the UHI intensity in Athens, Greece, during both day and night (Mihalakakou et al., 2004) using data for a two-year time period. Another study uses input data from meteorological stations as well as historic measured air temperatures within the city to predict the UHI intensity in London based on neural network architecture (Kolokotroni et al., 2010).

Comparison between LTS and ANN model (Khandelwal, 2012) has been carried out in the present study. ANN model has been developed by using three years data of Jaipur city from 2007 to 2009. LST data of various seasons of good quality has been used for the

development of ANN model. NDVI, distance from hotspots (DHS), RD and elevation have been used as input parameters for model generation. The model has been used to predict LST for all the pixels of the Jaipur study area for one year after the three year data and the performance of the model has been evaluated using the observed LST data for the year 2010. LTS model has also been developed using the same data and the output of the LTS model has been compared with the output of the ANN model. The comparison has been carried out using principal statistics (Table 4.52). Statistical parameters MAE, MAPE, MSE and R^2 have been calculated for both LTS and ANN model using predicted LST values from the model and observed LST values. MAE and MAPE of different periods, for which LST values have been predicted by the LTS model, range from 0.27 to 1.69 K and 0.10% to 0.60%, respectively. Correlation coefficient (R^2) between the observed and predicted values range from 0.52 to 0.98. Overall average MAE, average MAPE, and average R^2 of the prediction is 0.58 K, 0.20 %, and 0.89, respectively from the LTS model.

Table 4.52: Inter Comparison of Three Year LTS Model with ANN Model (Jaipur)

		LTS				**ANN**			
Sl. No.	Days No.	MAE	MAPE	MSE	R^2	MAE	MAPE	MSE	R^2
1	009	0.50	0.18	0.39	0.88	0.61	0.22	0.56	0.81
2	025	0.37	0.13	0.22	0.95	0.81	0.29	1.00	0.87
3	041	0.54	0.19	0.47	0.88	0.80	0.28	0.96	0.79
4	057	0.61	0.21	0.59	0.92	0.93	0.32	1.30	0.81
5	073	0.34	0.12	0.17	0.98	0.55	0.19	0.48	0.93
6	089	1.03	0.35	1.28	0.94	0.54	0.19	0.46	0.92
7	105	0.29	0.10	0.14	0.97	0.54	0.18	0.47	0.88
8	121	0.38	0.13	0.23	0.90	0.46	0.16	0.33	0.85
9	137	0.33	0.11	0.18	0.95	0.51	0.17	0.40	0.92
10	153	0.62	0.21	0.59	0.62	1.06	0.36	1.84	0.38
11	169	0.39	0.13	0.23	0.89	0.37	0.12	0.21	0.89
12	265	0.46	0.16	0.28	0.94	0.39	0.13	0.25	0.87
13	281	1.19	0.41	1.48	0.98	0.62	0.21	0.59	0.9
14	297	0.44	0.15	0.37	0.91	1.03	0.36	1.45	0.83
15	329	0.42	0.15	0.27	0.93	0.66	0.23	0.65	0.8
16	345	0.27	0.10	0.12	0.97	0.54	0.19	0.45	0.92
17	361	1.69	0.60	4.57	0.52	1.47	0.52	2.58	0.47
	Overall	**0.58**	**0.20**	**0.68**	**0.89**	**0.70**	**0.24**	**0.82**	**0.81**

MAE and MAPE of different periods, for which LST values have been predicted by the ANN model, range from 0.37 to 1.47 K and 0.12 to 0.52 %, respectively. Correlation coefficient (R^2) between the observed and predicted values range from 0.38 to 0.93. Overall

average MAE, average MAPE, and average R^2 of the prediction is 0.70 K, 0.24 %, and 0.81, respectively from the ANN model.

From the comparison between LTS and ANN model, it is observed that the LTS model gives better results than the ANN model. MAE and MAPE calculated for LTS model of different periods show comparatively lower error compared to the ANN model. Also correlation coefficients for prediction from LTS model have been observed to be higher than ANN model for most of the time periods which signifies the better results of prediction by LTS model. Data during the time periods of 153- 160^{th} and 361- 366^{th} days show the results of less accuracy with maximum error compared to other time periods.

4.6.3.1 Comparison of Skill Metric and skill score factor

The LTS model has been compared with ANN model to estimate the skill score of the LTS model (Forecasted) with reference to the ANN (Referred) model. Skill calculation has been carried out using the error metric 'Mean Squared Error (MSE)' and the associated skill score based on MSE has been calculated. A perfect forecast when the predicted and observed values are absolutely same will have ZERO MSE thereby resulting in a forecast skill metric having ZERO value. This will result in skill score being 1.0. When the forecast and reference models are of equal skill and have same MSE than the skill metric will be one and it will have a skill score of 0.0. In this case both the models are of equal quality with none of them being good or bad. If the skill metric is greater than one, i.e. MSE of forecast model is higher than MSE of referred model the skill score factor will be negative which means that forecast model is less skilful than the referred model. In such a case there may be unbounded negative skill score values. Skill metric and skill score factor for LTS (forecast) and ANN (reference) models for different periods have been calculated. Skill Metric and skill score factor of various periods have been shown in Table 4.53. In most of the periods, skill metric lies between 0 and 1 which results in positive skill score values i.e. LTS model has been observed to be more skilful than ANN model for most of the time periods. But, some of the time periods show skill metric values greater than 1 which results in negative skill score representing that LTS model has been observed to be less skilful than the ANN model. Skill metric values of different time periods range from 0.22 to 2.79 with an average skill metric value of 0.84. Also, skill score values of different time periods range from -1.79 to 0.78 with an average skill score of 0.16.

From the comparison between LTS and ANN model, it is observed that LTS model is more efficient than ANN model for most of the cases for the prediction of LSTs. Periods of April, October and December show high negative skill scores of -1.79, -1.51, and -0.77, respectively representing LTS model is less skilful than ANN model in those periods. Periods of June and September also show low negative skill scores of -0.10 and -0.13. There are large variations in LST during monsoon season as well as inter season variations are also significant. The change in season and corresponding variations may have resulted in lower skill of LTS model during the above months. However, for all the other periods of summer and winter seasons the LTS model gives better result than the ANN model signified by a positive skill score and hence the proposed LTS model has good capability of accounting the variations in the LST at different locations of the study areas.

Table 4.53: Skill Metric and Skill Score Factor for Different Periods

Sl. No.	Days No.	Skill Metric	Skill Score
1	009	0.68	0.32
2	025	0.22	0.78
3	041	0.49	0.51
4	057	0.45	0.55
5	073	0.36	0.64
6	089	2.79	-1.79
7	105	0.30	0.70
8	121	0.70	0.30
9	137	0.44	0.56
10	153	0.32	0.68
11	169	1.10	-0.10
12	265	1.13	-0.13
13	281	2.51	-1.51
14	297	0.25	0.75
15	329	0.41	0.59
16	345	0.28	0.72
17	361	1.77	-0.77

Chapter 5

Conclusions

Urbanization, one of the main factors causing unnatural changes in ordinary climate patterns around the globe, is infecting our world drastically. All cities of the world have witnessed rapid urbanization, which causes the natural landscape having predominantly vegetation cover and pervious areas, converted into built-up and impervious areas. The present study analyses the UHI phenomenon of Indian cities of Jaipur, Ahmedabad and Chandigarh of different climates. This work documents the spatial, diurnal and seasonal variations in the UHI intensity of approximately 1370, 887, 511 km^2 of area surrounding Jaipur, Ahmedabad and Chandigarh cities, respectively, utilizing predetermined quality remote sensing data from Landsat, MODIS and ASTER sensors. Spatio-temporal SUHI growth analysis of the three cities has been carried out using UHI_{index} and transect methods. The present study also documents the contrast diurnal SUHI effect over these cities. Hence, diurnal thermal behaviour of various land surface materials viz-a-viz air temperature, has been studied by in-situ temperature monitoring, for comparing diurnal SUHI and AUHI effects. Also, the efficacy of remote sensing data of different times during the day/night has been analyzed for SUHI studies, in order to understand the importance of time of observation. The present study has also improved understanding of the UHI characteristics and brings out the diurnal relationship between LST and different parameters representing urbanization, vegetation, soil, water and terrain of the cities. Understanding of relationships coupled with spatial SUHI growth impacts on human comfort and health are crucial for making rational and scientifically sound decisions in urban planning applications. Most of the studies on urban climates discuss only the qualitative description of thermal patterns and simple correlation analysis (Ruiliang et al., 2006). However, in the present study, the simultaneous effect of different parameters on LST variations has also been studied by developing a LTS model to predict the LST at a particular location for given values of the different parameters for SUHI assessment. This model can be used for planned development of a city in such a manner that UHI effect can be minimized. The reduction in UHI effect can help in reducing the energy demand.

5.1 Conclusions and Recommendations

Diurnal and seasonal variations in LSTs for the assessment of SUHI effect over three

Indian cities have been analyzed in the present study. Magnitude of SUHI of an image has been represented as maximum UHI intensity which is the difference between maximum (urban) and minimum (rural) LSTs of a particular image. From the analysis of night-time images, overall average of maximum SUHI intensity of the Jaipur study area during summer, monsoon, and winter seasons has been observed as 8.39 K, 6.83 K, and 9.6 K, respectively. Similarly overall average of maximum SUHI intensity of the Ahmedabad study area during summer, monsoon, and winter seasons is 6.26 K, 5.79 K, and 7.69 K, respectively. Overall average of maximum SUHI intensity of the Chandigarh study area during summer, monsoon, and winter seasons is 5.67 K, 4.64 K, and 5.04 K, respectively. Annual average maximum SUHI intensity of the Jaipur, Ahmedabad and Chandigarh study areas for all seasons is 8.5 K, 6.75 K, and 5.17 K, respectively, indicating significant SUHI effect during nighttime over all the three cities. The average night SUHI intensity for the entire 13 year study duration for Jaipur, Ahmedabad and Chandigarh study areas is 2.87 K, 2.64 K, and 1.14 K, respectively. On the other hand corresponding average day SUHI intensity of the Jaipur, Ahmedabad and Chandigarh study areas is -0.99 K, 0.57 K, and 1.53 K, respectively. **Existence of SUHI effect can be seen from nighttime LST images corresponding to all the seasons for all the three cities whereas weak or no such effect is visible from daytime LST images except for Chandigarh where daytime SUHI effect is comparable to that of the nighttime SUHI effect.**

UHI intensity exhibits diurnal and seasonal cycles and is modulated by meteorological conditions, such as cloud, wind conditions as well as anthropogenic heat release. The maximum and minimum temperatures for different periods of different years are highly variable, depending on the season of the year. Similarly, the UHI intensity at a particular location also varies considerably. Due to these reasons, it is very difficult to compare UHI intensity at a particular location during different periods. Further, it is not possible to calculate the consolidated UHI effect over the study area from the LST data for a long period. In order to facilitate such calculations, UHI_{index} has been used which is a normalized index with values between 0 and 1. The average value of UHI_{index} for the entire study period will indicate the combined UHI effect over different parts of the study area. Maximum value of average UHI_{index} for Jaipur city is 0.95 which is very close to 1 and hence indicating that this pixel encounters consistent maximum LSTs. Similarly, the corresponding maximum values of average UHI_{index} for Ahmedabad and Chandigarh are

0.92 and 0.89, respectively. The urban area has only high temperature pixels and the minimum value of average UHI_{index} in the urban area is 0.41, 0.31, 0.36, respectively for Jaipur, Ahmedabad and Chandigarh cities. The mean of average UHI_{index} of the urban area is 0.73, 0.74 and 0.66, respectively for Jaipur, Ahmedabad and Chandigarh cities. Pixels with average value of UHI_{index} more than 0.90 can be considered to indicate that high LST normally occurs on these pixels and they can be considered as hot spots (HS). The HS act as the centre of UHI of cities and other high-temperature pixels are located around these pixels. **Average UHI_{index} image of night period shows clear picture of SUHI for all three cities whereas no such clear SUHI pattern has been observed during day period.** The extreme temperature at any location due to some random event/specific meteorological conditions can make its UHI_{index} value higher for that particular image. However, if the UHI_{index} value is calculated for a long period of time, the error due to this bias introduced due to the random event will be reasonably low, thus facilitating correct location of the HS. On the other hand, if absolute temperatures are utilized for the analysis, the error may be comparatively higher. **This is the reason that UHI_{index} has been proposed to be a good way to study long-term effect.**

A temperature gradient, from the HS to the outer boundary of the study area, can be observed. This gradient may, however, be different in different directions. UHI_{index} and transect analysis has been carried out for analyzing SUHI growth using LST data at a gap of six years.

Area of HS of Jaipur, Ahmedabad and Chandigarh has increased by about 10.30 to 13.74 km^2; 12.02 to 25.76 km^2; and 6.01 to 16.31 km^2, respectively during the period between 2003 and 2015, which is an increase of up to 230%; 600% and 950% in the area of HS of Jaipur, Ahmedabad and Chandigarh cities and indicate significant areal SUHI growth over these cities. Corresponding decrease in the area of undeveloped land has also been observed between 2003 and 2015 that indicates conversion of natural land surfaces into human-made materials which increase the anthropogenic heat resulting into increase in temperature. High seasonal and spatial variations in SUHI growth of the study areas have been observed. The seasonal variations in LST profile of the urban area are very less as compared to the rural area. SUHI growth over rural regions shows different patterns depending on seasons.

Transect analysis has been done by analyzing the increase in temperature of the pixels

with respect to the pixels of maximum temperature i.e. HS. All the transects pass through centroid of HS and run from HS to outer boundary of the study area. Relative difference between the LST at HS and LST of all other pixels has been calculated. This relative difference is then plotted along the transects. Increase in area enclosed by different isothermal lines, varies from 20% to above 400% during different seasons between 2003 and 2015. It can be interpreted that there is a continuous increase in LST of the Jaipur and Ahmedabad cities and the temperature gradient between HS and area surrounding it is falling i.e. more and more area is noticing temperatures which are moving close to the temperature of HS. Consistent SUHI growth pattern has not been observed in Chandigarh study area compared to Ahmedabad and Jaipur because of the existence of lower SUHI intensity over the area compared to those cities. Clear SUHI growth has been observed up to 3^{o} C isothermal lines for different seasons covering urban and semi urban regions of the city indicating that the area where LST is up to 3^{o} C less than the LST of HS has increased during last decade.

Transit of satellites over different places is at different times and therefore the remote sensing data is available with different time of observation. Application of the remote sensing data for SUHI studies has been analyzed using Aqua-Terra MODIS data in order to study the importance of time of observation. The pass of Aqua and Terra satellites over the study cities has a lag of about 3 hours. Day and night LST images area available corresponding to both the satellites which have MODIS sensor onboard. Contrast diurnal LST variations have been observed during different time intervals by analyzing Aqua and Terra LST data. During day time, LST images show significantly higher temperature variations in the different parts of the study areas as compared to night time images. However, the LST profile over these cities, during night time, is different than that observed during day time. Inverse or negative SUHI effect has been observed over these cities during day time, whereas clear SUHI effect is observed during night time. The interaction of barren land with solar radiation during daytime results in the high surface temperature of the bare soil. Hence, when the day time images are used to determine the LST, this behavior of soil surface show the temperature of the surface which is highly dependent on the solar radiation. The effect of higher temperature of the bare soil is more pronounced in summer season as compared to the winter season as the temperature during the winter season is lower than during summer season and the effect of differential cooling rate is also not high. However, when the night time images are used for

determining the LST inverse behaviour of that observed from day time images is observed for Jaipur and Ahmedabad study areas. Thermal characteristics of various land surfaces during solar peak time may also affect alterations in LSTs in different areas. Hence the thermal behavior of various land use/ land covers may seriously influence the variations in surface temperatures.

Regression analysis of all the images (two day-time and two night-time) has been carried out for Jaipur and Ahmedabad cities. Good correlation, with R^2 value above 0.90, is observed between most of the night images (Aqua night and Terra night). The corresponding R^2 values for day images of the two satellites are comparatively lower (ranges from 0 to 0.82), whereas the coefficient of correlation is very low for day and night images (ranges from 0 to 0.59). In order to understand the reason for this varying behavior, study has been extended to Ludhiana city of India. This city shows similar SUHI effects during both the day and night times. The vegetation density in and around Ludhiana city is higher compared to Ahmedabad and Jaipur cities. Correspondingly higher NDVI values are observed in the Ludhiana non-urbanized areas as compared to Ahmedabad and Jaipur rural areas. R^2 analysis for three cities signifies good correlation between night-night LSTs and reasonable correlation between day to day LSTs. Lesser vegetation density and higher barren soil proportion in rural areas result in higher LSTs especially during day time because soil shows higher thermal profile than other surface materials due to its low thermal inertia. The R^2 values for day-night LSTs for Jaipur and Ahmedabad cities are almost negligible as day and night LST of rural area is highly variable. But in the case of Ludhiana corresponding R^2 values for day-night LST relationships are higher because of higher vegetation density in rural areas. The subtropical climate of the city provides favorable conditions to grow vegetation in the rural areas hence less barren land is available to heat up. LST variations are observed to be more uniform during night time as compared to day time from Aqua-Terra data analysis. The analysis indicates that night time images can be used for the analysis of SUHI effect over any area. If a city has good vegetation cover, then the day/night LST pattern does not vary by a large extent. However, when the city has low/moderate vegetation cover and has large areas of barren land/soil cover, the day images may show different pattern as compared to the night images. The pattern during different times of the day is also highly variable owing to the interactions in the presence of solar radiation. But the pattern during night time is more or less similar thereby making the night time

images best suited for analysis of UHI effects. This indicates that the time of observation of satellite images is very important when these images are to be used for carrying out studies on SUHI effect.

In-situ temperature measurements have also been carried out to investigate the thermal behaviour of different surfaces during different periods of a day. In-situ temperature monitoring has been conducted at 7 points spread within the study area (3 inside the urban boundary and 4 outside the urban boundary but inside study area boundary) of Jaipur city, in order to study the thermal pattern of various surfaces at these locations as well as to compare the SUHI and AUHI effects. AUHI and SUHI intensity has been calculated at the time of satellite pass (10.30 AM and 10.30 PM). UHI intensity has been calculated with respect to the location of observation of minimum air temperature at 10:30 PM. Positive AUHI intensity has been observed at most of the locations irrespective of time periods. Negative SUHI intensity has been observed at most of the locations during day period, whereas positive SUHI intensity has been observed during night. Direct relationship has been observed between AUHI and SUHI during night, whereas inverse relationship has been observed between AUHI and SUHI during day. i.e. AUHI has been observed during both day and night period. **The study shows that use of day time images for SUHI analysis depends on the surface cover and it may show a different effect which may not be similar to AUHI.**

All three seasons show similar observations of AUHI and SUHI effect for both day and night period. SUHI is more apparent at night, i.e. SUHI has been considered as a nocturnal phenomenon and not prominent during day period. AUHI has been observed during both day and night. Clear existence of AUHI and non-existence of SUHI has been observed over the study area during day period through the field survey analysis, whereas clear existence of both AUHI and SUHI has been observed during the night. Significant diurnal AUHI effect has been observed over the study area which depicts that urban area is warmer compared to rural area. Inverse or negative SUHI effect has been observed over some cities due to the variations in thermal behavior of various land surfaces. **In general, SUHI is not apparent at daytime. Daytime LST data have been used in many SUHI studies. SUHI varies during the day and it is more significant during the evening/night.**

The in-situ temperature study observes that soil gets heated quickly in the presence of

solar radiation and it also cool down quickly when solar radiation is low or it is absent. The temperature of soil is even higher than the temperature of road surface/concrete surface during peak sunshine hours of summer season. The higher temperature of soil as compared to other materials is observed up to about 3:00 PM and then the temperature starts falling. The rate of cooling of soil is maximum as compared to other materials. The field study also exhibits that vegetation remains cooler throughout the day when compared with other materials and the total change in temperature of vegetation over a period of 24 hours is significantly lower than the corresponding change in temperature of other surface materials. The diurnal temperature change of road and concrete surfaces is quite similar and there are minor variations in this behaviour with road or concrete surface registering slightly higher temperature depending on season. The temperature of different land covers has been observed in the order, soil> road> concrete> vegetation during day time of summer season. The corresponding order during night time has been observed as road and concrete > soil > vegetation during summer season. During monsoon and winter seasons this order modifies to concrete > road > soil > vegetation during daytime and road> concrete > soil > vegetation during nighttime.

The nonexistence of any significant SUHI effect in Ahmedabad and Jaipur is due to the fact that these cities have a hot semi-arid climate which does not favour vegetation cover due to lack of water and there are large plots of open land. When sunlight falls over this land predominantly having soil cover, the soil quickly heats up thereby making rural areas warm. Since the remote sensing data, for the study cities, has been captured during noon when the soil has an apparent higher temperature than the concrete/road surface, no UHI effect is observed during the daytime. However the nighttime images show a clear SUHI effect as the temperature of soil is within the range of vegetation. The study shows that for the purpose of UHI studies using remote sensing data, the time of observation is very important and solar radiation play an important role in modifying the heat island over a city which can be best studied in the absence of solar radiation i.e. during night time.

Diurnal LST relationship with various land surface parameters representing vegetation (NDVI), urbanization (%ISA, RD, NDBI), soil (NDBaI), water (MNDWI) and terrain (DEM), etc. has also been investigated in the present research. Various land surfaces play a significant role in the diurnal variations of LSTs. There is direct relationship between

LST and NDBI whereas inverse relationship exists between LST and NDVI. However, both these relationships are not similar during day and night time and the nighttime relationship is better than the corresponding relationship during daytime. LST has been found to have a positive relationship with NDBaI during daytime whereas it has inverse relationship with NDBaI during nighttime. On the other hand the relationship of LST with MNDWI, %ISA, RD and elevation is inverse during day and positive during night. The relationship of LST with different parameters undergoes both diurnal and seasonal variations. As can be seen from the results, though the coefficient of correlation of the relationship of LST with different parameters is highly variable during different times and seasons and some parameters have better relationship with LST compared to others, yet there is no single parameter that can be used to completely express the variations in LST. Most of the previous studies have analyzed the LST variations as an effect of single parameter individually and have not considered the simultaneous effect of several parameters. It may, therefore, be important to determine the effect of a combination of these parameters on LST.

Overall analysis of the relationship of LST with all the different parameters indicates that a very complex relationship exists between them. Though NDVI, %ISA, NDBI, RD, NDBaI, MNDWI and elevation are independent parameters and uniquely affect the LST, but they are influenced, to some extent, by each other also. In the present study, a LTS model has been developed to predict LST, using LST values for 10 years. In order to use LST relationship with different parameters as well as to get the simultaneous effect of these parameters on LST, NDVI, %ISA, RD and elevation have been used as input parameters to the model that has been developed separately for Ahmedabad, Chandigarh and Jaipur study areas.

A comparison of observed and model predicted LST values shows that most part of the urban area has error within ±0.5 K. The LST data from MODIS has been used for the present study and quality flag available with this data has been used to include only good quality data for the analysis. The maximum error that has been limited by use of quality flag is ±2 K. As the error in prediction from the model is less than half of this value for most part of the study area and nowhere in the study area is the error beyond this value, it can be concluded that the model predicts the LST for SUHI studies very accurately. From the graphs and scatterplots also, it can be concluded that good correlation exists between

the model predicted and observed LST values, where R^2 values range from 0.84 to 0.97. MAE and MAPE of the model range from 0.23 K to 0.36 K and 0.08 % to 0.12 %, respectively.

The LST so predicated can be used for the study of UHI effect over any area as it encompasses different parameters that affect the LST directly. The model has good capability of accounting the variations in the LST at different locations of the study area. So the proposed LTS model can be used as an effective tool for the prediction of LST for the assessment of SUHI effect. Hence by using LTS model, LST can be predicted from previous year LST images with good accuracy and will be helpful to monitor SUHI effect and can be used as an effective tool for planned development of city in a scientific manner to contain the SUHI effect. LTS model can also be used as an effective tool to retrieve missing data due to presence of cloud cover or any other disturbances using small year interval LTS models. The predicted LST from this model can be used by city planners to propose mitigation strategies for reducing SUHI effect and control the various anthropogenic heat sources causing SUHI effect. Hence proposed LTS model can be used as an effective tool for scientific planning of upcoming urban areas. Such planning can help in reducing the LST at a predetermined level and hence contribute in lowering the overall energy demand. If there is a requirement to develop some area within or outside a city, it is possible to plan the development of the city in a scientific manner using the LTS model generated in the present study. For this purpose, some options of the proposed development may be prepared having desired road density, green areas, permissible ground coverage and parking lots etc. The LST over the proposed areas corresponding to different such options may be calculated using the model and the option resulting in lower LST can be opted for better thermal comfort. This model can also be used for many climatological studies where LST is widely used in a variety of fields including evapotranspiration, climate change, hydrology, vegetation monitoring, surface energy, urban climate and environmental studies.

The LTS model has been compared with ANN model to estimate the skill score factor of the LTS model (Forecasted) with reference to the ANN (Referred) model. Skill scores calculated for most of the periods show positive values which clearly depicts the efficacy of LTS model compared to ANN model for better LST prediction.

5.2 Major Contributions of the Present Study

The proposed research is a step towards increasing the understanding of the diurnal UHI variations and the factors responsible for it. The proposed research will help to identify the extent of spatio-temporal SUHI growth which is required for more efficient city planning. The proposed research will also help in providing a scientific tool to optimally plan the development of a city in such a manner that the effect of UHI is minimized. Major contributions of the study have been summarized as under

1. Diurnal and temporal variations in UHI effect over three Indian cities has been studied.
2. New criterion/methods based on UHI_{index} and transect have been proposed to estimate the spatio-temporal SUHI growth.
3. It has been shown that the three cities are experiencing significant spatio-temporal SUHI growth and hence it is necessary to take proper mitigation strategies in order to control the extent of SUHI.
4. The study proposes that there is no existence of SUHI effect during day period in the study cities and striking SUHI can be observed during night. i.e. SUHI is predominantly a nocturnal phenomenon. Urban heat island varies during the day, and it is more significant during the evening/night and there is an apparent UCI effect during daytime. AUHI has been observed during both day and night periods.
5. Time of observation of satellite data and thermal characteristics of various land surfaces influence the diurnal variations in LSTs. Also, vegetation and soil in rural areas have significant role in the diurnal variations in SUHI effect. The study shows that for the purpose of UHI studies using remote sensing data, the time of observation is very important and solar radiation play an important role in modifying the heat island over a city which can be best studied in the absence of solar radiation i.e. during night time.
6. Simultaneous diurnal effect of various land surface parameters on LST has been investigated and it has been observed that different parameters have significant role in diurnal LST variations.
7. LTS model has been developed in the present study for short term prediction of LST data. The proposed LTS model has good capability of accounting the variations in the LST at different locations of the study

areas. So the proposed LTS model can be used as an effective tool for the prediction of LST for the assessment of SUHI effect. Also, LTS and ANN have been compared to find out the efficiency of LTS model.

5.3 Further Scope of Future Research

- UHI_{index} has been used as the primary parameter for the analysis of UHI effect and to find out the hot spots of the study area. In similar way, thermal comfort index also has to be developed using spatial correlation analysis in order to find out the thermal comfort zones over the study area which would be beneficial for future urban planning applications.
- SUHI growth over the study areas has been investigated in the present study using UHI_{index} method and transect analysis based on the hot spots. The number/direction of transects can be decided on the basis of other parameters depending on the specifics of a particular city.
- Field survey has been conducted in the present study in order to assess the diurnal thermal variations of various land surfaces. Diurnal thermal behaviour of various land surfaces contradicts each other. Hence thermal characteristics (thermal conductivity, thermal inertia, etc.) of various surfaces has to be investigated to find out the reason behind the contrast thermal behaviour.
- Development of AUHI model from the relationship of LST with various parameters using night data would be useful for atmospheric heat island studies.
- Short term prediction and validation have been done in the present study using past data. Long term prediction of LST based on various parameters would be helpful for scientific planning to control UHI effect, during master plan preparation of a city.
- In the study, MODIS data has been used for the SUHI analysis. If urbanization is a longer issue for a particular area, use of AVHRR data (1980–present) may be beneficial for better understanding of UHI variations over these cities as a long term concern.

References

Abutaleb, K., Ngie, A., Darwish, A., Ahmed, M., Arafat, S., Ahmed F., 2015. Assessment of Urban Heat Island Using Remotely Sensed Imagery over Greater Cairo. Egypt, Advances in Remote Sensing. 4, 35-47.

Aghdaei, N., Kokogiannakis, G., Daly, D., McCarthy, T., 2017. Linear regression models for prediction of annual heating and cooling demand in representative Australian residential dwellings. Energy Procedia. 121, 79-86.

Akbari, H., 1995. Cooling our communities: An overview of Heat Island project activities. Annual Report, Heat Island Group, Lawrence Berkeley National Laboratory, Berkeley, Calif.

Akbari, H., Konopacki, S., 2005. Calculating energy-saving potentials of heat-island reduction strategies. Energy Policy. 33(6), 721–756.

Akbari, H., Pomerantz, M., Taha, H., 2001. Cool surfaces and shade trees to reduce energy use and improve air quality in urban areas. Solar Energy. 70(3), 295-310.

Akbari, H., Pomerantz, M., Taha, H., Rosenfeld, A., Romm, J., 1996. Policies to reduce heat islands: magnitudes of benefits and incentives to achieve them. Proceedings ACEEE Summer study on energy efficiency in buildings. 9, 177.

Ali, J.M., Marsh, S.H., Smith, M.J., 2016. A comparison between London and Baghdad surface urban heat islands and possible engineering mitigation solutions. Sustainable Cities and Society. 29, 159–168.

Alshaikh, A.Y., 2015. Space applications for drought assessment in Wadi-Dama (West Tabouk), KSA. The Egyptian Journal of Remote Sensing and Space Sciences. 18, 543–553.

Aniello, C., Morgan, K., Busbey, A., Newland, L., 1995. Mapping micro-urban heat islands using LANDSAT TM and a GIS. Computers and Geosciences. 21(8), 965-969.

Anniballe, R., Bonafoni, S., Pichierri, M., 2014. Spatial and temporal trends of the surface and air heat island over Milan using MODIS data. Remote Sensing of Environment. 150, 163–171.

Arnfield, A., 2003. Two decades of urban climate research: a review of turbulence, exchanges in turbulence and water, and the urban heat island. International of Journal of Climatology. 23, 1–26.

Ash, C., Jasny, B.R., Roberts, L., Stone, R., Sugden, A.M., 2008. Reimagining cities. Science. 319 (5864), 739.

Aşıkgil, B., Erar, A., 2013. Polynomial tapered two-stage least squares method in nonlinear regression. Applied Mathematics and Computation. 219(18), 9743–9754.

Asimakopoulos, D.A., Santamouris, M., Farrou, I., Laskari, M., Saliari, M., Zere-fos, S.C., Antonakaki, T., Giannakopoulos, C., 2012. Modelling the energy demand projection of the building sector in Greece in the 21th century. Energy and Buildings. 49, 488–498.

Bagirov, A.M., Mahmood, A., Barton, A., 2017. Prediction of monthly rainfall in Victoria, Australia: Cluster wise linear regression approach. Atmospheric Research. 188, 20–29.

Becker, F., Li, Z.-L., 1993. Surface temperature and emissivity at various scales: Definition, measurement and related problems. Remote Sensing of Reviews. 12, 225-253.

Boonjawat, J., Niitsu, K., Kubo, S., 2000. Urban heat island: thermal pollution and climate change in Bangkok. Journal of health science. 9, 49–55.

Borbora, J., Das, A.K., 2014. Summertime Urban Heat Island study for Guwahati City, India. Sustainable Cities and Society, 11, 61–66.

Borden, K.A., Cutter, S.L., 2008. Spatial patterns of natural hazards mortality in the United States, International Journal of Health Geographics. 7(64), 1-13.

Borhani, T.N.G., Afzali, A., Bagheri, M., 2016a. QSPR estimation of the auto-ignition temperature for pure hydrocarbons. Process Safety and Environmental Protection. 103 (Part A), 115–125.

Borhani, T.N.G., Saniedanesh, M., Bagheri, M., Lim, J.S., 2016b. QSPR prediction of the hydroxyl radical rate constant of water contaminants. Water Research. 98, 344–353.

Brunsell, N. A., 2006. Characterization of land-surface precipitation feedback regimes with remote sensing. Remote Sensing of Environment. 100, 200–211.

Buchin, O., Hoelscher, M.T., Meier, F., Nehls, T., Ziegler, F., 2016. Evaluation of the health-risk reduction potential of countermeasures to urban heat islands. Energy and Buildings. 114, 27-37.

Buscail, C., Upegui, E., Viel, J.F., 2012. Mapping heatwave health risk at the community level for public health action. International Journal of Health Geographics. 11, 38.

Buyantuyev, A., Wu, J., 2010. Urban heat islands and landscape heterogeneity: Linking spatiotemporal variations in surface temperatures to land-cover and socioeconomic patterns. Landscape Ecology. 25(1), 17–33.

Campbell, J. B., 2002. Introduction to Remote Sensing. (3rd ed.). New York: The Guilford Press.

Cao, X., Onishi, A., Chen, J., Imura, H., 2010. Quantifying the cool island intensity of urban parks using ASTER and IKONOS data. Landscape and Urban Planning. 96(4), 224–231.

Carnahan, W. H., Larson, R. C., 1990. An analysis of an urban heat sink. Remote Sensing of Environment. 33, 65 – 71.

Census of India (2011). Office of the Registrar General and Census Commissioner, Ministry of Home affairs, Government of India. Available at http://www.censusindia.gov.in

Chander, G., Markham, B., 2003. Revised Landsat-5 TM radiometric calibration procedures and post calibration dynamic ranges. IEEE Transactions on Geoscience and Remote Sensing. 41(11), 2674−2677.

Chang, C., Li, M., Chang, S., 2007. A preliminary study on the local cool island intensity of Taipei city parks. Landscape and Urban Planning. 80 (4), 386–395.

Changnon, S. A., Kunkel, K. E., Reinke B C., 1996. Impacts and responses to the 1995 heat wave: A call to action. Bulletin of the American Meteorological Society. 77, 1497–1505.

Changnon, S.A., 1992. Inadvertent weather modification in urban areas: Lessons for global climate change. Bulletin of the American Meteorological Society. 73, 619-627.

Charabi, Y., Bakhit, Abdelhamid, 2011. Assessment of the canopy urban heat island of a coastal arid tropical city: the case of Muscat, Oman. Atmospheric Research. 101, 215–227.

Chen, F., Yang, X., Zhu, W., 2014. WRF simulations of urban heat island under hot-weather synoptic conditions: The case study of Hangzhou City, China. Atmospheric Research. 138, 364–377.

Chen, X.-L., Zhao, H.-M., Li, P.-X., Yin, Z.-Y., 2006. Remote sensing image-based analysis of the relationship between urban heat island and land use/cover changes. Remote Sensing of Environment. 104(2), 133-146.

Chen, Z., Gong, C.-F., Wu, J., Yu, S.-X., 2012. The influence of socioeconomic and topographic factors on nocturnal urban heat islands: a case study in Shenzhen, China. International Journal of Remote Sensing. 33(12), 3834–3849.

Cheval, S., Dumitrescu, A., 2009. The July urban heat island of Bucharest as derived from modis images. Theoretical Applied Climatology. 96, 145–153.

Cheval, S., Dumitrescu, A., Petrişor, A.-I., 2011. The July surface temperature lapse in the Romanian Carpathians. Carpathian Journal of Earth and Environmental Sciences. 6(1), 189 – 198.

Chow, W.T.L., Roth, M., 2006. Temporal dynamics of the urban heat island of Singapore. International Journal of Climatology. 26, 2243–2260.

Chun, B., Guldmann, J.-M., 2014. Spatial statistical analysis and simulation of the urban heat island in high-density central cities. Landscape and Urban Planning. 125, 76–88.

Chung, U., Choi, J., Yun, J. I., 2004. Urbanization effect on the observed change in mean monthly temperatures between 1951–1980 and 1971–2000 in Korea. Climatic Change. 66, 127–136.

City Development Plan Chandigarh, Chandigarh administration, under Jawaharlal Nehru National Urban Renewal Mission (JNNURM), Ministry of Urban Development, Government of India. Available at http://mcchandigarh.gov.in/cdp.pdf

Civco, D.L., Hurd, J.D., Wilson, E.H., Arnold, C.L., Prisloe Jr., M.P., 2002. Quantifying and describing urbanizing landscapes in the northeast United States. Photogrammetric Engineering and Remote Sensing. 68 (10), 1083–1090.

Clinton N., Gong, P., 2013. MODIS detected surface urban heat islands and sinks: Global locations and controls. Remote Sensing of Environment. 134, 294–304.

Crutzen, P. J., 2004. New directions: The growing urban heat and pollution “island” effect—impact on chemistry and climate. Atmospheric Environment. 38, 3539–3540.

Cui, L.L., Shi, J., Gao, Z.Q., 2007. Urban heat island in Shanghai, China. Proceedings of the SPIE-The International Society for Optical Engineering.

Dash, P., Gottsche, F.M., Olesen, F.S., Fischer, H., 2002. Land Surface Temperature and Emissivity Estimation from Passive Sensor Data: Theory and Practice-Current Trends. International Journal of Remote Sensing. 23, 2563-2594.

Deng, C., Wu, C., 2013. Examining the impacts of urban biophysical compositions on surface urban heat island: A spectral unmixing and thermal mixing approach. Remote Sensing of Environment. 131, 262–274.

Dettinger, M.D., Cayan, D.R., Meyer, M.K., Jeton, A., 2004. Simulated hydrologic responses to climate variations and change in the Merced, Carson, and American river basins Sierra Nevada, California, 1900-2099. Climate Change. 62, 283-317.

Dousset, B., Gourmelon, F., 2003. Satellite multi-sensor data analysis of urban surface temperatures and land cover. ISPRS Journal of Photogrammetry and Remote Sensing. 58, 43–54.

Effat, H.A., Hassan, O.A.K., 2014. Change detection of urban heat islands and some related parameters using multi-temporal Landsat images; A case study of Cairo City, Egypt. Urban Climate. 10, 171-188.

El-Fouly, T.H.M., El-Saadany, E.F., Salama, M.M.A., 2008. One day ahead prediction of wind speed and direction. IEEE Transactions on Energy Conversion. 23 (1), 191-201.

Enete, I. C., Officha, M., Ogbonna, C. E., 2012. Urban heat island magnitude and discomfort in Enugu urban area, Nigeria. Journal of Environment and Earth Science. 2(7), 77–83.

EPA., 2003. Beating the heat: mitigating thermal impacts. Nonpoint Source News Notes. 72, 23-26.

Epperson, D. L., Davis, J. M., Bloomfield, P., Karl, T. R., McNab, A. L. Gallo, K. P., 1995. Estimating the urban bias of surface shelter temperatures using upper-air and satellite data. Part II. Estimation of the urban bias. Journal of Applied Meteorology. 34, 358–370.

Erell, E., Pearlmutter, D., Williamson, T. J., 2011. Urban microclimate: Designing the spaces between buildings. London, Washington, DC: Earthscan.

Estoque, R.C., Murayama, Y., 2017. Monitoring surface urban heat island formation in a tropical mountain city using Landsat data (1987–2015). ISPRS Journal of Photogrammetry and Remote Sensing. 133, 18–29.

Feng, D.Y., Min, L.Y., Ming, J.J., 2014. Statistical downscaling of FGOALSs2 projected precipitation in eastern China. Atmospheric and Oceanic Science Letters. 7 (5), 388-394.

Feng, J.-M., Wang, Y.-L., Ma, Z.-G., Liu, Y.-H., 2012. Simulating the regional impacts of urbanization and anthropogenic heat release on climate across China. Journal of Climate. 25(20), 7187–7203.

Figuerola, P.I., Mazzeo, N.A., 1998. Urban-rural temperature differences in Buenos Aires. International Journal of Climatology. 18(15), 1709-1723.

Frey, C.M., Rigo, G., Parlow, E., 2007. Urban radiation balance of two coastal cities in a hot and dry environment. International Journal of Remote Sensing. 28 (12), 2675–2712.

Friedl, M.A., 2002. Forward and inverse modeling of land surface energy balance using surface temperature measurements. Remote Sensing of Environment. 79 (2–3), 344–354.

Frumkin, H., 2002. Urban sprawl and public health. Public Health Reports. 117(3), 201–217.

Fujibe, F., 2011. Urban warming in Japanese cities and its relation to climate change monitoring. International Journal of Climatology. 31(2), 162–173.

Gallo, K. P., McNab, A. L., Karl, T. R., Brown, J. F., Hood, J. J., Tarpley, J. D., 1993. The use of NOAA AVHRR data for assessment of the urban heat-island effect. Journal of Applied Meteorology. 32(5), 899–908.

Gallo, K. P., Owen, T. W., 1999. Satellite-based adjustments for the urban heat island temperature bias. Journal of Applied Meteorology. 38(6), 806–813.

Gallo, K.P., Easterling, D.R., Peterson, T.C., 1996. The influence of land use/land cover on climatological values of the diurnal temperature range. Journal of Climate. 9, 2941-2944.

Gallo, K.P., Owen, T.W., 1998. Assessment of urban heat Islands: a multi-sensor perspective for the Dallas-Ft. worth, USA region. Geocarto International. 13 (4), 35–41.

Gallo, K.P., Tarpley, J.D., 1996. The comparison of vegetation index and surface temperature composites of urban heat-island analysis. International Journal of Remote Sensing. 17, 3071-3076.

Ganbat, G., Han, Ji-Young, Ryu, Young-Hee, Baik, Jong-Jin, 2013. Characteristics of the urban heat island in a high-altitude metropolitan city, Ulaanbaatar, Mongolia. Asia-Pacific Journal of the Atmospheric Sciences. 49 (4), 535–541.

Gao, B.C., 1996. NDWI–A normalized difference water index for remote sensing of vegetation liquid water from space. Remote Sensing of Environment. 58(3), 257–266.

Giannaros, T.M., Melas, D., Daglis, I.A., Keramitsoglou, I., Kourtidis, K., 2013. Numerical study of the urban heat island over Athens (Greece) with the WRF model. Atmospheric Environment. 73, 103-111.

Gillies, R., Kustas, W., Humes, K., 1997. A verification of the 'triangle' method for obtaining surface soil water content and energy fluxes from remote measurements of the Normalized Difference Vegetation Index (NDVI) and surface. International Journal of Remote Sensing. 18(15), 3145–3166.

Giridharan, R., Lau, S.S.Y., Ganesan, S., 2005. Nocturnal heat island effect in urban residential developments of Hong Kong. Energy and Buildings. 37, 964–971.

Gobakis, K., Kolokotsa, D., Synnefa, A., Saliari, M., Giannopoulou K., Santamouris M., 2011. Development of a model for urban heat island prediction using neural network techniques. Sustainable Cities and Society. 1, 104– 115.

Golden, J. S., Kaloush, K. E., 2006. Mesoscale and microscale evaluation of surface pavement impacts on the urban heat island effects. International Journal of Pavement Engineering. 7(1), 37–52.

Gong, P., Liang, S., Carlton, E. J., Jiang, Q., Wu, J., Wang, L., Remais, J. V, 2012. Urbanisation and health in China. The Lancet. 379(9818), 843–852.

Green, A. A., Berman, M., Switzer, P., Craig, M. D., 1988. A transformation for ordering multispectral data in terms of image quality with implications for noise removal. IEEE Transactions on Geoscience and Remote Sensing. 26, 65-74.

Gunay, A., 2007. Application of nonlinear regression analysis for ammonium exchange by natural (Bigadiç) clinoptilolite. Journal of Hazardous Materials. 148(3), 708–713.

Guo, G., Wu, Z., Xiao, R., Chen, Y., Liu, X., Zhang, X., 2015. Impacts of urban biophysical composition on land surface temperature in urban heat island clusters. Landscape and Urban Planning. 135, 1–10.

Hafner, J., Kidder, S.Q., 1999. Urban heat island modeling in conjunction with satellite-derived surface / soil parameters. Journal of Applied Meteorology. 38, 448–465.

Harlan, S.L., Brazel, A.J., Prashad, L., Stefanov, W.L., Larsen, L., 2006. Neighborhood microclimates and vulnerability to heat stress Social Science & Medicine. 63 (11), 2847–2863.

Hart, M., Sailor, D., 2009. Quantifying the influence of land-use and surface characteristics on spatial variability in the urban heat island. Theoretical and Applied Climatology. 95(3–4), 397–406.

Hassid, S., Santamouris, M., Papanikolau, N., Linardi, A., Klitsikas, N., Geor-gakis, C., Assimakopoulos, D.N., 2000. Effect of the Athens heat island on air conditioning load. Energy and Buildings. 32 (2), 131–141.

Hathway, E., Sharples, S., 2012. The interaction of rivers and urban form in mitigating the Urban Heat Island effect: A UK case study. Building and Environment. 58, 14–22.

Hirano, Y., Fujita, T., 2012. Evaluation of the impact of the urban heat island on residential and commercial energy consumption in Tokyo. Energy. 37 (1) 371–383.

Holme, A. McR., Burnside, D. G., Mitchell, A. A., 1987. The development of a system for monitoring trend in range condition in the arid shrub lands of Western Australia. Australian Rangeland Journal. 9, 14-20.

http://en.wikipedia.org/wiki/K%C3%B6ppen climate classification

http://www.fluke.com/fluke/inen/electrical-testers/thermometers/fluke59. htm?pid=56093

http://www.imdpune.gov.in/Temp_Extremes/histext2010.pdf

https://lpdaac.usgs.gov/dataset_discovery/modis, LP DAAC, USGS Website.

https://lpdaac.usgs.gov/dataset_discovery/modis/modis_products_table/myd13q1. LP DAAC, USGS website.

https://lpdaac.usgs.gov/dataset_discovery/modis/modis_products_table/myd11a2, LP DAAC, USGS website.

Hu, L., Nathaniel, A., Brunsell, 2013. The impact of temporal aggregation of land surface temperature data for surface urban heat island (SUHI) monitoring. Remote Sensing of Environment. 134, 162–174.

Hulme, M., Zhao, Z.-C., Jiang, T., 1994. Recent and future climate change in East Asia. International Journal of Climatology. 14, 637–658.

Hung, T., Uchihama, D., Ochi, S., Yasuoka, Y., 2006. Assessment with satellite data of the urban heat island effects in Asian mega cities. International Journal of Applied Earth Observation and Geoinformation. 8 (1), 34–48.

Ibrahim, G.R.F., 2017. Urban Land Use Land Cover Changes and Their Effect on Land Surface Temperature: Case Study Using Dohuk City in the Kurdistan Region of Iraq. Climate. 5, 13, 1-18.

Ichinose, T., Shimodozono, K., Hanaki, K., 1999. Impact of anthropogenic heat on urban climate in Tokyo. Atmospheric Environment. 33(24-25), 3897–3909.

Ihara, T., Kusaka, H., Hara, M., Matsuhashi, R., Yoshida, Y., 2011. Estimation of mild health disorder caused by urban air temperature increase with midpoint-type impact assessment methodology. Journal of Environmental Engineering. 76, 459–467.

Imhoff, M. L., Zhang, P., Wolfe, R. E., Bounoua, L., 2010. Remote sensing of the urban heat island effect across biomes in the continental USA. Remote Sensing of Environment. 114 (3), 504–513.

IPCC. (2007).In Solomon, S., Qin, D., Manning, M., Chen, Z., Marquis, M., Averyt, K.B., Tignor, M., Miller, H.L. (Eds.), Climate change 2007: The physical science bases. Contribution of working group I to the fourth assessment report of the intergovernmental panel on climate change. Cambridge, UK, and New York, USA: Cambridge University Press.

Jasinski, M.F., 1990. Sensitivity of the Normalized Difference Vegetation Index to subpixel canopy cover, soil albedo, and pixel scale. Remote Sensing of Environment. 32, 169–187.

Jauregui, E., 1997. Heat island development in Mexico city. Atmospheric Environment. 31, 3821–3831.

Jin, M., Dickinson, R. E., Zhang, D.-L., 2005. The footprint of urban areas on global climate as characterized by MODIS. Journal of Climate. 18, 1551-1565.

Johnson, D. P., Stanforth, A., Lulla, V., Luber, G., 2012. Developing an applied extreme heat vulnerability index utilizing socioeconomic and environmental data. Applied Geography. 35(1), 23-31.

Jonsson, P., 2004. Vegetation as an urban climate control in the subtropical city of Gaborone, Botswana. International Journal of Climatology. 24, 1307–1322.

Jusuf, S. K., Wong, N. H., Hagen, E., Anggoro, R., Hong, Y., 2007. The influence of land use on the urban heat island in Singapore. Habitat International. 31(2), 232-242.

Kareiva, P., Wennergren, U., 1995. Connecting landscape patterns to ecosystem and population processes. Nature. 373(6512), 299–302.

Karl, T., Diaz, H. F., Kulka, G., 1988. Urbanization: Its detection and effect in the United States climate record. Journal of Climate. 1, 1099–1123.

Kaya, S., Basar, U.G., Karaca, M., Seker, D.Z., 2012. Assessment of Urban Heat Islands Using Remotely Sensed Data. Ekoloji. 21, 84, 107-113.

Khandelwal, S., (2012). Analysis of spatial and seasonal variations of surface temperatures of Jaipur city and its relationship with various parameters. Ph.D. thesis submitted to Malaviya National Institute of Technology Jaipur.

Khandelwal, S., Goyal, R., Kaul, N., Mathew, A., 2017. Assessment of land surface temperature variation due to change in elevation of area surrounding Jaipur, India. The Egyptian Journal of Remote Sensing and Space Sciences. http://dx.doi.org/10.1016/j.ejrs.2017.01.005

Kikon, N., Singh, P., Singh, S.K., Vyas, A., 2016. Assessment of urban heat islands (UHI) of Noida City, India using multi-temporal satellite data. Sustainable Cities and Society. 22, 19–28.

Kim Y, Baik J, 2005. Spatial and temporal structure of the urban heat island in Seoul. Journal of Applied Meteorology. 44, 591–605.

Kleerekoper, L., Esch, M. V, Salcedo, T. B., 2012. How to make a city climate-proof, addressing the urban heat island effect. Resources, Conservation and Recycling. 64, 30–38.

Klok, L., Zwart, S., Verhagen, H., Mauri, E., 2012. The surface heat island of Rotterdam and its relationship with urban surface characteristics, Resources, Conservation and Recycling. 64, 23– 29.

Kolokotroni, M., Davies, M., Croxford, B., Bhuiyan, S., Mavrogianni, A., 2010. A validated methodology for the prediction of heating and cooling energy demand for buildings within the Urban Heat Island: Case-study of London. Solar Energy. 84, 2246–2255.

Kolokotroni, M., Giridharan, R., 2008. Urban heat island intensity in London: an investigation of the impact of physical characteristics on changes in outdoor air temperature during summer. Solar Energy. 82 (11), 986–998.

Kolokotroni, M., Ren, X., Davies, M., Mavrogianni, A., 2011. London's urban heat island: Impact on current and future energy consumption in office buildings. Energy and Buildings. 47, 302–311.

Kong, F., Yin, H., James, P., Hutyra, L.R., He, H.S., 2014. Effects of spatial pattern of greenspace on urban cooling in a large metropolitan area of eastern China. Landscape and Urban Planning. 128, 35–47.

Konopacki, S., Akbari H., 2002. Energy savings for heat island reduction strategies in Chicago and Houston (including updates for Baton Rouge, Sacramento, and Salt Lake City). Draft Final Report, LBNL-49638, University of California, Berkeley.

Kourtidis, K., Georgoulias, A.K., Rapsomanikis, S., Amiridis, V., Keramitsoglouc, I., Hooyberghs H, Maiheu, B., Melas, D., 2015. A study of the hourly variability of the urban heat island effect in the Greater Athens Area during summer. Science of the Total Environment. 517, 162–177.

Kovats, R.S., Hajat, S., 2008. Heat stress and public health: a critical review. Annual Review of Public Health. 29, 41-55.

Kukla, G., Gavin, J., Karl, T.R., 1986. Urban Warming. Journal of climate and applied meteorology. 25, 1265-1270.

Kumar, K.S., Bhaskar, P.U., K Padmakumari, K., 2012. Estimation of land surface temperature to study urban heat island effect using Landsat ETM+ image. International Journal of Engineering Science and Technology. 4, 771-778.

Kumar, K.S., Kumari, K.P., Bhaskar P.U., 2013. Artificial Neural Network Model for Prediction of Land Surface Temperature from Land Use/Cover Images. International Journal of Advanced Trends in Computer Science and Engineering. 2(1), 87-92.

Lafortezza, R., Carrus, G., Sanesi, G., Davies, C., 2009. Benefits and well-being perceived by people visiting green spaces in periods of heat stress. Urban Forestry & Urban Greening. 8 (2), 97–108.

Landsberg, H.E., 1981. The Urban Climate (New York: Academic Press).

Larson, R. C., Carnahan, W. H., 1997. The influence of surface characteristics on urban radiant temperatures. Geocarto International. 12, 5 – 16.

Lazzarini, M., Marpu, P.R., Ghedira, H., 2012. Temperature-land cover interactions: The inversion of urban heat island phenomenon in desert city areas. Remote Sensing of Environment. 130, 136–152.

Lee, D. O., 1991. Urban-rural humidity differences in London. International Journal of Climatology. 11(5), 577–582.

Lee, Y.Y., Kim, J.T., Yun, G.Y., 2016. The neural network predictive model for heat island intensity in Seoul. Energy and Buildings. 110, 353–361.

Leroyer, S., Bélair, S., Mailhot, J., Strachan, I. B., 2011. Microscale numerical prediction over Montreal with the Canadian external urban modeling system. Journal of Applied Meteorology and Climatology. 50(12), 2410–2428.

Li, J., Song, C., Cao, L., Zhu, F., Meng, X., Wu, J., 2011. Impacts of landscape structure on surface urban heat islands: A case study of Shanghai, China. Remote Sensing of Environment. 115(12), 3249–3263.

Li, X., Zhou, W., Ouyang, Z., 2013. Relationship between land surface temperature and spatial pattern of greenspace: What are the effects of spatial resolution? Landscape and Urban Planning. 114, 1– 8.

Li, Y., Zhang, H., Kainz, W., 2012. Monitoring patterns of urban heat islands of the fast-growing Shanghai metropolis, China: Using time-series of Landsat TM/ETM+ data. International Journal of Applied Earth Observation and Geoinformation. 19, 127–138.

Liang, B.Q., Weng, Q.H., 2011. Assessing urban environmental quality change of Indianapolis (1998) United States, by the remote sensing and GIS integration. IEEE Journal of Selected Topics in Applied Earth Observations and Remote Sensing. 4 (1), 43–55.

Liu, H., Weng, Q., 2008. Seasonal variations in the relationship between land-scape pattern and land surface temperature in Indianapolis, USA. Environmental Monitoring and Assessment. 144(1–3), 199–219.

Liu, L., Zhang, Y., 2011. Urban heat island analysis using the Landsat TM data and ASTER data: A case study in Hong Kong. Remote Sensing. 3, 1535-1552.

Liu, W., Ji, C., Zhong, J., Jiang, X., Zheng, Z., 2007. Temporal characteristics of the Beijing urban heat island. Theoretical Applied Climatology. 87, 213–221.

Livada, I., Santamouris, M., Niachou, K., Papanikolaou, N., Mihalakakou, G., 2002. Determination of places in the great Athens area where the heat island effect is observed. Theoretical Applied Climatology. 71, 219–230.

Lo, C. P., Quattrochi, D. A., 2003. Land-use and land-cover change, urban heat island phenomenon, and health implications: a remote sensing approach. Photogrammetric Engineering & Remote Sensing. 69, 1053-1063.

Lo, C. P., Quattrochi, D. A., Luvall, J. C., 1997. Application of high-resolution thermal infrared remote sensing and GIS to assess the urban heat island effect. International Journal of Remote Sensing. 18(2), 287-304.

Lokoshchenko, M.A., 2014. Urban 'heat island' in Moscow. Urban Climate. 10, 550–562.

Mackey, C.W., Lee, X., Smith, R.B., 2012. Remotely sensing the cooling effects of city scale efforts to reduce urban heat island. Building and Environment. 49, 348-358.

Marrapu, P., 2012. Local and regional interactions between air quality and climate in New Delhi: A sector based analysis. University of Iowa.

Md Din, M. F., Lee, Y. Y., Ponraj, M., Ossen, D. R., Iwao, K., Chelliapan, S., 2014.Thermal comfort of various building layouts with a proposed discomfort index range for tropical climate. Journal of Thermal Biology. 41, 6–15.

Memon, R.A., Leung, D.Y.C., Liu, C.H., 2009. An investigation of urban heat island intensity (UHII) as an indicator of urban heating. Atmospheric Research. 94, 491–500.

Miao, S., Chen, F., LeMone, M. A., Tewari, M., Li, Q., Wang, Y., 2009. An observational and modeling study of characteristics of urban heat island and boundary layer structures in Beijing. Journal of Applied Meteorology and Climatology. 48(3), 484–501.

Mihalakakou, P., Santamouris, M., Papanikolaou, N., Cartalis, C., Tsangrassoulis, A., 2004. Simulation of the urban heat island phenomenon in Mediterranean climates. Journal of pure and applied geophysics. 161, 429–451.

Mirzaei, P.A., Haghighat, F., 2010. A novel approach to enhance outdoor air quality: pedestrian ventilation system. Building and Environment. 45, 1582-93.

Mohan, M., Yukihiro, Kikegawa, Gurjar, B.R., Bhati, Shweta, Kandya, Anurag, Ogawa, Koichi, 2012. Urban heat island assessment for a tropical urban Air shed in India. Atmospheric and Climate Sciences. 2, 127–138.

Montavez, J. P., Rodriguez, A., Jimenez, J. I., 2000. A study of the Urban Heat Island of Granada. International Journal of Climatology. 20(8), 899–911.

Mushore, T. D., Odindi, J., Dube, T., Mutanga, O., 2017. Prediction of future urban surface temperatures using medium resolution satellite data in Harare metropolitan city, Zimbabwe. Building and Environment. 122, 397-410.

NASA, Landsat 7 Science Data Users Handbook, https://landsat.gsfc.nasa.gov/wp-content/uploads/2016/08/Landsat7_Handbook.pdf

NASA, Landsat 8 Science Data Users Handbook, https://landsat.usgs.gov/documents/Landsat8DataUsersHandbook.pdf

Nassar, A.K., Blackburn, G.A., Whyatt, J. D., 2016. Dynamics and controls of urban heat sink and island phenomena in a desert city: Development of a local climate zone scheme using remotely-sensed inputs. International Journal of Applied Earth Observation and Geoinformation. 51, 76–90.

Nichol, J., Wong, M.S., 2005. Modeling urban environmental quality in a tropical city. Landscape and Urban Planning. 73 (1), 49–58.

O'Malley, C., Piroozfar, P., Farr, E.R.P., Pomponi, F., 2015. Urban Heat Island (UHI) mitigating strategies: A case-based comparative analysis. Sustainable Cities and Society. 19, 222–235.

Offerle, B., Grimmond, C. S. B., Fortuniak, K., 2005. Heat storage and anthropogenic heat flux in relation to the energy balance of a central European city centre. International Journal of Climatology. 25(10), 1405–1419.

Ogashawara, I., Bastos, V.D.S.B., 2012. A Quantitative Approach for Analyzing the Relationship between Urban Heat Islands and Land Cover. Remote Sensing. 4, 3596-3618.

Oke, T. R., 1981. Canyon geometry and the nocturnal urban heat island: Comparison of scale model and field observations. International Journal of Climatology. 1(3), 237–254.

Oke, T.R., 1973. City size and the urban heat island. Atmospheric Environment. 7 (8), 769–779.

Oke, T.R., 1982. The energetic basis of the urban heat island. Quarterly Journal of the Royal Meteorological Society. 108 (445), 1–24.

Oke, T.R., 1987. Boundary Layer Climates. Methuen, London, New York.

Oleson, K. W., Bonan, G. B., Feddema, J., Vertenstein, M., 2008. An urban parameterization for a global climate model. Part II: Sensitivity to input parameters and the simulated urban heat island in offline simulations. Journal of Applied Meteorology and Climatology. 47(4), 1061–1076.

Oleson, K.W., Bonan, G. B., Feddema, J., Jackson, T., 2010. An examination of urban heat island characteristics in a global climate model. International Journal of Climatology. 31(12), 1848–1865.

Owen, T., 1998. Using DMSP-OLS light frequency data to categorize urban environments associated with US climate observing stations. International Journal of Remote Sensing. 19(17), 3451–3456.

Owen, T.W., Carlson, T.N., Gillies, R.R., 1998. An assessment of satellite remotely-sensed land cover parameters in quantitatively describing the climatic effect of urbanization. International Journal of Remote Sensing. 19, 1663-1681.

Pal, S., Ziaul, S., 2016. Detection of land use and land cover change and land surface temperature in English Bazar urban centre. Egyptian Journal of Remote Sensing and Space Sciences. 20, 125-145.

Pandey, P., Kumar, D., Prakash, A., Masih, J., Singh, M., Kumar, S., Jain, V.K., Kumar, K., 2012. A study of urban heat island and its association with particulate matter during winter months over Delhi. Science of the Total Environment. 414, 494–507.

Pantavou, A., Theoharatos, G., Mavrakis, A., Santamouris, M., 2011. Evaluating thermal comfort conditions and health responses during an extremely hot summer in Athens. Building and Environment. 2 (46), 339–344.

Parida, B. R., Oinam, B., Patel, N.R., Sharma, N., Kandwal, R., Hazarika, M. K., 2008. Land surface temperature variation in relation to vegetation type using MODIS satellite data in Gujarat state of India. International Journal of Remote Sensing. 29(14), 4219-4235.

Patz, J.A., Campbell-Lendrum, D., Holloway, T., Foley, J.A., 2005. Impact of regional climate change on human health. Nature. 438, 310-317.

Pisello, A.L., Castaldo, V.L., Pignatta, G., Cotana, F., Santamouris, M., 2015. Experimental in-lab and in-field analysis of waterproof membranes for cool roof application and urban heat island mitigation. Energy and Buildings. 114, 180-190.

Pongracz, R., Bartholy, J., Dezso, Z., 2006. Remotely sensed thermal information applied to urban climate analysis. Advances in Space Research. 37 (12), 2191–2196.

Pongrácz, R., Bartholy, J., Dezso, Z., 2010. Application of remotely sensed thermal information to urban climatology of Central European cities. Physics and Chemistry of the Earth. 35, 95-99.

Poumadère, M., Mays, C., Mer, S. L., Blong, R., 2005. The 2003 Heat Wave in France: Dangerous Climate Change Here and Now. Risk analysis. 25, 1483–1494.

Price, J. C. (1990). Using spatial context in satellite data to infer regional scale evapotranspiration. I.E.E.E. Transactions on Geoscience and Remote Sensing, 28, 940−948.

Pu, R., Gong, P., Michishita, R., Sasagawa, T., 2006. Assessment of multi-resolution and multi-sensor data for urban surface temperature retrieval. Remote Sensing of Environment. 104, 211-225.

Purevdorj, T.S., Tateishi, R., Ishiyama, T., Honda, Y., 1998. Relationships between percent vegetation cover and vegetation indices. International Journal of Remote Sensing 19, 3519-3535.

Qiao, Z., Tian, G., Xiao, L., 2013. Diurnal and seasonal impacts of urbanization on the urban thermal environment: A case study of Beijing using MODIS data. ISPRS Journal of Photogrammetry and Remote Sensing. 85, 93–101.

Qin, Z., Karnieli, A., 1993. Progress in remote sensing of land surface temperature and ground emissivity using NOAA-AVHRR data. International Journal of Remote Sensing. 20, 2367-2393.

Qin, Z., Karnieli, A., 1999. Progress in the remote sensing of land surface temperature and ground emissivity using NOAA-AVHRR data. International Journal of Remote Sensing. 20, 2367-2393.

Quattrochi, D.A., Luvall, J.C., 1999. Thermal infrared remote sensing for analysis of landscape ecological processes: methods and applications. Landscape Ecology. 14, 577–598.

Quattrochi, D. A., Ridd, M. K., 1998. Analysis of vegetation within a semi-arid urban environment using high spatial resolution airborne thermal infrared remote sensing data. Atmospheric Environment. 32, 19 – 33.

Rajagopalan, P., Lim, K.C., Jamei, E., 2014. Urban heat island and wind flow characteristics of a tropical city. Solar Energy. 107, 159–170.

Ramamurthy, P., Sangobanwo, M., 2016. Inter-annual variability in urban heat island intensity over 10 major cities in the United States. Sustainable Cities and Society. 26, 65-75.

Rao, P.K., 1972. Remote sensing of urban ‘‘heat islands’’ from an environmental satellite. Bulletin of the American Meteorological Society. 53, 647–648.

Rasul, A., Balzter, H., Smith, C., 2015. Spatial variation of the daytime Surface Urban Cool Island during the dry season in Erbil, Iraqi Kurdistan, from Landsat 8. Urban Climate. 14, 176–186.

Ripley, E.A., Archibold, O.W., Bretell, D.L., 1996. Temporal and spatial temperature patterns in Saskatoon. Weather. 51, 398–405.

Rizwan, A.M., Dennis, Y.C., Liu, C., 2008. A review on the generation, determination and mitigation of Urban Heat Island. Journal of Environmental Sciences. 20 (1), 120–128.

Rosenfeld, A.H., Akbari, H., Romm, J.J., Pomerantz, M., 1998. Cool communities: Strategies for heat island mitigation and smog reduction. Energy and Buildings. 28(1), 51–62.

Rotem-Mindali, O., Michael, Y., Helman, D., Lensky, I.M., 2015. The role of local land-use on the urban heat island effect of Tel Aviv as assessed from satellite remote sensing. Applied Geography. 56, 145-153.

Roth, M., Oke, T.R., Emery, W.J., 1989. Satellite-derived urban heat islands from three coastal cities and the utilization of such data in urban climatology. International Journal of Remote Sensing. 10, 1699–1720.

Rouse, J.W., Haas, R.H., Schell, J.A., Deering, D.W., 1974. Monitoring vegetation systems in the Great Plains with ERTS, In: S.C. Freden, E.P. Mercanti, and M. Becker (eds) Third Earth Resources Technology Satellite–1 Symposium. Volume I: Technical Presentations, NASA SP-351, NASA, Washington, D.C., pp. 309-317.

Runnals, K.E., Oke, T.R., 2000. Dynamics and Control of the Near-Surface Heat Island of Vancouver, British Columbia. Physical Geography. 21, 283-304.

Rydin, Y., Bleahu, A., Davies, M., Dávila, J. D., Friel, S., Grandis, G.D, et al., 2012. Shaping cities for health: Complexity and the planning of urban environments in the 21st century. Lancet. 379 (9831), 2079-2108.

Saengsawang, S., Pankhao, P., Kaprom, C., Sriwongsitanon, N., 2017. Projections of future rainfall for the upper Ping River Basin using regression-based downscaling. Advances in Climate Change Research. 8 (4), 256-267.

Şahin M., 2012. Modelling of air temperature using remote sensing and artificial neural network in Turkey. Advances in Space Research. 50, 973–85.

Sailor, D. J., Fan, H., 2002. Modeling the diurnal variability of effective albedo for cities. Atmospheric Environment. 36(4), 713–725.

Saito, I., Ishihara, O., Katayama, T., 1990/91. Study of the effect of green area on the thermal environment in an urban area. Energy and Buildings. 15/16, 493–498.

Sakka, A., Santamouris, M., Livada, I., Nicol, F., Wilson, M., 2012. On the thermal performance of low income housing during heat waves. Energy and Buildings. 49, 69–77.

Sandholt, I., Rasmussen, K., Andersen, J., 2002. A simple interpretation of the surface temperature/vegetation index space for assessment of surface moisture status. Remote Sensing of Environment. 79, 213–224.

Santamouris, M., 2014. Cooling the cities-A review of reflective and green roof mitigation technologies to fight heat island and improve comfort in urban environments. Solar Energy. 103, 682–703.

Santamouris, M., Cartalis, C., Synnefa, A., Kolokotsa, D., 2015. On the impact of urban heat island and global warming on the power demand and electricity consumption of buildings — a review. Energy and Buildings. 98, 119-124.

Santamouris, M., Kolokotsa, D., 2015. On the impact of urban overheating and extreme climatic conditions on housing energy comfort and environmental quality of vulnerable population in Europe. Energy and Buildings. 98, 125-133.

Santamouris, M., Papanikolaou, N., Livada, I., Koronakis, I., Georgakis, C., Argiriou, A., Assimakopoulos, D.N., 2001. On the impact of urban climate on the energy consumption of buildings. Solar Energy. 70 (3), 201–216.

Santamouris, M., Synnefa, A., Karlessi, T., 2011. Using advanced cool materials in the urban built environment to mitigate heat islands and improve thermal comfort conditions. Solar Energy. 85 (12), 3085–3102.

Sarrat, C., Lemonsu, A., Masson, V., Guedalia, D., 2006. Impact of urban heat island on regional atmospheric pollution. Atmospheric Environment. 40, 1743-58.

Schmugge, T., Hook, S.J., Coll, C., 1998. Recovering surface temperature and emissivity from thermal infrared multispectral data. Remote Sensing of Environment. 65, 121–131.

Seguin, B., Itier, B., 1983. Using midday surface temperature to estimate daily evaporation from satellite thermal IR data. Remote Sensing. 4(2), 371–383.

Shwetha, H. R., Kumar, D. N., 2015. Prediction of Land Surface Temperature under Cloudy Conditions using Microwave Remote Sensing and ANN. Aquatic Procedia. 4, 1381 – 1388.

Skelhorn, C., Lindley, S., Levermore, G., 2014. The impact of vegetation types on air and surface temperatures in a temperate city: A fine scale assessment in Manchester, UK. Landscape and Urban Planning. 121, 129–140.

Skoulika, F., Santamouris, M., Boemi, N., Kolokotsa, D., 2014. On the thermal characteristics and the mitigation potential of a medium size urban park in Athens, Greece. Landscape and Urban Planning. 123, 73–86.

Snyder, W. C., Wan, Z., Zhang, Y., Feng, Y.-Z. 1998. Classification-based emissivity for land surface temperature measurement from space. International Journal of Remote Sensing. 19(14), 2753–2774.

Snyder, W., Wan, Z., 1998. BRDF models to predict spectral reflectance and emissivity in the thermal infrared. IEEE Transactions on Geoscience and Remote Sensing. 36(1), 214-225.

Sofer, M., Potchter, O., 2006. The urban heat island of a city in an arid zone: the case of Eilat, Israel. Theoretical Applied Climatology. 85, 81–88.

Srivastava, P. K., Majumdar, T. J., Bhattacharya, A. K., 2009. Surface temperature estimation in Singhbhum Shear Zone of India using Landsat-7 ETM+ thermal infrared data. Advances in Space Research. 43, 1563-1574.

Stathopoulou, M., Constantinos, C., 2007. Daytime urban heat islands from Landsat ETM+ and Corine land cover data: an application to major cities in Greece. Solar Energy. 81, 358–368.

Stathopoulou, Mihalakakou, G., Santamouris, M., Bagiorgas, H.S., 2008. Impact of temperature on tropospheric ozone concentration levels in urban environments. Journal of Earth System Science. 117, 227–236.

Stewart, I.D., Oke, T.R., 2012. Local climate zones for urban temperature studies. Bulletin of the American Meteorological Society. 93(12), 1879–1900.

Streutker, D.R., 2002. A remote sensing study of the urban heat island of Houston, Texas. International Journal of Remote Sensing. 23 (13), 2595–2608.

Streutker, D.R., 2003. Satellite-measured growth of the urban heat island of Houston, Texas. Remote Sensing of Environment. 85 (3), 282–289.

Sun. Q., Wu, Z., Tan, J., 2012. The relationship between land surface temperature and land use/land cover in Guangzhou, China. Environmental Earth Sciences. 65, 1687–1694.

Synnefa, A., Santamouris, M., 2012. Advances on technical, policy and market aspects of cool roof technology in Europe: the cool roofs project. Energy and Buildings. 55, 35–41.

Taha, H., 1997. Urban climates and heat islands: Albedo, evapotranspiration, and anthropogenic heat. Energy and Buildings. 25(2), 99–103.

Takebayashi, H., Masakazu, M., 2007. Surface heat budget on green roof and high reflection roof for mitigation of urban heat island. Buildings and Environment. 42(8), 2971–2979.

Tam, B.Y., Gough, W.A., Mohsin, T., 2015. The impact of urbanization and the urban heat island effect on day to day temperature variation. Urban Climate. 12, 1-10.

Tan, J., Zheng, Y., Tang, X., Guo, C., Li, L., Song, G., Zhen, X., Yuan, D., Kalkstein, A.J., Li, F., Chen, H., 2010. The urban heat island and its impact on heat waves and human health in Shanghai. International Journal of Biometeorology. 54, 75–84.

Tan, M., Li, X., 2015. Quantifying the effects of settlement size on urban heat islands in fairly uniform geographic areas. Habitat International. 49, 100-106.

The United Nations., 2013. World urbanization prospects: The 2012 revision. New York, NY: Department of Economic and Social Affairs, Population (Vol. I: Comprehensive Tables ST/ESA/SER.A/336).

Tiangco, M., Lagmay, A. M. F., Argete, J., 2008. ASTER-based study of the night-time urban heat island effect in Metro Manila. International Journal of Remote Sensing. 29(10), 2799-2818.

Turner, B L II, Clark, W C Kates, R W., 1990.The earth as transformed by human action: global and regional change in the biosphere over the past 300 years, Cambridge University Press, Cambridge.

Tyagi, A., Singh, O.P., Singh, S.S., Kumar, S., 2011. Climate of Jaipur, Meteorological Centre, Jaipur, India Meteorological Department, Ministry of Earth Sciences, Government of India. http://amssdelhi.gov.in/news_events/Jaipur_climate.pdf

Tyrväinen, L., Pauleit, S., Seeland, K., de Vries, S., 2005. Benefits and uses of urban forests and trees. In C. C. Konijnendijk, K. Nilsson, T. B. Randrup, & J. Schipperijn(Eds.), Urban forests and trees 81–114. Berlin: Springer.

Uejio, C. K., Wilhelmi, O. V., Golden, J. S., Mills, D. M., Gulino, S. P., Samenow, J.P., 2011. Intra-urban societal vulnerability to extreme heat: The role of heat exposure and the built environment, socioeconomics, and neighbourhood stability. Health & Place. 17(2), 498–507.

United Nations, Department of Economic and Social Affairs, Population Division (2014). World Urbanization Prospects: The 2014 Revision, Highlights (ST/ESA/SER.A/352).

Vardoulakis, R.E., Karamanis, D., Fotiadi, A., Mihalakakou, G., 2013. The urban heat island effect in a small Mediterranean city of high summer temperatures and cooling energy demands. Solar Energy. 94, 128–144.

Voogt, J.A., Oke, T.R., 2003. Thermal remote sensing of urban climates. Remote Sensing of Environment. 86 (3), 370–384.

Walsh, S.J., Moody, A., Allen, T.R., Brown, D.G., 1997. Scale dependence of NDVI and its relationship to mountainous terrain. In D.A. Quattrochi & M.F. Goodchild (Eds.). Scale in Remote Sensing and GIS (pp 27-55). Boca Raton, FL: Lewis Publishers.

Wan, Z., 1999. MODIS Land-Surface Temperature Algorithm Theoretical Basis Document (LST ATBD), Version 3.3, Contract Number: NAS5-31370. University of California, Santa Barbara. URL: http://modis.gsfc.nasa.gov/data/atbd/atbd_mod11.pdf.

Wan, Z., 2007. Collection-5, MODIS Land Surface Temperature Products Users' Guide, (ICESS, University of California, Santa Barbara). Available online at: http://www.icess.ucsb.edu/modis/LstUsrGuide/MODIS_LST_products_Users_guide_C5.pdf.

Wan, Z., Dozier, J., 1996. A generalized split-window algorithm for retrieving land-surface temperature from space. IEEE Transactions of Geoscience and Remote Sensing. 34 (4), 892–905.

Wan, Z., Li, Z.L., 1997. A physics-based algorithm for retrieving land-surface emissivity and temperature from EOS/MODIS data. IEEE Transactions of Geoscience and Remote Sensing. 35 (4), 980–996.

Weng, Q., 2001. A remote sensing-GIS evaluation of urban expansion and its impact on surface temperature in the Zhujiang Delta, China. International Journal of Remote Sensing. 22 (10), 1999–2014.

Weng, Q., Liu, H., Lu, D., 2007. Assessing the effects of land use and land cover patterns on thermal conditions using landscape metrics in city of Indianapolis, United States. Urban Ecosystems. 10(2), 203–219.

Weng, Q., Lu, D., Schubring, J., 2004. Estimation of land surface temperature–vegetation abundance relationship for urban heat island studies. Remote Sensing of Environment. 89(4), 467–483.

Weng, W.C., Zeng, Z., Karl, T.R., 1990. Urban heat islands in China. Geophysical Research Letters. 17(12), 2377-2380.

Wilby, R. L., 2003. Past and projected trends in London's urban heat island. Weather. 58(7), 251–260.

Wilby, R.L., Hay, L.E., Leavesley, G.H., 1999. A comparison of downscaled and raw GCM output: implications for climate change scenarios in the San Juan River basin. Colorado. Journal of Hydrology. 225, 67-91.

Wilby, R.L., Wigley, T.M.L., 1997. Downscaling General Circulation Model output: a review of methods and limitations. Progress in Physical Geography: Earth and Environment. 21, 530-548.

Wu, C., Murray, A. T., 2003. Estimating impervious surface distribution by spectral mixture analysis. Remote Sensing of Environment. 84, 493–505.

Wu, H., J. Jiang, J. Zhou, H. Zhang, L. Zhang, and L. Ai, 2005. Dynamics of urban expansion in Xi'an City using Landsat TM/ETM data. Acta Geographica Sinica. 60(1), 143–150.

Wu, H., Ye, L.-P., Shi, W.-Z., Clarke, K.C., 2014. Assessing the effects of land use spatial structure on urban heat islands using HJ-1B remote sensing imagery in Wuhan, China. International Journal of Applied Earth Observation and Geoinformation. 32, 67–78.

Xian, G., Crane, M., 2006. An analysis of urban thermal characteristics and associated land cover in Tampa Bay and Las Vegas using Landsat satellite data. Remote Sensing of Environment. 104, 147-156.

Xu, H. Q., 2006. Modification of normalised difference water index (NDWI) to enhance open water features in remotely sensed imagery. International Journal of Remote Sensing. 27, 3025–3033.

Xu, H., Lin, D., Tang, F., 2012. The impact of impervious surface development on land surface temperature in a subtropical city: Xiamen, China. International Journal of Climatology. 33(8), 1873–1883.

Xu, L.Y., Xie, X.D., Li, S., 2013. Correlation analysis of the urban heat island effect and the spatial and temporal distribution of atmospheric particulates using TM images in Beijing. Environmental Pollution. 178, 102-114.

Yamashita, S., Sekine, K., Shoda, M., Yamashita, K. Hara, Y., 1986. On relationships between heat island and sky view factor in the cities of Tama River basin, Japan. Atmospheric Environment. 20, 681–686.

Yang, J., Gong, P., Zhou, J., Huang, H., Wang, L., 2010. Detection of urban heat island in Beijing using HJ-1B satellite imagery. Science China Earth Sciences. 53, 67-73.

Yang, X., 2013. Temporal variation of urban surface and air temperature. University of Hong Kong. Retrieved from http://hub.hku.hk/handle/10722/195964.

Yuan, F., Bauer, M.E., 2007. Comparison of impervious surface area and normalized difference vegetation index as indicators of surface urban heat island effects in Landsat imagery. Remote Sensing of Environment. 106 (3), 375–386.

Yue, W., Liu, Y., Ye, X., Wu, C., 2012. Assessing spatial pattern of urban thermal environment in Shanghai, China. Stochastic Environmental Research and Risk Assessment. 26(7), 899-911.

Zha, Y., Gao, J., Ni, S., 2003. Use of normalized difference built-up index in automatically mapping urban areas from TM imagery. International Journal of Remote Sensing. 24 (3), 583–659.

Zhang, H., Qi, Z.F, Ye, X.Y., Cai, Y.B., Ma, W.C., Chen, M.N., 2013. Analysis of land use/land cover change, population shift, and their effects on spatiotemporal patterns of urban heat islands in metropolitan Shanghai, China. Applied Geography. 44, 121-133

Zhang, Y., Odeh, I.O.A., Han, C., 2009. Bi-temporal characterization of land surface temperature in relation to impervious surface area, NDVI and NDBI, using sub-pixel image analysis. International Journal of Applied Earth Observation and Geoinformation. 11, 256-264.

Zhangyan, J., Yunhao, C., Jing, L., 2006. On urban heat island of Beijing based on Landsat TM data. Geo-spatial Information. 9(4), 293-297.

Zhao, H., Chen, X., 2005. Use of normalized difference bareness index in quickly mapping bare areas from TM/ETM? Geoscience and Remote Sensing Symposium. 3(25–29), 1666–1668.

Zhao, S., Zhou, D., Liu, S., 2015. Data concurrency is required for estimating urban heat island intensity. Environmental Pollution. 208, 118-124.

Zhou, D., Zhao, S., Liu, S., Zhang, L., Zhu, C., 2014. Surface urban heat island in China's 32 major cities: Spatial patterns and drivers. Remote Sensing of Environment. 152, 51–61.

Zhou, L.-M., Dickinson, R. E., Tian, Y.-H., Fang, J.-Y., Li, Q.-X., Kaufmann, R. K., Tucker, C.J., Myneni, R.B., 2004. Evidence for a significant urbanization effect on climate in China. Proceeding of the National Academy of Science of the United States of America. 101(26), 9540–9544.

Zhou, W., Huang, G., Cadenasso, M. L., 2011. Does spatial configuration matter? Understanding the effects of land cover pattern on land surface temperature in urban landscapes. Landscape and Urban Planning. 102(1), 54–63.

Annexure I

Statistical Details of Mean LST Images

Table A.1: Statistical Details of Mean LST Images of the Jaipur Study Area for Different Seasons

years	Summer Day			Summer Night			Monsoon Day			Monsoon Night			Winter Day			Winter Night		
	Urban	Rural	Day Mean UHII	Urban	Rural	Night Mean UHII	Urban	Rural	Day Mean UHII	Urban	Rural	Night Mean UHII	Urban	Rural	Day Mean UHII	Urban	Rural	Night Mean UHII
2003	314.78	315.75	-0.97	295.12	292.56	2.56	313.78	313.97	-0.18	294.50	292.04	2.46	306.80	307.64	-0.84	283.35	280.20	3.15
2004	317.92	319.03	-1.11	295.76	292.98	2.78	309.23	309.18	0.04	295.66	294.11	1.55	305.01	306.14	-1.13	285.06	281.59	3.47
2005	316.48	317.92	-1.44	294.57	291.41	3.16	311.31	311.38	-0.08	297.23	295.50	1.73	305.98	307.00	-1.02	283.31	279.75	3.57
2006	315.84	317.24	-1.40	295.48	292.97	2.51	315.77	316.04	-0.27	296.92	295.10	1.83	306.90	308.07	-1.17	285.40	281.73	3.66
2007	314.67	315.76	-1.09	295.48	292.63	2.85	313.48	313.66	-0.19	296.42	294.52	1.90	306.34	307.61	-1.27	285.90	281.99	3.91
2008	315.89	316.94	-1.06	294.47	291.49	2.98	312.52	312.66	-0.14	296.46	294.36	2.10	306.30	308.03	-1.73	285.12	281.16	3.95
2009	317.19	319.10	-1.90	295.72	292.57	3.15	313.41	313.47	-0.06	297.79	296.05	1.74	306.95	308.17	-1.21	285.76	282.05	3.71
2010	317.67	319.24	-1.57	296.32	293.25	3.07	310.95	310.93	0.01	296.21	293.93	2.28	303.49	304.24	-0.75	285.63	282.44	3.18
2011	314.06	314.49	-0.42	295.61	292.45	3.16	312.01	312.12	-0.11	296.54	294.03	2.51	306.44	307.76	-1.32	286.31	282.66	3.66
2012	314.09	315.18	-1.10	295.12	291.87	3.26	313.09	313.24	-0.14	296.75	294.33	2.42	305.11	306.68	-1.57	284.83	280.95	3.88
2013	315.62	316.61	-0.99	296.36	293.21	3.15	309.16	309.02	0.14	297.18	295.16	2.02	304.72	305.63	-0.91	285.29	281.81	3.48
2014	313.54	314.48	-0.94	296.05	293.13	2.93	311.31	311.27	0.04	297.91	295.55	2.36	304.73	305.49	-0.76	285.68	281.98	3.70
2015	314.18	315.33	-1.15	295.51	292.91	2.60	316.08	316.31	-0.23	297.38	295.16	2.22	306.44	307.68	-1.25	285.74	282.25	3.49

Table A.2: Statistical Details of Mean LST Images of the Ahmedabad Study Area for Different Seasons

years	Summer Day			Summer Night			Monsoon Day			Monsoon Night			Winter Day			Winter Night		
	Urban	Rural	Day Mean UHII	Urban	Rural	Night Mean UHII	Urban	Rural	Day Mean UHII	Urban	Rural	Night Mean UHII	Urban	Rural	Day Mean UHII	Urban	Rural	Night Mean UHII
2003	320.00	320.18	-0.19	297.85	295.58	2.27	313.72	311.78	1.94	297.06	295.10	1.96	309.16	308.86	0.30	290.90	287.67	3.23
2004	320.41	320.58	-0.16	297.69	295.42	2.28	310.32	308.88	1.44	296.97	295.66	1.30	309.47	309.07	0.40	290.67	287.54	3.13
2005	320.81	321.06	-0.25	297.85	295.17	2.68	311.49	308.01	3.49	297.33	295.71	1.61	308.30	307.76	0.54	289.40	286.18	3.22
2006	319.90	320.00	-0.10	297.90	295.52	2.38	313.17	311.19	1.98	297.52	296.19	1.33	309.41	308.88	0.53	291.25	288.01	3.24
2007	319.90	319.99	-0.09	298.70	296.23	2.48	312.76	309.68	3.08	296.55	294.80	1.74	309.27	308.85	0.42	290.62	287.47	3.14
2008	318.49	317.76	0.73	297.84	295.22	2.63	312.70	309.86	2.84	297.42	295.76	1.66	308.75	308.10	0.65	290.18	286.81	3.37
2009	320.31	320.62	-0.31	298.70	296.10	2.60	314.17	312.23	1.95	297.54	295.64	1.90	309.64	309.31	0.33	290.99	287.65	3.34
2010	320.76	320.63	0.14	299.69	296.98	2.70	313.05	309.71	3.35	298.74	296.69	2.05	307.76	307.41	0.35	291.17	288.28	2.89
2011	318.80	318.56	0.24	298.22	295.72	2.50	312.97	310.88	2.09	297.96	296.24	1.72	308.48	307.90	0.59	291.34	288.12	3.22
2012	318.19	317.83	0.36	298.31	295.88	2.43	312.15	309.86	2.29	297.43	295.47	1.96	308.31	307.77	0.55	290.04	286.78	3.26
2013	319.65	319.50	0.14	298.74	296.03	2.71	310.59	307.00	3.59	297.52	296.04	1.48	308.06	307.27	0.79	290.73	287.61	3.12
2014	318.66	318.36	0.30	298.77	296.27	2.50	312.48	310.16	2.32	298.09	296.65	1.44	307.65	307.29	0.36	291.13	287.99	3.14
2015	317.73	317.59	0.13	298.49	296.08	2.41	313.50	310.52	2.98	298.92	296.81	2.11	308.77	308.36	0.41	291.40	288.07	3.34

Table A.3: Statistical Details of Mean LST Images of the Chandigarh Study Area for Different Seasons

years	Summer Day			Summer Night			Monsoon Day			Monsoon Night			Winter Day			Winter Night		
	Urban	Rural	Day Mean UHII	Urban	Rural	Night Mean UHII	Urban	Rural	Day Mean UHII	Urban	Rural	Night Mean UHII	Urban	Rural	Day Mean UHII	Urban	Rural	Night Mean UHII
2003	313.16	312.06	1.10	291.99	290.73	1.25	307.74	305.36	2.38	295.18	294.29	0.89	299.33	297.85	1.48	283.34	282.51	0.83
2004	313.23	311.68	1.54	293.14	291.77	1.37	307.82	305.03	2.80	295.18	294.15	1.03	298.47	297.07	1.40	282.98	282.11	0.86
2005	313.15	311.62	1.53	292.27	290.95	1.32	307.33	304.36	2.97	296.32	295.26	1.06	297.98	296.67	1.31	281.91	280.97	0.95
2006	311.71	309.98	1.73	293.01	291.76	1.25	308.37	305.63	2.75	295.92	294.88	1.05	299.61	298.35	1.27	283.32	282.41	0.91
2007	311.30	309.72	1.58	293.38	292.17	1.21	308.47	305.90	2.57	295.94	294.82	1.12	299.32	298.21	1.11	282.54	281.41	1.13
2008	312.56	311.08	1.48	292.83	291.42	1.40	307.28	304.32	2.97	296.42	295.46	0.95	298.90	297.78	1.13	282.62	281.60	1.02
2009	314.21	313.18	1.02	292.86	291.35	1.51	309.04	306.21	2.83	296.67	295.62	1.05	299.67	298.67	1.00	282.87	281.87	1.00
2010	314.78	313.44	1.34	294.15	292.64	1.50	307.72	305.06	2.66	296.31	295.28	1.03	299.79	298.56	1.23	282.42	281.54	0.88
2011	310.98	309.36	1.63	292.86	291.47	1.39	308.13	305.95	2.18	296.05	295.05	1.00	298.84	297.64	1.19	283.00	282.08	0.92
2012	312.29	310.76	1.52	292.46	290.96	1.49	307.02	304.72	2.29	296.70	295.47	1.22	297.97	296.85	1.12	282.58	281.48	1.10
2013	310.71	309.08	1.64	293.33	291.91	1.42	306.45	303.97	2.48	296.37	295.33	1.05	297.81	296.76	1.05	282.73	281.66	1.07
2014	311.94	310.59	1.35	292.84	291.46	1.39	308.28	306.13	2.15	296.89	295.83	1.07	298.12	297.11	1.00	283.41	282.25	1.16
2015	310.87	309.25	1.63	293.57	292.34	1.23	308.36	306.44	1.92	297.11	295.86	1.25	297.91	296.99	0.92	283.56	282.61	0.94

Annexure II

Site Locations for In-Situ Temperature Measurements

1. Kanwar Nagar

Fig. A.1. Various Surfaces at Kanwar Nagar Location

2. PGIS

Fig. A.2. Various Surfaces at PGIS Location

3. MNIT

Fig. A.3. Various Surfaces at MNIT Location

Annexure III

Curriculum-Vitae

1. Name : Aneesh Mathew

2. Designation : Assistant Professor, Department of Civil Engineering, Madanapalle Institute of Technology and Science, Madanapalle

3. Educational Qualifications (Starting from Graduation onwards):

S. No.	Degree	University	Year	Subjects	Percentage/CGPA
1	B.Tech	Mahatma Gandhi University	2011	Civil Engineering	76.59
2	M.Tech	MNIT Jaipur	2014	Water Resources Engineering	9.68 (Gold Medal)

4. Employment Record:

Organization/Employer	Designation	Period
Shapoorji Pallonji Engineering and Constructions	Graduate Engineer Trainee (Civil)	August 2011- July 2012
Madanapalle Institute of Technology and Science, Madanapalle	Assistant Professor	March 2018 and continuing

5. Publications

a) International Journal Publications

i. **Aneesh Mathew**, Sumit Khandelwal, Nivedita Kaul. "Spatio-temporal variations of surface temperatures of Ahmedabad city and its relationship with vegetation and urbanization parameters as indicators of surface temperatures". Published in Remote Sensing Applications: Society and Environment Journal (ELSEVIER). Digital Object Identifier: https://doi.org/10.1016/j.rsase.2018.05.003. Vol. 11 (2018) 119-139.

ii. **Aneesh Mathew**, Sumit Khandelwal, Nivedita Kaul. "Investigating spatio-temporal surface urban heat island growth over Jaipur city using geospatial techniques". Published in Sustainable Cities and Society Journal (ELSEVIER). Digital Object Identifier: https://doi.org/10.1016/j.scs.2018.04.018. Vol. 40 (2018) 484-500.

iii. **Aneesh Mathew**, Sumit Khandelwal, Nivedita Kaul, Shivam Chauhan. "Analyzing the diurnal variations of land surface temperatures for surface urban heat island (SUHI) studies: Is time of observation of remote sensing data important?" Published in Sustainable Cities and Society Journal (ELSEVIER) Digital Object Identifier: https://doi.org/10.1016/j.scs.2018.03.032. Vol. 40 (2018) 194-213.

iv. **Aneesh Mathew**, Sumit Khandelwal, Nivedita Kaul. "Analysis of diurnal surface temperature variations for the assessment of surface urban heat island effect over Indian cities". Published in Energy and Buildings journal (ELSEVIER). Digital Object Identifier: https://doi.org/10.1016/j.enbuild.2017.10.062. Vol. 159 (2017) 271-295.

v. **Aneesh Mathew**, Sumit Khandelwal, Nivedita Kaul. "Investigating Spatial and Seasonal Variations of Urban Heat Island Effect over Jaipur City and Its Relationship with Vegetation, Urbanization and Elevation Parameters". Published in Sustainable Cities and Society Journal (ELSEVIER). Digital Object Identifier: http://dx.doi.org/10.1016/j.scs.2017.07.013. Vol. 35 (2017) 157-177.

vi. **Aneesh Mathew**, Sumit Khandelwal, Nivedita Kaul. "Spatial and Temporal Variations of Urban Heat Island Effect and the effect of Percentage Impervious Surface Area and Elevation on Land Surface Temperature: Study of Chandigarh City, India". Published in Sustainable Cities and Society Journal (ELSEVIER). Digital Object Identifier: 10.1016/j.scs.2016.06.018, Vol. 26 (2016) 264–277.

vii. **Aneesh Mathew**, Sreenu Sreekumar, Sumit Khandelwal, Nivedita Kaul, Rajesh Kumar. "Prediction of Surface Temperatures for the Assessment of Urban Heat Island Effect over Ahmedabad City Using Linear Time Series Model". Published in Energy and Buildings journal (ELSEVIER). Digital Object Identifier: 10.1016/j.enbuild.2016.07.004, Vol. 128 (2016) 605–616.

viii. **Aneesh Mathew**, Sreenu Sreekumar, Sumit Khandelwal, Nivedita Kaul, Rajesh Kumar. "Prediction of Land-Surface Temperatures of Jaipur City Using Linear Time Series Model". Published in IEEE Journal of Selected Topics in Applied Earth Observations and Remote Sensing (IEEE). Digital Object Identifier: 10.1109/JSTARS.2016.2523552. Vol. 9, No. 8 (2016) 3546-3552.

b) International Conference Publications

i. **Aneesh Mathew**, Shivam Chauhan, Sumit Khandelwal, Nivedita Kaul. "Assessment of surface urban heat island growth over Ahmedabad city using geospatial techniques". Paper presented in International Conference on Sustainable Technologies for Intelligent Water Management, Department of Water Resources Development & Management, IIT Roorkee, Uttarakhand, 16-19th February 2018.

ii. **Aneesh Mathew**, Sumit Khandelwal, Nivedita Kaul. "Seasonal and spatial variations of surface urban heat island effect over Ahmedabad city using geospatial techniques". Paper presented in 22nd International Conference on Hydraulics, Water Resources and Environmental Engineering (ISH-Hydro 2017 International), LD Engineering college, Ahmedabad, Gujrat, 21-23, December, 2017.

iii. **Aneesh Mathew**, Sumit Khandelwal, Nivedita Kaul. "Assessment of Land Surface Temperature Relationship with Vegetation, Water and Built-up Parameters of Chandigarh City in India". Paper presented in 21st International Conference on Hydraulics, Water Resources and Environmental Engineering (ISH-Hydro 2016 International), CPWRDM Pune, Maharashtra, 8-10th December 2016.

iv. **Aneesh Mathew**, Neha Gupta, Sumit Khandelwal, Nivedita Kaul. "Assessment of Land Surface Temperature-Vegetation Relationship over Jaipur City Using Geospatial Techniques". Paper presented in International Conference on Recent Trends in Engineering and Material Sciences (ICEMS-2016), JNU Jaipur, Rajasthan, 17-19th March 2016.

v. **Aneesh Mathew**, Sumit Khandelwal, Nivedita Kaul. "Analysis of Spatial and Temporal Variations of Urban Heat Island Effect on Ahmedabad city and Its Relationship with Impervious Surfaces". Paper presented in 20th International Conference on Hydraulics, Water Resources and River Engineering (Hydro 2015 International), IIT Roorkee, Uttarakhand, 17-19th December 2015.

vi. **Aneesh Mathew**, Rishabh Chaudhary, Neha Gupta, Sumit Khandelwal, Nivedita Kaul. "Study of Urban heat Island Effect on Ahmedabad City and Its Relationship with Urbanization and Vegetation Parameters". Paper presented in International Conference on Emerging Trends of Engineering, Science, Management and Its Applications' 15 JNU Convention Centre, New Delhi, India, 1st March 2015.

6. Workshops

i. One day Training-cum-Workshop on 'ISRO's Geo-portals for developmental planning and e-governance' at Birla auditorium, Jaipur on April 12, 2016.

ii. Global Initiative of Academic Networks (GIAN), International Summer Course – 2016 on Land Use/ Land Cover Change Modelling and Prediction (July 04 – 08, 2016), Department of Civil Engineering, Malaviya National Institute of Technology Jaipur, Jaipur – 302017 (Rajasthan), India.

iii. One day Training-cum-Workshop on 'Sustainability of ODS Phase out, Kigali Amendment and India's way forward' on the occasion of International Ozone Day (16th September, 2017), Department of Civil Engineering, Malaviya National Institute of Technology Jaipur, Jaipur – 302017 (Rajasthan), India.

iv. One day Training-cum-Workshop on 'AIR-O2-THON International summit (20th January, 2018), Department of Civil Engineering, Malaviya National Institute of Technology Jaipur, Jaipur – 302017 (Rajasthan), India.

v. IUCEE – IIEECP, international engineering educator precertification Batch-2 Phase1 workshop conducted at VIT, Amaravathi from 12th July 2018 to 14th July 2018.

7. Professional recognition, awards, fellowships received: **Received**

M.Tech Gold Medal for securing Maximum marks in Water Resources Engineering 2014 batch